INFORMATION TO USERS

This manuscript has been reproduced from the microfilm master. UMI films the text directly from the original or copy submitted. Thus, some thesis and dissertation copies are in typewriter face, while others may be from any type of computer printer.

The quality of this reproduction is dependent upon the quality of the copy submitted. Broken or indistinct print, colored or poor quality illustrations and photographs, print bleedthrough, substandard margins, and improper alignment can adversely affect reproduction.

In the unlikely event that the author did not send UMI a complete manuscript and there are missing pages, these will be noted. Also, if unauthorized copyright material had to be removed, a note will indicate the deletion.

Oversize materials (e.g., maps, drawings, charts) are reproduced by sectioning the original, beginning at the upper left-hand corner and continuing from left to right in equal sections with small overlaps. Each original is also photographed in one exposure and is included in reduced form at the back of the book.

Photographs included in the original manuscript have been reproduced xerographically in this copy. Higher quality 6" x 9" black and white photographic prints are available for any photographs or illustrations appearing in this copy for an additional charge. Contact UMI directly to order.

UMI

A Bell & Howell Information Company
300 North Zeeb Road, Ann Arbor MI 48106-1346 USA
313/761-4700 800/521-0600

PHYSICOCHEMICAL CONTROLS OF GREISEN FORMATION AND CASSITERITE DEPOSITION AT THE EAST KEMPTVILLE TIN DEPOSIT, NOVA SCOTIA.

by

Werner E. Halter

December, 1996

A thesis submitted to the Faculty of Graduate Studies and Research in partial fulfillment of the requirements of the degree of Doctor of Philosophy

Department of Earth and Planetary Sciences
McGill University
Montréal, Québéc
Canada

0-612-29955-4

ABSTRACT

Prior to complete crystallization of leucogranitic magma at East Kemptville, tectonic fracturing induced a pressure drop, allowing a NaCl-HCl-HF-rich fluid phase to separate. This fluid caused pervasive sericitization and extracted the ore metals from the melt. It was then channeled into the fractures and caused greisenization in the apical part of the intrusion. During greisenization, the leucogranite was converted into quartz-sericite greisen through sequential replacement of K-feldspar and albite. Muscovite was replaced by topaz to form quartz-topaz greisen, host to sulphide and cassiterite mineralization. In this greisen, the OH^- of muscovite is replaced by H_2O and O^{2-}, which leads to its dehydration during microprobe analyses. Close to veins, suphides and cassiterite were re-dissolved in quartz greisen. The altering fluid had a pH of 3.0 and contained 4.8m Cl, 3.7m Na, 0.53m Fe and minor F, K, S and Sn as determined from fluid inclusions and mineral equilibria. The temperature of greisenization was determined to be 480 ± 15°C using a F-OH exchange geothermometer between topaz and muscovite and oxygen isotopic data on cassiterite and quartz; the pressure was estimated to be 4.1 ± 1.0 kbars using fluid inclusion isochores. Alteration occurred though a process of compensated infiltration in which small aliquots of fluid were exchanged between the rock and the vein, while the bulk flow was parallel to the vein. This created a distribution of the components controlled by chemical potential gradients; Fe, Sn, S and F were transported away from the vein and Na towards it. Changes in physicochemical parameters of the fluid were quantified using computer simulation, which, in conjunction with fluid inclusion data, indicates that cassiterite precipitated in response to a pH increase. Changes in a_{Cl^-} and fO_2 were insufficient to account for cassiterite precipitation or acted against it. Modeling further showed that sulphides and cassiterite re-dissolved close to the vein depressed fO_2 and increased the Sn content of the fluid in quartz-topaz greisen. This raised the chemical potential of Sn, creating a barrier across which tin could not be transported, possibly explaining the low tin grades at East Kemptville.

RÉSUMÉ

Le leucogranite de East Kemptville a subi une fracturation tectonique à laquelle fut associée une baisse subite de la pression, permettant ainsi la séparation d'une phase fluide, riche en NaCl, HCl et HF. Cette phase fluide fut responsable tant d'une sericitisation générale que de l'extraction du magma des métaux se trouvant dans le gisement. Ce fluide fut ensuite canalisé dans les fractures et provoqua l'altération en greisen dans la partie supérieure de l'intrusion. Lors de l'altération, le feldspath potassique et l'albite furent successivement dissous, ce qui transforma le leucogranite en un greisen à quartz et sericite. La muscovite fut par la suite remplacée par le topaz durant la formation de greisen à quartz et topaz. La minéralisation est associée avec cette seconde altération. Dans ce greisen, les groupes OH^- de la muscovite ont été remplacés par un ion O^{2-} et une molécule de H_2O. Cette substitution conduit à la deshydratation de ce minéral durant l'analyse à la microsonde. A proximité des veines, la formation de greisen à quartz fut accompagnée de la redissolution tant des sulfures que de la cassiterite. L'étude des inclusions fluides a démontré que le fluide à l'origine de l'altération avait un pH de 3.0 et contenait 4.8m de Cl, 3.7m de Na, 0.53m de Fe et des concentrations mineures de F, K, S et de Sn. La température de formation des greisens a été estimée à 480 ± 15°C par un geothermomètre basé sur l'échange de F et OH entre la muscovite et le topaz. Cette température fut confirmée par des données isotopiques sur le quartz et la cassiterite. La pression a été évaluée à 4.1 ± 1.0 kbars à l'aide d'isochores d'inclusions fluides. L'altération fut produite par un processus d'infiltration compensée. Par ce processus, de petites quantités de fluide ont été échangées entre la roche et la fracture (veine). Le flux global fut, toutefois, parallèle à la fracture. La distribution des composants de la roche et du fluide fut ainsi contrôlée par des gradiens de potentiels chimiques : Fe, Sn, S et F furent transportés de la fracture vers la roche et le Na de la roche vers la fracture. Les variations des paramètres physico-chimiques furent quantifiés par simulation sur ordinateur. Cette simulation, en association avec les données des inclusions fluides, indique que la précipitation de la cassiterite est due à une augmentation du pH. Les variations en a_{Cl^-} furent insuffisantes pour expliquer la précipitation de la cassiterite tandis que les

variations en fO_2 favorisaient sa dissolution. La modélisation permis également de montrer que la redissolution des sulfures et de la cassiterite proche de la veine diminua fO_2 et augmenta la concentration en Sn du fluide dans le greisen à quartz et topaz. Cette redissolution augmenta le potentiel chimique du Sn et forma ainsi une barrière efficace à travers laquelle Sn ne pouvait être transporté. Ceci pourrait expliquer les faibles teneurs en étain du gisement de East Kemptville.

ACKNOWLEDGMENTS

I wish to express my deepest thanks to my supervisor, Prof. A.E. Williams-Jones for his encouragements and enthusiasm which continuously stimulated my research interest, and for patiently reviewing my work.

Thanks are extended to Dr. D.J. Kontak who suggested the study area and provided important insights into the geology of the area. Many others have also provided stimulating discussions on my research, particularly C. Normand, but also V. Bodycomb, J. Clark, J. Fein, C. Gammons, A. Herzakani, R. Martin, G. Olivo, S. Salvi and B. Stefanini. Thanks to all of you.

The technical assistance provided by G. Poirier (electron microprobe), G. Keating (IC analyses), S. Shata (X-ray diffraction), G. Panagiotidis (rock preparation workshop) and S. McCauley (computer work) is greatly appreciated. Particularly helpful were the numerous E-mails from S. Salvi on how to run the gas chromatograph.

The author would like to thank John Horton, Jim Langille, Bill Palmer and Donnie Weir for their help during the core logging in Stellarton as well as the East Kemptville Tin Corp. (Rio Algom), and Mr. Brian Lewis for permission to work at the mine in the summer of 1993.

Financial support for this research was provided by the Canada-Nova Scotia Mineral Development Agreement through a contract with D. Kontak from the Nova Scotia Department of Natural Resources. Additional support was provided by an NSERC research grant to A.E.W.-J.

TABLE OF CONTENTS

PREFACE

The research presented in this thesis was initiated as a collaboration between the author and his advisor, Prof. A.E. Williams-Jones and Dr. D.J. Kontak from the Nova Scotia Department of Natural Resources. The thesis is divided into seven Chapters, five of which are manuscripts and the remaining two are a general introduction and conclusion. Chapter 2 was published in Economic Geology, 1996, v. 91, p. 368-385. Chapters 3, 4, 5 and 6 have yet to be submitted. Each manuscript is co-authored by Prof. A.E. Williams-Jones who provided advice on research methodology, helped evaluate and interpret the data and critically reviewed the text. Dr. D.J. Kontak is third author on Chapters 2 and 3. He suggested the field area, help to finance the project, provided logistical support during field work and useful information on the regional and local geology and helpful comments on Chapter 2. Field work and core logging were carried out by the author in the summer of 1993. Petrographic analyses, fluid inclusion microthermometry, SEM analyses of fluid inclusion decrepitates, IC analyses of fluid inclusion leachates and gas chromatographic analyses of fluid inclusions were also carried out by the author. Electron microprobe analyses were conducted by the author with the assistance of G. Poirier. Major and trace element compositions of whole rocks were analyzed using X-ray fluorescence by T. Ahmedali at the Department of Earth and Planetary Sciences, McGill University. Rare Earth elements were analysed using ICP-MS by Dr. S. Jackson at Memorial University, Newfoundland, and by Dr. E. Hoffmann at Activation Laboratories, Ancaster, Ontario. The latter laboratories also analysed cations in fluid inclusion leachate solutions using ICP-MS. Oxygen isotope compositions were determined by D. Pezderic at the University of Saskatchewan. Finally, computer modeling was carried out by the author using the program CHILLER and a data base modified by him.

The following is an excerpt from the "Guidelines Concerning Thesis Preparation as required by the Faculty of Graduate Studies and Research at McGill University:

> Candidates have the option of including, as part of the thesis, the text of one or more papers submitted or to be submitted for publication, or the clearly-duplicated text of one or more published papers. These texts must be bound as an integral part of the thesis.

If this option is chosen, **connecting texts that provide logical bridges between the different papers are mandatory**. The thesis must be written in such a way that it is more than a mere collection of manuscripts; in other words, results of a series of papers must be integrated.

The thesis must still conform to all other requirements of the "Guidelines for Thesis Preparation". **The thesis must include :** A Table of Contents, an abstract in English and French, an introduction which clearly states the rationale and objectives of the study, a review of the literature, a final conclusion and summary, and a thorough bibliography or reference list.

Additional material must be provided where appropriate (e.g. in appendices) and in sufficient detail to allow a clear and precise judgement to be made of the importance and originality of the research reported in the thesis.

In the case of manuscripts co-authored by the candidate and others, **the candidate is required to make an explicit statement in the thesis as to who contributed to such work and to what extent.** Supervisors must attest to the accuracy of such statements at the doctoral oral defense. Since the task of the examiners is made more difficult in these cases, it is in the candidate's interest to make perfectly clear the responsibilities of all authors of the co-authored papers.

CHAPTER I

GENERAL INTRODUCTION

INTRODUCTION

A large number of hydrothermal ore deposits are related to the formation of veins which provide local pathways for mineralizing fluids. Veins can host spectacular mineralization, but much of the ore associated with these deposits is disseminated in the altered host rocks. Understanding the formation of these deposits is therefore bound to the understanding of the chemical changes that the mineralizing fluid was subjected to during alteration. This problem has been addressed by a limited number of researchers, although only for gold bearing systems (e.g., Böhlke, 1989, Mountain and Williams-Jones, 1996). In this thesis, I investigate the formation of a different type of vein mineralization, i.e., a greisen-hosted tin deposit, for which the origin of the metals as well as the controls on cassiterite precipitation still remains controversial.

CURRENT KNOWLEDGE OF TIN DEPOSITS

Based on work by Daubrée (1841), Beaumont (1847) developed the first comprehensive theory on the formation of hydrothermal ore deposits in acid magmatic systems. These authors suggested that an important characteristic of tin-bearing granites is their high volatile content, which lowers their solidus temperature. They further proposed, that tin is leached from granitic rocks by an acid hydrothermal fluid and subsequently reprecipitated in apical parts of the intrusion during alteration of the granitic rocks. In essence, this theory for the formation of greisen-hosted tin deposits is still widely applicable a century and a half later. The main improvements to the model have been to better characterize the intrusive rock and the mineralizing fluid as well as to quantify some aspects of the processes.

Intrusions hosting tin mineralization, often referred to as "tin granites", are typically peraluminous S-type granites or monzogranites formed by partial melting of the continental crust (Taylor, 1979). The vast majority of tin granites are reduced, i.e., they belong to the ilmenite series granites (Lehmann, 1990), since tin is present as incompatible Sn^{2+} in these melts (Sn^{4+} in oxidized melts can substitute for Fe^{3+} and Ti^{4+} in early fractionated phases).

Tin mineralization is associated with the most differentiated part of these intrusions in which late magmatic volatiles are concentrated (Burnham, 1979). Volatiles, and particularly H_2O cause depolymerization of the melt (Mahood and Hildreth, 1983) and therefore favour the concentration of Na, Li, Be, F, Cl and large, highly charged cations such as Nb, Ta, Sb, Mo, Sn, W, U (Eugster, 1985) characteristic of highly specialized granites (Tischendorf, 1977). Textural evidence shows that the enrichment in Sn can be sufficient to precipitate primary cassiterite in pegmatites (Linnen et al., 1992).

At a late stage of the crystallization of the magma, volatiles can saturate in the residual melt and separate as a vapour-rich phase which accumulates at the roof of the chamber (Jackson et al., 1982). These fluids either remain trapped in the granite or fracture the intrusive and the surrounding rocks if fluid pressure exceeds lithostatic pressure. Partitioning of Sn between this fluid phase and the melt has been investigated by several authors (Nekrasov et al., 1982; Nekrasov, 1984; Taylor and Wall, 1984; Urabe, 1985; Manning and Pichavant, 1988) who have shown that the partition coefficients depend greatly on the melt and fluid composition. It is, however, generally agreed, that Sn^{2-} partitions into the vapour phase due to its high solubility in chloride-rich fluids at submagmatic conditions (Eugster and Wilson, 1985; Eugster, 1986; and Wilson and Eugster, 1990). In the fluid, Sn is transported mainly as a chloride complex; OH^- and F^- complexes are also present (Klintsova and Barsukov, 1973; Štemprock, 1982; Kovalenko et al., 1992) but significantly less important (Jackson and Helgeson, 1985).

Previous investigations of hydrothermal fluid associated with tin deposits (Durišová et al., 1979; Kelly and Rye, 1979; Haapala and Kinnunen, 1982; Norman and Trangcotchasan, 1982; Eadington, 1983; Rankin and Alderton, 1985; Shepherd et al., 1985; Taylor and Pollard, 1988; Schwartz and Askury, 1989) have shown that, in addition to Sn and Cl, the mineralizing fluid is characterized by high concentrations of Na, F, P, S, Fe, CO_2 and a low pH. Mineralization takes place at temperatures between 250 and 500°C and pressures between 0.2 and 5 Kbars when this fluid interacts with the intrusive or sedimentary rocks that host the intrusion. In the granite, the alteration progressively destroys feldspars and biotite by leaching of Na and K and enriches the rock in F, Fe, B, Li, S (Burt, 1981; Štemprock, 1987; Heinrich, 1990). This leads to the formation of greisens, consisting typically of quartz, muscovite, topaz, sulphides, cassiterite, fluorite and minor phases like molybdenite, wolframite or tourmaline, as documented by many authors (e.g., Rundquist, 1982; Eugster, 1985; Stone et al., 1985; Plimer, 1987; Schwartz and Askury, 1989; Lehmann, 1990; Richardson et al., 1990; Schwartz and Surjono, 1990; Kontak, 1993). The studies on the mineralizing fluid, mentioned above, also conclude that a decrease in temperature or acid neutralization though feldspar dissolution was responsible for cassiterite precipitation. The importance of these two parameters in the formation of hydrothermal tin deposits has been confirmed by theoretical modeling of fluid-rock interaction (Heinrich, 1990) but the role of other components present in the fluid needs yet to be evaluated.

The purpose of my study was to determine the origin of the mineralizing fluid and the ore metals, to quantify the chemical changes in a greisenizing fluid and the host leucogranite, and to establish the extent and the direction of mass transfer during the vein-forming process. The first step in this investigation was to determine the mineralogical and chemical changes that affected the leucogranite. This information provided a basis for evaluating chemical changes in fluid inclusions during alteration. Data from rock and fluid chemistry were in turn used to guide a computer simulation of the evolution of the greisenizing system. The integration of these studies provided a better insight into changes of physico-chemical parameters which control tin mineralization (pH, fO_2 and a_{Cl^-}) and permitted a better understanding of the direction and the mechanism of mass transfer.

Byproducts of this study were the development of a geothermometer based on the F-OH exchange between topaz and muscovite. An explanation for the nature of apparently anhydrous muscovite in highly altered greisen was also provided.

THE EAST KEMPTVILLE TIN DEPOSIT

The East Kemptville tin deposit was selected for this study because earlier investigations had reported the occurrence there of zoned greisens, formed of symmetrical alteration halos around central veins (Richardson, 1988; Kontak, 1990; Richardson et al., 1990). These zoned greisens present an excellent opportunity for studying the progressive alteration that affected the host rock during tin mineralization. The same alteration zones occur on the scale of the deposit and zoned greisens could therefore be used as a tool for investigating the large scale alteration processes. Moreover, the easily accessible open pit mine and the numerous drill cores available from Rio Algom and from the Nova Scotia Department of Natural Resources made it possible to undertake the closely spaced rock sampling needed to support detailed investigation of all the alteration facies.

The East Kemptville mine was the only primary tin deposit in North America. The deposit is located 25 km northeast of Yarmouth, Nova Scotia, and was exploited between 1982 and 1992 as an open pit mine by Rio Algom. Tin was recovered in two zones, a Main and a Baby Zone. The latter is much smaller but has significantly higher ore grades than the Main Zone. Initial reserves were estimated at 56 million tones grading 0.17% Sn, with Cu, Zn and Ag as by-products (Moyle 1985). Cassiterite was concentrated using a magnetic separator, designed to recover 80% of the ore.

The deposit formed in the Davis Lake Pluton located at the southwestern end of the 370 Ma peraluminous South Mountain Batholith in the Meguma Terrane of the Appalachian Orogen. Mineralization developed in the apical part of an evolved leucogranitic facies of the pluton derived by fractional crystallization of a biotite monzogranitic magma that produced most of the Davis Lake Pluton (Kontak, 1990, 1993; and Richardson et al., 1990). The leucogranite has been described extensively by Richardson et al. (1982), Richardson (1988) and Kontak (1990, 1991), and consists of quartz, albitic plagioclase, K-feldspar, muscovite and locally topaz, with accessory biotite, apatite and zircon. The major element chemistry of the leucogranite is characterized by high contents of SiO_2, Al_2O_3, F and P_2O_5 and low contents of MgO and TiO_2 (Chatterjee et al., 1985; Richardson et al., 1990; Kontak, 1990). In the deposit area, the leucogranite was pervasively sericitized and the plagioclase has a composition close to end-member albite.

Richardson (1985, 1988) and Richardson et al. (1990) suggested in previous studies of the East Kemptville deposit, that tin mineralization resulted from the separation of a fluid phase from the crystallizing magma, which subsequently accumulated under an impermeable cap of sediments. When hydrostatic pressure exceeded lithostatic pressure, the granite was fractured and the fluid deposited cassiterite in the leucogranite as it migrated downwards; the sediments on top were not affected by this fracturing. These authors further argue that tin mineralization and the formation of the alteration halos around central fractures were a result of successive pulses of fluid of different composition, i.e., that the first fluid caused albite-white mica replacement and a later fluid was responsible for the fluorine-rich greisenization.

THESIS ORGANIZATION

This thesis is divided into seven chapters, five of which (Chapters 2 to 6) are manuscripts. Chapter 2 details the chemical and mineralogical changes that affected the leucogranite during the formation of a zoned greisen, i.e., a symmetric alteration halo around a central vein. Results of this study showed that greisenization first converted the leucogranite into a quartz-sericite greisen during the replacement of the feldspars by muscovite. With further alteration, muscovite was, in turn, replaced by topaz in quartz-topaz greisen which formed next to the central vein. Cassiterite and sulphide mineralization is associated with this latter alteration. Mineralogical changes are used to evaluate variations in the composition of the hydrothermal fluid and hence to determine the controls of cassiterite precipitation.

In Chapter 3, we examine the effect of alteration on the leucogranite at the scale of the deposit. This was done by chemical, mineralogical and fluid inclusion analyses of selected samples from a 850m deep drill hole which cuts through all the alteration zones present in the deposit, and through 500m of leucogranite. The freshest leucogranite provided valuable information on pre-mineralization processes and permitted the formation and testing of a hypothesis for the origin of the mineralizing fluid and the ore forming elements. This fluid is interpreted to have exsolved from the leucogranite magma and to have interacted with the latter, converting it into quartz-topaz greisens in a sequence of stages similar to those established for the zoned greisen. The mineralogical and chemical changes in the rock were determined by whole rock geochemical analyses and mineral chemical analyses. The changes in the chemical composition of the mineralizing fluid during its interaction with the host rock were evaluated using microthermometry, leachate, decrepitate and gas chromatographic analyses of fluid inclusions from the various alteration zones. These data were used to quantify the mass transfer between the fluid and the rock and thus to determine the large scale controls on the mineralization and the process responsible for vein formation.

One of the most important parameters that controls the formation of hydrothermal ore deposits and the nature of the associated host rock alteration is temperature. Chapter 4 describes the calibration of a new geothermometer based on the F-OH exchange between muscovite and topaz that provides an accurate estimate for the temperature at which greisenizing systems form. This geothermometer yields temperatures which compare well with those estimated using the experimentally calibrated cassiterite-quartz oxygen isotopic geothermometer of Zhang et al. (1994) and, in conjunction with the fluid inclusions data, helped determine the temperature and the pressure of greisen formation at East Kemptville.

The chemical composition of the leucogranite, the mineralizing fluid, and the estimated pressure and temperature conditions provided the input for computer modeling of the fluid-rock interaction. This was done with the program CHILLER (Reed 1982, Spycher and Reed, 1989) specially modified for this purpose. Chapter 5 reports the changes that occur in the fluid and the rock for a multiple pass fluid flow model in which successive aliquots of fluid are passed though a segmented rock column. This model accurately simulates changes in fluid and rock compositions deduced from the natural samples. It could therefore be used for the quantification of the changes in physicochemical parameters which could not be obtained from fluid inclusions (pH, a_{Cl^-}), but which are potentially important in controlling cassiterite precipitation. It also helped understand the evolution of the mineralizing system through time and thus provided insight on the formation of the alteration halo.

During alteration, the composition of muscovite changed significantly with respect to its Fe^{2+}, F^- and Al^{3+} content and, in Chapter 6, a series of coupled substitution are suggested to account for this variation in the leucogranite and the greisens. In quartz-topaz greisen, electron microprobe analyses systematically yield totals close to 100%, suggesting that, in these rocks, muscovite might be anhydrous. An explanation is provided for this anomaly based on the replacement of hydroxide ions by O^{2-} and H_2O, and the dehydration of the muscovite during microprobe analyses.

REFERENCES

Beaumont, E. de, 1847, Note sur les émenations volcaniques et metallifères: Bulletin de la Société Géologique de France, 2ème Série, 4, p. 1249-1334.

Böhlke, J.K., 1989, Comparison of metasomatic reactions between a common CO_2-rich vein fluid and diverse wall rocks: Intensive variables, mass transfers and Au Mineralization at Alleghany, California: Economic Geology, v. 84, p. 291-327.

Burnham, C.W., 1979, Magmas and hydrothermal fluids, *in* H.L. Barnes, ed., Geochemistry of hydrothermal ore deposits, 2nd edition: New York, Wiley, p. 71-136.

Burt, D. M., 1981, Acidity-salinity diagrams - Application to greisen and porphyry deposits: Economic Geology, v. 76, p. 832-843.

Chatterjee, A.K., Strong, D.F., and Clarke, D.B., 1985, Petrology of the polymetallic quartz-topaz greisen at East Kemptville: Nova Scotia Department of Natural Resources, Open File Report 650, p. 151-196.

Daubrée, A., 1841, Mémoire sur le gisement, la constitution et l'origine des amas de minerai d'étain: Annale des Mines, 3ième Série 20, p. 65-112.

Durišová , J., Charoy, B., and Weisbrod, A., 1979, Fluid inclusion studies in minerals from the tin and tungsten deposits in the Krusné Hory Mountains (Czechoslovakia): Bulletin de Minéralogie, v. 102, p. 665-675.

Eadington, P.J., 1983, A fluid inclusion investigation of ore formation in a tin-mineralized granite, New England, New South Wales: Economic Geology, v. 78, p. 1204-1221.

Eugster, H.P., 1985, Granite and hydrothermal ore deposits: a geochemical framework: Mineralogical Magazine, v. 49, p. 7-23.

Eugster, H.P., 1986, Minerals in hot water: American Mineralogist, v. 71, p. 655-673.

Eugster, H.P., and Wilson, G.A., 1985, Transport and deposition of ore-forming elements in hydrothermal systems with granites, *in* High heat production granites, hydrothermal circulation and ore genesis: London, England, The Institution of Mining and Metallurgy, p. 87-98.

Haapala, I., and Kinnunen, K., 1982, Fluid inclusion evidence on the genesis of tin deposits, *in* A.M. Evans, ed., Metallizations associated with acid magmatism, New York, Wiley-Interscience, p. 101-110.

Heinrich, C.A., 1990, The chemistry of Hydrothermal tin (- tungsten) ore deposits: Economic Geology, v. 85, p. 457-481.

Jackson, K.J., and Helgeson, H.C., 1985, Chemical and thermodynamic constrains on the hydrothermal transport of tin: I. Calculation of the solubility of cassiterite at high pressures and temperatures: Geochimica et Cosmochimica Acta, v. 49, p. 1-22.

Jackson, N.J., Halliday, A.N., Sheppard, S.M.F., and Mitchell, J.G., 1982, Hydrothermal activity in the St. Just mining district, Cornwall, England; *in* A.M. Evans, ed., Metallizations associated with acid magmatism: New York, Wiley-Interscience, p. 137-179.

Kelly, W.C., and Rye, R.O., 1979, Geologic, fluid inclusion, and stable isotope studies of the tin-tungsten deposits of Panasqueira, Portugal: Economic Geology, v. 74, p. 1721-1823.

Klintsova, A.P., and Barsukov, V.L., 1973, Solubility of cassiterite in water and in aqueous NaOH solutions at eleveted temperatures: Geochemistry International, 1973, p. 540-547.

Kontak, D.J., 1990, The East Kemptville topaz-muscovite leucogranite, Nova Scotia. I. Geological setting and whole-rock geochemistry: Canadian Mineralogist, v. 28, p. 787-825.

Kontak, D.J., 1991, The East Kemptville topaz-muscovite leucogranite, Nova Scotia. II. Mineral chemistry: Canadian Mineralogist, v. 29, p. 37-60.

Kontak, D.J., 1993, Geological, geochemical and isotopic studies of the East Kemptville Sn-(Zn-Cu-Ag) deposit, Yarmouth County, Nova Scotia, Canada: Quadrennial IAGOD Symposium, Eighth, Stuttgart, Germany, E. Schweizerbart'sche Verlagsbuchhandlung, 1993, Proceedings, p. 383-409.

Kovalenko, N.I., Ryzhenko, B.N., Dorofeyeva, V.A., and Bannykh, L.N., 1992, The stability of $Sn(OH)_4^{2-}$, $Sn(OH)_2F^-$, and $Sn(OH)_2Cl^-$ at 500°C and 1Kbar: Geochemistry International, v. 29, p. 84-94.

Lehmann, B., 1990, Metallogeny of tin: Berlin, Germany, Springer-Verlag, 211p.

Linnen, R.L., Williams-Jones, A.E., and Martin, R.F., 1992, Evidence of magmatic cassiterite mineralization at the Nong Sua aplite-pegmatite complex, Thailand: Canadian Mineralogist, v. 30, p. 739-761.

Mahood, G., and Hildreth, W., 1983, Large partition coefficients for trace elements in high-silica rhyolites: Geochimica et Cosmochimica Acta, v. 47, p. 11-30.

Manning, D.A.C., and Pichavant, M., 1988, Volatiles and their bearing on the behaviour of metals in granitic systems, *in*: R.P. Taylor and D.F. Strong, eds. Recent advances in the geology of granite-related mineral deposits. Canadian Institute of Mining and Metallurgy Special Publication v. 39, p. 13-24.

Mountain, B.W., and Williams-Jones, A.E., 1996, Mass transfer and the path of metasomatic reactions in mesothermal gold deposits: an example from Flambeau Lake, Ontario, Economic Geology, v. 91, p. 302-321.

Moyle, J. E., 1985, East Kemptville tin project, *in* Guide to the granites and mineral deposits of southwestern Nova Scotia: Nova Scotia Department of Mines and Energy; Paper 85-3, p. 199-200.

Nekrasov, I.Y., 1984, Tin in magmatic and postmagmatic processes. Moscow, Nedra.

Nekrasov, I.Y., Epel'baum, M.B., and Sobolev, V.P., 1982, Partition of tin between melt and chloride fluid in the granite-SnO-SnO_2-fluid system: Dokl. Earth Sciences, Sect. 252, p. 165-168.

Norman, D. I., and Trangcotchasan, Y., 1982, Mineralization and fluid inclusion study of the Yod Nam tin mine, southern Thailand, *in* Metallizations associated with acid magmatism: New-York, Wiley-Interscience, p. 261-272

Plimer, I.R., 1987, Fundamental parameters for the formation of granite-related tin deposits: Geologische Rundschau, v. 76, p. 23-40.

Rankin, A.H., and Alderton, D.H.M., 1985, Fluids in granites from southwest England, *in* High heat production granites, hydrothermal circulation and ore genesis: London, England, Institution of Mining and Metallurgy, p. 287-299.

Reed, H.M., 1982, Calculation of multicomponent chemical equilibria and reaction processes in systems involving minerals, gases and an aqueous phase: Geochimica et Cosmochimica Acta, v. 46, p. 513-528.

Richardson, J.M., 1985, Magmatic fractionation and metasomatic alteration of the Davis Lake-East Kemptville Complex and its relationship to the rest of the South Mountain Batholith, *in* Guide to granites and mineral deposits of southwestern Nova Scotia: Nova Scotia Department of Natural Resources, Open File Report 650, p. 131-149.

Richardson, J.M., 1988, Field and textural relationships of alteration and greisen-hosted mineralization at the East Kemptville tin deposit, Davis Lake Complex, southwest Nova Scotia, *in* Recent advances in the geology of granite-related mineral deposits: Canadian Institute of Mining and Metallurgy Special Volume 39, p. 265-279.

Richardson, J.M., Bell, K., Watkinson, D.H., and Blenkinsop, J., 1990, Genesis and fluid evolution of the East Kemptville greisen-hosted tin mine, southwest Nova Scotia, Canada, *in* Ore-bearing granite systems; petrogenesis and mineralizing processes: Geological Society of America Special Paper 246, p. 181-203.

Richardson, J.M., Spooner, E.T.C., and McAuslan, D.A., 1982, The East Kemptville tin deposit, Nova Scotia: An example of a large tonnage, low grade, greisen-hosted deposit in the endocontact zone of a granite batholith: Geological Survey of Canada Current research, part B, paper 82-1B, p. 27-32.

Rundquist, D.V., 1982, Zoning of metallization associated with acid magmatism, *in* A.M. Evans, ed., Metallizations associated with acid magmatism: New York, Wiley-Interscience, p. 279-289.

Schwartz, M.O., and Surjono, A., 1990, Greisenization and albitization at the Tikus tin-tungsten deposit, Belitung, Indonesia: Economic Geology, v. 85, p. 691-713.

Schwartz, M.O., and Askury, A.K., 1989, Geologic, geochemical and fluid inclusion studies of the Tin Granites from the Bujang Melaka Pluton, Kinta Valley, Malaysia: Economic Geology, v. 84, p. 751-779.

Shepherd, T.J., Miller, M.F., Scrivener, R.C., and Darbyshire, D.P.F., 1985, Hydrothermal fluid evolution in the relation to mineralization in southwest England with special reference to the Dartmoor-Bodmin area, *in* High heat production granites, hydrothermal circulation and ore genesis: London, England, Institution of Mining and Metallurgy, p. 345-364.

Spycher, N.F., and Reed, M.H., 1989: CHILLER : A program for computing water-rock reactions, boiling, mixing and other reaction processes in aqueous-mineral-gas systems: Unpublished report, Dept. of Geological Sciences, University of Oregon, Eugene, Oregon.

Štemprok, M., 1982, Tin-fluorine relationships in ore-bearing assemblages, *in* A.M. Evans, ed., Metallizations associated with acid magmatism: New York, Wiley-Interscience, p. 321-337.

Štemprok, M., 1987, Greisenization (a review): Geologische Rundschau, v. 76, p. 169-175.

Štemprok, M., 1990, Solubility of tin, tungsten and molybdenum oxides in felsic magmas: Mineralium Deposita, v. 25, p. 205-212.

Stone, M. and Exley, C.S., and Phil, D, 1985: High heat production granites of southwest England and their associated mineralization: a review, *in* High heat production granites, hydrothermal circulation and ore genesis: London, England, Institution of Mining and Metallurgy, p. 571-593.

Taylor, R.G., 1979, Geology of tin deposits: Amsterdam, Netherlands, Elsevier, 543p.

Taylor, R.G., and Pollard, P.J., 1988, Pervasive hydrothermal alteration in tin-bearing granite and implications for the evolution of ore-bearing magmatic fluids, *in* Recent advances in the geology of granite-related mineral deposits: Canadian Institute of Mining and Metallurgy Special Volume 39, p. 86-95.

Taylor, J.R., and Wall, V.J., 1984, The mobilization of tin from granitoid magmas: 27th International Geological Congress, Moscow, Abstr. v. 4, p. 474.

Tischendorf, G., 1977, Geochemical and petrographic characteristics of silicic magmatic rocks associated with rare-element mineralization, *in* M. Štemprok, L Burnol, and G. Tischendorf, eds., Metallization associated with acid magmatism: Geological Survey of Czechoslovakia, v. 2, p. 41-98.

Urabe, T., 1985, Aluminous granite as a source of hydrothermal ore deposits: An experimental study: Economic Geology, v. 80, p. 148-157.

Wilson, G.A., and Eugster, H.P., 1990, Cassiterite solubility and tin speciation in supercritical chloride solutions, in Fluid-mineral interactions: A tribute to H.P. Eugster: The Geochemical Scociety, Special Publication No 2., p. 179-195.

Zhang, L.G., Liu, J.X., Chen, Z.S., and Zhou, H.B., 1994, Experimental investigation of oxygen isotopic fractionation in cassiterite and wolframite, Economic Geology, v. 89, p. 150-157.

CHAPTER II

THE ROLE OF GREISENIZATION IN CASSITERITE PRECIPITATION AT THE EAST KEMPTVILLE TIN DEPOSIT, NOVA SCOTIA.

WERNER E. HALTER

ANTHONY E. WILLIAMS-JONES

DEPARTMENT OF EARTH AND PLANETARY SCIENCES, MCGILL UNIVERSITY
3450 UNIVERSITY STREET, MONTRÉAL QUÉBEC H3A 2A7

DANIEL J. KONTAK

NOVA SCOTIA DEPARTMENT OF NATURAL RESOURCES
P.O. BOX 698, HALIFAX, NOVA SCOTIA B3J 2T9

ABSTRACT

The role of fluid/rock (leucogranite) interaction in forming the greisen-hosted tin (Cu-Zn-Ag) deposit at East-Kemptville, Nova Scotia was investigated by evaluating compositional and mineralogical changes in a representative zoned greisen, and by using this information to estimate physicochemical changes in the fluid/rock system at each step of the alteration. A large sample comprising one side of a symmetrically zoned greisen was cut into 1.5 cm wide slabs and each slab was analyzed for its major and trace element content. The results of these analyses were used to calculate the modal mineralogy of each slab which, in conjunction with petrographic observations, revealed two main alteration zones. First, or distal to the vein, the leucogranite was converted to a quartz-sericite greisen through the replacement of albite by muscovite. This alteration, specifically the dissolution of albite, created some porosity. Closer to the vein, the neo-formed muscovite was converted to topaz and quartz, creating a quartz-topaz greisen; pyrite, sphalerite and cassiterite precipitated in the earlier created pore space.

Mass balance calculations show that during alteration almost all major elements, including aluminum, were mobile. Only silicon was essentially immobile because the fluid was saturated with quartz due to earlier interaction with the leucogranite. The alteration of the leucogranite resulted in a quantitative removal of the alkalies, Mg and Mn, and an addition of Fe, S, F, Zn, and Sn. The difference in the modal mineralogy of each pair of adjacent slabs was used to quantify mineralogical changes in the two main alteration reactions responsible for the observed zonation. Variations in the molar abundances of species in solution were evaluated by balancing the alteration reactions and by estimating the water/rock ratios at each step of the alteration using oxygen isotopic data. The study indicates that there was an increase in the pH of the fluid and a decrease in fO_2 during alteration, and that these changes were most important close to the vein. Cassiterite deposition occurred contemporaneously with the alteration of muscovite to topaz and quartz, and is interpreted to have been caused by the sharp increase in pH that accompanied this reaction. Changes in fO_2 and Cl^- acted against cassiterite precipitation, but were apparently insufficient to prevent its saturation.

INTRODUCTION

The association of greisenization with tin mineralization in granitic rocks was first recognized over 150 years ago by Daubrée (1841). Since that time there have been numerous investigations of greisen-hosted tin deposits and of the fluids responsible for the greisenization (e.g., Barnes, 1979; Durišová et al, 1979; Burt, 1981; Haapala and Kinnunen, 1982; Norman and Trangcotchasan, 1982; Eadington, 1983; Rankin and Alderton, 1985; Shepherd et al., 1985; Štemprok, 1987; Taylor and Pollard, 1988; Schwartz and Askury, 1989; Schwartz and Surjono, 1990). These studies have established that greisenization occurs through interaction of the granitic host rock with a fluorine-bearing, acid, magmatic fluid of generally low salinity, at temperatures between 250°C and 450°C. Recent theoretical and experimental studies of the complexing of tin in hydrothermal solutions (Jackson and Helgeson, 1985a, 1985b; Eugster, 1986; Wilson and Eugster, 1990; Kovalenko et al., 1992) suggest that changes in pH and/or fO_2 and/or ligand concentration, are probably the main controls of cassiterite deposition in greisens. However, apart from a theoretical study by Heinrich (1990), there has been no attempt to quantitatively relate the cassiterite deposition to changes which occur in these parameters as a result of greisenization.

The purpose of our paper is to reconstruct the process of greisen formation in a natural setting and, by determining the stoichiometric coefficients of the greisenizing reaction(s), to establish the extent to which pH and/or fO_2 and/or ligand concentration could have contributed to cassiterite deposition. We have selected the East Kemptville tin deposit, Nova Scotia, for this study because of the occurrence there of zoned greisens which represent on a centimetre scale all stages of alteration affecting the host leucogranite at the deposit scale. The paper reports a study of a single, zoned greisen in which detailed petrographic and chemical analyses were conducted on a series of thin slabs of greisen cut parallel to the vein (c.f., Mountain and Williams-Jones, 1996). As a result of this approach it has been possible to document the nature of the progressive changes that occurred across the alteration zone, and thereby to both quantify the stoichiometry of the overall alteration reaction(s) and establish the path of fluid-rock interaction. This, in turn, has enabled us to demonstrate, at least in the case of East

Kemptville and perhaps many other greisen-hosted tin deposits, that increasing pH was the major and possibly sole control on cassiterite deposition.

GEOLOGICAL SETTING

The East Kemptville tin deposit is located 25 km northeast of Yarmouth, Nova Scotia, and had initial reserves of $56x10^6$ tons grading 0.17% Sn, with Zn, Cu and Ag as by-products (Moyle, 1985), which were exploited by open pit mining between 1985 and 1992. The immediate host to the mineralization is an evolved leucogranitic facies of the Davis Lake Pluton, which intruded the southwestern end of the 370Ma South Mountain Batholith and forms part of the Meguma Terrane of the Appalachian Orogen (Fig. 1). The leucogranite consists essentially of quartz, albitic plagioclase, K-feldspar, muscovite and topaz, with accessory biotite, apatite and zircon. According to Kontak (1990, 1993) and Richardson et al. (1990), the chemical variations within the Davis Lake Pluton indicate that the leucogranite was derived by fractional crystallization of biotite monzogranitic magma. The major element chemistry of the leucogranite is characterized by high SiO_2, Al_2O_3, F and P_2O_5 contents and low contents of MgO and TiO_2 (Chatterjee et al., 1985; Kontak, 1990; Richardson et al., 1990), which is typical of highly differentiated granite (Tischendorf 1977). Near the deposit, the leucogranite was pervasively sericitized and the plagioclase has a composition close to end-member albite.

The tin mineralization developed synchronously with or soon after emplacement of the leucogranite, (i.e. 366±4 Ma; Kontak and Chatterjee, 1992) and occurs in quartz-topaz-muscovite greisen, close to the contact of the leucogranite with surrounding Cambro-Ordovician Meguma Group metawacke (Fig. 2). The greisens are spatially associated with subvertical faults and in many cases, are localized around discrete fractures. These faults and fractures form part of the sub-vertical and NE-SW trending East Kemptville-East Dalhousie Fault Zone, a major structure which is believed to have controlled the location and geometry of the deposit, by providing a preferential path for the mineralizing fluid (Halter et al., 1994). Movement in this fault zone also resulted in the introduction of slices of sedimentary rock into the main ore body which have been previously misinterpreted bt Richardson (1988) as

Figure 1 : Location of the East Kemptville tin deposit on a simplified geological of the Meguma terrane, Nova Scotia (after Keppie, 1979, and Kontak, 1990). The enlarged area of the South Mountain Batholith shows the Davis Lake Pluton (after MacDonald, 1994, and Ham and MacDonald, 1994), which hosts the mineralization. The fault that runs through the leucogranite is part of the East Kemptville-East Dalhousie fault zone (EKEDFZ), and controlled the location and geometry of the mineralization at East Kemptville. TFZ refers to the Tobiatic Fault Zone.

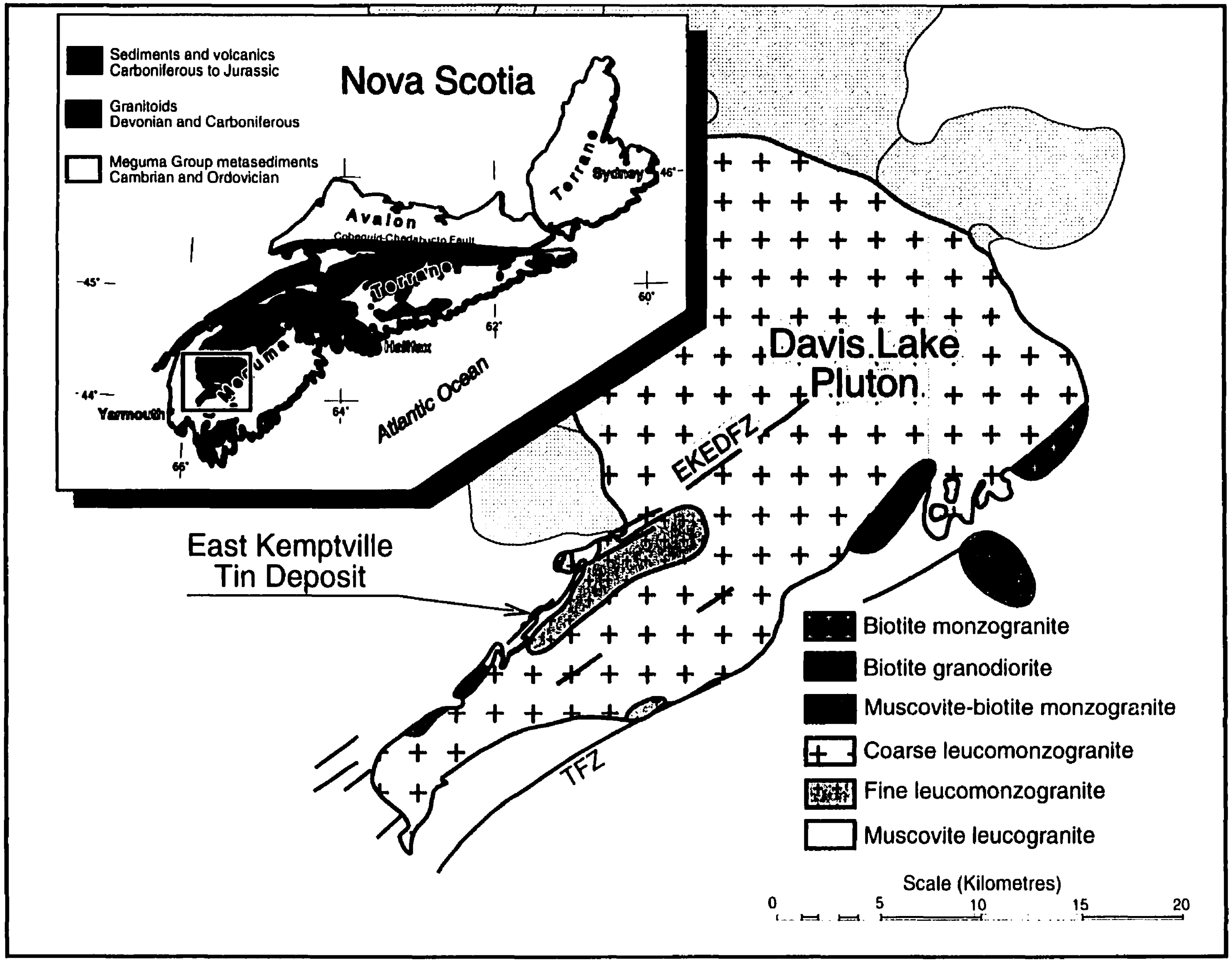
Sediments and volcanics
Carboniferous to Jurassic
Granitoids
Devonian and Carboniferous
Meguma Group metasediments
Cambrian and Ordovician
Nova Scotia
Avalon
Cobequid-Chedabucto Fault
Terrane
Sydney
46°
45°
60°
62°
Halifax
Meguma
Terrane
44°
Yarmouth
64°
66°
Atlantic Ocean
Davis Lake
Pluton
EKEDFZ
East Kemptville
Tin Deposit
TFZ
Biotite monzogranite
Biotite granodiorite
Muscovite-biotite monzogranite
Coarse leucomonzogranite
Fine leucomonzogranite
Muscovite leucogranite
Scale (Kilometres)
0
5
10
15
20

Figure 2 : A horizontal section through the East Kemptville deposit at the 94m elevation. Bodies of sedimentary rock in the Main Zone display sub-vertical tectonic contacts with the leucogranite along their western margins and westerly dipping intrusive contacts on their eastern margins. Greisens are centered on, or run parallel to the major NE - SW fault system, suggesting that the latter controlled the path of the greisenizing fluid. Sample N106ZG used in this study was located at the NE end of the deposit.

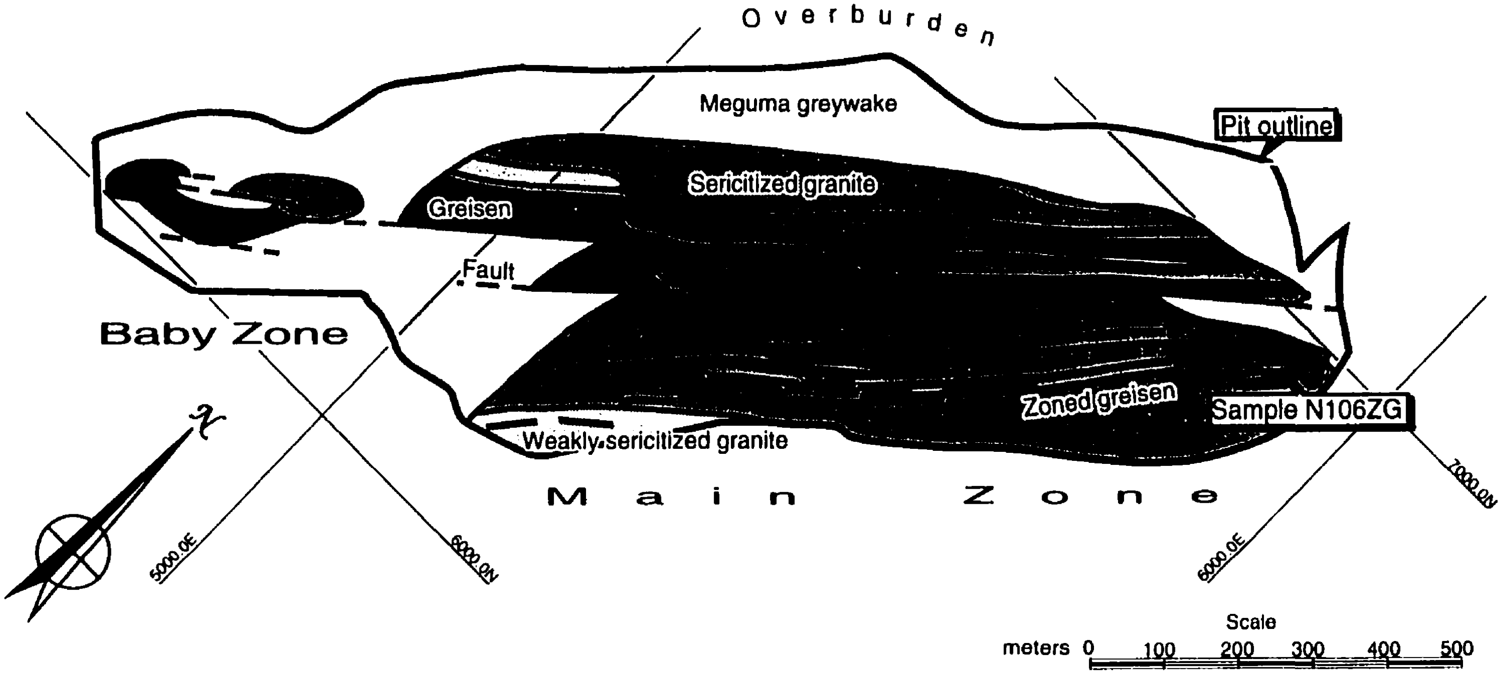
Overburden
Meguma greywake
Pit outline
Sericitized granite
Greisen
Fault
Baby Zone
Zoned greisen
Sample N106ZG
Weakly sericitized granite
Main Zone
5000.0E
6000.0N
6000.0E
7000.0N
Scale
meters 0 100 200 300 400 500

sedimentary keels, i.e., roof pendants. The latter display sub-vertical tectonic contacts with the leucogranite along their western margins, and westerly dipping intrusive contacts on their eastern margins.

Greisen formation and tin mineralization was followed by the development of quartz-sulphide veins that are typically within or close to the greisens. These veins can be up to one metre wide and contain mainly pyrite, sphalerite, chalcopyrite, and minor galena and arsenopyrite. Phosphate veins consisting of quartz, triplite ($(Mn, Fe^{2+}, Mg, Ca)_2(PO_4)(F, OH)$), vivianite ($Fe^{2+}_3(PO_4)_2 \cdot 8H_2O$) and apatite, are locally present in the leucogranite, and post-date sulphide mineralization (Richardson 1985). Later hyrothermal activity is represented by open fractures containing fluorite, pyrite, zeolites and dolomite or quartz, calcite, dickite and epidote.

GREISEN PETROGRAPHY

The greisens may be classified into two groups; zoned greisens which range from 20 to 50 cm in width and are localized around narrow cassiterite-rich veins (1 to 3 cm wide), and massive greisens which range from 1 to 10 metres in width and show no clear relationship to veining (Fig. 3). The veins associated with zoned greisens typically contain cassiterite and sulphides (most commonly pyrite and sphalerite) in their cores and topaz along their walls. Adjacent to the vein, the wallrock is altered to a quartz-topaz greisen containing cassiterite and sulphide minerals, and progressively outwards is altered to less mineralized quartz-sericite greisen and sericitized leucogranite. Massive greisens are usually well mineralized but do not show the systematic zonation that characterizes the zoned greisens. However, the massive greisens display the same paragenesis as the zoned greisens, i.e. they contain irregularly distributed quartz-sericite and quartz-topaz domains. This, and field evidence for the overprinting of outer zones of zoned greisens by the inner zones of adjacent zoned greisens, suggest that massive greisens are composites of closely spaced zoned greisens developed in highly fractured zones.

The sample selected for this study (N106ZG) is from the northeastern end of the deposit (Fig. 2) and represents a complete section across one side of a single, symmetrically-zoned greisen centered on a quartz-topaz-cassiterite-sulphide vein (Fig. 4). A hairline fracture

Figure 3 : An example of zoned and massive greisen at the NE end of the deposit. Zoned greisens are between 10 and 50cm wide and typically display a topaz and cassiterite rich core which grades outwards into quartz-topaz and quartz-sericite greisen. Sample N106ZG was taken from this location. Massive greisens can be several metres thick and probably represent the overlap of numerous zoned greisens.

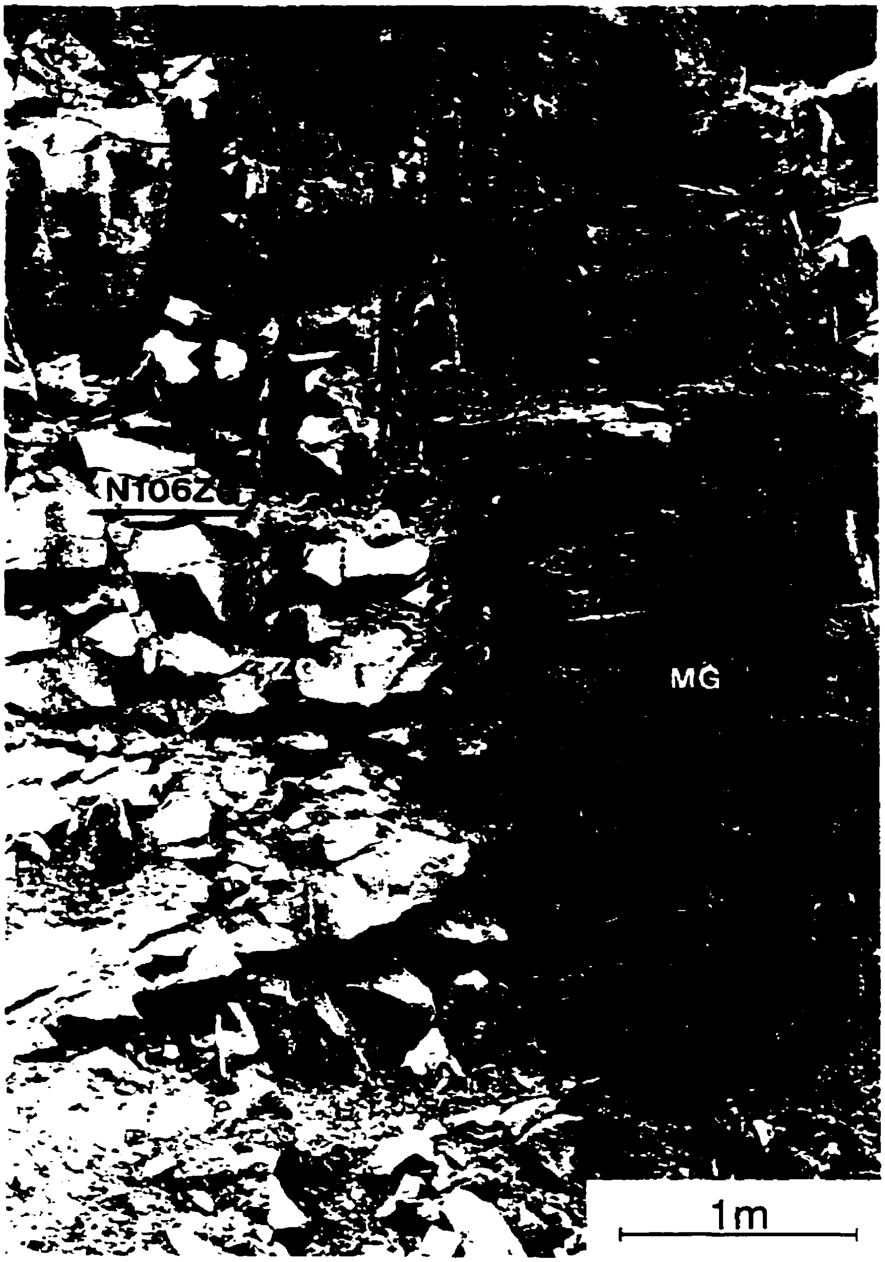
N106Z6
MG
1m

with a 2mm wide bleached halo crosses the outer part of the greisen. The greisen was cut into eight, 1.5 cm wide slabs parallel to the vein, which were analyzed for major and trace elements, and studied petrographically. The vein was not analysed chemically as it reflects open space filling rather than alteration. The least altered slab (8), some 12 cm away from the vein, is a sericitized leucogranite consisting essentially of quartz, muscovite and slightly sericitized albite. Additional phases are apatite, present as small crystals in albite, relicts of magmatic topaz and traces of sphalerite. X-ray diffraction analysis also revealed the presence of minor kaolinite. Slabs 7 and 6, closer to the vein, display essentially the same mineralogy except that muscovite increases in abundance at the expense of albite. In slab 6, kaolinite is observed to have replaced albite (Fig. 5A). The small amounts of kaolinite (less than 2 wt %) present in slabs 8 to 6 are interpreted to reflect post-greisen alteration of the albite in a 2 mm wide zone by fluids that entered the rock along the earlier mentioned hairline fracture. Kaolinite was not detected when albite was absent, and the later event therefore only affected albite and not the associated muscovite. Quartz and muscovite are the only major phases present in slab 5; albite is absent, having been replaced competely by muscovite. Owing to the high concentration of quartz and muscovite (95% of the rock), this rock is referred to as quartz-muscovite greisen. The remaining 5% of this greisen comprises topaz, fluorite, sphalerite, and traces of cassiterite and pyrite. The disappearance of albite coincided with the development of porosity (3-4 vol. %) in this slab and those close to the vein. With increasing alteration towards the vein (slabs 4, 3 and 2), muscovite was progressively replaced by topaz (Fig. 5B) and the rock grades into a quartz-topaz greisen (slab 3). Sphalerite, pyrite, fluorite and cassiterite, which increase in abundance from slab 5 to slab 2, crystallized in the pore space (Fig. 5C). Slab 1 contains essentially the same proportions of major minerals as slab 2, but slightly less pyrite and cassiterite. Topaz was the first mineral to fill the vein and occurs as euhedral crystals along the walls (Fig. 5D). Cassiterite was next to form, and precipitated on topaz, also as euhedral crystals. Quartz and sphalerite are interstitial to topaz and cassiterite, or occur in fractures in cassiterite. The center of the vein is occupied by very fine-grained muscovite intergrown with coarser apatite. The highest concentration of cassiterite is in the vein and the next highest concentration is in slab 2.

Microprobe analyses were conducted on all minerals, except accessory phases and quartz, and representative compositions of these minerals are given in Table 1. The feldspar is

Figure 4 : Sample N106ZG of a zoned greisen and schematic representation of the slabs cut for geochemical analysis. Each slab has a thickness of 1.5cm and is cut parallel to the vein. The vein is a sealed fracture with euhedral topaz that crystallized from the walls. The central part of the vein was filled by cassiterite, sphalerite, quartz, and subsequently sericite and apatite. The most altered part of the alteration halo (quartz-topaz greisen) extends from slab 1 to slab 3. The latter slab and slab 4 mark the transition to the quartz-muscovite greisen. Beyond slab 5 the rock is sericitized leucogranite and slab 8 is the least altered part of the alteration halo. Also shown is the hairline fracture that caused local kaolinitization of the albite.

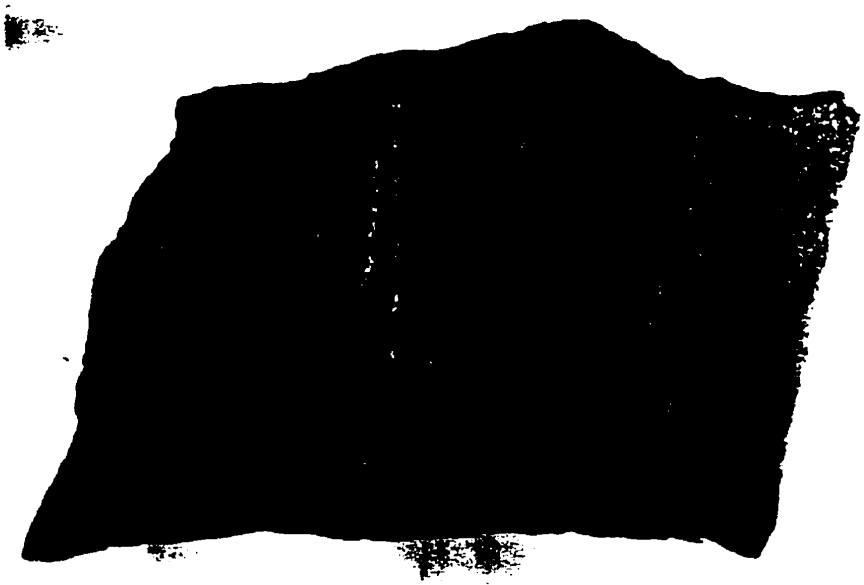

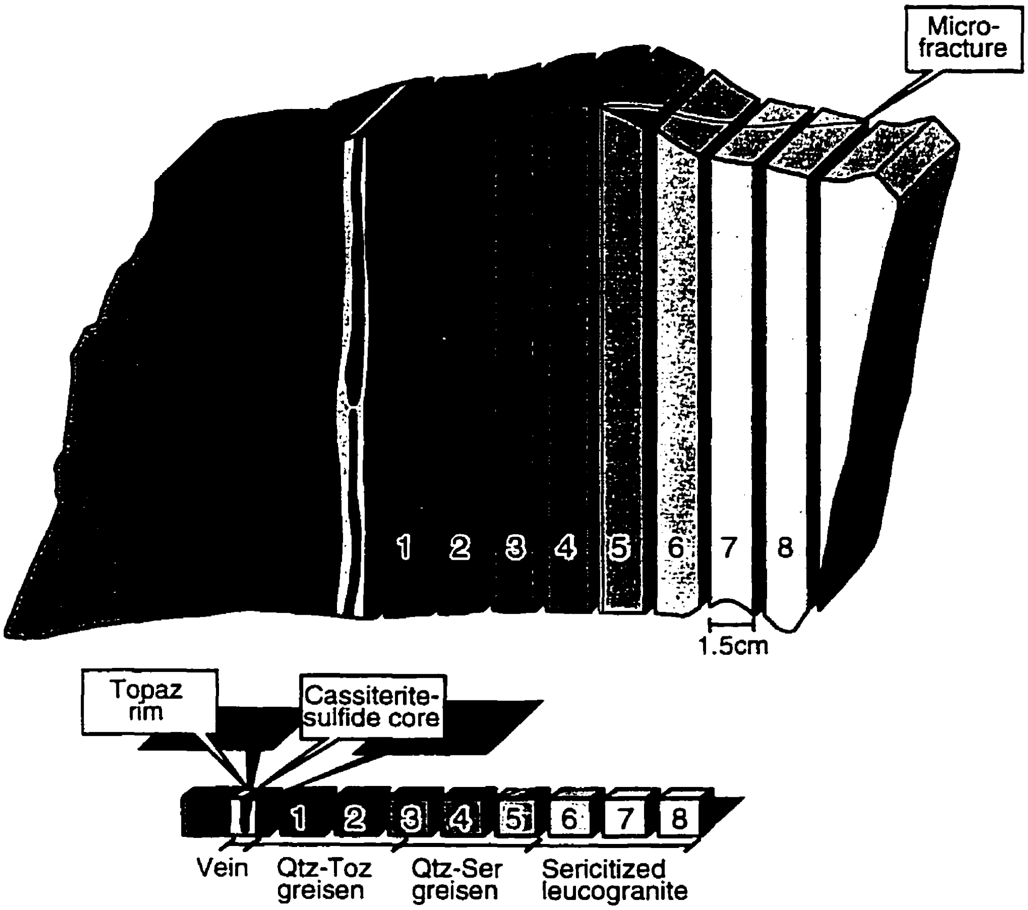
Micro-
fracture
1
2
3
4
5
6
7
8
1.5cm
Topaz
rim
Cassiterite-
sulfide core
1
2
3
4
5
6
7
8
Vein
Qtz-Toz
greisen
Qtz-Ser
greisen
Sericitized
leucogranite

Figure 5 : Microphotographs of sample N106ZG showing : a.) Replacement of albite by kaolinite in slab 6. In the absence of albite (i.e. slabs 5 to 1), kaolinite could not be detected. b.) Replacement of muscovite by topaz in slab 3. c.) A pore in quartz-muscovite greisen of slab 4 that has been partially filled with fluorite, sphalerite, pyrite, cassiterite and topaz. d.) Euhedral topaz on the walls of the vein displaying primary fluid inclusions. Cassiterite crystallized around the topaz, followed by quartz and sphalerite. Muscovite and apatite filled in the remaining space in the center of the vein.

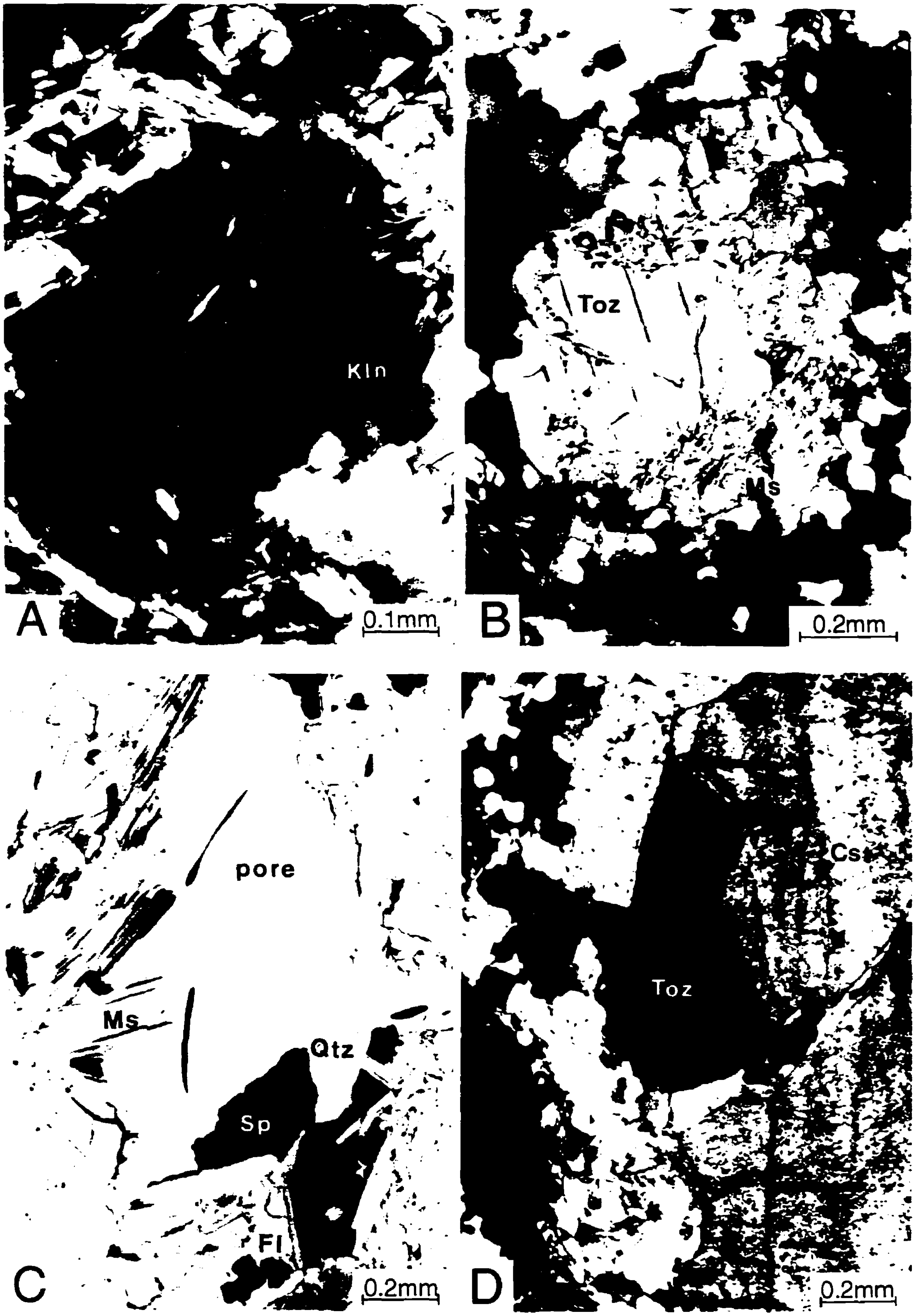
Kln
A
0.1mm
Toz
Ms
B
0.2mm
pore
Ms
Qtz
Sp
Fl
C
0.2mm
Cs
Toz
D
0.2mm

Table 1 : Representative compositions of silicate minerals in sample N106ZG

	Muscovite		Topaz		Albite		Kaolinite	
	wt. %	cations	wt %	cations	wt. %	cations	wt. %	cations
SiO_2	47.34	6.50	31.85	0.99	68.39	2.98	45.33	4.07
TiO_2	0.21	0.02	N.A.		0.00	0.00	0.00	0.00
Al_2O_3	29.70	4.81	54.80	2.01	20.18	1.04	36.24	3.84
FeO	5.89	0.68	0.03	0.00	0.03	0.00	1.00	0.07
MnO	0.23	0.02	N.A.		0.00	0.00	0.00	0.00
MgO	0.18	0.04	N.A.		0.00	0.00	0.03	0.00
CaO	0.00	0.00	0.02	0.00	0.03	0.00	0.07	0.01
Na_2O	0.12	0.03	N.A.		11.51	0.97	0.07	0.01
K_2O	11.32	1.98	N.A.		0.07	0.00	0.07	0.01
F	2.41	1.04	16.09	1.58	0.02	0.00	0.00	0.00
O correction for F	-1.01		-6.78		0.00		0.00	
Total	96.38		96.01		100.23		82.81	

N.A. : Not analysed

almost end-member albite (Ab99) and is unzoned. Muscovite compositions are essentially the same throughout the alteration halo, and no compositional variation could be observed between coarse- and fine-grained varieties. The approximate structural formula derived for this mineral, based on 22 oxygen atoms, is $K_2Al_{3.3}Fe_{0.7}Si_{6.5}Al_{1.5}O_{20}((OH)_3F)$. The Fe and F contents are too high to fit the standard definition of muscovite, and may reflect the presence of a zinnwaldite component (lithium has been shown to be present in muscovite separates from East Kemptville (Kontak, 1991). However, for convenience, the term "muscovite" is retained to refer to this mineral in the paper. As was the case for muscovite and albite, no zonation could be observed in any of the other phases. Topaz has a composition close to $Al_2SiO_4(F_{1.5}(OH)_{0.5})$. Cassiterite composition changes on a micron scale with respect to its iron and titanium concentration but no systematic trend could be observed. The average concentration, of these two components are 0.11 wt. % FeO and 0.23 wt. % TiO_2, and the corresponding ranges are 0.00 to 0.33 wt. %, and 0.01 to 0.61 wt. % respectively. Sphalerite contains 10.11±0.6 wt. % Fe, and apatite has a composition close to the fluorine endmember (fluorapatite) with 5.6±0.1 wt. % F.

WHOLE ROCK GEOCHEMISTRY

Major and trace elements were analyzed by X-ray fluorescence and results are presented in Table 2. The detection limit was 0.01% for major elements, 10 ppm for TiO_2 and 2 ppm for trace elements, except for As, Mo and Sn, which have a detection limit of 1 ppm and W, which has a detection limit of 3 ppm. The concentration of FeO was determined by titration with ammonium metavanadate, and was detectable down to 0.01%. Sulfur was analyzed by titration, and fluorine by a specific ion electrode method involving a NaOH fusion. Because of their low concentrations, some elements (Zr, Y, Nb, Ba, Hf, Ta, Th) were re-analyzed using ICP-MS (Table 3), and these data are considered more reliable than those determined by XRF analysis. Rare earth element (REE) concentrations were also analyzed by ICP-MS.

Results of whole rock analyses of slabs 1 to 8 are presented in Table 2. The two dominant oxides in all slabs are SiO_2 and Al_2O_3, which form up to 90 wt. % of the rock. In the least altered leucogranite, only K_2O, Na_2O and to a lesser extent FeO contribute significantly to

Table 2 : XRF analyses of slabs 1 to 8 in the zoned greisen.
Major element contents are in wt-% and those of trace elements are in ppm

Samples	*1*	*2*	*3*	*4*	*5*	*6*	*7*	*8*
SiO_2	72.7	70.2	71.6	73.2	75.0	74.2	74.4	74.2
TiO_2	0.041	0.064	0.048	0.039	0.030	0.030	0.031	0.030
Al_2O_3	15.6	15.7	15.7	14.5	14.0	14.6	14.7	14.9
FeO	3.46	4.62	3.74	3.73	2.53	2.02	1.85	1.94
Fe_2O_3	<0.01	<0.01	0.59	0.06	<0.01	0.33	0.28	<0.01
MnO	0.03	0.03	0.05	0.08	0.12	0.11	0.09	0.08
MgO	<0.01	<0.01	0.02	0.03	0.04	0.13	0.11	0.10
CaO	0.64	0.67	0.62	0.60	0.59	0.71	0.49	0.45
Na_2O	0.74	0.47	0.41	0.31	0.29	0.32	1.19	2.10
K_2O	0.13	0.29	1.46	2.75	4.46	4.54	4.00	3.61
P_2O_5	0.60	0.47	0.11	0.46	0.48	0.55	0.50	0.41
LOI	2.99	3.09	2.79	2.61	2.18	2.30	1.94	1.77
Total	96.93	95.64	97.14	98.42	99.67	99.77	99.58	99.58
S	3.03	3.45	2.77	2.00	0.46	0.04	0.05	0.10
F	4.60	4.60	3.70	2.40	1.40	1.40	1.30	1.20
BaO	Int.	Int.	Int.	Int.	Int.	Int.	Int.	Int.
Ce	<2	15	<2	Int.	3	<2	33	<2
Co	<2	3	<2	2	34	30	41	31
Cr_2O_3	44	38	64	43	<2	<2	<2	<2
Cu	300	505	411	187	143	66	83	47
Ni	22	25	24	19	11	10	23	9
Sc	1	<2	<2	2	8	9	8	2
V	11	11	11	13	15	4	8	10
Zn	17166	12529	8954	5777	4028	778	1093	1421
Ga	<2	<2	17	43	45	40	37	37
Nb	20	27	25	26	27	27	28	30
Pb	<2	3	<2	<2	<2	<2	<2	<2
Rb	15	52	338	631	1056	1040	960	895
Sr	26	24	21	20	26	29	23	22
Th	<2	4	8	16	12	7	12	3
U	17	14	16	15	17	15	18	18
Y	11	11	8	6	4	4	6	6
Zr	31	30	28	24	18	18	18	20
Sn	2610	6049	1819	1231	428	116	95	87
As	1.6	<1	<1	<1	<1	<1	<1	<1
W	Int	<3	<3	<3	269.2	210	264.9	255.3
Mo	1.1	<1	1.4	<1	<1	<1	<1	<1

Detection limit is 0.01% for major elements, Fe_2O_3, F and S, 10ppm for TiO_2, 2ppm for traces, 3ppm for W and 1ppm for As and Mo. Accuracies are 0.5% for SiO_2, 1% for the other major elements and 5% for the trace elements.

Int. : Not analysed because of interferences.

TiO2 analysed as a trace element

< : below detection limit

Table 3 : ICP-MS analyses of some trace elements and REE in slab 1 to 8 (in ppm)

Sample	*1*	*2*	*3*	*4*	*5*	*6*	*7*	*8*
Y	3.3	3.1	3.5	3.3	2.7	3.2	2.8	3.3
Zr	22.1	20.5	20.7	23.3	20.0	24.8	23.0	23.1
Nb	22.2	36.9	32.2	31.0	8.8	9.7	13.6	11.2
Ba	4.9	5.6	10.2	17.4	21.8	21.4	18.4	17.6
Hf	1.6	1.6	1.5	1.8	1.6	2.1	1.8	1.9
Ta	5.0	6.5	5.3	8.1	4.4	5.4	7.4	7.8
Th	3.3	3.4	3.6	4.2	3.6	4.1	4.4	4.6
La	0.74	0.67	0.61	0.49	0.44	0.66	0.75	0.76
Ce	2.0	2.0	2.0	2.0	1.4	2.1	2.2	2.3
Pr	0.25	0.22	0.24	0.21	0.20	0.27	0.30	0.28
Nd	1.01	0.86	0.68	0.66	0.75	0.78	0.99	0.93
Sm	0.56	0.58	0.65	0.49	0.54	0.58	0.56	0.58
Eu	0.086	0.042	0.027	0.028	0.014	0.019	0.010	0.003
Gd	0.51	0.55	0.52	0.54	0.43	0.53	0.59	0.56
Tb	0.14	0.13	0.14	0.13	0.12	0.14	0.13	0.14
Dy	0.74	0.82	0.84	0.74	0.69	0.83	0.69	0.83
Ho	0.11	0.08	0.11	0.09	0.09	0.10	0.08	0.10
Er	0.22	0.24	0.24	0.22	0.19	0.24	0.21	0.24
Tm	0.030	0.040	0.050	0.040	0.030	0.030	0.040	0.042
Yb	0.16	0.22	0.19	0.27	0.18	0.32	0.24	0.21
Lu	0.020	0.020	0.020	0.020	0.020	0.020	0.020	0.023

All analysis are at least one order of magnitude above the detection limit.

the whole rock composition. The concentrations of MnO, MgO and CaO are very low, reflecting the highly differentiated nature of the unaltered leucogranite. Some trace elements (Zr, Sc, Th, Ni) also have very low abundances, which is a common characteristic of specialized granites (Tischendorf, 1977). Concentrations of S and F are high close to the vein, but low in the least altered rock. Throughout the alteration halo, iron is present mainly as Fe^{2+}; the Fe^{3+} concentration is close to zero, except in slab 3 (0.59 wt. %) and to a lesser extent in slabs 6 and 7 (0.33 and 0.28 wt. %, respectively).

Chondrite-normalized profiles of mass-corrected REE values (see below) are presented in Figure 6. All samples are characterized by very low abundances of REE, and especially of the HREE, and the profiles are very similar. These profiles have a gullwing form (i.e., strongly negative Eu anomalies, and maxima at Sm and Tb). There are also maxima at Ce and Tm or Yb. These profiles compare well with previously published REE profiles of East Kemptville leucogranite (Chatterjee and Strong 1984, Kontak, 1990).

NORMATIVE CALCULATION AND GREISEN ZONATION

The normative composition of each slab was calculated using the whole rock analyses discussed above, and microprobe analyses of the constituent minerals. This was done by solving the inexact matrix equation AX=B, where A is the matrix of the stoichiometric coefficients of the elements in each mineral, B is the matrix of the molar concentrations of the elements obtained from the whole rock analysis and X is the desired matrix of molar concentrations of each mineral determined by linear least squares regression (Spear et al., 1982). The molar concentrations were converted to weight-percentages of minerals using the molecular weights of each mineral and, in turn, to volume percentages using mineral densities. The amount of kaolinite estimated to be in slabs 8 to 6 by this calculation is less than 2 wt. % (concentrated in a post-greisen bleached halo: see above). As the kaolinite was only the product of albite alteration, it was possible to estimate the amount of albite that was replaced by kaolinite by assuming aluminum conservation, and attributing to the albite any whole rock alumina in excess of that required for muscovite, topaz and unaffected albite. This was necessary in order to

Figure 6 : Chondrite-normalized REE profiles for each slab corrected using the corresponding mass factor (see Fig. 8). The shaded area represents the range of compositions of all slabs. With the exception of Eu (increases towards the vein) all REEs were immobile during alteration and variations are attributed to heterogeneities due to the small size of the samples in the rock and/or analytical errors.

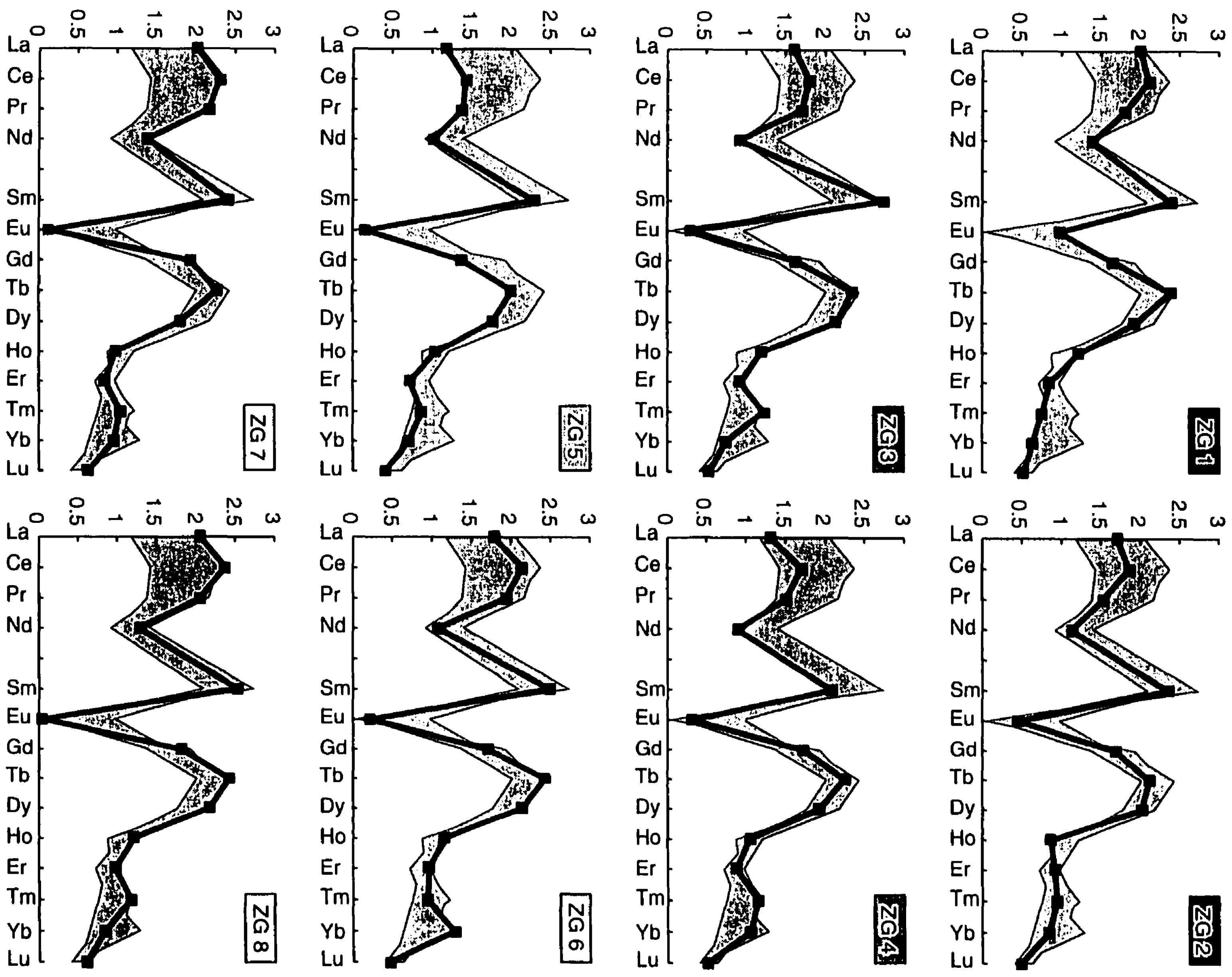
ZG 1
ZG 2
ZG 3
ZG 4
ZG 5
ZG 6
ZG 7
ZG 8
0
0.5
1
1.5
2
2.5
3
La
Ce
Pr
Nd
Sm
Eu
Gd
Tb
Dy
Ho
Er
Tm
Yb
Lu

quantitatively evaluate the mineralogical changes associated with greisen formation. Errors in estimating normative mineralogy due to this later event are considered to be minor because of the small size of the fracture and the small amount of albite replaced. The normative composition of each slab and the calculated density obtained from this norm are shown in Figure 7.

Changes in normative mineralogy permit subdivision of the alteration halo into three main mineralogical zones that coincide with zones established from petrographic observations. The distal, least altered zone, is characterized by sericitized leucogranite and comprises slabs 8 to 6. The bulk composition of the rock in this zone, and in particular slab 8, is considered to represent the starting rock composition, prior to greisen formation. This assumption might not be rigorously true, since chemical and mineralogical compositions change from slab 7 to 8 and elsewhere in the deposit, samples of least altered rock have been collected which have higher concentrations of Na_2O than slab 8 and contain K-feldspar. However, this will not affect the following interpretations of the alteration reactions, which are based on comparisons between slabs.

The next zone inwards is the quartz-muscovite greisen of which slab 5 is the most representative sample. Slab 4 also belongs to this zone, however, some muscovite in this sample has been replaced by topaz. Slab 3 has equal proportions of muscovite and topaz, and is considered to represent the boundary between the quartz-muscovite greisen and the quartz-topaz greisen, formed next to the vein (slabs 2 and 1). The quartz-topaz greisen is interpreted to represent the mineralogical assemblage in equilibrium with the vein fluid.

MASS CHANGES DURING GREISENIZATION

Mass Factors

In order to use the chemical analyses given in Table 2 to determine the mass changes of each element during greisen formation, it was necessary to determine whether there was an overall change in mass and/or volume of the rock. One of the ways to determine the mass factor

Figure 7 : Variations in normative mineralogy (wt-%) across the zoned greisen of Figure 4. The kaolinite present in slabs 8 to 6 is represented by equivalent proportions of albite (see text). From slab 8 towards the vein, albite first reacted to form muscovite and quartz. Subsequently, muscovite was converted to topaz and quartz. However, muscovite never completely disappears, even in the most altered rock. Sulphide minerals and cassiterite are only important in the quartz-topaz greisen, between slabs 4 and 1. The highest concentration of cassiterite is in slab 2. The density profile was obtained by summing the multiples of weight proportion and density for the different minerals in each slab. Density increases significantly between slab 5 and 2 due to increases in the proportion of sulphide minerals, cassiterite and topaz. The profile for the pore volume was obtained by calculating the volume change accompanying alteration reactions between pairs of adjacent slabs using the coefficients of table 6. A sharp increase in the pore volume occurs between slabs 6 and 4, as albite disappears. A second increase between slabs 2 and 1 is associated with a decrease in the amount of pyrite and muscovite.

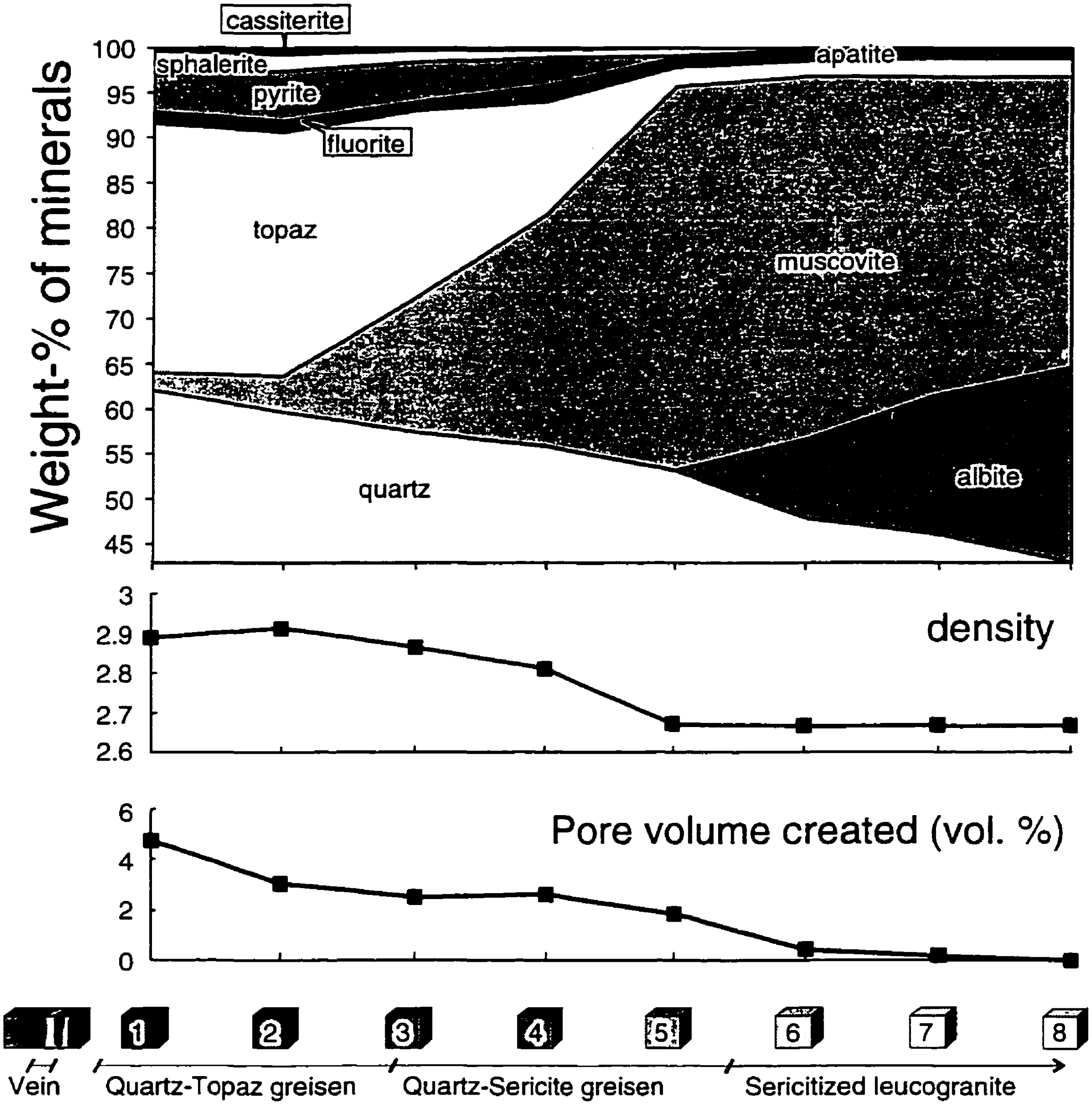
cassiterite
sphalerite
pyrite
fluorite
apatite
topaz
muscovite
quartz
albite
Weight-% of minerals
100
95
90
85
80
75
70
65
60
55
50
45
density
3
2.9
2.8
2.7
2.6
Pore volume created (vol. %)
6
4
2
0
II
1
2
3
4
5
6
7
8
Vein
Quartz-Topaz greisen
Quartz-Sericite greisen
Sericitized leucogranite

needed for the correction of whole rock analyses is to use Grant's (1986) isocon technique, in which the abundances of selected elements in an unaltered sample are plotted against their abundances in the altered sample, and a line defined by the concentrations of immobile elements (isocon) is identified. In our sample, slab 8, the furthest away from the vein, is the least altered and was taken as the reference sample. Isocon diagrams for four of the seven altered slabs are shown in Figure 8. Also plotted on these diagrams are the densities of each slab determined from the normative calculations (Fig. 7). Unfortunately, the trace elements that are most commonly immobile (e.g., Zr, REE and Nb), and normally constrain isocons, have very low concentrations in these samples and the associated nugget effect prohibits their use. However, SiO_2 aq. can be assumed to have had a constant activity, on the grounds that the fluid would have been saturated with quartz by its previous interaction with the leucogranite, and the activity of SiO_2 in a quartz saturated solution is essentially independent of pH at constant temperature (the pH above which silicic acid (H_2SiO_4) dissociates varies between 8.9 and 10 between 100 and 350°C and increases with increasing temperature; Seward 1974). For the purposes of our calculation SiO_2 can therefore be assumed to be immobile. If this assumption is made, isocons drawn from the origin through SiO_2 have a mass factor of approximately 1, implying that alteration occurred at constant mass and close to constant volume. The validity of the assumption that the masses of SiO_2 accurately define the isocon is supported by the fact that many elements, including Zr, plot close to this line, and that density plots slightly above the line as expected from the observation that alteration produced minor but measurable porosity (3 to 5 vol. % in slabs 5 to 1). Moreover, any errors in this assumption are minimized by the fact that silica has a high abundance in the rock and that absolute variations in the SiO_2 concentration (comparable to those of some other elements) will represent very small variations relative to the total SiO_2 concentration.

As a further test of our assumption that SiO_2 could be used to establish the mass factor, we plotted the contents of a variety of potentially immobile elements against that of SiO_2 for all samples. As shown by Finlow-Bates and Stumpfl (1981) and MacLean and Kranidiotis (1986), such plots should produce linear correlations which regress through the origin if both elements in each pair are immobile. As can be seen from Figure 9, a number of elements, including Zr, display such linear correlations. Elements that are commonly considered immobile but that do

Figure 8 : Isocon diagrams for slabs 1, 3, 5 and 7 using slab 8 as a reference. Solid lines are for constant mass and dashed lines are isocons on or adjacent to which the largest number of immobile elements are concentrated. The best constraint on the mass change is given by SiO_2 since most major elements were mobile during the alteration and trace elements have very low concentrations. Zirconium, which is one of the most immobile elements in nature, plots on the isocons deduced for Figures a and d and is close to the corresponding isocons in figures b and c Also plotted is the calculated density (den) obtained from Figure 7 which should lie close to, but above the isocon. Only those elements used for the constructions of the isocon are labeled. m.f. : mass factor.

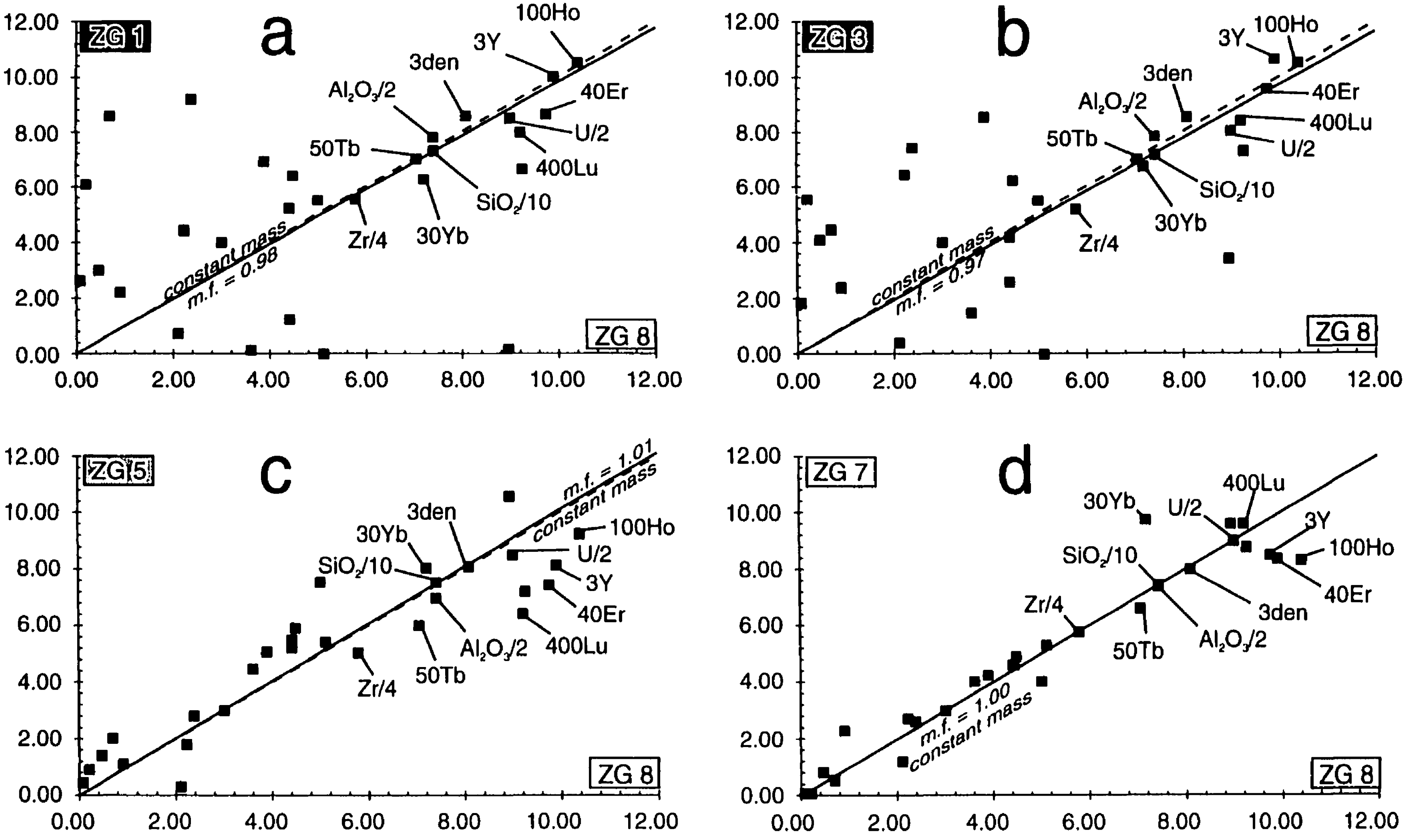
a
ZG 1
ZG 8
constant mass
m.f. = 0.98
100Ho
3Y
3den
Al2O3/2
40Er
U/2
50Tb
400Lu
SiO2/10
Zr/4
30Yb
b
ZG 3
ZG 8
constant mass
m.f. = 0.97
3Y
100Ho
3den
Al2O3/2
40Er
50Tb
400Lu
U/2
SiO2/10
30Yb
Zr/4
c
ZG 5
ZG 8
m.f. = 1.01
constant mass
3den
30Yb
100Ho
U/2
SiO2/10
3Y
40Er
Al2O3/2
400Lu
50Tb
Zr/4
d
ZG 7
ZG 8
m.f. = 1.00
constant mass
400Lu
30Yb
U/2
3Y
100Ho
SiO2/10
40Er
Zr/4
3den
50Tb
Al2O3/2
0.00
2.00
4.00
6.00
8.00
10.00
12.00

Figure 9 : Diagram correlating wt-% SiO_2 in slabs 1 to 8 with other probable immobile elements and the calculated density. Also shown is the profile for Sn which was clearly mobile. The excellent correlations for most of the elements confirms that SiO_2 was immobile and that ratios of SiO_2 concentrations can be used as a good approximation of the mass factor. The mass factors obtained are given in table 4.

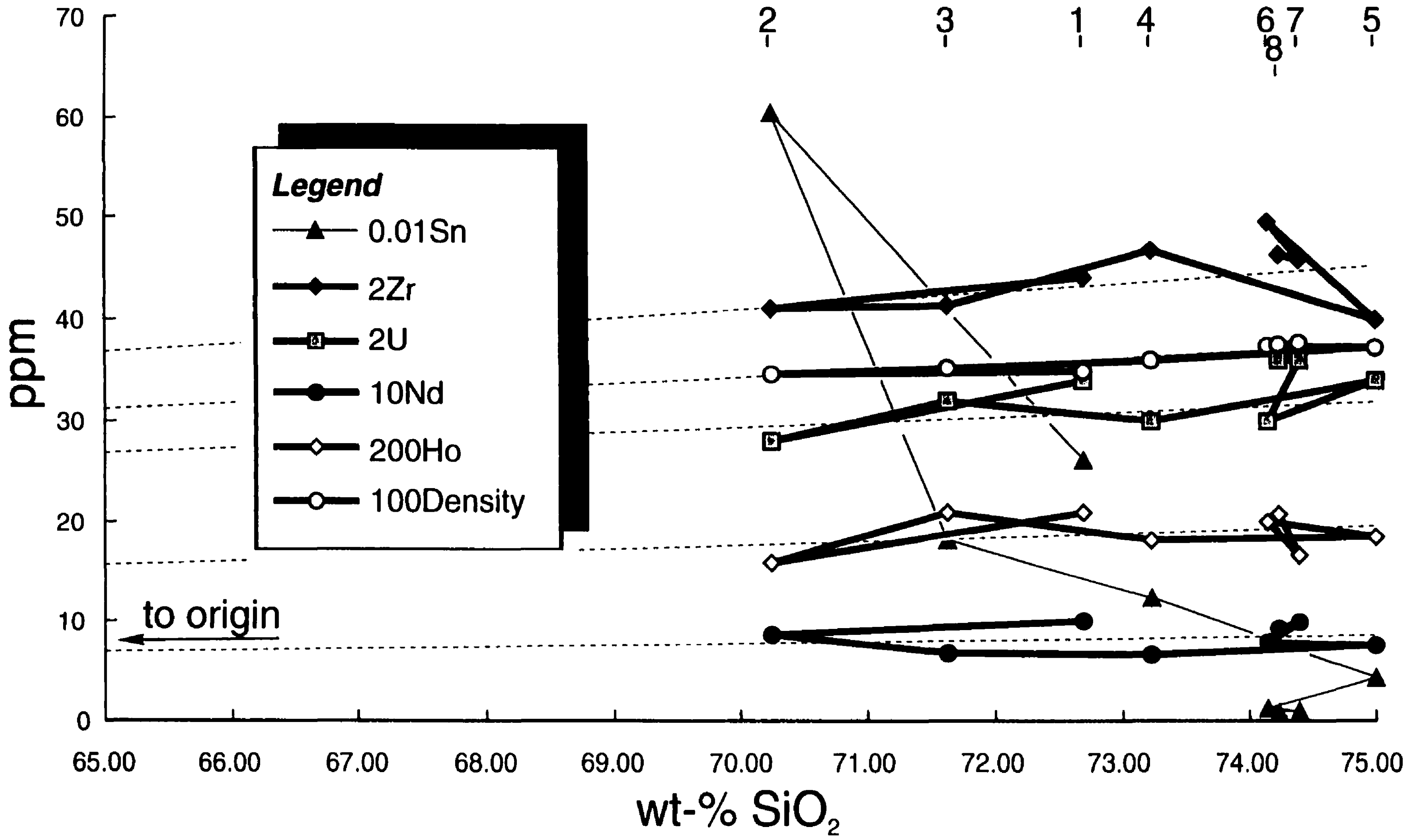

2
3
1
4
6
7
8
5
70
60
50
40
30
20
10
0
ppm
Legend
0.01Sn
2Zr
2U
10Nd
200Ho
100Density
to origin
65.00
66.00
67.00
68.00
69.00
70.00
71.00
72.00
73.00
74.00
75.00
wt-% SiO2

not produce linear correlations are Nb and Ti (not plotted). The concentrations of these elements vary by up to a factor of 5, and therefore cannot represent overall mass changes in the rock. Moreover, Nb and Ti concentration are much higher in samples 1 to 4, i.e. closer to the vein, than in samples further out in the alteration halo, which may indicate that these elements were added during alteration. Significantly, the concentration of Sn is also much higher in samples 1 to 4 and, as shown below, was deposited by the vein fluid during its infiltration into the rock. It is also well known that Nb and Ti substitute for Sn in cassiterite (Möller et al., 1988) and we therefore conclude that the behaviour of Nb and Ti reflect their concurrent addition with Sn from the fluid (c.f., Fig. 9).

Mass Changes

Corrected chemical analyses are shown in Tables 4 and 5 along with the mass factors (ratios of silica concentrations). The mass changes during the alteration of major and selected trace elements are plotted in Figure 10. Since silica was used to constrain the isocon, it shows no variation. Zirconium, which is considered to be immobile, shows only minor variation in concentration. Alumina content also displays minor variation, but this element is clearly depleted in the quartz-sericite zone and enriched in the quartz-topaz zone relative to the sericitized granite. This contrasts with the assumption of many authors that aluminum is an immobile element during alteration and, in particular, with Leitch and Lentz (1994) who used this assumption for mass balance calculations at East Kemptville. As expected from the mineralogical zonation, Fe, Zn, Cu, F and S are progressively enriched towards the vein and, with the exception of Fe, were entirely added by the mineralizing fluid. The high concentration of cassiterite in slab 2 corresponds to a 3 fold enrichment in Sn relative to the adjacent slabs. Similarly, Ti, Fe and S have lower concentrations in slab 1 than in slab 2. The magnitude of the changes and the fact that these elements are present in different phases suggests that enrichments in slab 2 are real and do not result from a nugget effect. This indicates that the fluid which altered slab 1 was undersaturated with respect to Sn, Ti, Fe and S, and became saturated in these elements in slab 2 due to its interaction with the wall rock. The behaviour of Ca, which is present only in apatite and fluorite, was similar to the above elements i.e., it increased in the

Figure 10 : Mass change across the alteration halo for all major and selected trace elements. Percentage changes are relative to the concentrations in sample 8. Corrections for the mass change of the rock during alteration was made using the mass factor obtained from isocons such as those shown in Figure 9. See text for discussion of the significance of individual profiles.

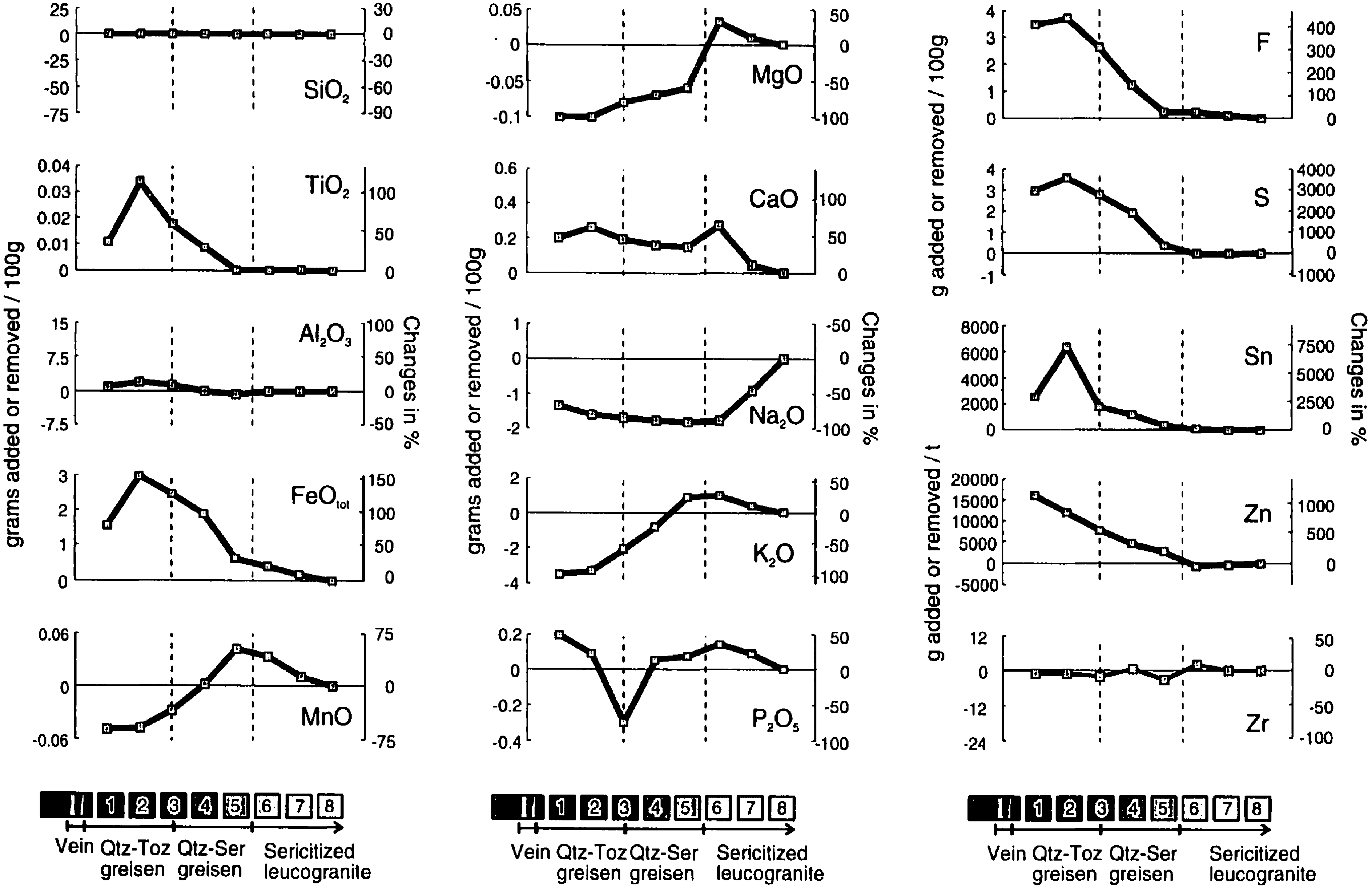
grams added or removed / 100g
Changes in %
SiO2
TiO2
Al2O3
FeOtot
MnO
MgO
CaO
Na2O
K2O
P2O5
g added or removed / 100g
F
S
g added or removed / t
Sn
Zn
Zr
V 1 2 3 4 5 6 7 8
Vein
Qtz-Toz greisen
Qtz-Ser greisen
Sericitized leucogranite

Table 4 : Mass factors obtained by ratios of SiO_2 and corrected XRF analyses. Major element contents are in wt-% and those of trace elements are in ppm

Samples	*1*	*2*	*3*	*4*	*5*	*6*	*7*	*8*
Si/Si mass fac.	0.98	0.95	0.96	0.99	1.01	0.99	1.00	1.00
SiO_2	74.2	74.2	74.2	74.2	74.2	74.2	74.2	74.2
TiO_2	0.042	0.067	0.050	0.040	0.030	0.031	0.031	0.030
Al_2O_3	16.0	16.6	16.3	14.7	13.8	14.6	14.7	14.9
FeO	3.53	4.88	3.88	3.78	2.50	2.02	1.85	1.94
Fe_2O_3	0.00	0.00	0.61	0.06	0.00	0.33	0.28	0
MnO	0.03	0.03	0.05	0.08	0.12	0.11	0.09	0.08
MgO	0.00	0.00	0.02	0.03	0.04	0.13	0.11	0.1
CaO	0.65	0.71	0.64	0.61	0.58	0.71	0.49	0.45
Na_2O	0.76	0.50	0.42	0.31	0.29	0.32	1.19	2.1
K_2O	0.13	0.31	1.51	2.79	4.41	4.54	3.99	3.61
P_2O_5	0.61	0.50	0.11	0.47	0.48	0.55	0.50	0.41
LOI	3.02	3.29	2.87	2.64	2.21	2.33	1.94	1.77
S	3.09	3.65	2.87	2.03	0.46	0.04	0.05	0.10
F	4.70	4.88	3.83	2.43	1.39	1.40	1.30	1.20
BaO	Int.	Int.	Int.	Int.	Int.	Int.	Int.	Int.
Ce	<2	16	<2	Int.	3	<2	33	<2
Co	<2	3	<2	2	34	30	41	31
Cr_2O_3	45	40	66	44	<2	<2	<2	<2
Cu	306	534	426	190	142	66	83	47
Ni	22	26	25	19	11	10	23	9
Sc	1	<2	<2	2	8	9	8	2
V	11	12	11	13	15	4	8	10
Zn	17529	13241	9279	5855	3987	779	1090	1421
Ga	<2	<2	18	44	46	40	37	37
Nb	20	29	26	26	27	27	28	30
Pb	<2	3	<2	<2	<2	<2	<2	<2
Rb	15	55	345	640	1045	1041	957	895
Sr	27	26	22	20	26	29	23	22
Th	<2	4	8	16	12	7	12	3
U	17	15	16	15	17	15	18	18
Y	11	12	8	6	4	4	6	6
Zr	31	32	29	24	18	18	18	20
Sn	2665	6442	1885	1248	423	116	95	87
As	2	<1	<1	<1	<1	<1	<1	<1
W	Int	<3	<3	<3	266	210	264	255
Mo	1	<1	1	<1	<1	<1	<1	<1

Detection limit and accuracies as for Table 1

Int. : Not analysed because of interferences.

< : below detection limit

Table 5 : ICP-MS analyses corrected for the mass factor obtained from isocons (in ppm)

Sample	*1*	*2*	*3*	*4*	*5*	*6*	*7*	*8*
mass factor	0.98	0.95	0.96	0.99	1.01	1.00	1.00	1.00
Y	3.4	3.3	3.7	3.3	2.7	3.2	2.8	3.3
Zr	22.5	21.7	21.4	23.7	19.8	24.8	22.9	23.1
Nb	22.6	39.0	33.4	31.4	8.7	9.7	13.6	11.2
Ba	5.1	6.0	10.5	17.6	21.6	21.4	18.4	17.6
Hf	1.7	1.6	1.6	1.8	1.6	2.1	1.8	1.9
Ta	5.1	6.9	5.5	8.2	4.3	5.4	7.4	7.8
Th	3.4	3.6	3.8	4.2	3.6	4.1	4.4	4.6
La	0.76	0.70	0.63	0.49	0.44	0.66	0.74	0.76
Ce	2.0	2.1	2.1	2.0	1.4	2.1	2.2	2.3
Pr	0.26	0.23	0.25	0.21	0.19	0.27	0.30	0.28
Nd	1.03	0.91	0.70	0.67	0.74	0.78	0.99	0.93
Sm	0.57	0.61	0.68	0.49	0.54	0.58	0.55	0.58
Eu	0.088	0.044	0.028	0.028	0.014	0.019	0.010	0.003
Gd	0.52	0.58	0.53	0.54	0.43	0.53	0.59	0.56
Tb	0.14	0.14	0.15	0.13	0.12	0.14	0.13	0.14
Dy	0.76	0.86	0.87	0.75	0.68	0.83	0.69	0.83
Ho	0.11	0.08	0.11	0.09	0.09	0.10	0.08	0.10
Er	0.22	0.26	0.25	0.23	0.18	0.24	0.21	0.24
Tm	0.031	0.042	0.052	0.041	0.030	0.030	0.040	0.042
Yb	0.16	0.23	0.20	0.27	0.18	0.32	0.24	0.21
Lu	0.020	0.021	0.021	0.020	0.020	0.020	0.020	0.023

All analysis are at least one order of magnitude above the detection limit.

rock towards the vein. Since the P concentration of the rock remained essentially unchanged during alteration, this increase in Ca must reflect an increase in the fluorite concentration. This is consistent with the increase in whole-rock F concentration towards the vein. The abnormally high Ca concentration of slab 6, as well as the low P content of slab 3, may be significant, but cannot be satisfactorily explained. In contrast to the elements discussed above, K, Mn and Rb (not shown) were enriched during sericitization of albite, and depleted during replacement of white mica by topaz, suggesting that these three elements were present only in the mica. Magnesium behaved similarly, but its depletion took place earlier i.e. between slabs 6 and 5. Albite is the only sodium-bearing phase and controlled the abundance of Na. The Na concentrations of slabs 6 to 8 were higher by approximately 0.14 wt. % prior to kaolinitization, but the profile is identical and this effect was not corrected for in Figure 10. The slight increase in the Na concentration between slabs 5 and 1 might reflect an increase in the amount of halite-bearing fluid inclusions, since the only Na-bearing phase, albite, is absent.

Except for Eu, the abundance of rare earth elements, corrected for mass changes, is essentially unchanged, and chondrite-normalized patterns are consistent across the alteration halo, i.e. there is no evidence for preferential leaching or addition of the HREE or the LREE (Fig. 6). The Eu concentration increases steadily from the least altered slab (8) to the most altered slab (1) (Fig. 11) indicating that Eu was added by the fluid. The difference in behaviour between Eu and the other REE suggests that it was transported as Eu^{2-} during greisenization and substituted for Ca^{2-} in the crystal structures of fluorite or apatite.

ALTERATION REACTIONS

The reactions characterizing the alteration that converted each slab into the next more altered slab were reconstructed using the differences in molar abundance between pairs of adjacent slabs (Figure 7), corrected for constant Si. These differences determines the reaction coefficients at each step of the alteration. The alteration reactions were balanced for each element using the appropriate dominant species in solution. Hydrogen was balanced by adding H_2O to the equation and oxygen was balanced by O_2. The coefficients for the reactions between

Figure 11 : Profile showing the concentration of europium across the alteration halo. See text for further detail.

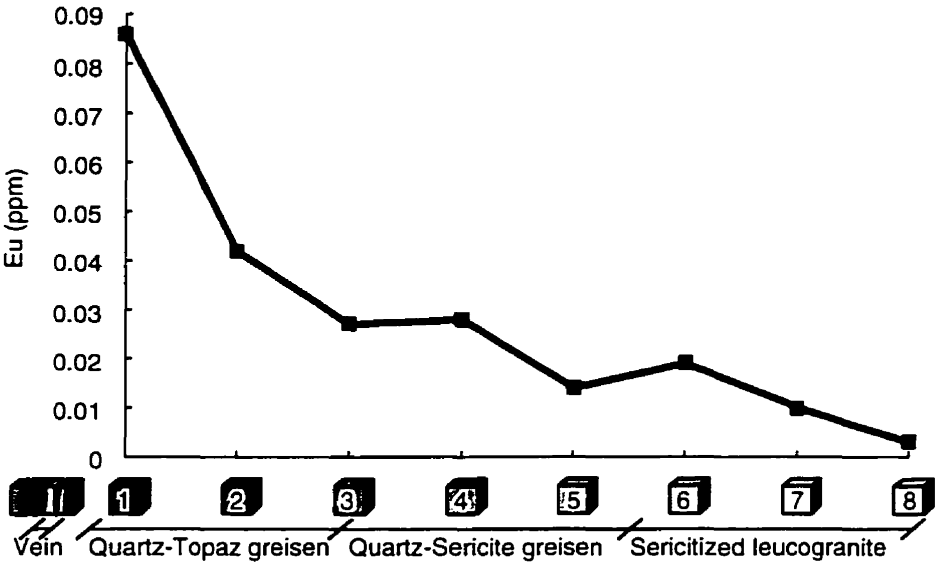
0.09
0.08
0.07
0.06
0.05
0.04
0.03
0.02
0.01
0
Eu (ppm)
1
2
3
4
5
6
7
8
Vein
Quartz-Topaz greisen
Quartz-Sericite greisen
Sericitized leucogranite

adjacent slabs are given in Table 6, with negative values indicating that the phase/aqueous species is a reactant, and positive values that it is a product in the reaction from slab 8 to 1. The coefficient of each phase is the number of moles reacting between two slabs each hypothetically containing 10kg of material. Fluorite and apatite, which are present only in trace amounts, were not considered in this calculation.

Speciation

For the purpose of identifying the dominant species in solution, we assumed that temperature and pressure were constant across the alteration halo. The values used for these parameters were 420°C and 2800bars and were based on microthermometric data for primary fluid inclusions, oxygen isotopic fractionation between quartz and cassiterite and contact metamorphic mineral assemblages (Halter, unpublished data.). These conditions are similar to those reported for other greisen-hosted tin deposits (Roedder, 1984). Based on dissolution temperatures for halite in the fluid inclusions and on EDS analyses of fluid inclusion decrepitates the total salinity fo the fluid was estimated to be 30 to 33 wt. % NaCl eq. and the Na/K ratio, 10/1. Dissociation constants for $NaCl^0$ and KCl^0 were calculated using SUPCRT92 (Johnson et al., 1991) and indicate that at the assumed P-T conditions NaCl and KCl were dominant over Na^- and K^- in the fluid. The distribution of these species was used to calculate the activity Cl^- in the fluid and to show in turn that $FeCl^-$ and $ZnCl_2^0$ were the dominant species of Fe and Zn, respectively (Johnson et al., 1991). Fluorine was assumed to be in the form of HF^0 as this species has a very small dissociation constant (Johnson et al., 1991). At the above conditions, the ratio of H^- over HCl^0 is approximately 1/3 (Frantz and Marshall, 1984) and HCl^0 was therefore assumed to be dominant over H^-. The pH of the fluid was predicted to be low from the mineral assemblage. Hence, sulfur was assumed to have been present mainly as H_2S and aluminum to have formed a neutral hydroxyl $Al(OH)_3^0$ complex (Ragnarsdottir and Walther, 1985). Aluminum-fluoride complexes are considered to have been unimportant because their activities only become significant at unreasonably high HF^0 activities, and the latter activity is predicted to have been relatively low judging by the measured F/OH ratio (3) in the topaz which is close to the minimum reported in nature.

Table 6: Coefficients of alteration reactions for each pair of ajacent samples (in moles per 10 kg of rock)

Reactions:	8⇨7	7⇨6	6⇨5	5⇨4	4⇨3	3⇨2	2⇨1
Phases							
Quartz	4.40	4.30	8.75	6.97	3.90	5.22	1.71
Muscovite	0.41	0.59	0.20	-1.94	-1.30	-1.36	-0.26
Albite	-2.25	-2.65	-3.42	0.00	0.00	0.00	0.00
Topaz	0.02	-0.18	0.25	5.94	4.83	3.82	-0.01
Pyrite	0.00	0.00	0.20	2.59	1.21	1.06	-1.49
Sphalerite	-0.12	-0.06	0.78	0.08	0.45	0.54	1.02
Aqueous species							
$Al(OH)_3$	0.36	0.16	2.00	-2.14	-3.04	-0.81	1.27
KCl	-0.81	-1.16	-0.39	3.84	2.58	2.70	0.52
NaCl	2.98	2.83	0.89	0.06	0.04	0.04	0.01
$FeCl^-$	-0.26	-0.38	-0.32	-1.35	-0.38	-0.19	1.65
$ZnCl_2$	0.12	0.06	-0.78	-0.08	-0.45	-0.54	-1.02
HF	-0.50	-0.39	-0.61	-6.88	-5.90	-4.29	0.31
H_2S	0.12	0.06	-1.17	-5.26	-2.87	-2.65	1.95
HCl	-1.89	-1.03	1.70	-1.04	-0.98	-1.28	-1.79
H_2O	-0.69	-0.60	-0.18	13.81	11.59	7.70	-2.74
O_2	-0.03	-0.02	-0.14	-1.77	-1.00	-0.82	0.76

Positive values indicate that a mineral/complex is formed during the reaction, negative values that it is consumed.

Reactions

The formation of the greisen can be described by the progress of two main reactions. The first of these reactions converted albite to muscovite and quartz, between slabs 8 and 5 (Fig. 7) as follows:

$$8.42Ab + 2.36KCl^{0}_{aq} + 0.96FeCl^{-} + 0.60ZnCl_2^{0} + 1.5HF^{0} + 1.22HCl^{0} + 0.99H_2S^{0} + 1.47H_2O + 0.19O_2 + 0.96Cl^{-} \rightleftharpoons$$

$$17.45Qtz + 0.27Toz + 1.2Ms + 0.6Sp + 0.2Py + 2.52Al(OH)_3^{0} + 6.70NaCl^{0}_{aq} \qquad (1)$$

The phases on the left-hand side of the reaction were consumed from slab 8 to 5, whereas those on the right were produced. Coefficients are moles per 10kg of rock. Albite was converted to muscovite and quartz, and disappeared between slabs 6 and 5. The amount of topaz, which presumably reflects original magmatic topaz, only increased slightly at this stage of the alteration. Pyrite and sphalerite also increased slightly towards the vein, but remained at trace levels in the rock. The small consumption in oxygen reflects pyrite precipitation. Important changes in fluid composition were the sharp increase in the Na content due to albite dissolution, and the decrease in the K content due to the precipitation of muscovite. The reaction also increased the Al content of the fluid significantly and decreased the concentrations of HF^{0} and HCl^{0}, which were consumed by the crystallization of muscovite and by the formation of the $NaCl^{0}$ ion pair, respectively. This consumption of HF^{0} and HCl^{0} caused increased association of H^{+} with F^{-} and Cl^{-}, respectively, as a result of the reactions:

$$H^{+} + Cl^{-} \rightleftharpoons HCl^{0}$$

and

$$H^{+} + F^{-} \rightleftharpoons HF^{0}$$

and a corresponding increase of the pH of the fluid. The extent to which pH changed would have depended on the starting pH (the pH of the fluid in equilibrium with slab 5), on the amount of fluid involved in the reaction and on the dissociation constants of HCl^{0} and HF^{0}.

The second important alteration reaction, which took place closer to the vein, converted muscovite to topaz and quartz between slabs 5 and 2 as follows:

$$4.50\mathrm{Ms} + 5.99\mathrm{Al(OH)_3}^0 + 1.92\mathrm{FeCl}^- + 1.07\mathrm{ZnCl_2}^0 + 17.07\mathrm{HF}^0 + 3.30\mathrm{HCl}^0 + 10.78\mathrm{H_2S}^0 + 3.59\mathrm{O_2} + 1.92\mathrm{Cl}^- \rightleftharpoons 16.09\mathrm{Qtz} + 14.59\mathrm{Toz} + 4.86\mathrm{Py} + 1.07\mathrm{Sp} + 9.12\,\mathrm{KCl}^0 + 0.14\mathrm{NaCl}^0 + 33.10\mathrm{H_2O} \quad (2)$$

This reaction consumed significant amounts of Al in the production of topaz. Simultaneously, large amounts of K were released to the fluid by the dissolution of muscovite. Precipitation of pyrite lowered the activity of FeCl^- and O_2, sphalerite the activity of $\mathrm{ZnCl_2}^0$ and both minerals the activity of H_2S. However, the most important change, particularly in comparison to Reaction (1), was the consumption of very large amounts of HF^0 and lesser amounts of HCl^0 which produced a large increase in pH.

Fluid Path

Alteration around a vein develops as a series of steps characterized by distinctive low variance mineral assemblages which are separated by sharp fronts representing equilibrium boundaries between adjacent zones, (Thompson, 1959). The system is open and components are transported into or out of the alteration halo by diffusion, advection or a combination of the two processes. In most cases, the contribution of diffusion to the overall alteration is probably very small because of the extremely slow rate at which material is transferred by this process. At the conditions estimated for the East Kemptville deposit, we calculated that it would take 5 Ma to form a 1 cm wide halo by grain boundary diffusion and 500 Ma to form a 10cm wide halo (Fisher, 1978). Clearly, these periods of time are unreasonably long for individual veins to remain open. We therefore envisage the alteration halo described in this paper as having formed mainly in response to the infiltration of fluid along complex paths provided by innumerable microfractures in the rock adjacent to a main fracture now represented by the vein. According to this model, aliquots of fluid migrate to different distances into the alteration halo before returning to the vein, and the mineral assemblage formed at a given location represents equilibrium for a specific integrated fluid/rock ratio. Reaction fronts separating mineralogical zones in the halo identify distances from the vein beyond which the fluid/rock ratio is too low to permit continued equilibrium with the mineral assemblage of the preceding zone. The widths of the various zones in the alteration halo depend on the rate of change of the fluid/rock ratio with distance from the vein and the chemical nature of water-rock interaction.

From Figure 7 it is apparent that the alteration of muscovite to topaz and the associated cassiterite precipitation did not terminate at a sharp front, but persisted over a transition zone of 4 to 5 centimetres from slab 2 to slab 5. The same is true for the conversion of albite to muscovite and quartz, i.e., this reaction did not stop at slab 5 but its importance decreased progressively from slab 5 and 8 and it may even have extended beyond slab 8. We do not interpret this to represent local disequilibrium, but suggest instead, that the absence of sharp alteration fronts is evidence that some fluid was able to make its way deeper into the alteration zone without equilibrating with the bulk rock. An explanation for how the latter may have occurred is provided by the observation that pores are common, particularly from slab 5 inwards. These pores, if interconnecting, could have provided paths along which the mineralizing fluid would have been preferentially channeled. Such channels would have locally raised the water/rock ratio, thereby preserving the capacity of the fluid to alter rock further from the vein. Thus, the widths of the alteration zones are considered to reflect the integrated water/rock ratio, and the widths of the transitions between them, the extent of heterogeneity in the physical path of the fluid.

WATER/ROCK RATIO

Oxygen isotope analyses

Estimates of the integrated water/rock ratio as a function of distance from the vein were made using the analysed oxygen isotopic compositions of a subset of the slabs and calculated oxygen isotopic compositions of the water which would have been in equilibrium with each slab. The following slabs were analysed: 1,3,5,6,7 and 8, and yielded $\delta^{18}O$ values of 10.1, 9.9, 9.5, 9.9, 10.3 and 11.6 respectively (Fig. 12). Isotopic compositions of the water were calculated for a temperature of 420°C using the modal proportions of the major silicates in each slab and the appropriate fractionation equation for each silicate-water pair. The fractionation coefficients used for quartz-water, muscovite-water and albite-water were 3.6‰ (Clayton et al., 1972), -0.2‰ (Zheng, 1993) and 2.4‰ (Matsuhisa et al., 1979), respectively. The initial (unmodified) water composition (6.8‰) was determined from the $\delta^{18}O$ of quartz in the vein (10.1‰). The isotopic composition of topaz in the vein was also measured (9.2 ‰), and was used, in conjunction with the data for quartz, to obtain an estimate of the fractionation between topaz and water at 420°C (2.4‰). Fractionation factors for topaz-water have been estimated theoretically by Zheng (1993) for F-free topaz, but yield results that are inconsistent with the other isotopic data, (e.g., an unreasonably high temperature of 920°C is predicted from quartz-topaz fractionation).

Water/rock ratios for each slab were calculated using the equation of Taylor (1974) assuming that the water/rock ratio of slab 8 was zero. Even if the latter is not rigorously true, it is unlikely that the original $\delta^{18}O$ value of slab 8 would have been significantly above its present value (11.6), as this value is close to the maximum reported for granite (cf., Taylor, 1974), i.e., the water/rock ratio of slab 8 could not have been much above zero. Water/rock ratios so calculated for the various slabs are shown in Figure 12 and range from a high of 14 in slab 1 to less than 1 in slab 7 (oxygen isotopic measurements were not made for slabs 2 and 4; their w/r values are estimates based on interpolations of the $\delta^{18}O_{H_2O}$ values for adjacent slab. The distribution of the data, i.e., a concave upwards profile, is a predictable consequence of infiltration. Immediately adjacent to the fracture occupied by the vein, infiltration would have been considerable because of a high density of associated microfractures, and would have decreased sharply with distance from the vein because of correspondingly lower permeability.

Quantitative changes of aqueous species

Changes in the concentrations of aqueous species predicted by the alteration reactions (Table 6) were converted to changes in moles per liter using the water/rock ratios from Figure 12, and

Figure 12 : a. Variation in $\delta^{18}O$ values of the whole rock and distribution of $\delta^{18}O$ values in the fluid across the greisen, calculated assuming equilibrium with the rock. The general increase in values towards slab 8 is consistent with interaction of the fluid with isotopically heavier leucogranite at progressively lower water/rock ratios. b. Water/rock ratios obtained using the equation of Taylor (1974) and assuming a water/rock ratio of 0 in slab 8. Slabs 2 and 4 were not analyzed, and the water/rock ratio for these two slabs was obtained by interpolation of $\delta^{18}O$ values in the fluid calculated for adjacent slabs.

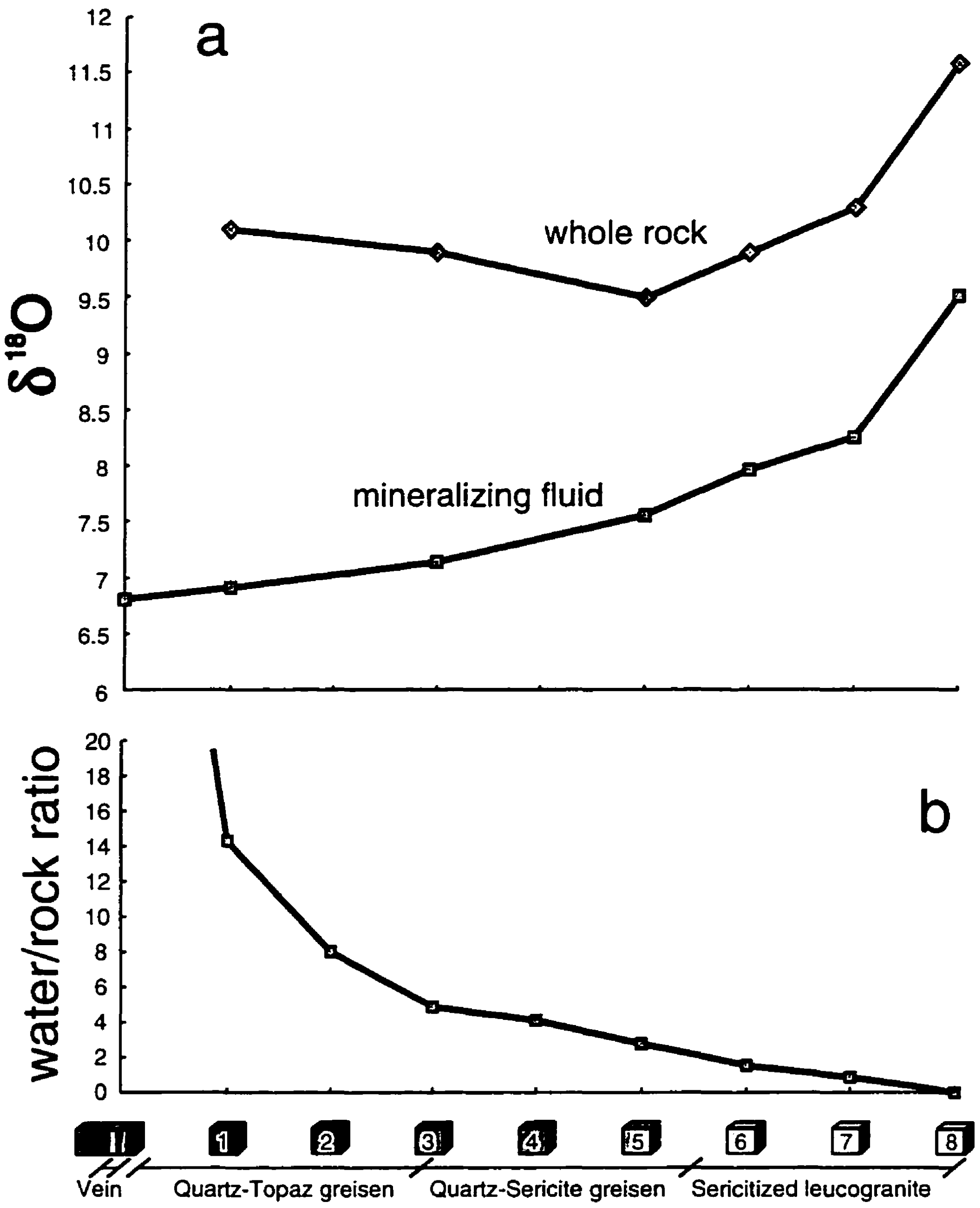a
b
δ18O
water/rock ratio
whole rock
mineralizing fluid
12
11.5
11
10.5
10
9.5
9
8.5
8
7.5
7
6.5
6
20
18
16
14
12
10
8
6
4
2
0
1
2
3
4
5
6
7
8
Vein
Quartz-Topaz greisen
Quartz-Sericite greisen
Sericitized leucogranite

are plotted in Figure 13. The profile for $SnCl^-$ was obtained using the differences in Sn concentrations of adjacent slabs. The diagram is constructed from left to right (i.e. from slab 1 to 8), since our purpose was to evaluate the evolution of the mineralizing fluid and not the alteration of the rock. The addition of an aqueous species to the fluid (from left to right) results from the destruction of a mineral and the consequent increase of the dissolved components in the fluid. The equilibrium between rock and fluid in slab 4, for example, reflects the interaction of a less altered rock (slab 5) with a more pristine fluid (from slab 3). Hence, the reaction that converted slab 5 to slab 4 documents the changes that the fluid underwent between slab 3 and slab 4. This creates an apparent shift of the data in the diagram of Figure 13 since reaction 5⇒4 characterizes the change undergone by the fluid from 3⇒4. The profiles of most of the species are a function of the difference in the composition of adjacent slabs, and errors in the profiles are due only to errors in the estimates of the water/rock ratio. Changes in HCl^0 and O_2 were obtained by balancing the alteration reactions, and are therefore dependent on the assumed speciation. Since the speciation has been simplified, the profiles for these two species are subject to some uncertainties, but the general trend is expected to be representative.

It is apparent from Figure 13, that between the vein and slab 1 the fluid composition changed very little as the system was essentially fluid buffered. Away from the vein, the system became progressively more rock buffered as the water/rock ratio decreased, and there were much larger changes in fluid composition. At the edge of the alteration halo, i.e. between slab 6 and 7, the changes in fluid composition are probably overestimated (e.g., the decrease in H^+ concentration would be greater than the starting concentration) because of the sharp increase in errors as the water/rock ratio approaches zero.

The changes were most important between slab 2 (i.e. after the water/rock ratio had decreased to 6), and slab 4. In this inner part of the alteration zone the quartz-muscovite greisen was converted to quartz-topaz greisen. As already discussed, changes in the pH of the fluid in this zone resulted from a decrease in the activities of HF^0 and HCl^0. It is apparent that most of the increase in the pH occurred between slabs 2 and 4. In the same interval, precipitation of sulphides and cassiterite decreased the activity of H_2S^0, $FeCl^+$, $ZnCl_2$ and $SnCl^-$ in the fluid, whereas the activity of KCl^0 increased due to dissolution of muscovite. In the outer part of the alteration halo, the concentration of most species in solution remained virtually unchanged due

Figure 13 : Cumulative changes in the concentration of selected aqueous species during greisen formation. Values were calculated using the reaction coefficients of table 6 and the appropriate water/rock ratios from Figure 12. The profile for tin was obtained using whole rock analyses; the profile for Cl^- (not shown) is identical to the one for $FeCl^-$. Next to the vein, the system was essentially fluid buffered and the fluid composition changed little. Away from the vein, the system became progressively rock buffered, causing more important changes in fluid composition. At the edge of the alteration halo, unreasonably high changes in certain elements are estimated due to the calculation method; as the water/rock ratio approaches the abitrarily imposed zero value any errors in analyses or original heterogeneities in rock composition are magnified enormously.

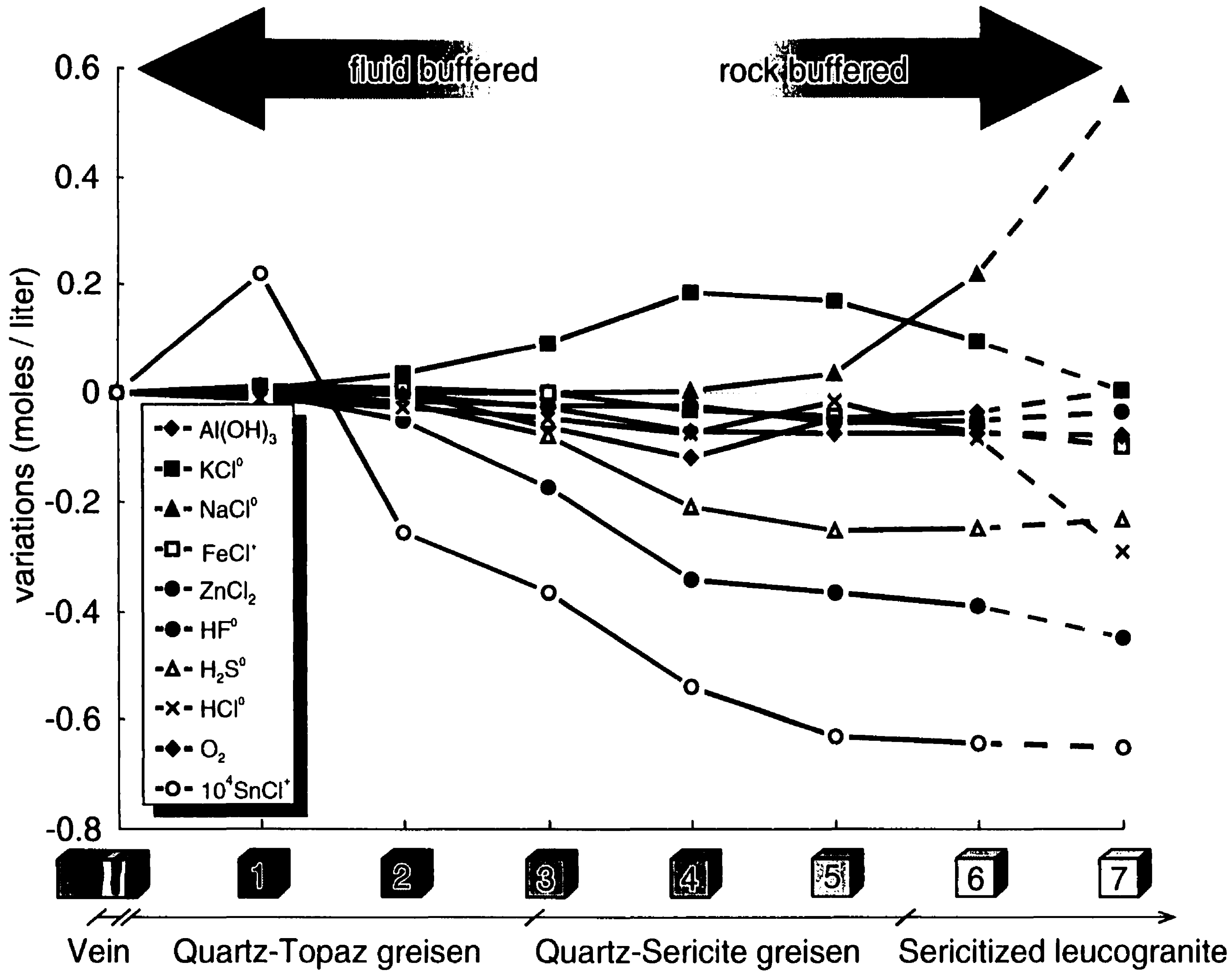
fluid buffered
rock buffered
0.6
0.4
0.2
0
-0.2
-0.4
-0.6
-0.8
variations (moles / liter)
$Al(OH)_3$
KCl^0
$NaCl^0$
$FeCl^+$
$ZnCl_2$
HF^0
H_2S^0
HCl^0
O_2
10^4SnCl^+
1
2
3
4
5
6
7
Vein
Quartz-Topaz greisen
Quartz-Sericite greisen
Sericitized leucogranite

to the lack of further mineral precipitation. Large variations are observed only for $NaCl^0$ which increased in the fluid, and KCl^0 and HCl^0 which decreased, all due to the replacement of albite by muscovite and quartz.

CASSITERITE DEPOSITION

Experimental studies by Eugster and Wilson (1985), Eugster (1986), Wilson and Eugster (1990), and Kovalenko et al. (1992), and theoretical studies by Jackson and Helgeson (1985a, 1985b) and Heinrich (1990) have shown that tin is dissolved in hydrothermal solutions predominantly as Sn^{2-} complexes with Cl^-, F^- or OH^- depending on temperature, fO_2-pH conditions, and ligand activity. At the conditions interpreted for East Kemptville (high temperature, low pH and high Cl^- activity) the most stable complex is $SnCl^-$ (Eugster, 1986). This, in turn, implies that cassiterite precipitated through the reaction

$$SnCl^- + H_2O + {}^1/_2O_2 + Cl^- \rightleftharpoons SnO_2 + 2HCl^0 \qquad (3)$$

Owing to the partial dissociation of HCl^0, Reaction (3) can be written using charged species even if HCl^0 is dominant in the fluid.

$$SnCl^- + H_2O + {}^1/_2O_2 \rightleftharpoons SnO_2 + 2H^- + Cl^- \qquad (4)$$

From Reactions (3) and (4), it is apparent that cassiterite precipitation can be caused by an increase in the pH of the fluid, an increase in fO_2 and/or a variation in a_{Cl^-}. A pH increase accompanied both alteration reactions (1) and (2) due to the consumption of HF^0 and HCl^0. The consumption of O_2 in these reactions decreased the fO_2 of the fluid and had a negative effect on cassiterite precipitation. These reactions (1 and 2) also decreased the free chloride ion concentration in the fluid by consuming Cl^- to form $NaCl^0$ and KCl^0, respectively. This, and the dominance of HCl^0 over Cl^- in Reaction (3) similarly acted against cassiterite precipitation. Assuming, as discussed earlier, that temperature remained constant, it then follows that pH is the only parameter that could have controlled the precipitation of cassiterite in the greisen, and we therefore propose, that the latter occurred as a result of the pH increase which accompanied alteration of muscovite to topaz and quartz. Changes in fO_2 and Cl^- acted against cassiterite precipitation, but were apparently insufficient to prevent its saturation.

It has been proposed by (Heinrich 1990), that cassiterite deposition in greisens occurs due to an increase in pH as a result of the sericitization (Reaction 1). In our sample no cassiterite precipitation accompanied this reaction. This does not necessarily mean that, in the absence of topaz formation, cassiterite precipitation will not occur. However, it is clear that Reaction (2) will produce a much larger increase in pH than Reaction (1) and, therefore, will be much more effective in causing cassiterite deposition. Accordingly, we attribute the lack of cassiterite in the quartz-muscovite greisen to near complete removal of Sn from solution before the fluid attained equilibrium with muscovite.

As already mentioned, cassiterite is also present in the vein, and precipitated after topaz but before quartz, sphalerite, muscovite and apatite. Precipitation of this cassiterite could have resulted from a decrease in the temperature of the fluid or from a change in the physico-chemical characteristics of the fluid due to its interaction with the wallrock. It seems likely that the latter was less important since in the vein, the amount of altered fluid was probably small relative to the amount of pristine fluid. Therefore, we tentatively conclude that cassiterite precipitation in the vein resulted mainly from a decrease in the temperature of the hydrothermal system. The genesis of the vein-hosted cassiterite mineralization will be further evaluated in a future paper.

DISTRIBUTION OF TUNGSTEN

Tungsten is commonly associated with tin in greisen-style deposits but its concentration is below the detection limit (<3ppm) in the greisens of slabs 1 to 4. On the other hand, it has a constant concentration between 210 and 270 ppm in slabs 5 to 8. It therefore follows that the fluid in equilibrium with the first four slabs was W-undersaturated, and W originally present in the rock was removed during alteration. The concentrations of W in slabs 5 to 8 are much higher than the 10 to 40 ppm reported for unaltered leucogranite by Kontak (1990) and either represent a higher original W concentration in the rock, or re-precipitation of W leached by the fluid in slabs 1 to 4. It is not clear in which phase(s) W is present in this greisen, but wolframite has been observed with cassiterite elsewhere in the deposit (Richardson et al., 1982, Richardson, 1988), and it is likely that this mineral is also present in trace amounts in sample N106ZG. Assuming this to be the case, wolframite saturation must have occurred between slabs 4 and 5. The precipitation reaction for wolframite was most likely

$$H_2WO_4^0 + FeCl^- + Cl^- \rightleftharpoons FeWO_4 + 2HCl^0 \qquad (5)$$

This reaction is similar to the precipitation reaction for cassiterite in that it depends on a_{HCl} and a_{Cl^-}. but it also depends on a_{FeCl^-} in the fluid (Heinrich, 1990). The decreases in the concentrations of Cl^- and $FeCl^-$ caused by alteration reactions (1) and (2) would have helped increase wolframite solubility whereas the decrease in pH would have promoted wolframite precipitation. We therefore conclude that a_{Cl^-} and a_{FeCl^+} were the dominant factors controlling wolframite behaviour in slabs 1 to 4, and that if wolframite was reprecipitated in slabs 5 to 8, this occurred as a result of the combined effects of increasing $a_{H_2WO_4^0}$ and increasing pH.

DISCUSSION AND CONCLUSION

The following conclusions can be drawn form the study presented above:

1. Petrographic observations and norm calculations show that the leucogranite was first altered to a quartz-muscovite greisen with the replacement of albite by muscovite between slabs 8 and 5. Closer to the vein, muscovite was progressively converted to topaz, and the rock was altered to a quartz-topaz greisen. Cassiterite mineralization is spacially associated with the second alteration.

2. During greisenization, almost all major elements, including aluminum, were mobile. However, silicon was effectively immobile as the fluid was saturated with quartz. The

greisenization of the leucogranite resulted in a quantitative removal of the alkalies, Mg and Mn, and an addition of Ti, Fe, S, F, Zn, and up to 6400 ppm of Sn.

3. From the measured changes in rock composition and the corresponding changes (calculated) in the concentrations of aqueous species, it is apparent that both alteration reactions (i.e., albite to muscovite and muscovite to topaz), were accompanied by an increase in the pH and decreases in fO_2 and a_{Cl^-}. However, the major changes in these fluid parameters were caused by the fomation of topaz.

4. Oxygen isotopic compositions indicate that the water/rock ratio decreased from 14 in slab 1 to less than one in slab 7, located only 10cm from the vein. As a result, the system was fluid-buffered close to the vein and became progressively rock-buffered further out. Changes in the hydrothermal fluid were important for mineralization only after the water/rock ratio had dropped below 6.

5. Precipitation of cassiterite was caused by the increase in pH that accompanied the alteration of muscovite to topaz. The other two factors commonly invoked as causes of cassiterite deposition, fO_2 and a_{Cl^-}, increased cassiterite solubility, but were apparently insufficient to prevent its saturation.

ACKNOWLEDGMENTS

The research presented in this paper was supported by the Nova Scotia Department of Natural Resources, Mines and Energy Branch and NSERC and FCAR research grants to AEW-J. Two ECONOMIC GEOLOGY reviewers provided comments which helped to improve the manuscript.

Reproduced from Economic Geology, 1996, Vol. 91, p. 368-385

REFERENCES

Barnes, H.L., 1979, Geochemistry of hydrothermal ore deposits (2nd ed.): New-York, Wiley-interscience, 798 p.

Burt, D.M., 1981, Acidity-salinity diagrams - Application to greisen and porphyry deposits: Economic Geology, v. 76, p. 832-843.

Chatterjee, A.K., and Strong D.F., 1984, Rare-Earth and other element variation in greisen and granites associated with the East Kemptville Tin Deposit, Nova Scotia, Canada: Institute of Mining and Metallurgy Transactions, Section B, v. 93, p. B59-B70.

Chatterjee, A.K., Strong, D.F., and Clarke, D.B., 1985, Petrology of the polymetallic quartz-topaz greisen at East Kemptville: Nova Scotia Department of Natural Resources, Open File Report 650, p. 151-196.

Clayton, R.N., O'Neil, R.J., and Mayeda, T.K., 1972, Oxygen isotope exchange between quartz and water: Journal of Geophysical Research, v. 77, p. 3057-3067.

Daubrée, A., 1841, Mémoire sur le gisement, la constitution et l'origine des amas de minerai d'étain: Annale des Mines, 3ième Série 20, p. 65-112.

Durišová , J., Charoy, B., and Weisbrod, A., 1979, Fluid inclusion studies in minerals from the tin and tungsten deposits in the Krusné Hory Mountains (Czechoslovakia): Bulletin de minéralogie, v. 102, p. 665-675.

Eadington, P.J., 1983, A fluid inclusion investigation of ore formation in a tin-mineralized granite, New England, New South Wales: Economic Geology, v. 78, p. 1204-1221.

Eugster, H. P., 1986, Minerals in hot water: American Mineralogist, v. 71, p. 655-673.

Eugster, H.P., and Wilson, G.A., 1985, Transport and deposition of ore-forming elements in hydrothermal systems with granites, *in* High heat production granites, hydrothermal circulation and ore genesis: London, England, The Institution of Mining and Metallurgy, p. 87-98.

Finlow-Bates, T., and Stumpfl, E.F., 1981, The behavior of so-called immobile elements in hydrothermally altered rocks associated with volcanogenic submarine-exhalative deposits: Mineralium Deposita, v. 16, p. 319-328.

Fisher , G.W., 1978, Rate laws in metamorphism: Geochimica et Cosmochimica Acta, v. 42, p. 1035-1050.

Frantz, J.D., and Marshall, W.L., 1984, Electrical conductances and ionization constants of salts, acids, and bases in supercritical aqueous fluids: I. Hydrochloric acid from 100 to 700°C and at pressures to 4000 bars: American Journal of Sciences, v. 284, p. 651-667.

Grant, J.A., 1986, The isocon Diagram - A simple solution to Gresens equation for metasomatic alteration: Economic Geology, v. 81, p. 1976-1982.

Haapala, I., and Kinnunen, K., 1982, Fluid inclusion evidence on the genesis of tin deposits, *in* Metallizations associated with acid magmatism: New York, Wiley-Interscience, p. 101-110.

Halter, W.E., Williams-Jones, A.E., and Kontak, D.J., 1994, Greisen zonation and mineralization process at the East Kemptville tin deposit, Yarmouth Country, Nova Scotia, *in* Mines and Minerals branch report of activities 1993: Nova Scotia Department of Natural Resources, Mines and Energy Branches, Report 94-1, p. 161-173.

Ham, L.J., and MacDonald, M.A., 1994, Geological map of Wentworth Lake: Nova Scotia Department of natural Resources, Mines and Energy Branches, map 94-03.

Heinrich, C.A., 1990, The chemistry of Hydrothermal tin (- tungsten) ore deposits: Economic Geology, v. 85, p. 457-481.

Jackson, K.J., and Helgeson, H.C., 1985a, Chemical and thermodynamic constrains on the hydrothermal transport of tin: I. Calculation of the solubility of cassiterite at high pressures and temperatures: Geochimica et Cosmochimica Acta, v. 49, p. 1-22.

Jackson, K.J., and Helgeson, H.C., 1985b, Chemical and thermodynamic constrains on the hydrothermal transport of tin: II. Interpretation of phase relations in the southeast Asian tin belt: Economic Geology, v. 80, p. 1365-1378.

Johnson, J.W., Oelkers, E.H., and Helgeson H.C., 1991, SUPCRT92, a software package for calculating the standard molal thermodynamic properties of minerals, gases, aqueous species, and reactions from 1 to 5000 bars and 0 to 1000°C: Computers and Geosciences, v. 17, p. 899-947.

Keppie, J.D., 1979, Geological map of Nova Scotia: Nova Scotia Department of Mines and Energy.

Kontak, D.J., 1990, The East Kemptville topaz-muscovite leucogranite, Nova Scotia. I. Geological setting and whole-rock geochemistry: Canadian Mineralogist, v. 28, p. 787-825.

Kontak, D.J., 1991, The East Kemptville topaz-muscovite leucogranite, Nova Scotia. II. Mineral chemistry: Canadian Mineralogist, v. 29, p. 37-60.

Kontak, D.J., 1993, Geological, geochemical and isotopic studies of the East Kemptville Sn-(Zn-Cu-Ag) deposit, Yarmouth County, Nova Scotia, Canada: Quadrennial IAGOD Symposium, Eighth, Stuttgart, Germany, E. Schweizerbart'sche Verlagsbuchhandlung, 1993, Proceedings, p. 383-409.

Kontak, D.J., and Chatterjee A.K., 1992, The East Kemptville tin deposit, Yarmouth County, Nova Scotia: a Pb-isotope study of the leucogranite and the mineralized greisens-evidence for a 366Ma metallogenic event: Canadian Journal of Earth Sciences, v. 29, p. 1180-1196.

Kovalenko, N.I., Ryzhenko, B.N., Dorofeyeva, V.A., and Bannykh, L.N., 1992, The stability of $Sn(OH)_4^{2-}$, $Sn(OH)_2F^-$, and $Sn(OH)_2Cl^-$ at 500°C and 1Kbar: Geochemistry International, v. 29, p. 84-94.

Leitch, C.H.B., and Lentz, D.R., 1994, The Gresens approach to mass balance constraints of alteration systems: Methods, pitfalls, examples, *in* Alteration and alteration processes associated with ore-forming systems: Geological Association of Canada, Short Course Notes, v. 11, p. 161-192.

MacDonald, M.A., 1994, Geological map of the South Mountain Batholith, western Nova Scotia: Nova Scotia Department of Natural Resources, Mines and Energy Branches, map 94-01.

MacLean, W.H., and Kranidiotis, P., 1986, Immobile elements as monitor of the mass transfers in hydrothermal alteration: Phelps Dodge massive sulphide deposit, Matagami, Quebec: Economic Geology, v. 82, p. 951-962.

Matsuhisa, T., Goldsmith, J.R., and Clayton, R.N., 1979, Oxygen isotopic fractionations in the system quartz-albite-anorthite-water: Geochimica et Cosmochimica Acta, v. 43, p. 1131-1140.

Möller. P., Dulski, P., Szacki, W., Malow, G., and Riedel, E., 1988, Substitution of tin in cassiterite by tantalum, niobium, tungsten, iron and manganese: Geochimica et Cosmochimica Acta, v. 52, p. 1497-1503.

Mountain, B.W., and Williams-Jones, A.E., 1996, Mass transfer and the path of metasomatic reactions in mesothermal gold deposits: an example from Flambeau Lake, Ontario, Economic Geology, in press.

Moyle, J.E., 1985, East Kemptville tin project, *in* Guide to the granites and mineral deposits of southwestern Nova Scotia: Nova Scotia Department of Mines and Energy, Paper 85-3, p. 199-200.

Norman, D.I., and Trangcotchasan, Y., 1982, Mineralization and fluid inclusion study of the Yod Nam tin mine, southern Thailand, *in* Metallizations associated with acid magmatism: New-York, Wiley-Interscience, p. 261-272

Ragnarsdòttir, K.V., and Walther, J.V., 1985, Experimental determination of corundum solubilities in pure water between 400-700°C and 1-3kbars: Geochimica et Cosmochimica Acta, v. 49, p. 2109-2115.

Rankin, A.H., and Alderton, D.H.M., 1985, Fluids in granites from southwest England, *in* High heat production granites, hydrothermal circulation and ore genesis: London, England, Institution of Mining and Metallurgy, p. 287-299.

Richardson, J.M., 1985, Magmatic fractionation and metasomatic alteration of the Davis Lake-East Kemptville Complex and its relationship to the rest of the South Mountain Batholith, *in* Guide to granites and mineral deposits of southwestern Nova Scotia: Nova Scotia Department of Natural Resources, Open File Report 650, p. 131-149.

Richardson, J.M., 1988, Field and textural relationships of alteration and greisen-hosted mineralization at the East Kemptville tin deposit, Davis Lake Complex, southwest Nova Scotia, *in* Recent advances in the geology of granite-related mineral deposits: Canadian Institute of Mining and Metallurgy Special Volume 39, p. 265-279.

Richardson, J.M., Bell, K., Watkinson, D.H., and Blenkinsop, J., 1990, Genesis and fluid evolution of the East Kemptville greisen-hosted tin mine, southwest Nova Scotia, Canada, *in* Ore-bearing granite systems; petrogenesis and mineralizing processes: Geological Society of America Special Paper 246, p. 181-203.

Richardson, J.M., Spooner, E. T.C., and McAuslan, D.A., 1982, The East Kemptville tin deposit, Nova Scotia: An example of a large tonnage, low grade, greisen-hosted deposit in the endocontact zone of a granite batholith: Geological Survey of Canada Current research, part B, paper 82-1B, p. 27-32.

Roedder, E., 1984, Fluid inclusions: Mineralogical Society of America, Reviews in Mineralogy, v. 12, 456 p.

Schwartz, M.O., and Askury, A.K., 1989, Studies of the tin granites from the Bujang Geological, geochemical, and fluid inclusion Melaka Pluton, Kinta Valley, Malasia: Economic Geology, v. 84, p. 751-779.

Schwartz, M.O., and Surjono, A., 1990, Greisenization and albitization at the Tikus tin-tungsten deposit, Belitung, Indonesia: Economic Geology, v. 85, p. 691-713.

Seward, T. M., 1974, Determination of the first ionization constant of silicic acid from quartz solubility in borate buffer solutions to 350°C: Geochimica et Cosmochimica Acta, v. 38, p. 1657-1664.

Shepherd, T.J., Miller, M.F., Scrivener, R.C., and Darbyshire, D.P.F., 1985, Hydrothermal fluid evolution in the relation to mineralization in southwest England with special reference to the Dartmoor-Bodmin area, *in* High heat production granites, hydrothermal circulation and ore genesis: London, England, Institution of Mining and Metallurgy, p. 345-364.

Spear, F.S., Rumble D. III, and Ferry, J.M., 1982, Linear algebraic manipulation of n-dimensional composition space, *in* Characterization of metamorphism through mineral equilibria: Mineralogical Society of America, Reviews in Mineralogy, v. 10, p. 105-152.

Štemprok, M., 1987, Greisenization (a review): Geologische Rundschau, v. 76, p. 169-175.

Taylor. H.P., 1974, The application of oxygen and hydrogen isotope studies to problems of hydrothermal alteration and ore deposition: Economic Geology, v. 69, p. 843-883.

Taylor, R.G., and Pollard, P.J., 1988, Pervasive hydrothermal alteration in tin-bearing granite and implications for the evolution of ore-bearing magmatic fluids, *in* Recent advances in the geology of granite-related mineral deposits: Canadian Institute of Mining and Metallurgy Special Volume 39, p. 86-95.

Thompson, J.B.,1959, Local equilibrium in metasomatic processes, *in* Research in geochemistry: New York, John Wiley and Sons, p. 427-457.

Tischendorf, G., 1977, Geochemical and petrographic characteristics of silicic magmatic rocks associated with rare-element mineralization, *in* M. Štemprok, L Burnol, and G. Tischendorf, eds., Metallization associated with acid magmatism: Geological Survey of Czechoslovakia, v. 2, p. 41-98.

Wilson, G.A., Eugster, H.P., 1990, Cassiterite solubility and tin speciation in supercritical chloride solutions, *in* Fluid-mineral interactions: A tribute to H.P. Eugster: The Geochemical Society Special Publication No. 2, p. 179-195.

Zheng, Y.F., 1993, Calculation of oxygen isotope fractionation in hydroxyl-bearing silicates: Earth and Planetary Science Letters, v. 120, p. 247-263.

INTRODUCTION TO CHAPTER III

In Chapter II, we examined the effect of fluid-rock interaction on the chemistry of the mineralizing fluid in a single zoned greisen. This permitted the evaluation of changes in physicochemical parameters potentially important in controlling cassiterite solubility, i.e., pH, fO_2 and a_{Cl^-}, and indicated that cassiterite precipitated as a function of a pH increase.

In the following chapter, we examine the applicability of the above conclusions drawn from a single sample, to the scale of the deposit. We further investigate the origin of the fluid and the metals as well as the process that lead to the formation of veins as these questions could not be properly addressed with the zoned greisen.

CHAPTER III

ORIGIN AND EVOLUTION OF THE GREISENIZING FLUID AT THE EAST KEMPTVILLE TIN DEPOSIT, NOVA SCOTIA, CANADA

WERNER E. HALTER

ANTHONY E. WILLIAMS-JONES

DEPARTMENT OF EARTH AND PLANETARY SCIENCES, MCGILL UNIVERSITY
3450 UNIVERSITY STREET, MONTRÉAL QUÉBEC H3A 2A7

DANIEL J. KONTAK

NOVA SCOTIA DEPARTMENT OF NATURAL RESOURCES
P.O. BOX 698, HALIFAX, NOVA SCOTIA B3J 2T9

ABSTRACT

The process responsible for greisen-hosted tin mineralization at East Kemptville was investigated using petrographic, chemical and fluid inclusion analyses of samples from a single deep drill hole (90-1) in the western part of the deposit (Baby Zone). Based on their trace element chemistry, the greisens intersected in the hole appear to have all formed from a single leucogranite protolith.

Alteration developed as symmetrically zoned halos around central fractures as a result of the interaction of a fluoride-rich orthomagmatic fluid with evolved leucogranite. During alteration, K-feldspar was first replaced by albite. With further alteration, albite was replaced by muscovite during the formation of quartz-sericite greisen. Some ore minerals can be present in that zone. Closer to veins, muscovite is, in turn, replaced by topaz and quartz, in quartz-topaz greisen with which the most intense mineralization is associated. This greisen is enriched in F, Fe, S, Zn, and Sn, suggesting that these elements were added by the mineralizing fluid. Next to the vein, dissolution of pyrrhotite, sphalerite and cassiterite characterizes quartz-greisen in which the concentration in ore forming elements (Sn, Fe, S, F, Zn, Cu) is lower than in the quartz-topaz greisen. Microthermometric measurements of fluid inclusions in quartz from these various alteration zones show that this alteration sequence was formed by only one greisenizing event and that temperature was approximately constant in the greisen (480°C). The fluid responsible for this alteration was an NaCl-brine, containing subordinate and variable concentrations of Fe, Mn and K.

During alteration, eutectic temperatures of fluid inclusions are lowest in quartz-topaz greisen as a result of an increase in the Fe concentration due to pyrrhotite dissolution. Oxygen fugacity, which was calculated from the CO_2/CH_4 ratio in gases released by crushing fluid inclusion-rich samples, displays the same minimum since pyrrhotite preferentially releases Fe^{2-}. The distribution of pyrrhotite and the fluid inclusion data indicate that pyrrhotite was precipitated close to the vein during early stages of the alteration, and re-precipitated further out as alteration progressed. This suggests that alteration zones moved away from the vein and widened with time.

The salinity of fluid inclusions varies between 27 and 41 wt-% NaCl equivalent, and increases linearly with increasing distance from the vein, even in the absence of Na-bearing phases. It therefore follows that sodium was transported towards the fracture (vein) down a chemical potential gradient. This occurred through "compensated infiltration", i.e., a regime in which flow was dominantly parallel to the fracture but individual aliquots of fluid followed complex paths back and forth between the fracture and the rock.

Cassiterite precipitated in quartz-topaz greisen in response to a pH increase of the mineralizing fluid due to its interaction with the wall rock. Other components affecting cassiterite solubility were either constant (temperature) or acted against its precipitation (fO_2 and a_{Cl^-}).

INTRODUCTION

Investigations of greisen-hosted tin deposits (e.g. Durišová et al, 1979; Burt, 1981; Haapala and Kinnunen, 1982; Norman and Trangcotchasan, 1982; Eadington, 1983; Rankin and Alderton, 1985; Shepherd et al., 1985b; Štemprok, 1987; Taylor and Pollard, 1988; Schwartz and Askury, 1989; Schwartz and Surjono, 1990) have established that this alteration is generally caused by an acid orthomagmatic fluid of intermediate salinity at temperatures between 300 and 500°C. Temporally, the hydrothermal system commonly evolves from an early stage dominated by a high temperature CO_2-CH_4 rich fluid, to a greisen-forming stage in which the principal fluid is an NaCl-rich brine, and to a later, lower temperature stage during which lower salinity fluid produces sulphide- and phosphate-bearing veins. Cassiterite precipitation is most frequently interpreted to result from a drop in temperature between the early and the late stages. Less commonly, it is attributed to changes in fluid chemistry due to fluid-rock interaction (Heinrich, 1990) and this appears to have been the case for the East Kemptville tin deposit, Nova Scotia, where the available evidence suggests that temperature was constant during mineralization. This deposit offers an excellent opportunity to evaluate the role of fluid-rock interaction in producing a tin greisen, because of the zonal distribution of alteration minerals and cassiterite around central veins, which provides a spatial context in which to reconstruct the temporal evolution of the hydrothermal system.

The purpose of this study is to establish the origin of the fluid and the metals that were concentrated during greisen formation at East Kemptville, and to document the changes in rock and fluid composition during greisenization as a means of evaluating the possible role of the alteration in cassiterite precipitation. These objectives were addressed by detailed analyses of the mineralogy and the chemistry of samples from fresh and variably altered leucogranite, and analyses of fluid inclusion compositions in the same samples. The data are used to quantify the direction and mechanisms of mass transfer during fluid-rock interaction and thereby aim to better our understanding of alteration and tin mineralizing processes in greisenizing systems.

GEOLOGICAL SETTING

The East Kemptville tin deposit is located 25 km northeast of Yarmouth, Nova Scotia, and had initial reserves of 56×10^6 tones grading 0.17% Sn, with Zn, Cu and Ag as by-products (Moyle, 1985). Two zones were distinguished during exploitation; a Main and a Baby Zone, separated by metasediments. The latter zone is much smaller but has significantly higher ore grades than the Main Zone. The immediate host to the mineralization is an evolved leucogranitic facies of the Davis Lake Pluton, located at the southwestern end of the 370 Ma South Mountain Batholith in the Meguma Terrane of the Appalachian Orogen (Fig. 1). Mineralization developed close to the contact of the intrusives with the metasediments of the Meguma Group.

The leucogranite of the Main Zone has been described extensively by Richardson et al. (1982), Richardson (1988) and Kontak (1990, 1991). It consists of quartz, albitic plagioclase, K-feldspar, muscovite and topaz, with accessory biotite, apatite and zircon. According to Kontak (1990, 1993) and Richardson et al. (1990), the chemical variations within the Davis Lake Pluton indicate that the leucogranite was derived by fractional crystallization of a biotite monzogranitic magma that produced most of the Davis Lake Pluton. The major element chemistry of the leucogranite is characterized by high contents of SiO_2, Al_2O_3, F and P_2O_5, and low contents of MgO and TiO_2 (Chatterjee et al., 1985; Richardson et al., 1990; Kontak, 1990), which is typical of highly differentiated granites (Tischendorf, 1977). In the deposit area, the leucogranite was pervasively sericitized and the plagioclase has a composition close to end-member albite.

A simplified map of the deposit, presented in Figure 2, shows that greisens are spatially associated with subvertical faults. These faults and fractures form part of the subvertical and NE-SW trending East Kemptville-East Dalhousie Fault Zone, and acted as a preferential path for the mineralizing fluid (Halter et al., 1994). As a result, greisens developed as symmetrical halos around central fractures (zoned greisens), and, in highly fractured zones, the halos overlapped to create massive greisens. The leucogranite and the mineralizing event have been dated with Pb isotopes at approximately 366 ± 4Ma (Kontak and Chatterjee, 1992).

Figure 1: Location of the East Kemptville tin deposit on a simplified geological of the Meguma Terrane, Nova Scotia (after Keppie, 1979, and Kontak, 1990). The enlarged area of the South Mountain Batholith shows the Davis Lake Pluton, which hosts the mineralization (after MacDonald, 1994, and Ham and MacDonald, 1994). The fault that runs through the leucogranite is part of the East Kemptville-East Dalhousie fault zone (EKEDFZ), and controlled the location and the geometry of the mineralization at East Kemptville. TFZ refers to the Tobiatic Fault Zone.

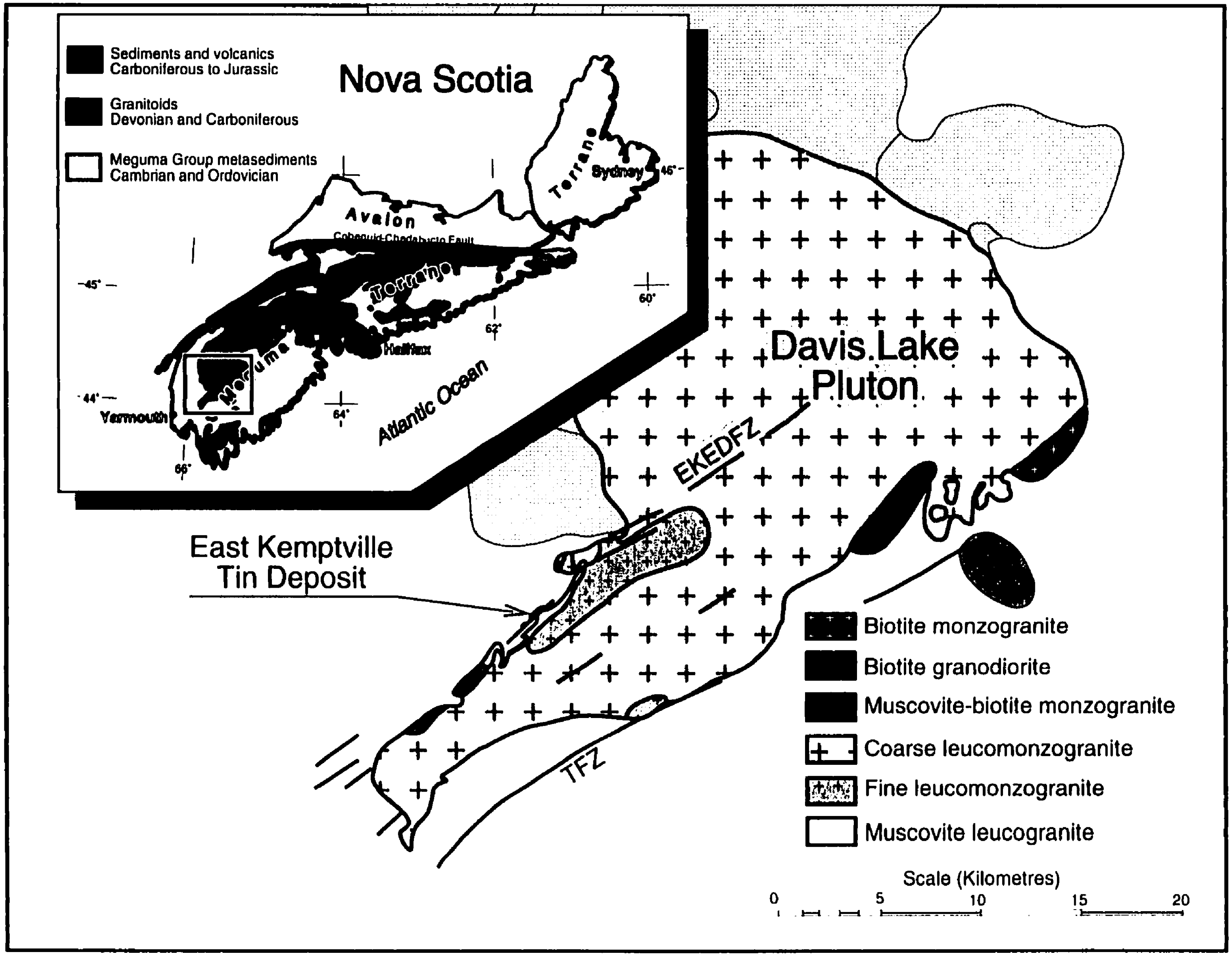
Sediments and volcanics
Carboniferous to Jurassic
Granitoids
Devonian and Carboniferous
Meguma Group metasediments
Cambrian and Ordovician
Nova Scotia
Avalon
Cobequid-Chedabucto Fault
Terrane
Terrane
Sydney
46°
45°
60°
62°
Halifax
Meguma
44°
Yarmouth
64°
66°
Atlantic Ocean
Davis Lake
Pluton
EKEDFZ
TFZ
East Kemptville
Tin Deposit
Biotite monzogranite
Biotite granodiorite
Muscovite-biotite monzogranite
Coarse leucomonzogranite
Fine leucomonzogranite
Muscovite leucogranite
Scale (Kilometres)
0
5
10
15
20

Figure 2: Horizontal section through the East Kemptville deposit at the 94m elevation. Bodies of sedimentary rock in the Main Zone display sub-vertical tectonic contacts with the leucogranite along their western margins and westerly dipping intrusive contacts on their eastern margins. Greisens are centered on, or run parallel to the major NE - SW fault system, suggesting that the latter controlled the path of the greisenizing fluid.

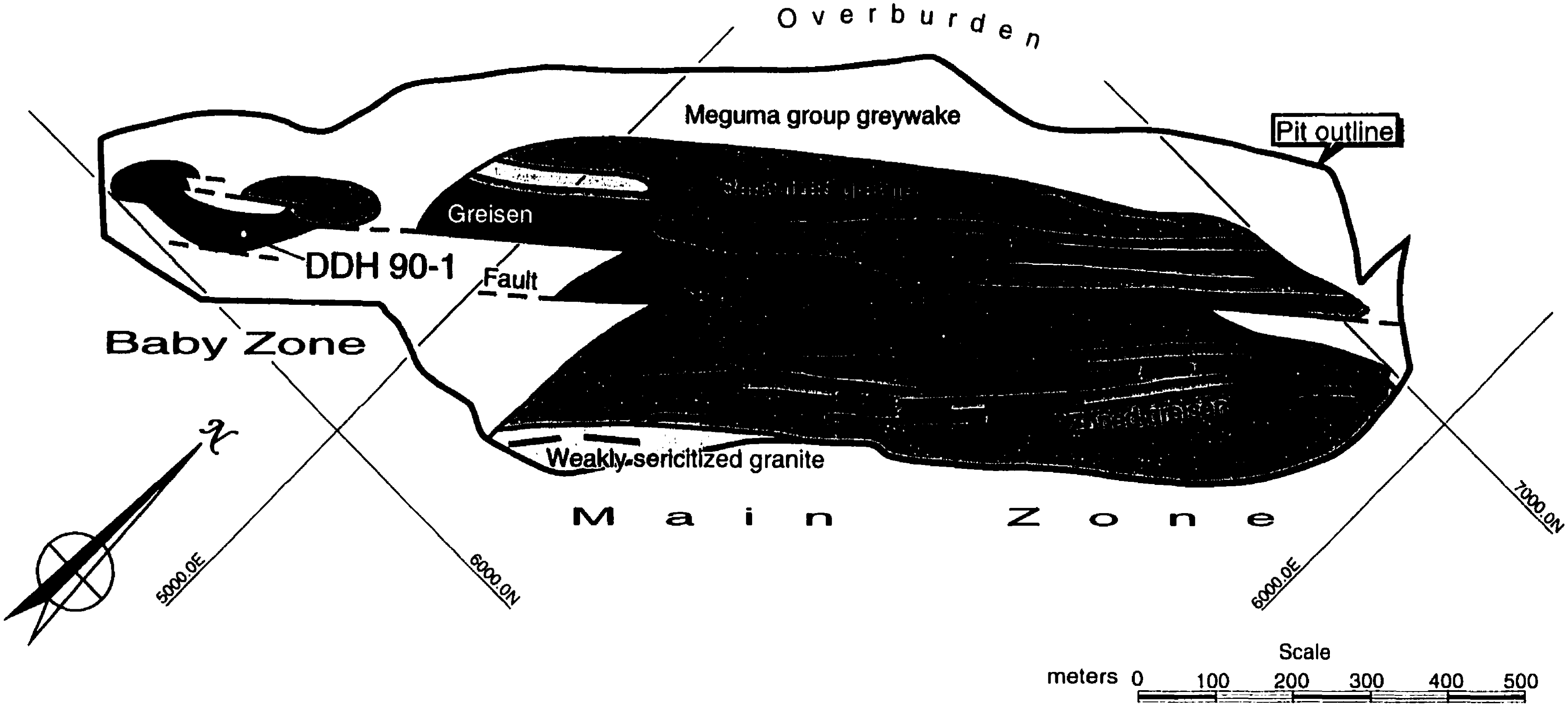
Overburden
Meguma group greywake
Pit outline
Greisen
DDH 90-1
Fault
Baby Zone
Weakly-sericitized granite
Main Zone
5000.0E
6000.0N
6000.0E
7000.0N
Scale
meters 0 100 200 300 400 500

DESCRIPTION AND PETROGRAPHY OF DDH 90-1

In order to obtain a representative continuous sample suite with which to investigate the detailed mineralogical and chemical changes that occurred during greisenization, we have based our study on the only deep hole drilled in the deposit (90-1), sited on surface in the better mineralized Baby Zone and extending vertically downwards over 851 meters (O'Reilly and Kontak, 1992). The hole intersects all the alteration zones present in the deposit

The top 103m of the hole cuts a greisen consisting of topaz, quartz, and minor but variable proportions of muscovite, pyrrhotite, sphalerite, chalcopyrite, cassiterite and fluorite (Fig. 3). The first 10m are particularly low in sulphides and cassiterite. Locally, annite and chlorite are present and formed contemporaneously with or slightly after other phases. This part of the hole is cut by numerous topaz, cassiterite and sulphide-bearing veins which commonly have a "bleached halo" containing little or no sulphide or cassiterite. Wolframite and molybdenite are present in a small proportion of the veins. Between 103 and 110m, the rock is a quartz-sericite greisen consisting of quartz-sericite-topaz ± pyrrhotite ± chalcopyrite. This is followed by 40m of alternating greisen, sericitized granite and metasediments of the Meguma Group. The contacts between the intrusive rock and the metasediments are either tectonic (sheared) or intrusive. In the latter case, the rock resembles a breccia with variably digested clasts of metasediments in an aplitic matrix. Throughout this section, the Fe content of the leucogranite is high (due probably to assimilation of Fe-rich metasediments) which helped stabilize garnet and biotite. This high Fe-content is most likely due to the incorporation of Fe-rich metasediments (Kontak and Dorsal, 1992) into the granite. Some metasediment was also intersected at 230m and 253m, but between 150 and 270m the core is mostly leucogranite which has been variably greisenized. Sulphides and cassiterite are also present, mainly in the quartz-topaz greisen. At 270m the hole passes into a sericitized leucogranite containing quartz, muscovite, albite and minor K-feldspar. With increasing depth, the proportion of muscovite decreases at the expense of albite and K-feldspar, and below 350m the hole intersects the least altered leucogranite, i.e., very homogenous quartz-

Figure 3: Simplified log of drill hole 90-1 in the Baby Zone. See text for description.

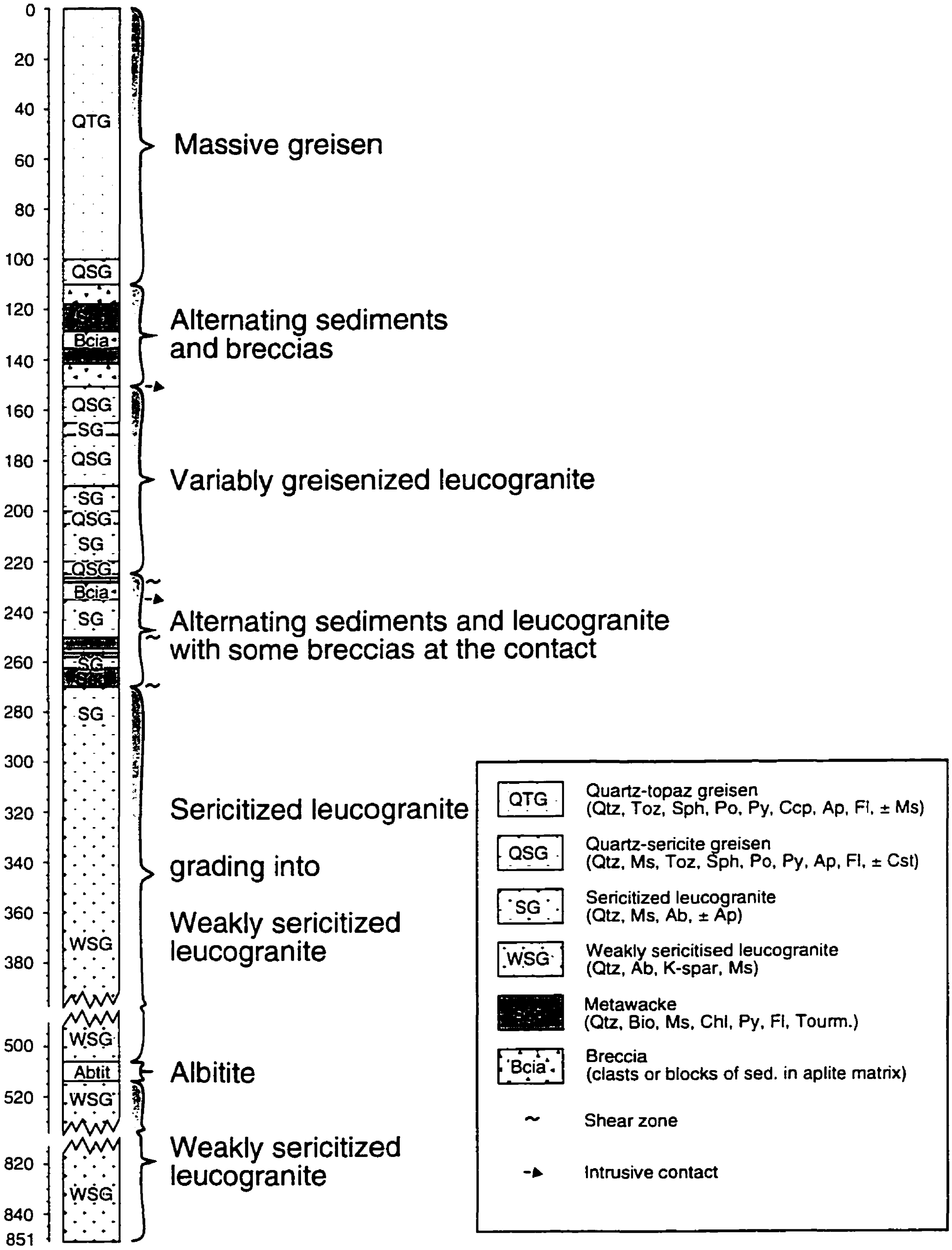
0
20
40
60
80
100
120
140
160
180
200
220
240
260
280
300
320
340
360
380
500
520
820
840
851
QTG
QSG
Bcia
QSG
SG
QSG
SG
QSG
SG
QSG
Bcia
SG
SG
SG
WSG
WSG
Abtit
WSG
WSG
Massive greisen
Alternating sediments and breccias
Variably greisenized leucogranite
Alternating sediments and leucogranite with some breccias at the contact
Sericitized leucogranite
grading into
Weakly sericitized leucogranite
Albitite
Weakly sericitized leucogranite
QTG
Quartz-topaz greisen (Qtz, Toz, Sph, Po, Py, Ccp, Ap, Fl, ± Ms)
QSG
Quartz-sericite greisen (Qtz, Ms, Toz, Sph, Po, Py, Ap, Fl, ± Cst)
SG
Sericitized leucogranite (Qtz, Ms, Ab, ± Ap)
WSG
Weakly sericitised leucogranite (Qtz, Ab, K-spar, Ms)
Metawacke (Qtz, Bio, Ms, Chl, Py, Fl, Tourm.)
Bcia
Breccia (clasts or blocks of sed. in aplite matrix)
~ Shear zone
-▸ Intrusive contact

muscovite-albite-K-feldspar leucogranite, similar to that described in the Main Zone by Kontak (1990) but without magmatic topaz. This rock also contains traces of zircon, U-oxides, monazite, xenotime and thorite as inclusions in large muscovite crystals interpreted to have formed during an early stage of sericitization that affected K-feldspar and albite. Apatite is present as inclusions in albite and small relicts of biotite are included in quartz. At 510 m the leucogranite is interrupted by 5m of albitite (Halter et al., 1995).

MINERAL CHEMISTRY

The compositions of all major minerals, except muscovite, remain essentially unchanged through the various alteration zones. Average compositions of these phases (except muscovite) determined by electron microprobe analyses are given in Table 1. Albite has a near end-member composition of Ab_{99} to Ab_{97}, with the highest concentration of Ca being in albite in the freshest leucogranite at the bottom of the hole. K-feldspar also has an end-member composition. The composition of the topaz varies in respect to F from 14.5 to 16.6 wt.%. No Cl could be detected in topaz. The main sulphide minerals are pyrrhotite and sphalerite; chalcopyrite is a minor phase. Pyrrhotite has an average composition of $Fe_{47.6}S_{52.4}$ and sphalerite contains between 9.0 and 9.7 wt.% Fe (the average Fe content is 9.3 wt%). Cassiterite has a near end-member composition with the main impurities being TiO_2 (0.5 wt %) and Fe_2O_3 (0.1 wt %). Locally, the content of Nb_2O_5 can reach 0.6 wt % and that of WO_3 up to 1.6wt %, but the concentrations of these oxides are usually below detection. Neither Ta nor Mn were detected. Annite $\{KAl_1Fe_{2.5}Mg_{0.3}Si_{3.2}O_{10}(F_{0.1}OH_{1.9})\}$ and chlorite are present in the upper part of the drill hole. Biotite, with an average composition of $KAl_2(Fe, Mg)_{1.5}Si_3O_{10}(F_{0.8}\ OH_{1.2})$ is present as inclusions in large quartz grains in the freshest leucogranite, and is thought to represent an early magmatic phase.

The composition of muscovite (Table 2) varies significantly with rock composition, particularly in respect to Fe and F (see Chapter 6 for details of chemical changes in muscovite compositions). In the leucogranite and in the quartz-sericite greisen, the most important substitution is phengitic, i.e., compositions in the least altered rocks

Table 1: Average mineral compositions and calculated number of ions or element proportions

	Albite			K-feldspar			Topaz	
	wt-%	ions (10O)		wt-%	ions (10O)		wt-%	ions (5O)
SiO_2	68.57	2.99	SiO_2	64.39	2.99	SiO_2	32.56	1.00
Al_2O_3	19.65	1.01	Al_2O_3	18.23	1.00	Al_2O_3	55.34	2.00
FeO	0.02	0.00	FeO	0.03	0.00	FeO	0.02	0.00
MgO	0.00	0.00	MgO	0.00	0.00	MgO	0.00	0.00
CaO	0.22	0.01	CaO	0.07	0.00	CaO	0.01	0.00
Na_2O	11.61	0.98	Na_2O	0.35	0.03	F	15.51	1.50
K_2O	0.11	0.01	K_2O	17.13	1.01	Cl	0.02	0.00
Total	100.17			100.20			96.92	

	Cassiterite			Sphalerite			Pyrrhotite	
	wt-%	ele. prop.		wt-%	ele. prop.		wt-%	ele. prop.
TiO_2	0.39	0.01	Fe	9.33	0.08	Fe	60.80	0.48
FeO	0.07	0.00	Mn	0.10	0.00	Mn	0.00	0.00
MnO	0.01	0.00	S	32.95	0.50	S	38.34	0.52
SnO2	99.85	0.99	Sn	0.00	0.00	Sn	0.00	0.00
WO_3	0.27	0.00	Zn	57.13	0.42	Zn	0.01	0.00
Nb_2O_5	0.15	0.00	Cu	0.08	0.00	Cu	0.03	0.00
Ta_2O_5	0.00	0.00						
Total	100.74			99.60			99.18	

Table 2: Average muscovite analyses and normative compositions (based on 22 oxygens) in selected samples

Sample	38.6		71.8		81		100		189		181	
	wt-%	norm. 22O	wt-%	norm. 22O	wt-%	norm. 22O	wt-%	norm. 22O	wt-%	norm. 22O	wt-%	norm. 22O
SiO_2	50.02	6.35	45.20	6.36	46.46	6.50	49.26	6.55	49.03	6.46	46.66	6.42
TiO_2	0.06	0.00	0.16	0.00	0.22	0.02	0.11	0.01	0.02	0.00	0.03	0.00
Al_2O_3	35.82	5.36	24.70	4.09	25.71	4.23	29.22	4.58	31.72	4.92	30.43	4.94
FeO	1.14	0.12	14.91	1.77	11.20	1.33	8.00	0.89	6.06	0.67	5.52	0.64
MnO	0.05	0.01	0.74	0.09	0.48	0.06	0.27	0.03	0.28	0.03	0.34	0.04
MgO	1.15	0.22	1.40	0.30	1.14	0.24	0.70	0.14	0.28	0.06	0.17	0.03
Na_2O	0.33	0.08	0.14	0.04	0.17	0.05	0.13	0.03	0.17	0.04	0.27	0.07
K_2O	10.81	1.75	10.29	1.85	10.65	1.90	10.90	1.85	10.83	1.82	11.32	1.99
F	1.57	0.63	5.26	2.36	4.79	2.14	3.68	1.55	2.93	1.22	2.09	0.91
OH		3.37		1.64		1.86		2.45		2.78		3.09
Total	100.31		100.61		98.84		100.73		100.12		95.93	

Sample	222		198		211		273		290		850	
	wt-%	norm. 22O	wt-%	norm. 22O	wt-%	norm. 22O	wt-%	norm. 22O	wt-%	norm. 22O	wt-%	norm. 22O
SiO_2	47.28	6.44	49.75	6.57	46.59	6.49	45.33	6.49	47.50	6.90	46.75	6.53
TiO_2	0.09	0.01	0.15	0.01	0.13	0.01	0.28	0.00	0.10	0.01	0.41	0.04
Al_2O_3	30.85	4.95	30.11	4.73	28.71	4.71	26.02	4.76	22.76	3.87	27.53	4.53
FeO	5.00	0.57	6.69	0.73	6.88	0.81	10.47	0.75	9.35	1.18	7.72	0.90
MnO	0.22	0.03	0.46	0.05	0.48	0.06	0.31	0.04	0.90	0.12	0.38	0.05
MgO	0.41	0.08	0.24	0.05	0.20	0.04	0.83	0.04	0.17	0.04	0.45	0.09
Na_2O	0.15		0.12	0.03	0.14		0.14	0.04	0.12		0.14	
K_2O	11.31	1.97	10.56	1.78	11.29	2.01	11.19	1.99	11.02	2.04	11.32	2.02
F	2.05	0.88	3.56	1.46	2.74	1.22	3.39	0.89	5.89	2.78	2.18	0.97
OH		3.12		2.54		2.78		3.11		1.22		3.03
Total	96.51		100.18		96.03		96.61		95.34		96.01	

Sample	450		350		650		830	
	wt-%	norm. 22O	wt-%	norm. 22O	wt-%	norm. 22O	wt-%	norm. 22O
SiO_2	46.65	6.58	47.46	6.69	46.43	6.49	45.61	6.47
TiO_2	0.25	0.00	0.26	0.00	0.48	0.00	0.50	0.00
Al_2O_3	26.98	4.48	26.27	4.36	28.27	4.64	27.07	4.52
FeO	7.24	0.86	7.53	0.89	6.76	0.80	8.49	1.01
MnO	0.38	0.05	0.41	0.05	0.36	0.04	0.36	0.04
MgO	0.53	0.11	0.28	0.06	0.40	0.08	0.43	0.09
Na_2O	0.13	0.03	0.12	0.03	0.26	0.07	0.12	0.03
K_2O	11.41	2.05	11.26	2.02	11.33	2.02	11.29	2.04
F	3.27	1.46	3.64	1.62	2.66	1.19	2.10	0.95
OH		2.54		2.38		2.81		3.05
Total	95.49		95.71		95.83		95.11	

varied mainly as a result of the exchange reactions

$$2.33\mathrm{Al} + \mathrm{OH} \rightleftharpoons \mathrm{Fe} + 1.25\ \mathrm{Si} + \mathrm{F}$$

and

$$1.47\mathrm{Si} + 1.7\mathrm{F} \rightleftharpoons \mathrm{Fe} + 1.29\mathrm{Al} + 1.7\mathrm{OH}$$

In quartz-sericite greisen, the exchange reaction is approximately

$$\mathrm{Fe} + 0.7\mathrm{Si} + 1.4\mathrm{F} \rightleftharpoons 1.6\mathrm{Al} + 1.4\mathrm{OH}$$

By contrast, cation substitution in quartz-topaz greisen affected only Fe and Al (the Si concentration remained unchanged) and the F concentration increased with the Fe content. High totals for electron microprobe analyses of muscovite in the quartz-topaz greisen are possibly related to the presence of H_2O in the structure in place of OH^- groups and to dehydration (Chapter 6).

CHEMISTRY OF THE LEAST ALTERED LEUCOGRANITE

Chemical analyses of 47 representative samples of the different types of greisens and leucogranite are presented in Table 3. Samples followed by the letter "c" are 3 meter long composites, free of veins (Kontak, unpublished data).

To evaluate chemical changes owing to greisenization, the first step was to determine whether or not the altered rocks in the deep hole have the same protolith. Commonly, this is done by making pairwise comparisons of the concentrations of immobile elements in the samples. If the protolith is the same, binary plots of the data should yield linear trends that regress through the origin (Finlow-Bates and Stumpfl, 1981; MacLean and Kranidiotis, 1986). Unfortunately, at East Kemptville, no immobile element pair could be identified. Elements usually considered to be immobile (Al, Ti, REE, Zr) display some degree of mobility in these rocks, most likely

Table 3: Whole rock analyses of selected samples in the DDH 90-1

Sample	10	26	30	66	81c	93	100	106c	175c	178c	181c	189c
SiO_2	83.52	78.96	74.13	72.5	72.41	71.13	75.31	71.86	73.85	73.48	76.05	74.23
TiO_2	0.02	0.02	0.03	0.04	0.03	0.03	0.02	0.02	0.04	0.04	0.04	0.03
Al_2O_3	11.35	11.54	14.09	14.89	11.51	12.86	13.33	13.65	12.24	12.44	11.59	15.45
FeO	2.7	5.4	6.3	7.2	7.1	7.23	6.3	6.87	4	3.57	4.31	3.62
MnO	0.02	0.02	0.04	0.04	0.05	0.05	0.03	0.1	0.23	0.13	0.08	0.07
MgO	0	0	0	0.02	0	0.01	0	0.14	0.07	0.09	0.08	0
CaO	0.35	0.29	0.35	0.56	0.26	0.45	0.59	1.18	0.82	1.12	0.77	0.57
Na_2O	0.06	0.51	0.57	0.06	0.25	0.16	0.67	0.56	0.16	0.13	0.23	0.12
K_2O	0.62	0.1	0.11	0.43	0.3	0.35	0.31	3.48	4.31	4.41	2.05	1.27
P_2O_5	0.16	0.17	0.2	0.17	0.16	0.18	0.27	0.22	0.16	0.16	0.19	0.31
LOI	0.54	1.47	1.43	1.58	6	6.1	1.51	2.9	2.5	2.2	2.7	2.1
Total	99.34	98.48	97.25	97.49	98.07	98.55	98.34	101	98.38	97.77	98.09	97.77
F	3.3	3.9	4.5	4.8	3.4	3.8	4.5	2.8	1.35	1.87	1.98	4.48
S	0.76	2.63	2.74	3	3.7	3.3	2.75	2.23	0.22	0.16	1.61	1.23
Fe_2O_3	0.39	0	0	0	N/A	N/A	0	N/A	4.44	3.97	4.79	4.02
Cl	194	159	169	89	N/A	N/A	229	N/A	N/A	N/A	N/A	N/A
CO_2	2000	250	4250	1000	N/A	N/A	5001	N/A	N/A	N/A	N/A	N/A
BaO	0	int	int	int	23	12	int	98	43	35	33	8
Ce	13	15	15	21	N/A	N/A	8	N/A	N/A	N/A	N/A	N/A
Co	5	7	1	6	N/A	N/A	3	N/A	N/A	N/A	N/A	N/A
Cr_2O_3	0	8	int	0	472	414	int	252	202	217	324	442
Cu	452	1160	1225	1708	1624	958	3564	2569	454	186	512	1208
Ni	2	4	2	2	14	16	1	7	7	5	10	10
Sc	1	4	0	3	N/A	N/A	0		N/A	N/A	N/A	N/A
V	7	0	8	6	0	7	2	0		0	0	0
Zn	234	7223	5830	475	6099	2613	4557	1746	711	943	5249	2085
Br	2	2	2	3	N/A	N/A	3	N/A	N/A	N/A	N/A	N/A
Ga	4	8	8	9	9	12	7	19	35	40	36	11
Mo	0	0	0	0	N/A	N/A	0	N/A	N/A	N/A	N/A	N/A
Nb	14	17	28	17	42	24	18	24	22	27	20	13
Pb	0	2	7	4	80	28	2	18	0	23	0	13
Rb	157	38	46	171	133	145	79	551	1384	1360	671	401
Sr	17	18	23	23	12	20	35	50	26	33	29	27
Th	13	13	13	14	N/A	N/A	12	N/A	33	24	31	22
Y	14	10	13	26	7	8	13	0	0	0	8	15
Zr	21	25	22	36	20	21	24	22	35	38	37	34
U	20	21	19	24	N/A	N/A	18	N/A	N/A	N/A	N/A	N/A
Cs	8	2	2	9	N/A	N/A	4	N/A	N/A	N/A	N/A	N/A
Hf	2	2	2	2	N/A	N/A	2	N/A	N/A	N/A	N/A	N/A
As	12	3	14	1	140	120	4	90	0.007	0.006	0.008	0.006
Bi	27	40	48	12	160	80	30	80	0.003	0	0.002	0.004
Sb	4	5	10	2	N/A	N/A	0	N/A	N/A	N/A	N/A	N/A
Sn	876	1430	4467	2244	1017	3340	843	1560	0.061	0.263	0.099	0.088
Ta	4	13	12	9	N/A	N/A	23	N/A	N/A	N/A	N/A	N/A
W	16	49	766	13	N/A	N/A	18	N/A	N/A	N/A	N/A	N/A
Li	151	229	35	365	135	98	916	327	1200	1315	313	242

Major elements. F and S are in weight percent. others in ppm. REE in ppb

N/A: not ananlysed. O: below detection limit. Int: interferences. "c": 3m composites

Table 3: cont.

Sample	196c	198	208c	211c	216	222	237	246	262	290	350	370
SiO_2	74.59	74.62	75.01	74.76	76.22	72.96	75.74	75.39	75.58	74.81	75.59	76.43
TiO_2	0.04	0.04	0.02	0.03	0.04	0.03	0.04	0.05	0.04	0.02	0.04	0.05
Al_2O_3	13.46	14.26	14.23	13.46	13.35	14.73	13.96	14.07	14.27	14.6	13.96	13.39
FeO	3.9	2.7	2.34	2.32	1.8	2.7	1.8	1.8	1.8	1.8	0.9	0.9
MnO	0.14	0.17	0.1	0.12	0.11	0.09	0.09	0.09	0.12	0.13	0.07	0.07
MgO	0.02	0	0	0.02	0	0.1	0	0	0	0	0	0.02
CaO	0.31	0.37	0.38	0.36	0.76	1.41	0.66	0.45	0.33	0.47	0.27	0.34
Na_2O	1.4	2.06	3.53	3.44	3.37	1.59	4.51	3.65	4.47	4.03	3.65	3.53
K_2O	3.7	3.75	2.75	2.52	2.86	3.99	2.22	3.68	2.61	2.77	4.41	3.9
P_2O_5	0.15	0.14	0.16	0.17	0.15	0.17	0.13	0.13	0.15	0.21	0.19	0.15
LOI	1.5	1.62	1.2	1.3	1.24	1.91	0.99	0.96	0.93	1.16	0.67	0.8
Total	99.21	99.73	99.72	98.5	99.9	99.68	100.1	100.3	100.3	100	99.75	99.58
F	1.17	1.1	0.99	1.04	1.2	1.7	1.2	1.2	1.3	1	0.66	0.66
S	0.62	0.39	0.27	0.06	0.01	0.21	0.04	0.02	0.01	0.01	0	0
Fe_2O_3	N/A	0.13	N/A	N/A	0.1	0.26	0	0	0	0	0	0
Cl	N/A	179	N/A	N/A	129	172	266	284	226	134	67	111
CO_2	N/A	5003	N/A	N/A	2749	500	3501	2747	2501	2998	1250	1250
BaO	46	64	9	41	79	100	44	69	35	46	0	22
Ce	N/A	4	N/A	N/A	26	24	8	23	0	0	16	31
Co	N/A	0	N/A	N/A	4	1	1	0	6	3	0	2
Cr_2O_3	244	0	230	207	3	0	2	0	3	0	6	0
Cu	185	209	97	87	132	426	261	199	138	96	99	73
Ni	8	8	9	6	7	3	7	2	0	6	8	4
Sc	N/A	0	N/A	N/A	0	7	3	5	6	3	9	2
V	0	5	7	5	5	2	3	4	7	3	0	4
Zn	2783	2151	1037	594	301	698	785	182	263	202	89	156
Br	N/A	3	N/A	N/A	4	3	6	7	4	2	2	3
Ga	42	37	37	37	32	37	33	33	32	44	29	28
Mo	N/A	0	N/A	N/A	1	0	0	0	0	0	0	0
Nb	23	25	26	24	23	28	28	26	25	36	24	22
Pb	0	1	0	0	1	1	1	2	1	2	4	2
Rb	1129	1060	797	898	894	1034	719	901	868	1007	964	916
Sr	25	31	34	40	62	49	73	56	47	57	6	12
Th	N/A	17	N/A	N/A	15	12	14	18	16	14	17	N/A
Y	0	57	0	0	53	45	44	53	50	40	53	53
Zr	38	42	25	30	44	24	40	48	37	18	46	54
U	N/A	25	N/A	N/A	24	19	28	29	30	20	32	N/A
Cs	N/A	37	N/A	N/A	39	31	29	38	46	29	36	N/A
Hf	N/A	2	N/A	N/A	3	2	2	3	2	2	2	N/A
As	40	2	70	60	4	7	N/A	N/A	0	3	1	1
Bi	10	7	30	30	N/A	9	1	3	5	57	N/A	N/A
Sb	N/A	2	N/A	N/A	N/A	N/A	N/A	3	1	2	0	0
Sn	280	104	100	70	72	85	41	54	28	58	14	29
Ta	N/A	8	N/A	N/A	9	14	5	5	6	27	13	7
W	N/A	11	N/A	N/A	120	51	9	21	37	106	21	N/A
Li	458	1522	1038	1028	1413	1101	1672	2356	2728	1722	1419	1305

Major elements. F and S are in weight percent. others in ppm. REE in ppb

N/A: not ananlysed. O: below detection limit. Int: interferences. "c": 3m composites

Table 3: cont.

Sample	390	410	430	450	470	490	530	550	570	590	610	630
SiO_2	75.55	76.21	75.94	76.58	75.7	76.4	76	76.98	75.9	76.91	75.55	76.55
TiO_2	0.04	0.05	0.05	0.05	0.06	0.05	0.06	0.06	0.06	0.06	0.07	0.06
Al_2O_3	14.05	13.51	13.77	13.13	13.64	13.48	13.6	13.08	13.65	12.89	13.68	13.32
FeO	0.9	0.9	1.8	1.8	1.8	0.9	0.9	1.8	1.8	1.8	1.8	1.8
MnO	0.07	0.08	0.07	0.07	0.08	0.07	0.07	0.08	0.07	0.06	0.07	0.07
MgO	0	0.01	0	0.02	0.02	0.01	0	0.01	0	0.01	0.02	0.01
CaO	0.31	0.34	0.33	0.33	0.32	0.25	0.31	0.39	0.18	0.23	0.35	0.35
Na_2O	3.65	3.6	3.58	3.35	3.5	3.56	3.62	3.27	3.46	3.33	3.49	3.47
K_2O	4.4	4.19	4.35	4.17	4.45	4.23	4.4	4.11	4.41	4.19	4.58	4.28
P_2O_5	0.16	0.16	0.15	0.14	0.15	0.15	0.14	0.16	0.14	0.13	0.14	0.15
LOI	0.74	0.76	0.75	0.77	0.78	0.73	0.55	0.71	0.74	0.67	0.74	0.71
Total	99.87	99.81	100.8	100.4	100.5	99.83	99.65	100.7	100.4	100.3	100.5	100.8
F	0.7	0.59	0.61	0.68	0.61	0.52	0.57	0.62	0.3	0.42	0.54	0.56
S	0	0	0	0	0	0	0	0	0.02	0	0	0
Fe_2O_3	0	0	0	0	0	0	0	0	0.07	0	0	0
Cl	202	245	202	293	237	174	127	210	202	143	122	190
CO_2	1249	1748	1499	4496	0	2001	0	1249	3248	1499	750	0
BaO	0	13	13	32	32	22	16	31	38	4	23	15
Ce	32	27	20	12	21	8	9	30	0	32	37	22
Co	0	1	7	0	0	2	0	6	4	1	0	8
Cr_2O_3	0	0	0	0	0	0	3	0	4	0	0	0
Cu	149	100	85	281	73	101	89	69	41	109	94	95
Ni	1	1	7	4	1	4	4	9	7	1	4	2
Sc	4	5	7	9	3	5	6	0	9	6	3	3
V	2	3	3	3	7	3	1	3	5	5	10	5
Zn	123	96	109	154	91	89	95	84	75	86	93	94
Br	4	5	4	6	5	5	2	4	3	1	1	1
Ga	28	28	27	27	27	27	26	27	27	25	27	26
Mo	0	0	0	0	0	0	0	0	0	0	0	1
Nb	22	21	20	21	22	21	19	21	21	18	20	20
Pb	2	4	5	5	5	3	4	4	3	12	7	6
Rb	957	888	869	834	873	833	845	833	808	765	843	782
Sr	10	11	9	11	19	13	7	14	15	10	9	9
Th	N/A	N/A	N/A	16	N/A	N/A	N/A	18	N/A	N/A	N/A	N/A
Y	52	52	50	53	55	51	50	55	50	51	54	51
Zr	44	48	44	57	54	50	53	56	52	57	59	58
U	N/A	N/A	N/A	26	N/A	N/A	N/A	31	N/A	N/A	N/A	N/A
Cs	N/A	N/A	N/A	48	N/A	N/A	N/A	43	N/A	N/A	N/A	N/A
Hf	N/A	N/A	N/A	2	N/A	N/A	N/A	3	N/A	N/A	N/A	N/A
As	1	0	1	8	1	1	N/A	1	2	N/A	0	N/A
Bi	N/A	0	1	3	0	1	N/A	4	N/A	16	N/A	N/A
Sb	1	2	N/A	0	1	1	1	N/A	3	N/A	N/A	N/A
Sn	25	17	23	44	16	19	25	38	17	12	18	20
Ta	9	8	6	7	10	8	7	5	7	3	7	10
W	N/A	N/A	N/A	15	N/A	N/A	N/A	65	N/A	N/A	N/A	N/A
Li	1351	1205	1310	1445	1371	1087	910	724	702	981	1326	1263

Major elements. F and S are in weight percent, others in ppm, REE in ppb

N/A: not ananlysed. O: below detection limit. Int: interferences. "c": 3m composites

Table 3: cont.

Sample	650	670	690	710	730	750	770	790	810	830	850
SiO_2	76.29	75.79	77.05	75.21	76.55	76.28	75.44	76.29	75.43	75.06	77.52
TiO_2	0.06	0.08	0.07	0.07	0.07	0.05	0.07	0.09	0.08	0.07	0.06
Al_2O_3	13.44	13.39	13.08	13.82	13.19	13.38	13.73	13.15	13.83	13.71	12.84
FeO	1.8	1.8	1.8	1.8	0.9	1.8	1.8	1.8	1.8	1.8	1.8
MnO	0.07	0.07	0.07	0.07	0.06	0.07	0.05	0.05	0.07	0.06	0.06
MgO	0.01	0.03	0.01	0.03	0.03	0.01	0.02	0.03	0.03	0.01	0.03
CaO	0.24	0.36	0.31	0.34	0.3	0.33	0.41	0.37	0.44	0.37	0.4
Na_2O	3.5	3.43	3.36	3.51	3.36	3.5	3.53	3.35	3.4	3.36	3.47
K_2O	4.63	4.49	4.36	4.65	4.54	4.05	4.61	4.55	4.51	4.89	3.71
P_2O_5	0.14	0.13	0.13	0.13	0.13	0.14	0.13	0.13	0.13	0.13	0.12
LOI	0.65	0.7	0.7	0.77	0.68	0.77	0.69	0.7	0.83	0.75	0.74
Total	100.8	100.3	100.9	100.4	99.81	100.4	100.5	100.5	100.6	100.2	100.8
F	0.52	0.51	0.5	0.54	0.42	0.5	0.42	0.36	0.49	0.4	0.46
S	0	0	0	0.02	0	0.02	0	0	0.02	0	0.01
Fe_2O_3	0	0	0	0	0	0	0	0	0	0	0.06
Cl	170	114	166	220	210	95	165	217	208	216	187
CO_2	2251	1250	250	1001	250	2996	3002	0	2999	0	3752
BaO	26	32	37	47	31	17	6	40	29	44	10
Ce	18	1	34	18	23	25	44	34	43	21	10
Co	0	2	0	0	6	0	0	2	0	10	2
Cr_2O_3	0	int	int	int	0	0	0	0	0	18	0
Cu	148	53	97	167	78	51	93	104	244	57	359
Ni	2	7	0	2	1	3	0	4	5	19	0
Sc	5	7	4	2	1	0	2	4	11	5	5
V	0	9	3	11	2	1	5	2	5	0	10
Zn	113	88	84	117	96	100	88	109	134	93	137
Br	2	2	2	4	3	3	3	3	4	5	4
Ga	26	26	25	27	25	26	25	25	26	25	24
Mo	0	0	0	0	0	0	0	0	0	0	0
Nb	18	21	20	20	18	18	17	18	21	19	19
Pb	7	8	7	7	9	5	9	8	7	7	3
Rb	782	794	801	850	744	738	704	708	751	756	664
Sr	10	11	8	11	10	13	14	16	14	14	9
Th	13	N/A	N/A	N/A	N/A	19	N/A	N/A	N/A	N/A	13
Y	50	54	54	53	52	47	51	56	50	53	42
Zr	56	62	60	54	68	44	65	75	55	54	40
U	24	N/A	N/A	N/A	N/A	32	N/A	N/A	N/A	N/A	19
Cs	47	N/A	N/A	N/A	N/A	27	N/A	N/A	N/A	N/A	27
Hf	2	N/A	N/A	N/A	N/A	3	N/A	N/A	N/A	N/A	2
As	1	1	8	1	N/A	N/A	0	0	1	N/A	N/A
Bi	1	N/A	N/A	N/A	3	1	0	N/A	0	N/A	1
Sb	N/A	1	N/A	2	0	N/A	N/A	1	N/A	1	N/A
Sn	16	12	11	39	32	55	11	10	22	14	39
Ta	4	6	3	6	4	5	3	4	7	5	3
W	12	N/A	N/A	N/A	N/A	10	N/A	N/A	N/A	N/A	9
Li	1103	1130	1249	1133	982	1149	950	1006	1105	980	911

Major elements, F and S are in weight percent, others in ppm, REE in ppb
N/A: not ananlysed. O: below detection limit. Int: interferences. "c": 3m composites

Table 3: cont.

Sample	10	30	66	100	198	216	222	237	246
La	2.61	2.61	4.56	2.95	6.08	5.80	2.72	5.13	6.83
Ce	6.74	7.35	11.69	7.80	16.04	15.14	8.23	14.39	19.56
Pr	0.76	0.86	1.34	0.96	1.97	1.65	0.96	1.66	1.98
Nd	2.99	3.08	4.90	3.67	7.26	6.57	4.09	6.39	7.91
Sm	1.28	1.42	1.85	1.30	2.58	2.10	1.58	2.41	2.90
Eu	0.13	0.08	0.08	0.17	0.08	0.08	0.08	0.08	0.09
Gd	1.25	1.25	2.34	1.31	2.99	2.41	1.40	2.63	3.09
Tb	0.29	0.29	0.49	0.29	0.69	0.58	0.29	0.59	0.64
Dy	1.85	1.94	3.49	2.14	4.29	3.63	1.97	3.95	4.64
Ho	0.33	0.33	0.77	0.38	0.86	0.76	0.38	0.77	0.86
Er	0.88	0.92	2.19	1.05	2.52	2.25	0.98	2.20	2.50
Tm	0.23	0.23	0.38	0.23	0.46	0.38	0.31	0.38	0.51
Yb	1.46	1.52	3.28	1.61	3.34	2.84	1.62	3.09	3.78
Lu	0.19	0.23	0.53	0.26	0.59	0.33	0.26	0.40	0.52

Sample	262	290	350	450	550	650	750	850
La	5.75	1.56	5.15	6.43	8.20	6.61	6.99	7.01
Ce	16.20	5.15	14.96	16.92	21.10	16.80	18.23	18.39
Pr	1.83	0.61	1.63	1.86	2.31	1.87	1.97	2.05
Nd	7.25	2.53	6.39	7.38	9.44	7.23	7.53	8.24
Sm	2.18	1.38	2.29	2.59	3.28	2.38	1.99	2.41
Eu	0.00	0.09	0.00	0.00	0.09	0.08	0.09	0.08
Gd	2.87	1.12	2.57	2.63	3.28	2.87	2.87	2.58
Tb	0.63	0.32	0.53	0.59	0.63	0.63	0.64	0.48
Dy	4.19	1.73	3.59	4.14	4.81	4.30	4.51	3.52
Ho	0.85	0.21	0.75	0.77	0.96	0.85	0.85	0.75
Er	2.21	0.79	1.87	2.29	2.48	2.54	2.22	1.96
Tm	0.42	0.17	0.42	0.46	0.50	0.45	0.51	0.37
Yb	3.27	1.35	3.12	3.23	4.15	3.38	3.44	2.69
Lu	0.37	0.22	0.45	0.46	0.59	0.49	0.52	0.35

Major elements. F and S are in weight percent, others in ppm, REE in ppb
N/A: not ananlysed. O: below detection limit. Int: interferences. "c": 3m composites

because of the high F content of the mineralizing fluid and the ability of F to form stable complexes with these elements in hydrothermal systems (Wood, 1990; Aja et al., 1996). Good correlations were obtained for U versus the REE, and Th versus the REE (particularly La), but the regressions do not pass through the origin (Fig 4). This suggests that these elements were mobile, but behaved coherently by being concentrated in a single mineral, possibly monazite, and were depleted during dissolution of this phase by the F-rich hydrothermal fluid. The fact that Th and La correlate linearly, indicates, however, that all the rocks intersected in the deep hole had the same original Th/La ratio, i.e., the same protolith.

In view of the above observations, the least altered leucogranite in the bottom 500m of the hole was taken to represent the protolith of all the greisens. The homogeneity of rock in this interval was examined by evaluating the variation of each element with increasing depth. The concentrations of major elements remain essentially constant, but some trace elements display a systematic enrichment/depletion with increasing depth (Fig. 5). These variations probably represent primary magmatic differentiation trends, controlled by the crystallization of albite, quartz, muscovite, K-feldspar and biotite. In such a system, Zr and Ca behave as incompatible elements, and since they are enriched towards the bottom of the hole, this suggests that crystallization occurred towards the inside of the intrusion. By contrast, Rb, Li, F behave as compatible elements since they are incorporated in muscovite; these elements decrease in concentration with increasing depth. Similarly Nb and Ta are incorporated in biotite and Ga substitutes for Al in feldspars, and these elements also decrease in abundance with depth. These variations are, however, minor compared to those induced by the greisenization, and for the purpose of our evaluation of the alteration, the protolith can be considered homogenous.

The chemical composition of the least altered leucogranite in hole 90-1 is close to that of the leucogranite in the Main Zone (Kontak, 1990) and reflects a highly evolved granite, i.e., one characterized by high concentrations of Si, Al and F, and low concentrations of Ti, Fe, Mn, Mg and Ca. However, the REE content (Fig. 6), and particularly the LREE content, is consistently higher than that reported for the Main Zone (Kontak, 1990). This reflects higher proportions of monazite and xenotime due perhaps to

Figure 4: A plot of whole rock La vs Th for the Baby Zone (diamonds). Fresh leucogranite has high La and Th values and altered greisens have lower values, particularly for La. The good correlation between these two elements and the fact that the linear regression (line) does not pass through the origin suggest that both elements were present in a phase that dissolved during greisenization. This also implies that the same protolith was present throughout the drill hole. Also shown are the plots of Th vs U and Lu, and these show similar correlations. Squares represent compositions of samples of fresh leucogranite in the Main Zone (Kontak, 1990).

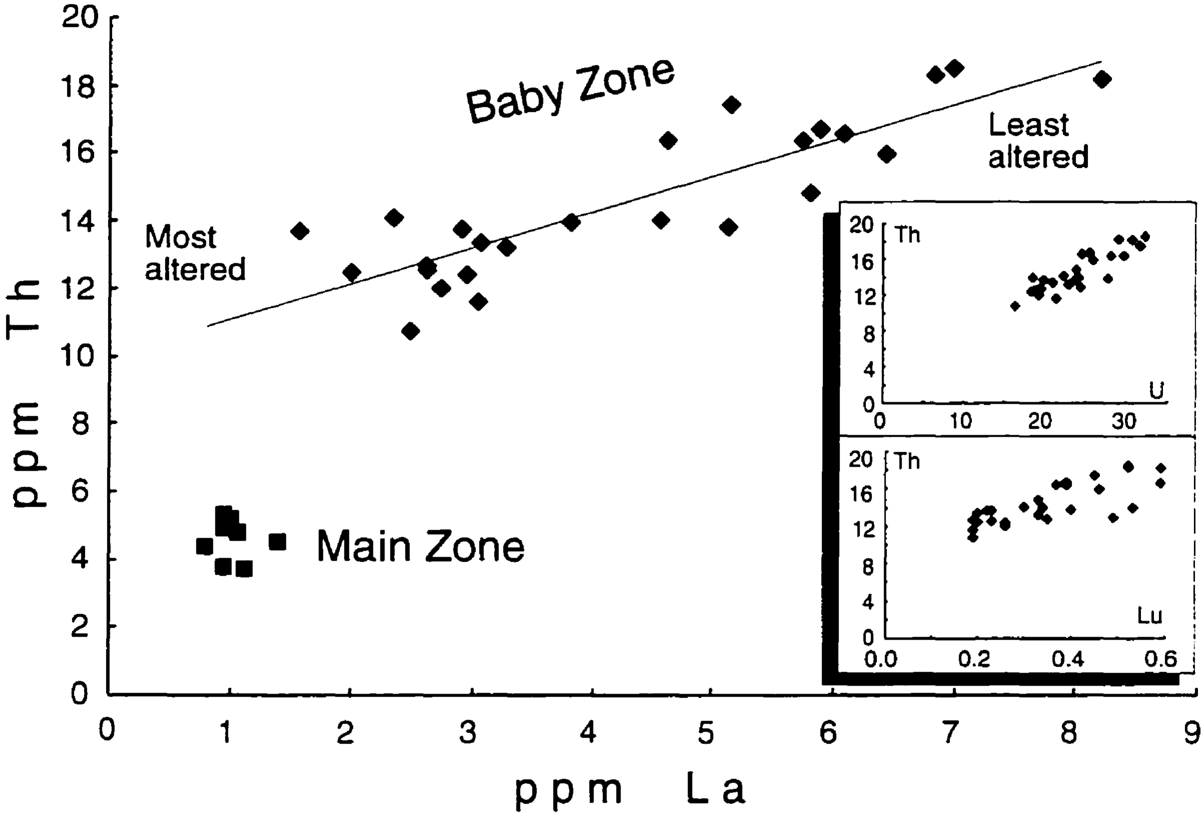
Baby Zone
Most altered
Least altered
Main Zone
ppm Th
ppm La
0
2
4
6
8
10
12
14
16
18
20
0
1
2
3
4
5
6
7
8
9
Th
U
0
4
8
12
16
20
0
10
20
30
Th
Lu
0
4
8
12
16
20
0.0
0.2
0.4
0.6

Figure 5: Variations in the concentration of selected elements with depth in the fresh leucogranite from the deeper part of drill hole 90-1. The increase in incompatible elements (Ca, Zr) and decrease in compatible elements (Nb, Li, Rb, Ta, F, Ga) with depth suggests magmatic differentiation. Lines are linear regressions obtained by least squares fit.

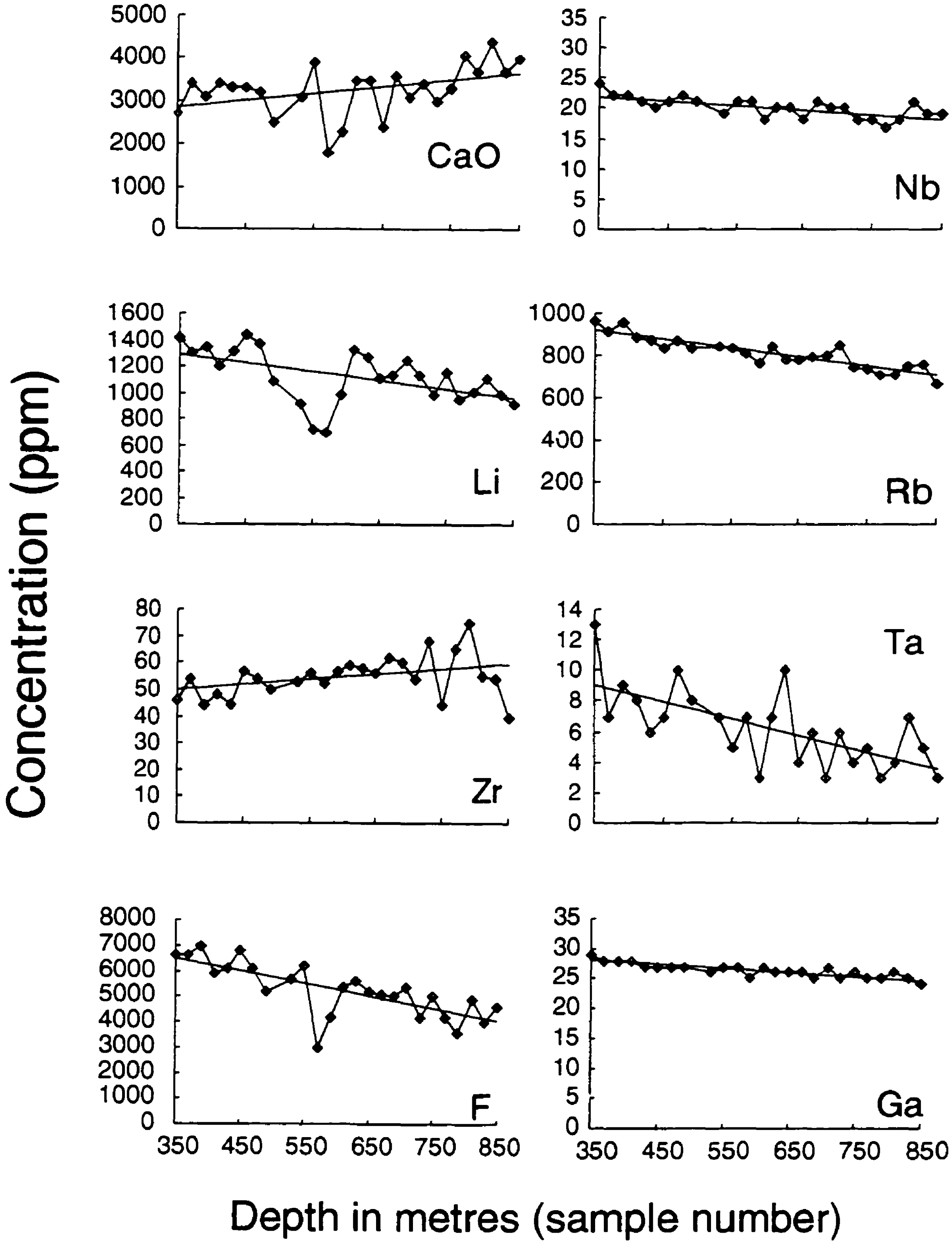
CaO
5000
4000
3000
2000
1000
0
Nb
35
30
25
20
15
10
5
0
Li
1600
1400
1200
1000
800
600
400
200
0
Rb
1000
800
600
400
200
0
Zr
80
70
60
50
40
30
20
10
0
Ta
14
12
10
8
6
4
2
0
F
8000
7000
6000
5000
4000
3000
2000
1000
0
Ga
35
30
25
20
15
10
5
0
350
450
550
650
750
850
Concentration (ppm)
Depth in metres (sample number)

Figure 6: Chondrite-normalized REE profiles from the least altered leucogranite in DDH 90-1. The profiles are characterized by a high LREE content and a very strong negative Eu anomaly, and are consistent with the highly differentiated nature of the leucogranite in this hole. Main: average REE analyses of leucogranite from the Main Zone (Kontak 1990).

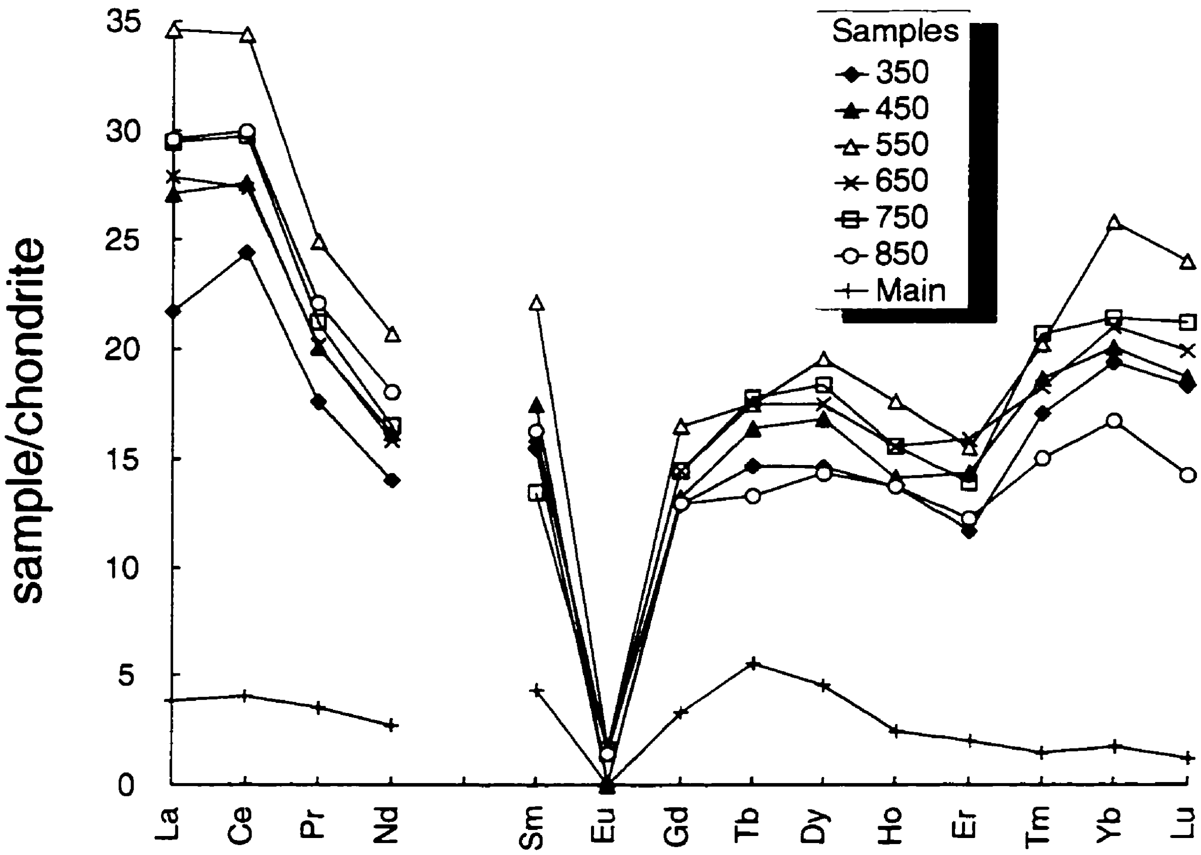
sample/chondrite
35
30
25
20
15
10
5
0
La
Ce
Pr
Nd
Sm
Eu
Gd
Tb
Dy
Ho
Er
Tm
Yb
Lu
Samples
350
450
550
650
750
850
Main

a higher F content, and thus a more evolved magma. The Eu content is close to zero, probably as a result of its early removal through fractional crystallization of plagioclase in the biotite monzogranite of the Davis Lake Pluton.

ALTERATION

Two types of greisen are distinguished at East Kemptville: zoned and massive. Zoned greisen formed around a central fracture and are up to a few meters wide. Massive greisens are several tens of meters wide and are the result of overlap of the alteration halos of numerous zoned greisens in highly fractured leucogranite. Petrographic observations revealed that the first alteration affecting the leucogranite (Fig. 7A) was replacement of K-feldspar. This occurred by the formation of "chess-board albite" in sericitized leucogranite (Fig 7B); locally K-feldspar was replaced completely (Fig. 7C). In K-feldspar-free rocks, albite was subsequently sericitized, and at an advanced stage of this alteration gave rise to an albite-K-feldspar-free quartz-sericite greisen (Fig. 7D). Close to veins and in highly altered zones, quartz-sericite greisen gives way to quartz-topaz greisen in which topaz replaced muscovite (Fig 7E). The immediate wall to veins is a quartz-greisen characterized by high quartz concentrations (Fig 7F). We interpret the alteration described above to reflect a single greisenizing event in which fluid of relatively constant initial composition reacted in varying proportions with homogeneous leucogranite at roughly constant temperature (see below).

The alteration facies discussed here are very similar to those described in a zoned greisen from the Main Zone (Chapter 2). We therefore used the spatial distribution of alteration facies observed in the zoned greisen to classify all the samples of the deep hole in order of increasing alteration, and thereby reconstruct an idealized alteration halo around a central vein (Fig. 8). In the leucogranite, samples were sorted by decreasing K-feldspar content with increasing alteration, as K-feldspar was replaced by albite (not observed in the zoned greisen but apparent from petrographic observations). Samples containing albite but no K-feldspar (sericitized leucogranite) were ordered by decreasing abundance of albite. Similarly, samples in the quartz-muscovite and the quartz-topaz

Figure 7: Photomicrographs of variably altered rocks. A. Least altered leucogranite containing quartz, muscovite, albite and K-feldspar. B. Partial replacement of K-feldspar by albite at the onset of the alteration. C. Complete replacement of K-feldspar by albite, which is, in turn, replaced by muscovite in the "albite zone". D., Quartz-muscovite greisen composed nearly exclusively of muscovite and quartz (albite was completely replaced by muscovite). E. Highly mineralized quartz-topaz greisen, formed after almost all the muscovite was replaced by topaz. F. Quartz-topaz greisen depleted in sulfides and cassiterite close to a vein. Scale bar: 0.25mm

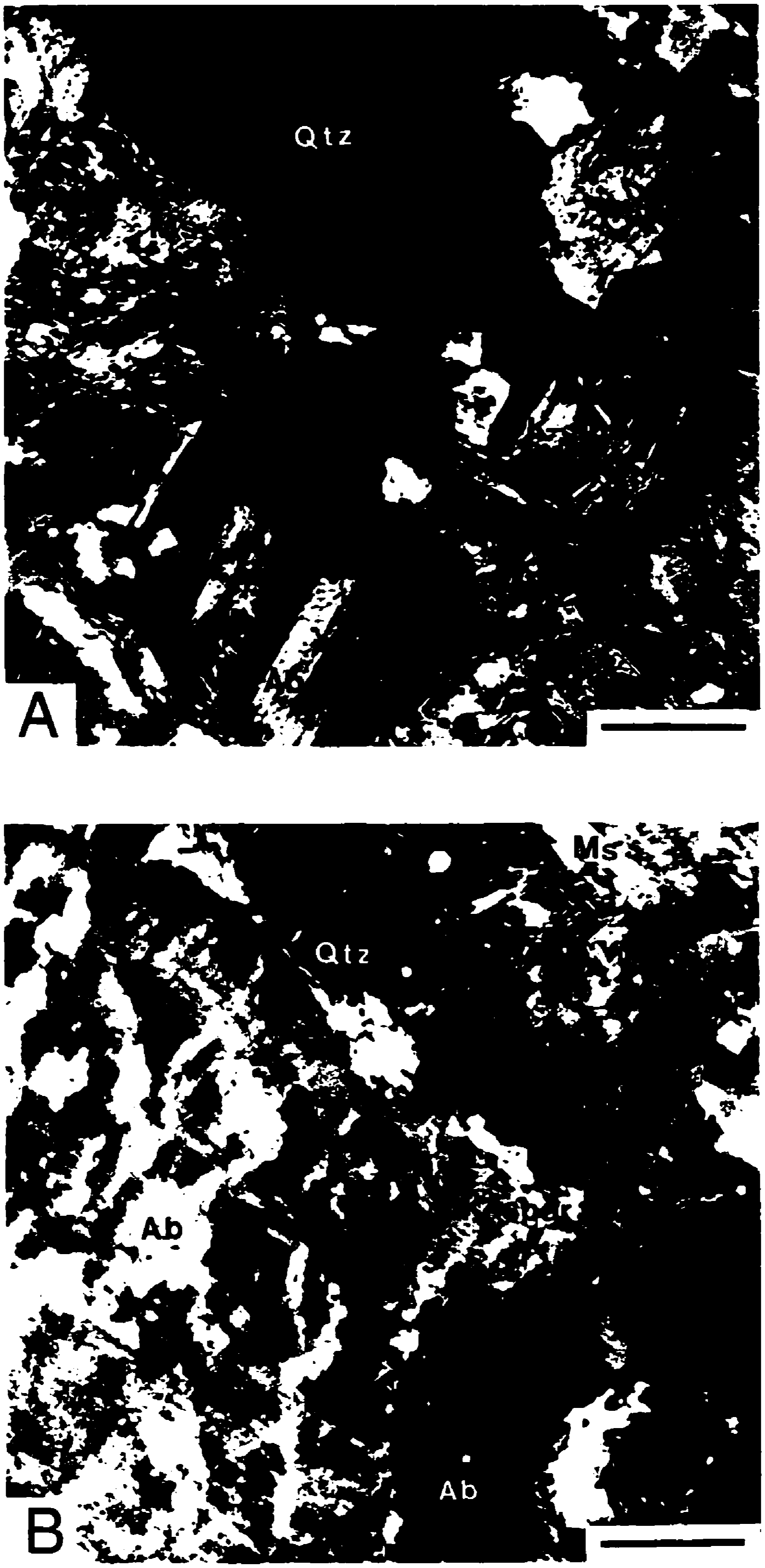
Qtz
Ab
A
Ms
Qtz
Ab
Ab
B

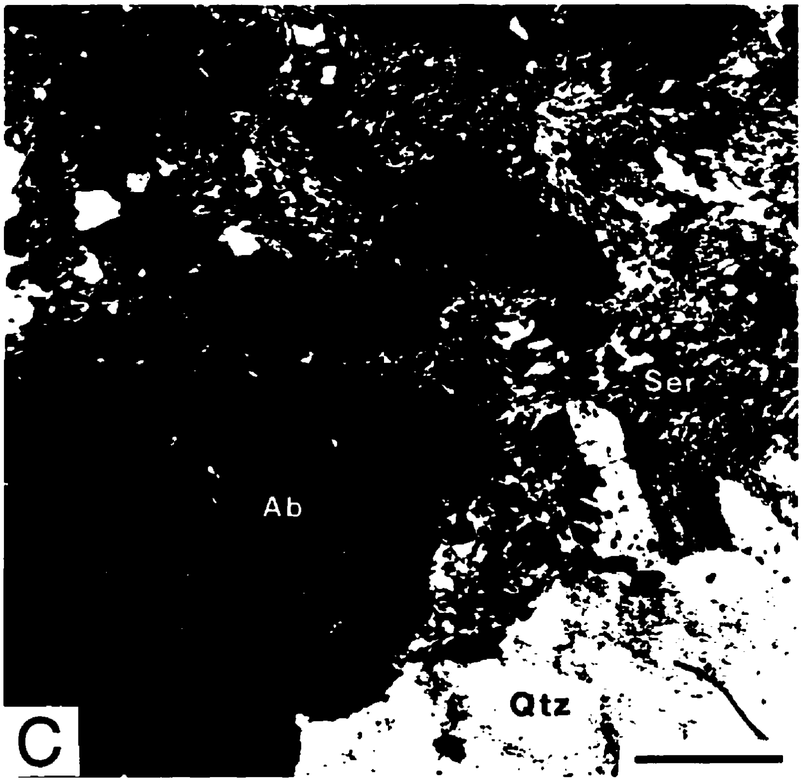
Ser
Ab
Qtz
C

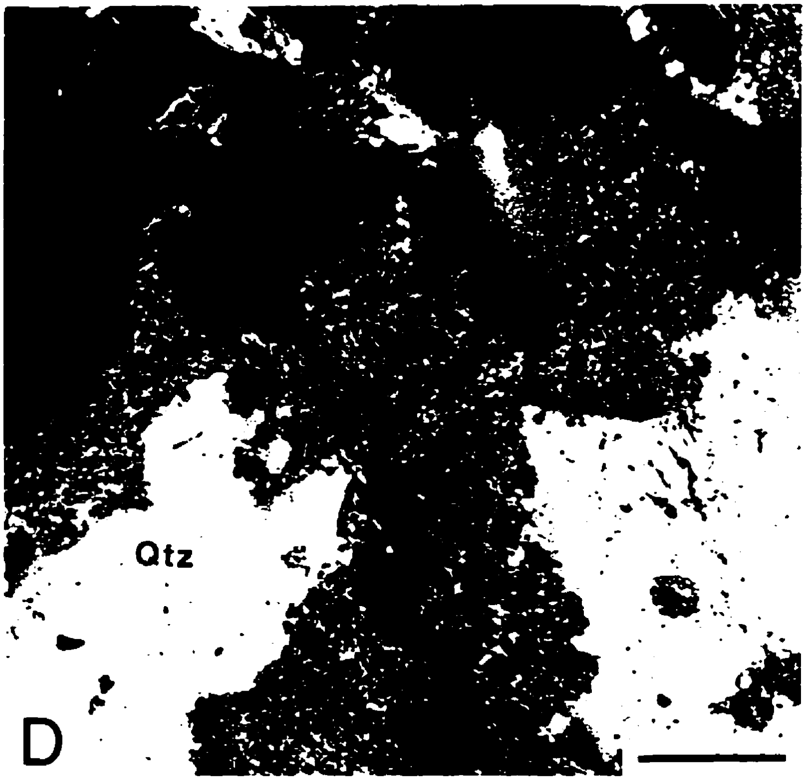
Qtz
D

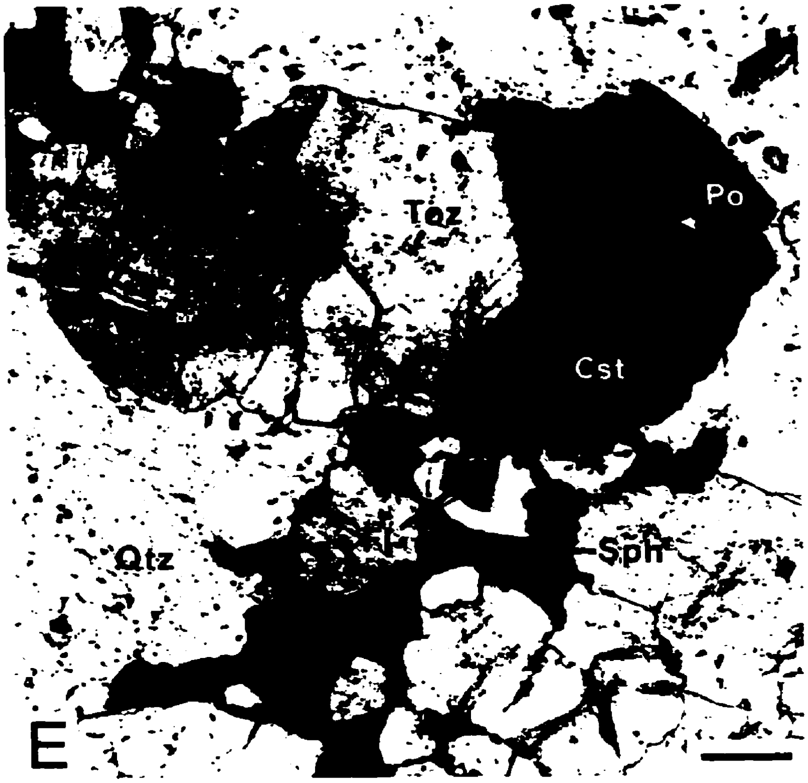
Tpz
Po
Cst
Fl
Qtz
Sph
E

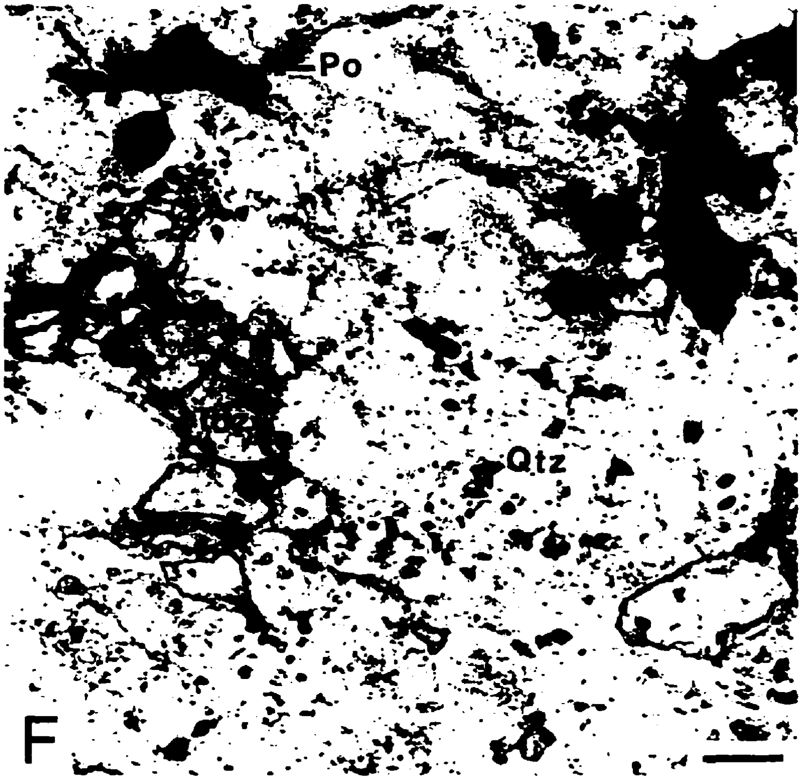
Po
Tpz
Qtz
F

greisen (albite free) were ordered by the decreasing abundance of muscovite. Only sample 10 was not sequenced according to this scheme. This sample contains more muscovite than samples 30 to 66, but was considered to reflect a higher degree of alteration because of its high quartz and low topaz and sulphide contents, i.e., to be similar to quartz-greisen observed next to veins. The mineralogical compositions required to order the samples were calculated using an inexact matrix equation that combines whole rock and microprobe mineral analyses (Spear et al.. 1982).

Since the number of samples taken in a specific alteration zone is arbitrary, the size of each zone needs also to be evaluated. This is commonly done by using a parameter (abundance of a phase or an element) which varies systematically with increasing alteration. Unfortunately, no such parameter could be found at East Kemptville. However, we showed that in a zoned greisen from the Main Zone (Chapter 2), decreases in the proportion of albite, where replaced by muscovite, and in the proportion of muscovite where replaced by topaz, are linear with distance from the vein. The same was shown to be true for quartz, which increases in proportion towards the vein. We used these relationships to approximate the degree of alteration of a sample in the deep hole, i.e., to establish the relative proximity of that sample to a hypothetical central vein. The spacing of samples in the ordered sequence of Figure 8 was accordingly adjusted in order to satisfy these linear trends as closely as possible. The left hand column in Figure 9 shows the changes in quartz, muscovite, albite and K-feldspar concentration assuming constant spacing of the samples, and the right hand column the concentration after adjusting the spacing. Also shown are correlation coefficients for linear regression assuming that a mineral concentration varies linearly with distance from the vein. It is evident from Figure 9 that once the spacing of samples is adjusted as described above, the distributions in the concentrations of all major minerals all vary linearly with distance from the vein; the concentration of quartz increases while those of K-feldspar, albite and muscovite all decrease.

The adjusted profile described above (Fig. 8) provides information about the effect of greisenization on the abundance of each minerals. Thus, at the onset of the alteration, (where K-feldspar decreases) the proportions of albite and quartz increase. Complete

Figure 8: Normative compositions of the analyzed samples in DDH 90-1. The abscissa indicates the depth at which the samples were taken (see text for an explanation of how the samples were ordered and spaced). Samples used for fluid inclusion analysis are framed.

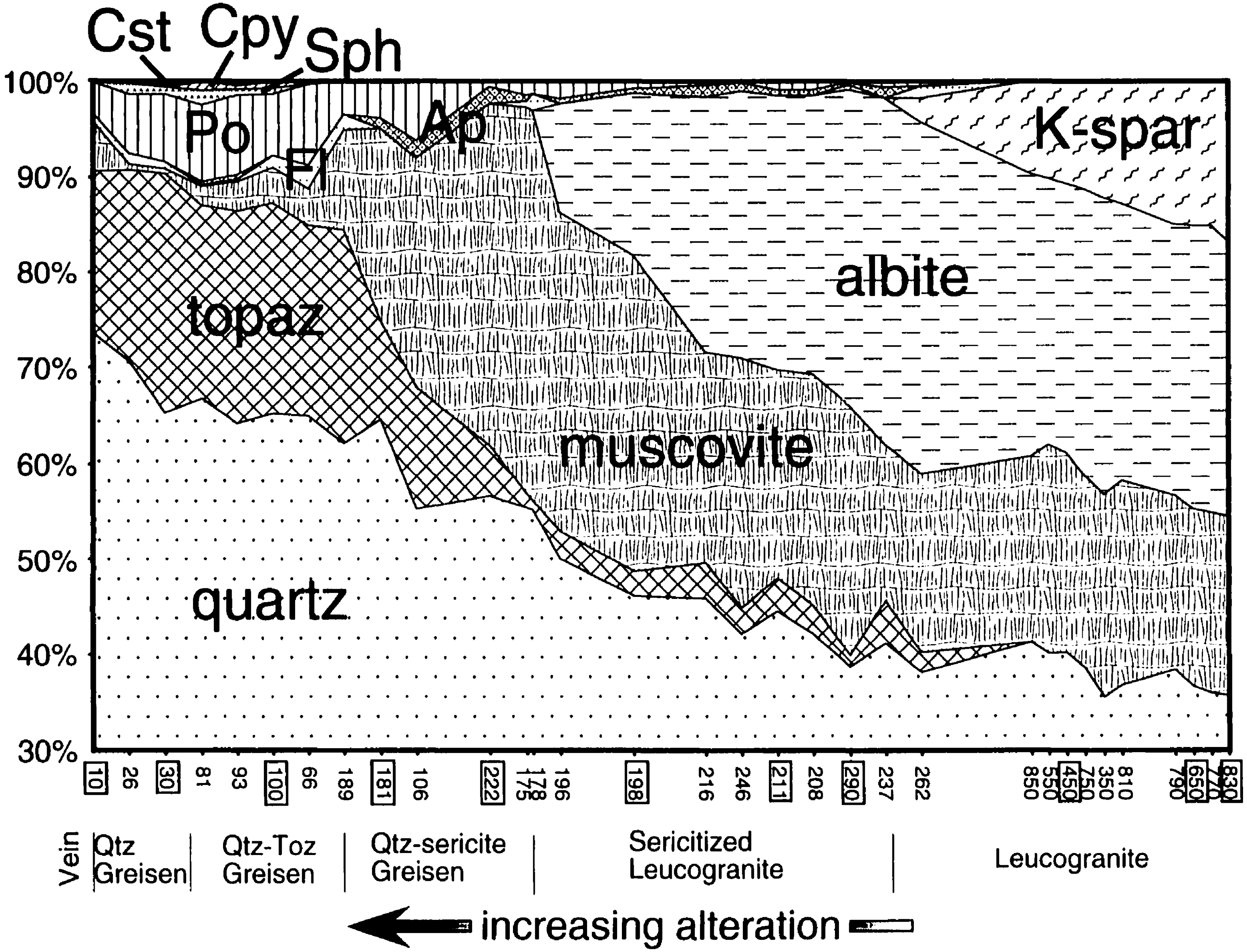
Cst
Cpy
Sph
Po
Fl
Ap
K-spar
albite
topaz
muscovite
quartz
100%
90%
80%
70%
60%
50%
40%
30%
10
26
30
81
93
100
66
189
181
106
222
175
178
196
198
216
246
211
208
290
237
262
850
550
450
750
350
810
790
650
770
830
Vein
Qtz Greisen
Qtz-Toz Greisen
Qtz-sericite Greisen
Sericitized Leucogranite
Leucogranite
increasing alteration

Figure 9: Distribution of quartz and muscovite in the greisens, quartz and albite in sericitized leucogranite and K-feldspar in relatively unaltered leucogranite, as a function of sample order and spacing. Samples in the diagrams on the left hand side are separated by a constant interval and those on the right a variable interval designed to produce the best linear correlations for each mineral (see text for further detail).

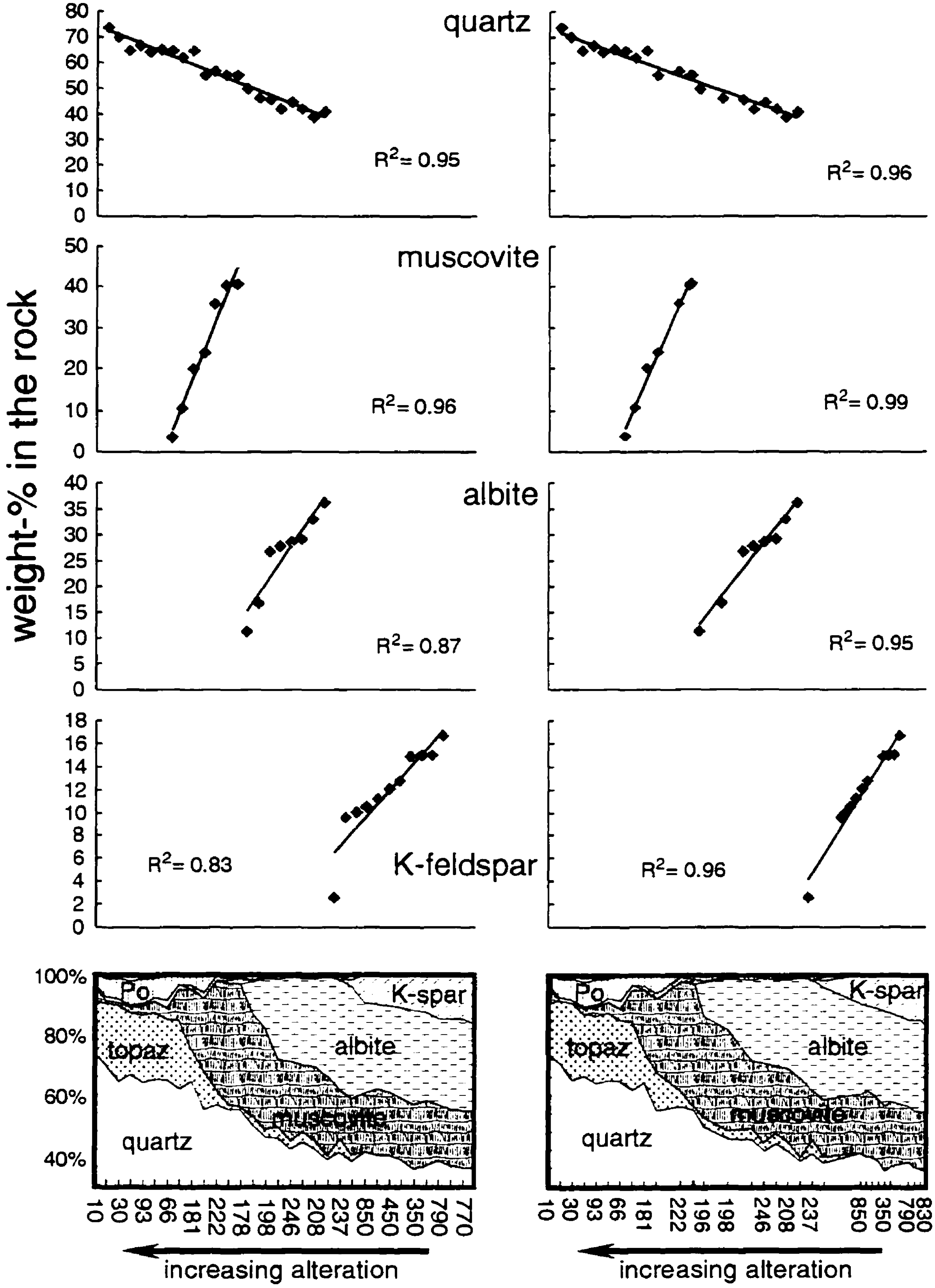
weight-% in the rock
quartz
R2= 0.95
R2= 0.96
muscovite
R2= 0.96
R2= 0.99
albite
R2= 0.87
R2= 0.95
K-feldspar
R2= 0.83
R2= 0.96
80
70
60
50
40
30
20
10
0
50
40
30
20
10
0
40
35
30
25
20
15
10
5
0
18
16
14
12
10
8
6
4
2
0
100%
80%
60%
40%
Po
K-spar
topaz
albite
muscovite
quartz
10 30 93 66 181 222 178 198 246 208 237 850 450 350 790 770
10 30 93 66 181 222 196 198 246 208 237 850 350 790 830
increasing alteration
increasing alteration

replacement of K-feldspar coincided with the first appearance of small proportions of topaz as an alteration product. With further alteration in the sericitized leucogranite, the proportions of topaz remained essentially unchanged. Trace amounts of pyrrhotite, apatite or fluorite can also be present in this interval. In the quartz-sericite greisen, pyrrhotite becomes increasingly important and trace amounts of cassiterite can be present. The dominant Ca-bearing phase in quartz-topaz greisen is fluorite, as opposed to apatite in less altered rocks, which presumably reflects an increase in the F-content of the mineralizing fluid. Another feature of this zone is that the proportions of pyrrhotite, sphalerite, chalcopyrite and cassiterite increase sharply and reach a maximum in sample 93. Further alteration is characterized by decreases in the proportion of these phases in the most altered rocks and by an increase in the proportion of quartz (quartz-greisen). This rock is evident as a sulphide-poor halo immediately adjacent to veins.

Despite the fact that the order of the samples is based only on the variation of muscovite, albite or K-feldspar, the abundance of all other phases displays the same variation as in the zoned greisen, thereby confirming that essentially the same alteration sequence affected the zoned greisen and the samples from drill hole 90-1.

CHEMICAL VARIATIONS

Variations in normative composition with increasing alteration are reflected in variations in the chemical composition of the rocks. In order to quantify changes that occurred in the rock during greisenization, the mass factor, i.e., the mass change that affected each altered sample, needed first to be determined. As noted earlier, most of the elements commonly considered to be immobile underwent some mobility, and therefore techniques normally used to determine the mass factor could not be applied (Grant, 1986; MacLean and Kranidiotis, 1986). However, quartz was almost certainly saturated in the mineralizing fluid due to previous interaction with the leucogranite, and since quartz solubility is dependent only on temperature (which remained constant, see below) except at extremes of pH (Seward, 1974), it follows that Si was effectively immobile during alteration. Assuming the latter to have been the case, the lack of significant variation in Si content among most of the samples indicates that the mass factor was close to one. The same conclusions, i.e., that Si was immobile and that the mass factor was close to unity, were reached in Chapter 2 for the zoned greisen from the Main Zone. The conclusion that the mass factor was close to one is also supported by the good linear correlation between La and Th in fresh and altered samples (Fig. 4). If the mass factor had been other than unity this would have caused departure from a linear relationship, as total mass gain or loss would have shifted the analyses of highly altered samples away from, or closer to the origin in Figure 4, respectively. For the above reasons, we suggest that, as a first approximation, no mass factor correction is necessary to compare chemical analyses of the leucogranite and the greisens. Only in samples 10 and 26, next to the vein, are contents of Si significantly higher, and this can be attributed to enhanced porosity adjacent to the vein: Mass factors of 1.13 and 1.07 were estimated for samples 10 and 26, respectively, based on the assumption of constant Si.

Variations in chemical composition that occurred during alteration are evaluated graphically in Figure 10 as percentage changes of an element added/depleted with respect to the average leucogranite. The abscissa orders and spaces the samples according to the criteria discussed earlier and shown in Figure 8. As indicated above, Si remained essentially unchanged during alteration; its increase close to the vein is due to a mass loss caused by the removal of sulphides in quartz greisen. Next to Si, Zr (not shown) was the most immobile element. Overall, Al was also largely immobile, but locally was enriched or depleted significantly. Calcium, likewise, did not vary systematically and was enriched only in quartz-sericite greisen, as is evident from the higher abundance of apatite in this zone. Magnesium and manganese were also enriched in the quartz-sericite greisen, although absolute concentrations remained very low (Table 3). Sodium, which is present only in albite, was enriched in the sericitized leucogranite and strongly depleted in the greisens. Potassium was depleted in the quartz-topaz greisen and in the albite zone, i.e., during the replacement of K-feldspar and muscovite; Rb which substitutes for K has a similar distribution. Fluorine, sulfur, iron, copper and zinc were all enriched significantly during alteration, but in the most altered rock, i.e., in the quartz greisen, the concentration of these elements is significantly lower than in slightly less altered rocks. This is evident by

Figure 10: Compositional variations with increasing alteration (right to left) of major and selected trace elements in bulk samples. Analyses were not corrected for mass change since the mass factor has been shown to be close to unity. Only the increase in Si in the most altered greisens is interpreted to reflect a change in total mass. This occurred due to the leaching of most other elements. See text for details of the profiles.

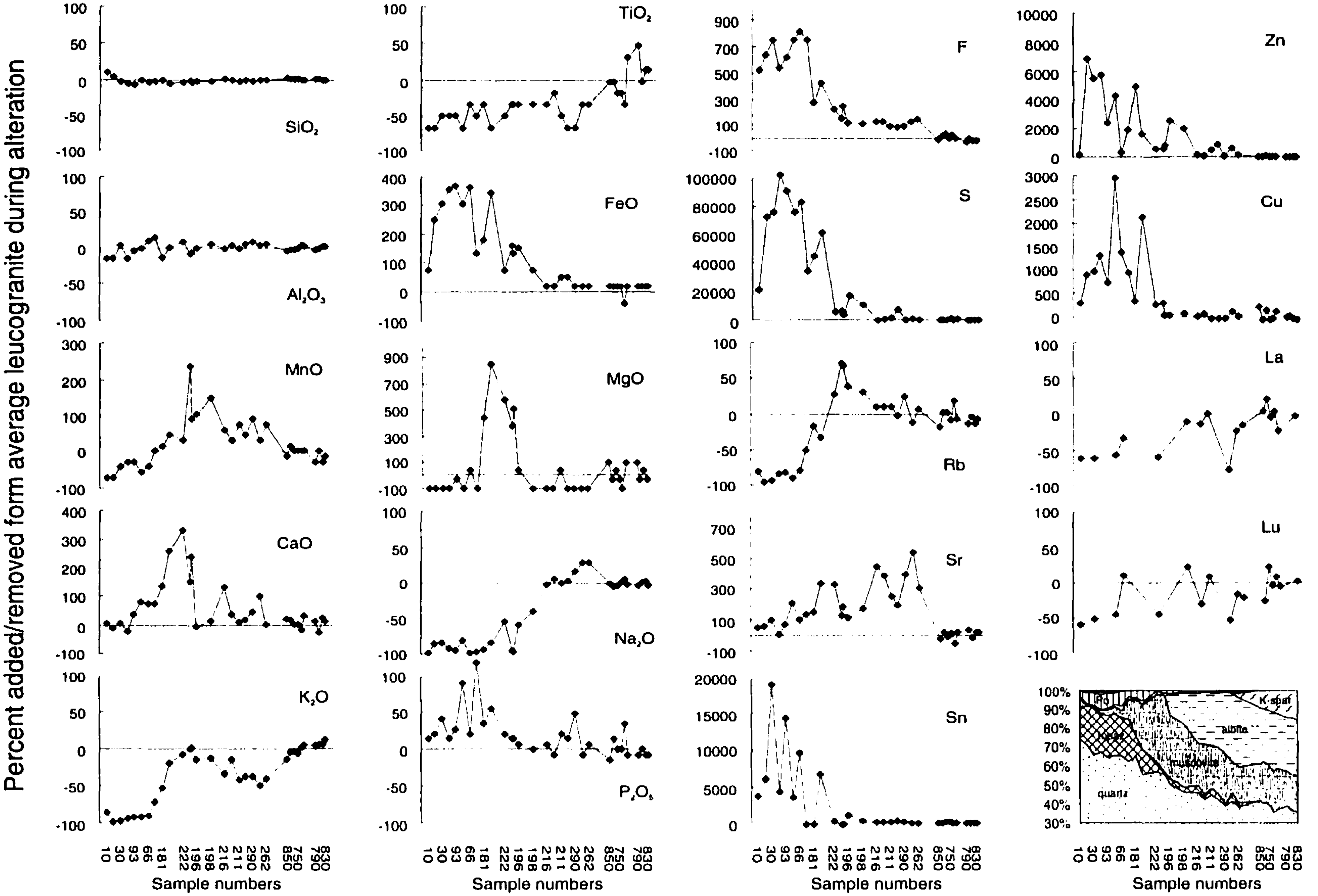Percent added/removed form average leucogranite during alteration
SiO₂
TiO₂
F
Zn
Al₂O₃
FeO
S
Cu
MnO
MgO
Rb
La
CaO
Na₂O
Sr
Lu
K₂O
P₂O₅
Sn
Ro
K-spar
albite
muscovite
quartz
100%
90%
80%
70%
60%
50%
40%
30%
10 30 93 66 181 222 196 198 216 211 290 262 850 750 790 830
Sample numbers
Sample numbers
Sample numbers
Sample numbers

the low abundance of sulphides. The REE and Ti appear to be depleted in quartz-topaz greisen, i.e., in the rocks where F is most abundant, suggesting mobility of these elements as fluoride complexes. Tin is most abundant in sulphide-rich quartz-topaz greisen; the erratic pattern is likely due to a nugget effect induced by the restriction of only being able to take small samples that can be taken from drill cores.

FLUID INCLUSIONS

Petrography

In order to obtain information on possible variations in the composition of the mineralizing fluid as a result of its interaction with the host rock, fluid inclusions were analyzed in 11 samples (framed in Figure 8) representing the different alteration zones in drill hole 90-1, and in one vein sample. Only quartz contained fluid inclusions large enough (5 to 30μm) for petrographic and microthermometric studies. All inclusion types described below are immature and are generally grouped in planar clusters or aligned on trails, suggesting a secondary origin. Some inclusions are isolated and could be primary, but compositionally these inclusions resemble secondary inclusions and were therefore considered to be of the same generation.

Fluid inclusions in vein material consist of liquid, vapour and one or two solids (L-V-S±H). The most common solids are small, rounded birefringent crystals with high relief and may be a Fe-chloride mineral. This is suggested by the high Fe and Cl content of fluid inclusion leachates and decrepitates (see below). Only a small proportion (5-10%) of these inclusions are halite-bearing, but there is no obvious difference in the nature and the distribution of halite and non-halite bearing inclusions. In the greisens, a vast majority of fluid inclusions contain liquid, vapour, halite, and a second solid (L-V-H±S). The second solid, which forms small rounded birefringent crystals, is present in all large inclusions and, as in veins, is interpreted to be a Fe-chloride mineral. This solid is commonly not visible in small inclusions, but this may reflect its small size rather than its absence from the inclusions. In view of the above, both halite and the Fe-chloride mineral are considered to be daughter minerals. In addition to L-V-H-S inclusions, some secondary L-V inclusions are aligned along planes in quartz in the greisen samples, but these do not exceed 2-3% of the fluid inclusion population. Most fluid inclusions in the freshest leucogranite (95%) contain liquid, vapour and the small birefringent solid (Fe-chloride), but generally no halite (L-V±S). The remaining 5% are L-V inclusions similar to those in the greisens.

Microthermometry

Microthermometric data for the fluid inclusions are given in Table 4. Temperatures of vapour disappearance (the temperature of homogenization between the liquid and the vapour phase $Th_{(L-V)}$) distinguish two populations with maxima at 150°C and at 250°C (Fig. 11). The low temperature population comprises L-V inclusions (light gray in Fig. 11) in the greisen and the leucogranite, whereas the high $Th_{(L-V)}$ population consists of solid-bearing fluid inclusions hosted by the vein, greisens and the leucogranite. If the latter population is subdivided by host rock, it is evident that the $Th_{(L-V)}$ distributions are very similar except in the leucogranite where $Th_{(L-V)}$ is generally slightly lower (Fig. 11). This indicates that there was only one important episode of greisenization, and that temperature was similar in the vein and the greisens.

Temperatures of halite dissolution (Td_{halite}) vary between 150 and 300°C, and are lower than those of disappearance of the vapour phase in samples close to the vein (Fig. 12). The opposite is true in sericitized leucogranite where the vapour phase disappears first, because of a higher salinity (see below). In Figure 12, apparent trends in each alteration zone are not significant and caused only by a few samples. Salinities of L-V-H-S inclusions were calculated from the halite dissolution temperatures, and vary between 29 and 38 wt.% NaCl equivalent using the equation of Zhang and Franz (1987) for the system NaCl-KCl-H_2O (solid symbols in Fig. 13A). No halite is present in the freshest leucogranite or in the vein. In L-V-S inclusions hosted by these samples, salinity was calculated from hydrohalite and ice melting temperatures using the equation developed by Sterner et al., (1988) for the system NaCl-KCl-H_2O (Table 4). These salinities vary

Table 4: Microthermometric data from fluid inclusions

Sample	Type	T_e	Tm_{ice}	$Th_{(l-V)}$	T_{Hdiss}	T_{S2diss}	T_{HHdiss}	NaCl eq. (Wt-%)		
								$T_{H\,diss}$	Tm_{ice}	$T_{HH\,diss}$
90-1-10	L-V	-25	-21.2				-16			27.1
90-1-10	L-V	-25	-21.1	185			-19.6			26.5
90-1-10	L-V	-30	-6.1				-0		9.4	
90-1-10	L-V-H	-39	-30.5							
90-1-10	L-V-H-S	-42	-31.2	292						
90-1-10	L-V-H-S	-42	-26.5				-0			
90-1-10	L-V-H-S	-42	-26.5							
90-1-10	L-V-H-S	-38	-27.0	310						
90-1-10	L-V-H-S	-35	-24.8	285						
90-1-10	L-V-H-S	-41	-26.0				-0			
90-1-10	L-V-H-S	-40	-24.5		181	-385		30.9		
90-1-10	L-V-H-S-S	-50	-32.0	246	226		-0	33.3		
90-1-30	L-H-S			247	155			29.9		
90-1-30	L-V		-3.2	152						
90-1-30	L-V-H	-47	-28.0	252	200			31.9		
90-1-30	L-V-H	-45	-26.3							
90-1-30	L-V-H	-48	-27.7							
90-1-30	L-V-H			280	190			31.4		
90-1-30	L-V-S		-5.0							
90-1-30		-55	-40.0	229	145			29.5		
90-1-74.7	L-V	-28	-22.5	290					24.4	
90-1-74.7	L-V	-29	-22.5	247					24.4	
90-1-74.7	L-V	-43	-26.2	228			-0			
90-1-74.7	L-V	-44	-24.5	275			-16.9			27.0
90-1-74.7	L-V	-30	-23.0							
90-1-74.7	L-V		-23.1	295						
90-1-74.7	L-V-S	-28	-21.7						23.8	
90-1-74.7	L-V-S	-30	-22.5	255					24.4	
90-1-74.7	L-V-S	-29	-22.4	268					24.3	
90-1-74.7	L-V-S	-25	-22.5	258					24.4	
90-1-74.7	L-V-S	-23	-22.1	250					24.1	
90-1-74.7	L-V-S	-28	-22.8						24.5	
90-1-74.7	L-V-S	-47	-24.2				-19.9			26.5
90-1-100	L-V	-50	-25.5							
90-1-100	L-V			225						
90-1-100	L-V			235						
90-1-100	L-V			229						
90-1-100	L-V			235						
90-1-100	L-V			235						
90-1-100	L-V-H	-50	-33.3							
90-1-100	L-V-H	-55	-33.0	223	165		-41.8	30.3		
90-1-100	L-V-H	-50		236	152		-39.5	29.7		
90-1-100	L-V-H				168			30.4		
90-1-100	L-V-H			260	183			31.1		
90-1-100	L-V-H				165			30.3		
90-1-100	L-V-H				180			30.9		
90-1-100	L-V-H	-52	-33.2							
90-1-100	L-V-H	-54	-32.3		178			30.8		
90-1-100	L-V-H	-50	-31.2		152			29.7		
90-1-100	L-V-H	-53	-29.5	232	134			29.1		
90-1-100	L-V-H	-62	-42.9	310	207			32.2		
90-1-100	L-V-H	-60	-41.5	290	207			32.2		
90-1-100	L-V-H	-52	-37.0							
90-1-100	L-V-H			275	157			29.9		
90-1-100	L-V-H			277	153			29.8		
90-1-100	L-V-H				170			30.5		
90-1-100	L-V-H			330	212			32.5		
90-1-100	L-V-H			235	142			29.4		
90-1-100	L-V-H				150			29.7		
90-1-100	L-V-H				160			30.1		
90-1-100	L-V-H				165			30.3		
90-1-100	L-V-H				173			30.6		
90-1-100	L-V-H-S	-55	-39.3							
90-1-100	L-V-H-S	-52	-32.5							
90-1-100	L-V-H-S			270	145			29.5		
90-1-181	L-V-H	-53	-33.1	243	154			29.8		
90-1-181	L-V-H				212			32.5		
90-1-181	L-V-H			235						
90-1-181	L-V-H			252	247			34.5		
90-1-181	L-V-H			245	237			33.9		
90-1-181	L-V-H			254	224			33.1		
90-1-181	L-V-H			257	227			33.3		
90-1-181	L-V-H-S	-50	-31.7	290	259			35.3		
90-1-181	L-V-H-S	-50	-31.0							
90-1-181	L-V-H-S			258	273			36.2		
90-1-181	L-V-H-S	-53	-32.9	232	200			31.9		
90-1-181	L-V-H-S			325		390				
90-1-181	L-V-H-S	-52	-32.5	160	215			32.7		
90-1-181	L-V-H-S			245	240	340		34.1		
90-1-181	L-V-H-S	-53	-28.8							
90-1-181	L-V-H-S	-51	-30.5	245	246	330		34.4		
90-1-181	L-V-H-S				176			30.7		
90-1-181	L-V-H-S			339						
90-1-181	L-V-H-S-S	-45	-31.0	225						
90-1-181	L-V-H-S-S	-50	-29.2	230	220			32.9		
90-1-198	L-V-H			215	195			31.6		
90-1-198	L-V-H-S	-44	-24.7	230	180			30.9		

Table 4cont.: Microthermometric data from fluid inclusions

Sample	Type	T_e	Tm_{ice}	$Th_{(L-V)}$	T_{Hdiss}	T_{S2diss}	T_{HHdiss}	NaCl eq. (Wt-%)		
								$T_{H diss}$	Tm_{ice}	$T_{HH diss}$
90-1-198	L-V-H-S	-42	-26.4	250						
90-1-198	L-V-H-S	-39	-24.0	242	310			38.9		
90-1-198	L-V-H-S	-50	-32.0	260	240			34.1		
90-1-212	L-V-H	-40	-28.5	250						
90-1-212	L-V-H			201	269			35.9		
90-1-212	L-V-H			210						
90-1-212	L-V-H			220						
90-1-212	L-V-H			270						
90-1-212	L-V-H			238						
90-1-212	L-V-H			215						
90-1-212	L-V-H			224	269			35.9		
90-1-212	L-V-H-S	-40	-27.4	180	140		29.2			
90-1-212	L-V-H-S		-24.5	268						
90-1-212	L-V-H-S	-42	-26.8	228						
90-1-212	L-V-H-S	-42		220	270			36.0		
90-1-212	L-V-H-S	-40	-26.3		300			38.2		
90-1-212	L-V-H-S		-25.2	215	257			35.1		
90-1-222	L-V-H			180						
90-1-222	L-V-H			265						
90-1-222	L-V-H			310	298			38.0		
90-1-222	L-V-H-S	-48	-30.0	185	200			31.9		
90-1-222	L-V-H-S	-47	-30.8	206	212			32.5		
90-1-222	L-V-H-S	-50	-31.2							
90-1-290	L-V-H			220						
90-1-290	L-V-H			230						
90-1-290	L-V-H-S	-48	-29.3	285	240			34.1		
90-1-290	L-V-H-S	-36	-24.7	210	230	410		33.5		
90-1-290	L-V-H-S	-37	-25.6							
90-1-290	L-V-H-S	-36.5	-24.3							
90-1-290	L-V-H-S			236	308			38.8		
90-1-290	L-V-S	-26	-19.6	139	-350				22.1	
90-1-450	L-V	-33	-23.8	233						
90-1-450	L-V-H			285						
90-1-450	L-V-H			287						
90-1-450	L-V-H			261	299			38.1		
90-1-450	L-V-H-S	-33	-25.4	234	277	413		36.5		
90-1-450	L-V-H-S			265	285			37.0		
90-1-450	L-V-H-S			273	335			41.0		
90-1-450	L-V-H-S	-38	-25.7	211	288			37.3		
90-1-450	L-V-H-S	-34	-22.9	233	280			36.7		
90-1-450	L-V-S	-32	-21.5	134						

Sample	Type	T_e	Tm_{ice}	$Th_{(L-V)}$	T_{Hdiss}	T_{S2diss}	T_{HHdiss}	NaCl eq. (Wt-%)		
								$T_{H diss}$	Tm_{ice}	$T_{HH diss}$
90-1-650	L-V			247						
90-1-650	L-V	-32	-7.5	153					11.1	
90-1-650	L-V		-13.8				-22		17.6	
90-1-650	L-V	-33	-12.5	180					16.5	
90-1-650	L-V	-29	-14.0	211			-22.1		17.8	
90-1-650	L-V	-28.5	-14.3	193			-21.8		18.1	
90-1-650	L-V-S	-28	-19.0	264			-22.3			26.6
90-1-650	L-V-S	-29	-19.4	242			-23			26.6
90-1-650	L-V-S	-28	-18.9	219			-22.7			26.7
90-1-650	L-V-S	-28	-19.0	267			-23.2			26.6
90-1-650	L-V-S	-29	-7.6	142			-21.5		11.3	
90-1-650	L-V-S	-28	-7.5	148					11.1	
90-1-650	L-V-S	-36	-14.1	128					17.9	
90-1-650	L-V-S-S	-29		262			-23.3			
90-1-830	L-V	-32	-6.1	188			-23		9.4	
90-1-830	L-V	-32	-5.2	123			-20.9		8.1	
90-1-830	L-V-H-S		-22.5	222		-450			25.2	
90-1-830	L-V-H-S	-27	-23.3	173						
90-1-830	L-V-S	-30	-23.1						25.9	
90-1-830	L-V-S		-24.4	255		-375				
90-1-830	L-V-S	-29	-22.2	218			-12		25.2	
90-1-830	L-V-S	-30	-22.7	240			-0		27.0	
90-1-830	L-V-S	-34	-23.2	216			-0		27.0	
90-1-830	L-V-S	-31	-23.2	251			-0		27.0	
90-1-830	L-V-S	-30	-23.0	261			-0		27.0	
90-1-830	L-V-S		-23.0	236			-0		27.0	
90-1-830	L-V-S	-30	-22.7	158			-10.8		25.4	
90-1-830	L-V-S	-30	-22.3	140			-0		27.0	
90-1-830	L-V-S	-32	-24.0	146			-10		25.5	
90-1-830	L-V-S		-22.2				-0		27.0	
90-1-830	L-V-S			137						
90-1-830	L-V-S			150						
90-1-830	L-V-S			155						
90-1-830	L-V-S			145						
90-1-830	L-V-S			211						

T_e Eutectic temperature
Tm_{ice} Final ice melting temperature
$Th_{(L-V)}$ Temperature of homogenization between the liquid and the vapour phase
T_{Hdiss} Temperature of halite dissolution
T_{S2diss} temperature of dissolution of the second solid
T_{HHdiss} Temperature of hydrohalite dissolution
NaCl eq (Wt-%) Claculated salinity in equivalent NaCl using $T_{H diss}$, Tm_{ice} or $T_{HH diss}$

Figure 11: Histogram of the distribution of liquid-vapour homogenization temperatures $Th_{(L-V)}$ of fluid inclusions in quartz from selected samples in a vein and the various alteration zones. Two populations are distinguished: one with a peak at 150°C, consisting of low salinity two phase inclusions (light gray) and another with a peak at 250°C, comprising high salinity inclusions (dark gray). Histograms of $Th_{(L-V)}$ in individual zones of the alteration halo indicate that temperature was constant in the greisen, but decreased slightly in the outer parts of the alteration halo.

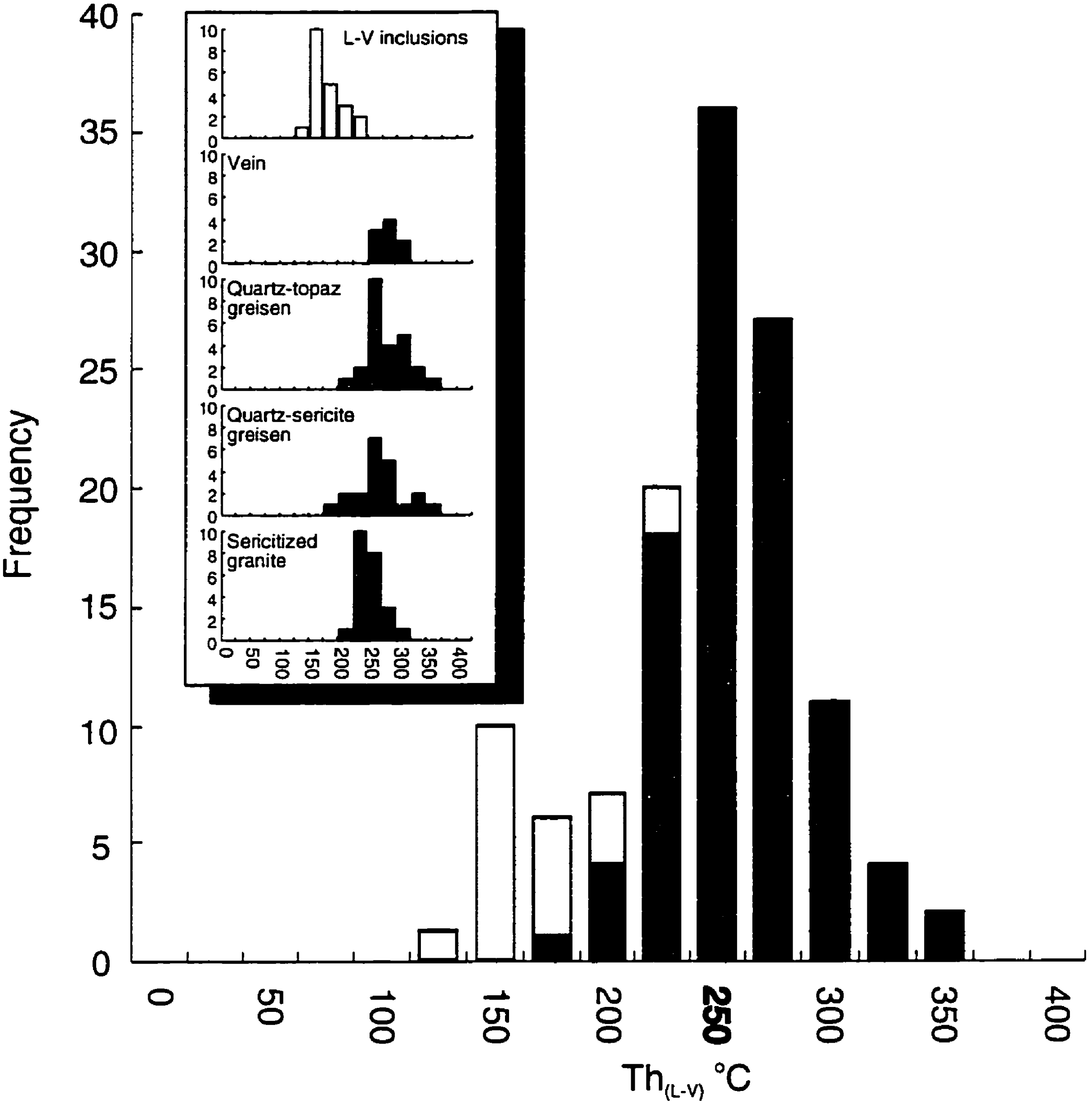
Frequency
40
35
30
25
20
15
10
5
0
0
50
100
150
200
250
300
350
400
Th(L-V) °C
L-V inclusions
Vein
Quartz-topaz greisen
Quartz-sericite greisen
Sericitized granite
10
8
6
4
2
0
0
50
100
150
200
250
300
350
400

Figure 12: A plot of halite dissolution temperatures (Td_{Halite}) vs liquid-vapour homogenization temperature ($Th_{(L-V)}$) of L-V-H-S fluid inclusions. The dashed line indicates $Td_{Halite} = Th_{(L-V)}$.

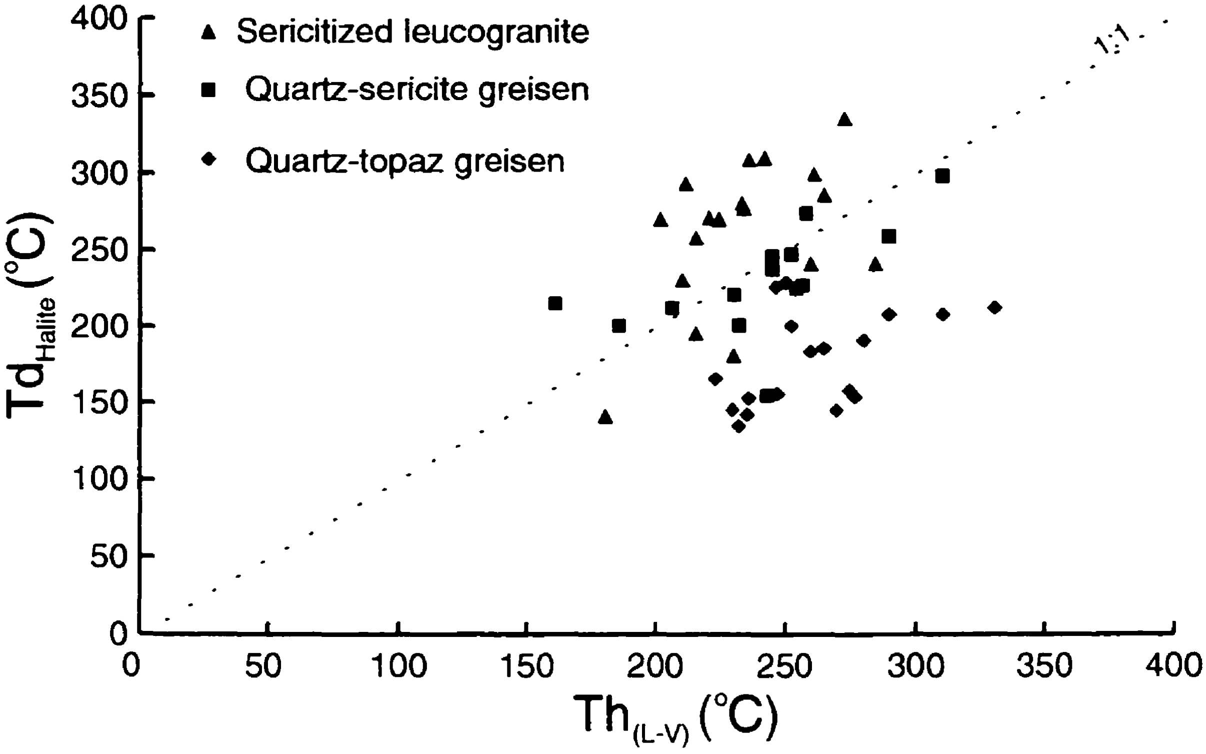

400
350
300
250
200
150
100
50
0
▲ Sericitized leucogranite
■ Quartz-sericite greisen
◆ Quartz-topaz greisen
1:1
Td_{Halite} (°C)
0
50
100
150
200
250
300
350
400
$Th_{(L-V)}$ (°C)

between 25 and 27 wt-% NaCl equivalent (open symbols in Fig. 13A) in the system NaCl-KCl-H_2O (Sterner et al., 1988). The NaCl/(NaCl+KCl) ratio used in these calculations was 0.95 and was based on an estimate of KCl molality of 0.08 made from calculations of muscovite solubility (Chapter 7). It is apparent from Figure 13A, that salinities of fluid inclusions increase steadily towards less altered rock but drop to lower values in the freshest leucogranite, i.e. in the presence of K-feldspar.

The second solid (Fe-chloride) dissolves at temperatures between 390 and 413°C, but this could only be observed in very few inclusions before decrepitation. Salinities of L-V inclusions (not shown in Figure 13A) vary between 9 and 17wt-% NaCl equivalent and average around 11 wt-% NaCl equivalent. These inclusions, which form a very small proportion of the fluid inclusion population, probably represent a later event. They will therefore not be discussed further here.

Temperatures of final ice melting (Tm_{ice}) in L-V-H-S inclusions and eutectic temperatures (T_e) of all inclusions are plotted in Figure 13B as a function of alteration. Eutectic temperatures initially decrease away from the vein, i.e., from -27°C to a minimum of -50°C, and then increase steadily towards less altered rock. Low values of T_e are generally interpreted to reflect the presence of appreciable $CaCl_2$ in the fluid. However, analyses of the residues of decrepitated fluid inclusions (see below), which provide little evidence of significant Ca, require an alternative explanation. We suggest that the low eutectic temperatures result from the presence of significant amounts of Fe, Mg and Mn, which are present in relatively high concentrations in analyses of fluid inclusion decrepitates (see below). Since determination of T_e depends on the ability to detect the onset of melting in the fluid inclusions, the variations in T_e probably reflect variations in the concentration of Fe, Mg and Mn in the fluid, i.e., the proportion of liquid formed at the eutectic, rather then an actual variation in T_e. Similarly, in the presence of halite, Tm_{ice} is a measure of the peritectic at which ice disappears. Since a peritectic is depressed with increasing complexity of a system, the decrease in Tm_{ice} also reflects addition of components to the mineralizing fluid.

Figure 13: A: Calculated salinities of fluid inclusions in wt% NaCl equivalent using halite dissolution temperature (solid symbols) and final ice melting and hydrohalite dissolution temperatures (open symbols). Samples are plotted as a function of alteration. Dashed lines represent the normative mineral boundaries from Figure 2. B: Eutectic temperature (Te) and temperature of final ice melting (Tm_{ice}) of fluid inclusions as a function of alteration. Both Te and Tm_{ice} show a minimum between samples 30 and 100, i.e., in the zone with the highest sulphide content, suggesting that the fluid has its highest concentration of Na and Fe in this zone. Dotted lines represent the normative mineral boundaries from Figure 8.

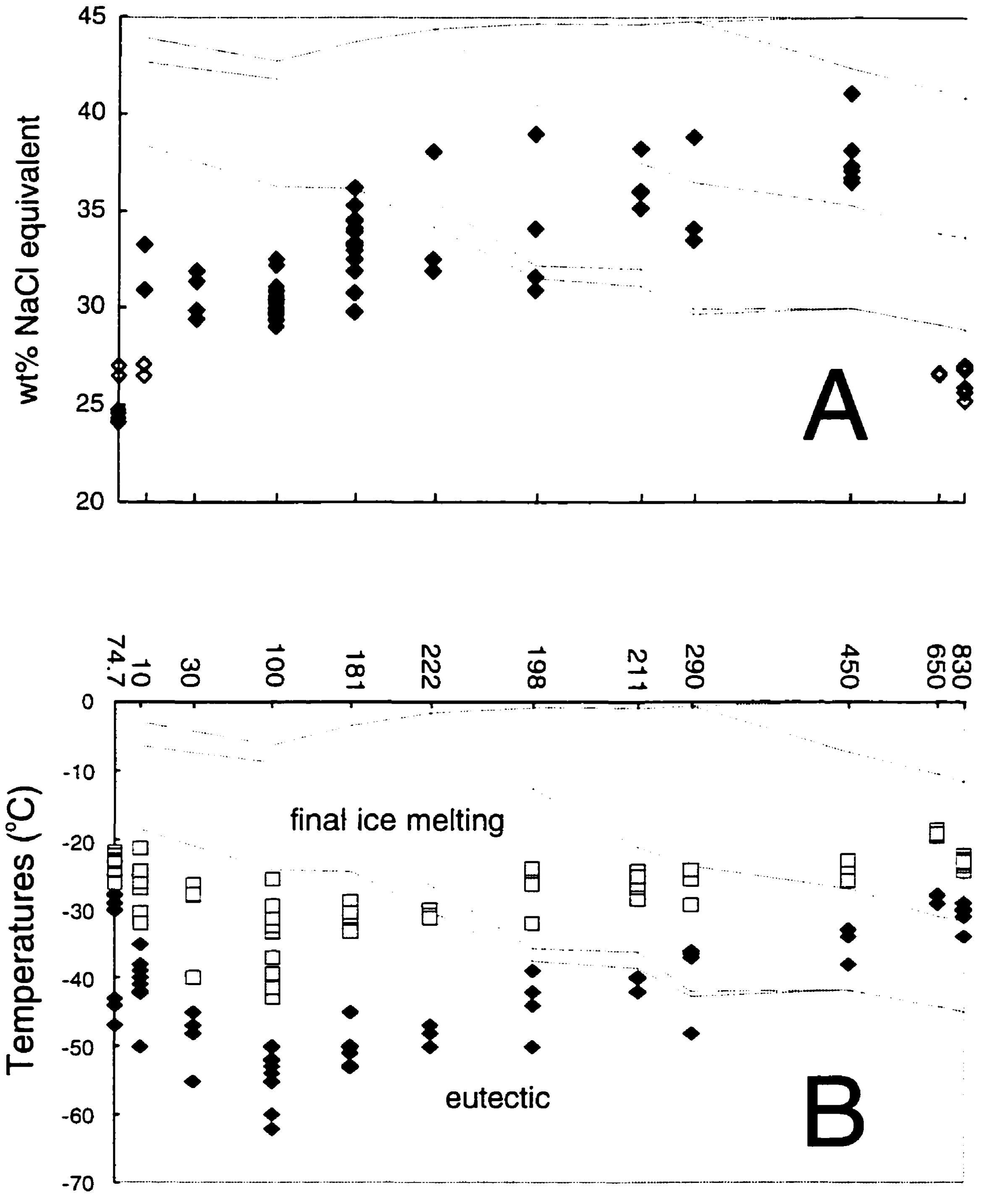
45
40
35
30
25
20
wt% NaCl equivalent
A
74.7
10
30
100
181
222
198
211
290
450
650
830
0
-10
-20
-30
-40
-50
-60
-70
Temperatures (°C)
final ice melting
eutectic
B

Decrepitates

Additional data on the compositions of the mineralizing fluid were obtained from analyses of residues of decrepitated fluid inclusions using an energy dispersive system (EDS) detector attached to a scanning electron microscope. Results of these decrepitate analyses are reported in Table 5, and shown graphically as a function of alteration in Figure 14. It is apparent from this figure that the fluid contains mainly Na and Cl throughout the entire alteration halo. Close to the vein, the fluid also contains appreciable Fe and Mn but both become decreasingly important away from the vein. The proportion of these components also appears to be lower in the vein than in the greisens. Potassium is significant only in sample 222 and those further away from the vein, i.e., in samples with significant muscovite. The distributions of Ca and S concentrations are similar to those of K but the maximum levels are much lower and the analyses for these elements might not be significant, i.e., the analytical errors are quite high and values below one to two percent are not considered reliable.

Leachate analyses

In order to further document the composition of the mineralizing fluid and particularly to better evaluate the variation in Na, Cl, and Fe concentration with alteration, we crushed selected samples and analyzed leachates from fluid inclusions. Several procedures have been described for sample preparation (Roedder, 1958; Shepherd et al., 1985a, Botrell et al., 1988). All these require preliminary cleaning of the samples to eliminate adsorbed species that could contaminate the leachate. This cleaning is usually achieved using an electrolytic cleaning cell as described in Roedder (1958). We modified this cleaning step by washing the samples (in our case quartz grains) in hot concentrated nitric acid for two hours, followed by a one hour wash in de-ionized water, and then we repeated the procedure. The acid wash creates a highly positive charge on the surface of the quartz grains, thereby effectively repelling most singly- or doubly-charged cations. More highly charged cations can, however, still be adsorbed on the surface after the acid wash.

Table 5: Analyses of fluid inclusion decrepitation residues (in wt-%)

Sample	host	Na	K	Cl	Ca	Fe	Mn	S	Zn	Mg
74.7	Toz	62	1	36	0	0	0	1	0	
74.7	Toz	61	1	37	0	0	0	1	0	
74.7	Toz	59	4	34	0	0	0	3	0	
74.7	Toz	60	5	35	0	0	0	0	0	
74.7	Toz	60	2	36	0	0	0	1	0	
74.7	Toz	55	2	37	0	3	2	0	1	
30	Qtz	61	0	38	0	0	0	1	0	
30	Qtz	59	2	39	0	0	0	0	0	
30	Qtz	56	0	36	0	3	4	0	0	
30	Qtz	59	0	37	0	1	0	1	0	
30	Qtz	55	0	38	1	2	3	1	0	
30	Qtz	57	0	38	0	1	2	1	0	
30	Qtz	58	0	38	0	1	1	0	0	
30	Qtz	49	1	32		4	5	1	1	
30	Qtz	47	0	40	3	5	4	0	1	
30	Qtz	44	0	29		8	8	0	2	
100	Qtz	32	1	59	1	5	2	0	1	
100	Qtz	54	1	39	0	2	3	1	1	
100	Qtz	47	2	37	1	6	7	0	1	
100	Qtz	51	1	44	0	2	2	0	0	
100	Si glass	59	1	37	0	1	1	1	0	
100	Si glass	50	7	30	0	5	5	1	2	
181	Qtz	63	0	34	0	1	1	0	1	
181	Qtz	55	1	39	0	1	2	1	1	
181	Qtz	61	1	36	0	0	1	0	0	
181	Qtz	57	0	40	0	1	0	0	1	
181	Qtz	53	1	43	0	2	0	1	1	
181	Qtz	54	1	41	0	1	2	0	1	
181	Qtz	60	1	38	0	1	1	0	0	
181	Qtz	60	0	38	0	0	0	0	0	
181	Qtz	62	0	37	0	0	1	1	0	
181	Qtz	52	1	41	0	2	3	0	0	
181	Qtz	57	1	38	0	1	2	1	0	
181	Qtz	58	1	38	1	0	2	1	0	
198	Si glass	42	3	54	0	0	0	0	0	
198	Si glass	44	1	55	0	0	0	0	0	
198	Si glass	45	1	52	0	0	0	1	1	
198	Qtz	37	7	55	1	0	0	0	0	
198	Qtz	39	13	45	2	0	0	2	0	
198	Qtz	46	4	44	4	2	0	0	0	
198	Qtz	25	5	46	1	1	0	1	0	
198	Qtz	22		46	0	0	0	1	0	
198	Qtz	41	8	41	1	0	0	1	0	
198	Qtz	42	3	51	1	1	0	2	0	
222	Qtz	44	6	47	3	0	0	0	1	21
222	Qtz	45	9	40	0	0	6	0	0	0
222	Qtz	41	12	42	1	1	0	2	1	6
222	Qtz	43	5	41	4	0	3	4	0	0
222	Qtz	43	19	35	3	0	0	0	0	2
450	Qtz	45	3	45	0	2	3	0	0	2
450	Qtz	46	2	47	1	1	1	1	2	0
450	Qtz	42	8	50	0	0	0	0	0	0
450	Qtz	44	7	43	0	0	0	0	0	6
450	Qtz	40	7	47	2	2	0	3	0	0
450	Qtz	45	0	49	1	1	0	2	0	2

Figure 14: Concentrations of major components in residues of decrepitated fluid inclusions from various parts of the alteration halo. These residues are composed mainly of NaCl and contain significant Fe and Mn close to the vein, and K in muscovite-rich samples. The content of calcium is generally low.

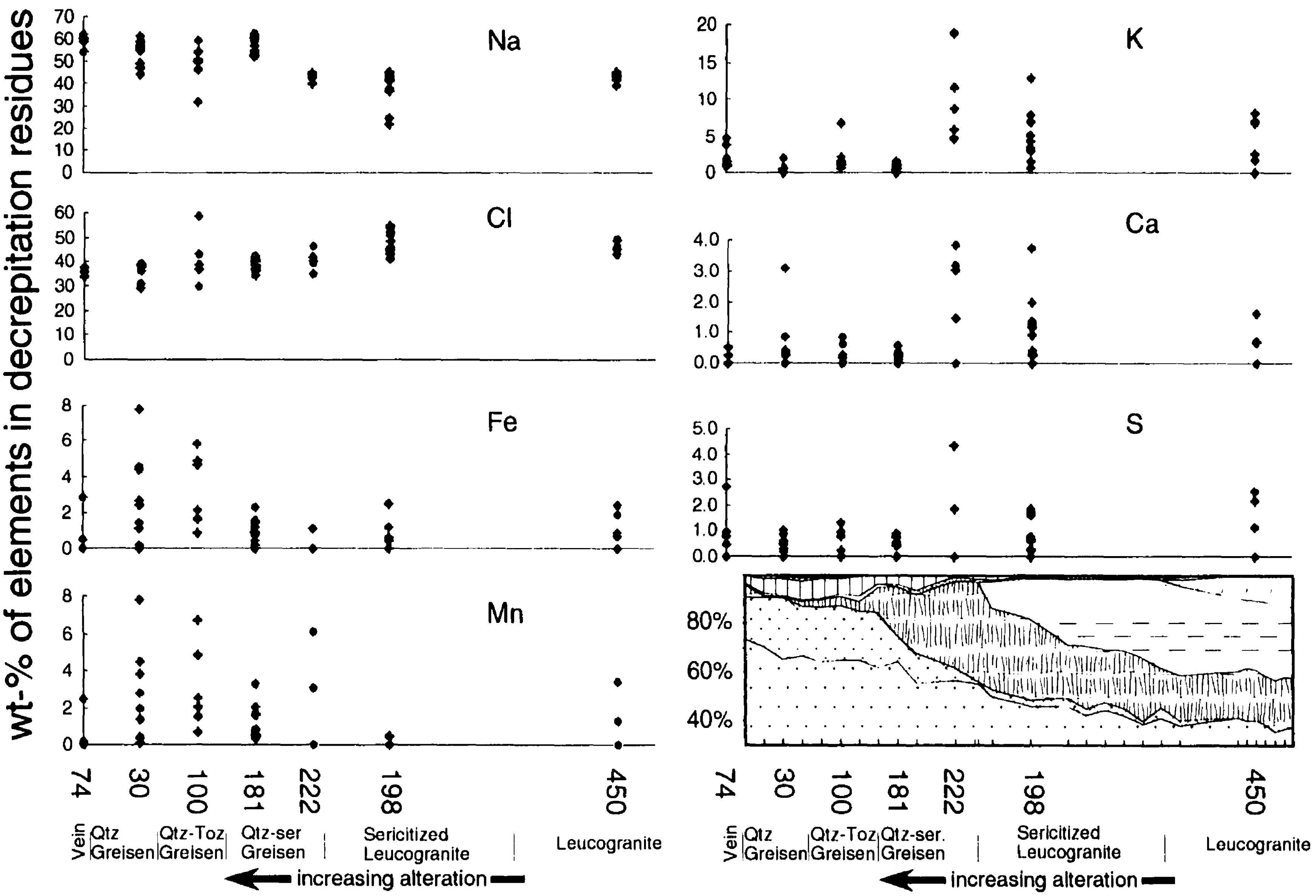
wt-% of elements in decrepitation residues
Na
70
60
50
40
30
20
10
0
Cl
60
50
40
30
20
10
0
Fe
8
6
4
2
0
Mn
8
6
4
2
0
K
20
15
10
5
0
Ca
4.0
3.0
2.0
1.0
0.0
S
5.0
4.0
3.0
2.0
1.0
0.0
80%
60%
40%
74
30
100
181
222
198
450
Vein
Qtz Greisen
Qtz-Toz Greisen
Qtz-ser Greisen
Sericitized Leucogranite
Leucogranite
increasing alteration
74
30
100
181
222
198
450
Vein
Qtz Greisen
Qtz-Toz Greisen
Qtz-ser. Greisen
Sericitized Leucogranite
Leucogranite
increasing alteration

Samples were therefore washed for an additional hour using a 0.13M HNO_3 solution containing 200ppm La, which has proven to be effective in preventing adsorption of highly charged cations onto the quartz surface (Botrell et al., 1988). Samples were then washed again with de-ionized water for one hour. After this cleaning, each sample was washed repeatedly (20 times) in de-ionized water to remove the nitric acid, which can interfere with other anions during ion chromatographic analyses, if its concentration is too high. Samples were then crushed dry in an agate mortar, split in two equal parts and leached, one with de-ionized water for anion analyses and the other with the 0.13M HNO_3 solution containing 200ppm La as recommendend by Botrell et al (1988) for cation analyses. Anions were analyzed by ion chromatography and cations by ICP-MS. Both splits were analyzed for Na, K and Br in order to relate the two sets of analyses. Blanks run with this cleaning technique indicate that it efficiently removes any contaminant that could influence the leachate analyses.

We separated 0.5 to 1g of quartz grains for leachate analyses from 9 samples selected to represent the various alteration zones; the vein did not contain enough quartz for separation (Table 6). Unfortunately, because of the fine grain-size of the samples, especially in the highly altered rocks, and because of the absence of colour in most of the minerals, we were not able to completely remove topaz, muscovite and fluorite from some of our samples. Consequently, because of the use of an acidic leaching solution, values of K, Al, F, and Ca are erratic, anomalously high, and therefore not considered to be reliable. Sulphides, however, could be detected easily and effectively removed from samples before analysis. A significant number of elements analysed (Ti, Mo, Ru, Pd, Ag, Sb, Te, I, Sm, Eu, Gd, Dy, Ho, Er, Tm, Re, Os, Pt, Au and Hg) were below the detection limit in all the samples and the blanks. Other elements (Li, Sc, Cr, Cu, As, Se, Ba, W and Pb) have a blank value close to the concentrations measured in the samples, and could not be analysed reliably.

Results of the analyses were normalized to the apparent salinity of the fluid assuming that the latter is equal to the equivalent weight percent NaCl determined by microthermometry. The apparent salinity ($S_{apparent}$), expressed in moles per liter, is

Table 6: Leachate analyses of fluid inclusions (in ppb)

Sample	10	100	181	198	210	271	450	650	830	blank
ICP-MS analyses										
Na	162	295	1532	530	658	2282	678	331	1238	8
Li	12	9	31	28	26	4	8	13	491	50
Mg	23	19	31	24	20	17	23	14	55	12
Al	152	152	660	543	772	2490	613	299	953	12
Si	2477	1833	4005	1330	2028	1710	460	1842	6272	3623
K	237	305	1225	766	910	681	549	363	1153	16
Ca	491	789	3226	789	1543	4190	1207	297	1839	91
Sc	6.9	3.8	9.5	4.1	7.8	1.1	0.2	3.3	10.1	3.7
Ti	<0.04	<0.04	<0.04	<0.04	<0.04	0.23	<0.04	<0.04	0.05	<0.04
V	1.6	1.4	1.5	1.5	1.4	0.8	0.9	0.9	1.0	0.4
Cr	5.6	5.4	6.4	4.7	5.2	3.9	3.0	4.7	4.1	2.7
Mn	24.9	66.3	316.2	103.6	64.1	54.6	35.5	11.8	68.3	0.4
Fe	68.1	86.7	326.0	137.0	159.0	127.1	73.1	28.1	182.2	0.2
Co	0.04	0.02	0.08	0.05	0.05	0.07	0.05	0.05	0.06	0.09
Ni	0.31	0.88	3.76	1.29	3.98	<0.004	<0.004	<0.004	3.64	<0.004
Cu	1.1	1.2	3.0	0.9	0.7	0.6	1.7	1.7	1.8	1.1
Zn	24	34	93	39	31	30	28	25	32	19
Ga	0.14	0.15	0.36	0.30	0.37	1.39	0.40	0.20	0.26	0.05
Ge	0.10	<0.004	0.06	0.03	0.14	0.14	0.02	0.10	0.03	0.03
As	0.10	0.13	0.88	0.34	0.39	0.11	0.72	0.39	0.87	0.10
Se	<0.04	<0.04	2.3	0.2	0.5	<0.04	1.2	<0.04	1.6	1.0
Br	180	174	201	160	155	122	134	122	138	99
Rb	4.04	6.82	21.65	18.17	19.76	25.64	17.20	10.44	21.20	0.08
Sr	2.57	7.02	24.17	5.36	5.30	17.47	1.86	0.52	2.08	0.04
Y	1.2	2.2	5.2	2.9	2.7	3.9	2.6	2.7	3.5	1.0
Zr	0.329	0.26	3.018	0.948	1.057	2.677	1.009	0.204	1.762	0.008
Nb	0.053	0.044	0.029	0.017	0.024	0.123	<0.004	0.026	0.032	<0.004
Mo	<0.04	<0.04	<0.04	<0.04	<0.04	<0.04	<0.04	<0.04	<0.04	<0.04
Ru	<0.04	<0.04	<0.04	<0.04	<0.04	<0.04	<0.04	<0.04	<0.04	<0.04
Pd	<0.04	<0.04	<0.04	<0.04	<0.04	<0.04	<0.04	<0.04	<0.04	<0.04
Ag	<0.004	<0.004	<0.004	<0.004	<0.004	<0.004	<0.004	<0.004	0.005	<0.004
Cd	0.05	0.19	1.08	0.15	0.11	0.18	0.10	<0.004	1.37	0.02
In	0.018	0.012	0.044	0.009	0.034	0.022	0.008	0.013	0.045	0.007
Sn	0.24	0.58	0.60	0.10	2.44	0.66	0.35	0.06	0.20	0.08
Sb	0.06	0.1	0.06	<0.04	<0.04	0.04	0.05	<0.04	0.05	<0.04
Te	<0.04	<0.04	<0.04	<0.04	<0.04	<0.04	<0.04	<0.04	<0.04	<0.04
I	<0.08	<0.08	<0.08	<0.08	<0.08	<0.08	<0.08	<0.08	<0.08	<0.08

Sample	10	100	181	198	210	271	450	650	830	blank
ICP-MS analyses										
Cs	1.44	3.09	10.11	3.66	2.27	3.00	5.57	2.81	6.26	0.06
Ba	1.1	1.3	11.1	5.2	4.2	8.4	12.9	0.9	1.5	1.1
Ce	0.9	1.3	3.5	2.1	1.9	1.7	2.6	3.9	1.7	0.4
Pr	0.10	0.18	0.35	0.21	0.22	0.17	0.29	0.42	0.18	0.04
Nd	0.18	0.45	0.99	0.48	0.59	0.56	0.82	1.35	0.64	0.08
Sm	<0.004	<0.004	<0.004	<0.004	<0.004	<0.004	<0.004	<0.004	<0.004	<0.004
Eu	<0.004	<0.004	<0.004	<0.004	<0.004	<0.004	<0.004	<0.004	<0.004	<0.004
Gd	<0.004	<0.004	<0.004	<0.004	<0.004	<0.004	<0.004	<0.004	<0.004	<0.004
Tb	0.08	0.14	0.26	0.12	0.12	0.12	0.09	0.12	0.14	0.05
Dy	<0.004	<0.004	<0.004	<0.004	<0.004	<0.004	<0.004	<0.004	<0.004	<0.004
Ho	<0.004	<0.004	<0.004	<0.004	<0.004	<0.004	<0.004	<0.004	<0.004	<0.004
Er	<0.004	<0.004	<0.004	<0.004	<0.004	<0.004	<0.004	<0.004	<0.004	<0.004
Tm	<0.004	<0.004	<0.004	<0.004	<0.004	<0.004	<0.004	<0.004	<0.004	<0.004
Yb	0.18	0.30	0.80	0.40	0.42	0.33	0.26	0.33	0.53	0.03
Lu	0.043	0.049	0.149	0.063	0.077	0.058	0.053	0.056	0.074	0.006
Hf	0.009	0.034	0.197	0.036	0.062	0.155	0.029	0.018	0.057	<0.004
Ta	0.033	<0.004	0.048	0.024	0.012	0.042	0.008	0.011	0.061	<0.004
W	0.1	0.3	0.5	0.3	0.5	0.5	0.6	0.3	0.8	0.2
Re	<0.004	<0.004	<0.004	<0.004	<0.004	<0.004	<0.004	<0.004	<0.004	<0.004
Os	<0.004	<0.004	<0.004	<0.004	<0.004	<0.004	<0.004	<0.004	<0.004	<0.004
Pt	<0.004	<0.004	<0.004	<0.004	<0.004	<0.004	<0.004	<0.004	<0.004	<0.004
Au	<0.004	<0.004	<0.004	<0.004	<0.004	<0.004	<0.004	<0.004	<0.004	<0.004
Hg	<0.04	<0.04	<0.04	<0.04	<0.04	<0.04	<0.04	<0.04	<0.04	<0.04
Tl	0.10	0.12	0.79	0.26	0.25	0.17	0.21	0.06	0.31	0.01
Pb	1.7	3.3	18.0	5.9	4.5	3.9	5.0	2.5	11.9	2.6
Bi	0.03	0.24	0.57	0.12	0.20	0.04	0.11	0.05	0.07	0.02
Th	1.49	3.57	11.15	4.02	5.75	2.66	3.88	5.56	9.24	0.05
U	5.73	8.78	<0.004	16.78	24.00	<0.004	11.70	<0.004	67.69	0.05
Ion Chromatographic analyses										
F	102	124	261	124	425	349	219	81	238	38
Cl	120	293	1246	454	444	494	352	121	150	57
Br	22	8	5		3	6	18	2	7	20
P	10	14	12	21	9	13	27	54	42	11
S	9		8							
Na	180	360	143	650	920	1660	400	360	960	107
K	130	150	92	610	650	340	540	450	790	77

approximated by the equation

$$S_{apparent} = \text{Molality}_{NaCl} + 0.5\ \Sigma\ \text{Molality}_{M^{n-}Cl^{-}_{n}}$$

where $M^{n-}Cl^{-}_{n}$ represents all other mono- and divalent metal chlorides in solution; because of their low concentration, higher charged cations do not contribute significantly to $S_{apparent}$. This empirical relationship is based on similarities between the $NaCl$-KCl-H_2O and $NaCl$-$CaCl_2$-H_2O systems and assumes that other mono- and divalent cations behave similarly to K or Ca in the presence of NaCl (Heinrich et al., 1992).

Figure 15 shows changes in the abundance of selected elements in the fluid as a function of alteration. The concentration of Na was calculated using fluid inclusion salinities as mentioned above, and the Cl content was calculated from the sum of cation charges. It is apparent from this figure, that the Fe and Mg contents of the fluid decrease with decreasing alteration, suggesting that these elements were added to the rock by the mineralizing fluid. Zinc and Manganese increase in concentration in the fluid away from the vein in the quartz-topaz greisen and decrease linearly in less altered rock until they reach a very low value in sample 290. The concentration of Rb apparently increases slightly towards less altered rocks, and strontium increases up to sample 93 and then decreases linearly towards the leucogranite. Bromine and Niobium behave similarly; these elements decrease sharply in concentration through the quartz-topaz greisen, and are then at near background values in the other samples. Thorium and phosphorus remain approximately unchanged in the fluid suggesting that they were essentially immobile during alteration; the high values in sample 650 are likely due to contamination from xenotime. The distributions of Nd and Y (not shown) are very similar to those of Th and P. Tin is most abundant in highly altered rocks, i.e., in quartz-topaz greisen, where most of the cassiterite precipitated, and is low in less altered rocks (the high value in sample 211 is again likely due to contamination).

Figure 15: Concentrations of various elements in fluid inclusion leachates. Samples are plotted as a function of alteration. See text for detailed discussion of the profiles.

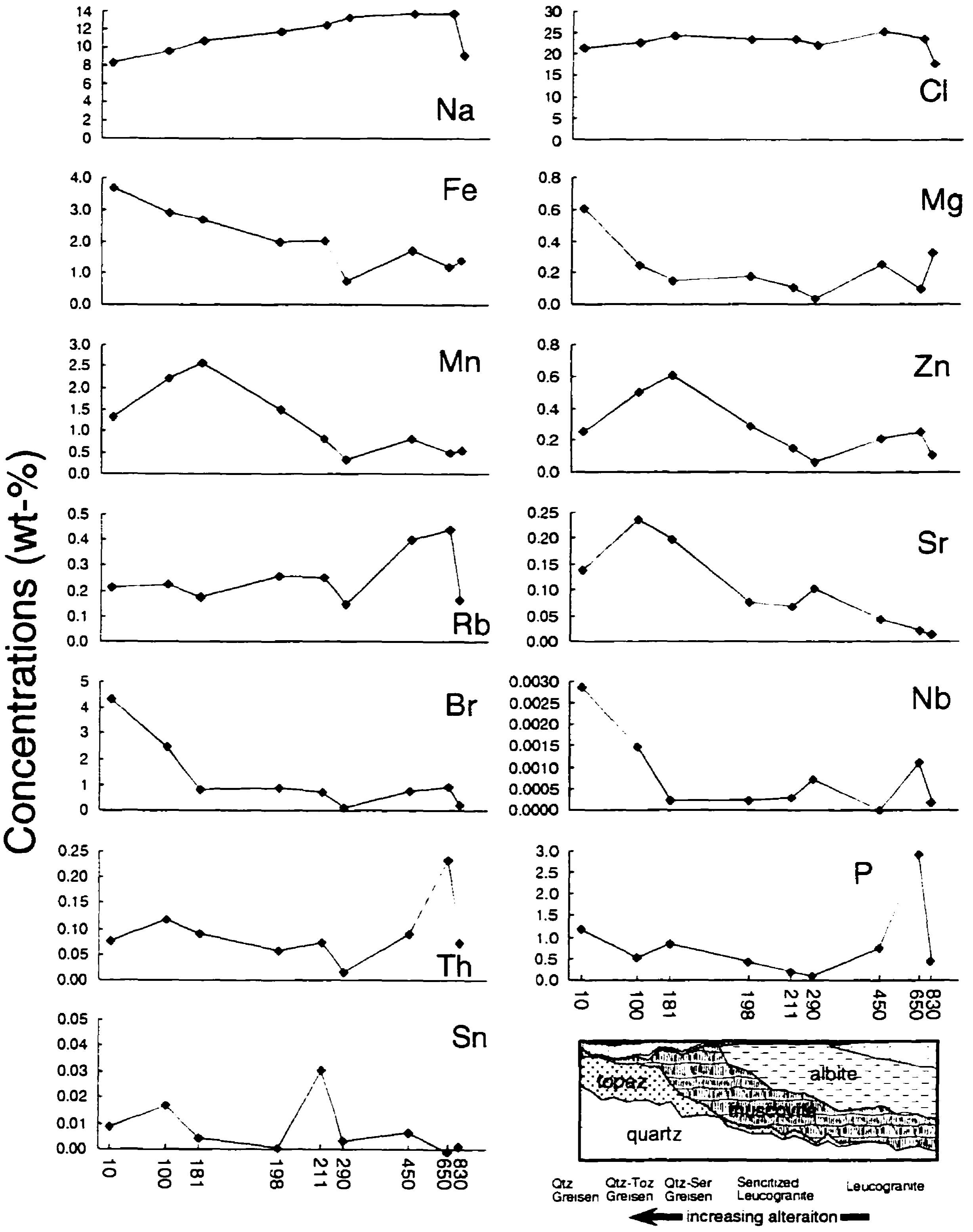
Concentrations (wt-%)
Na
0
2
4
6
8
10
12
14
Cl
0
5
10
15
20
25
30
Fe
0.0
1.0
2.0
3.0
4.0
Mg
0.0
0.2
0.4
0.6
0.8
Mn
0.0
0.5
1.0
1.5
2.0
2.5
3.0
Zn
0.0
0.2
0.4
0.6
0.8
Rb
0.0
0.1
0.2
0.3
0.4
0.5
Sr
0.00
0.05
0.10
0.15
0.20
0.25
Br
0
1
2
3
4
5
Nb
0.0000
0.0005
0.0010
0.0015
0.0020
0.0025
0.0030
Th
0.00
0.05
0.10
0.15
0.20
0.25
P
0.0
0.5
1.0
1.5
2.0
2.5
3.0
Sn
0.00
0.01
0.02
0.03
0.04
0.05
10
100
181
198
211
290
450
650
830
topaz
albite
muscovite
quartz
Qtz Greisen
Qtz-Toz Greisen
Qtz-Ser Greisen
Sericitized Leucogranite
Leucogranite
increasing alteraiton

Hydrocarbons and fO_2 conditions

Although there is no microthermometric evidence of dissolved carbonic gases in the fluid inclusions, analyses with a gas chromatograph using the method described by Bray and Spooner (1992), and modified by Salvi and Williams-Jones (1996), revealed the presence of small concentrations of N_2, CO_2, CH_4 and higher hydrocarbons. The analyses were conducted by crushing 1 to 1.5g of rock and analyzing the released gases with an "on line" HP5890 gas chromatograph equipped with thermal conductivity and photoionization detectors. The measured amounts of the various gas species are given in Table 7. In all samples, CO_2 and N_2 were the dominant gas species, the proportion of CH_4 low and C_2H_6, C_3H_6 and C_3H_8 at trace levels in highly altered samples, i.e., where fluid inclusions are abundant.

We used the CO_2/CH_4 ratio measured for each sample to estimate the fO_2 in the fluid from the reaction:

$$CO_2 + 2H_2O = CH_4 + 2O_2$$

Log fO_2 values were estimated from the value of log K calculated for this reaction (-49.72) at the conditions estimated for East Kemptville, i.e. 480°C and 4.1kb (see below) using SUPCRT92 (Johnson et al; 1991) and assuming unit activity for H_2O. The CO_2/CH_4 ratio used to calculate log fO_2 was corrected by a factor of 0.9948 calibrated by Dubessy (1984) to reflect the difference in this ratio at the temperature of analysis from that at the temperature of entrapment. The values of fO_2 so calculated fall between the NNO and the FMQ buffers at the temperature estimated for the formation of the greisen (480°C), and are plotted a function of alteration in Figure 16. The value of log fO_2 in the vein is -24.7 and decreases to a minimum of -25.2 in the most intensely mineralized quartz-topaz greisen. Log fO_2 values then increase linearly with decreasing alteration to a high of -24.0 in sample 650. The low fO_2 value in sample 850 is real (it was duplicated) but no adequate explanation could be found for why it is low.

Table 7: Gas analyses of fluid inclusions (in nanomoles)

Sample	10	30	74	74d	100	100d	198	211	222	271	450	650	830	830d
N_2	3.43	3.25	7.67	1.81	5.34	8.66	8.82	2.64	2.62	6.09	2.17	5.96	0.76	2.21
CH_4	10.88	9.84	11.37	2.69	17.25	30.83	11.25	2.43	6.05	1.87	0.52	1.37	1.77	5.66
CO_2	9.58	7.82	24.78	5.49	5.12	7.91	20.13	7.19	3.90	11.88	14.18	54.95	2.74	8.06
C_2H_6	0.14	0.17	0.25		0.33									
C_3H_6	0.11	0.18	0.29		0.24									
C_3H_8	0.00		0.01		0.01									
CO_2/CH_4	1.136	1.259	0.459	0.489	3.371	3.896	0.559	0.338	1.552	0.157	0.036	0.025	0.647	0.702
CO_2/CH_4 at 480°C	1.130	1.252	0.457	0.487	3.353	3.876	0.556	0.336	1.544	0.157	0.036	0.025	0.644	0.699
$\log fO_2$	-24.89	-24.91	-24.69	-24.70	-25.12	-25.15	-24.73	-24.62	-24.95	-24.46	-24.14	-24.06	-24.76	-24.78
N_2/tot moles	0.168	0.184	0.212	0.222	0.239	0.224	0.281	0.275	0.263	0.443	0.148	0.106	0.168	0.161

Figure 16: Variation of fO_2 with alteration (decreasing from left to right). The values were calculated from the CO_2/CH_4 ratio in fluid inclusion gases which were extracted by crushing, and analyzed using gas chromatography. fO_2 decreases between the vein and sample 93, i.e. in the interval in which cassiterite and pyrrhotite precipitated. Further away from the vein, fO_2 increases steadily with decreasing alteration. Sample 830 has an anomalously low fO_2 for reasons that are unknown. NNO represents the nickel-nickel oxide buffer and FMQ the quartz-magnetite-fayalite buffer at 475°C. Dashed lines represent the normative mineral boundaries from Figure 2.

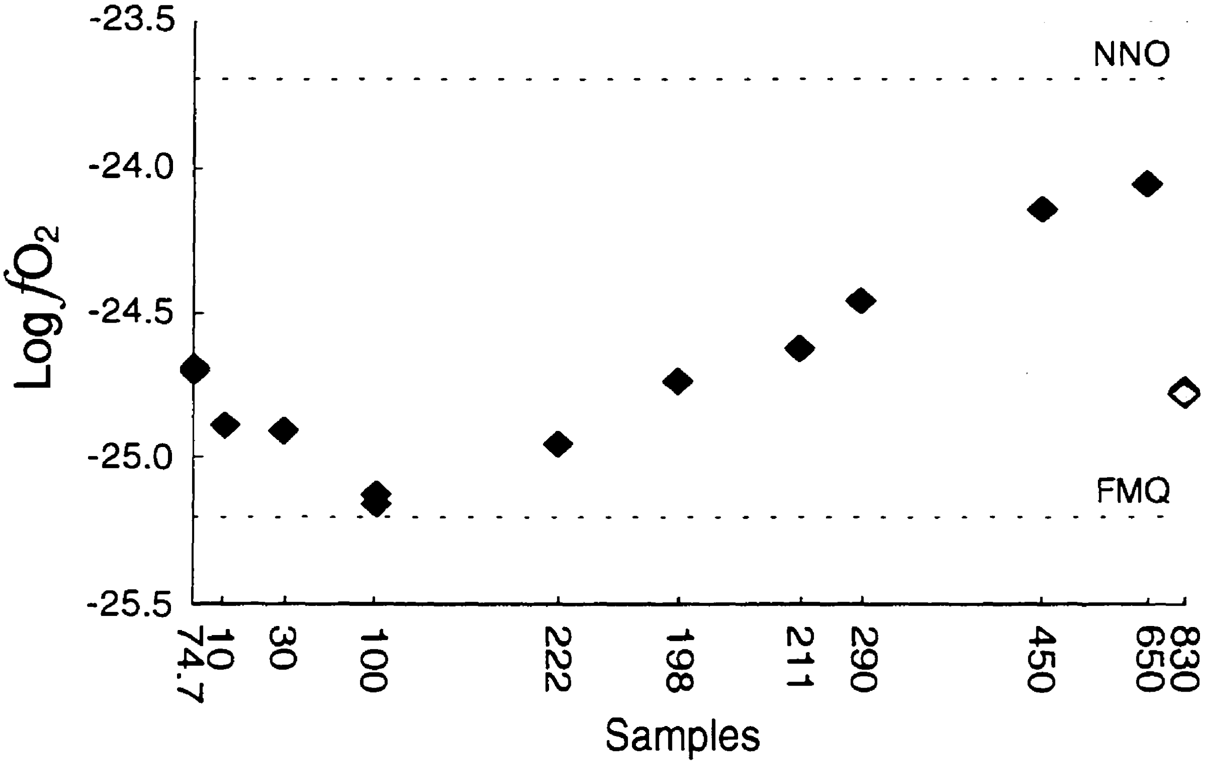
-23.5
-24.0
-24.5
-25.0
-25.5
Log fO_2
NNO
FMQ
74.7
10
30
100
222
198
211
290
450
650
830
Samples

P-T CONDITIONS

The temperature and pressure of formation of the greisen assemblage were estimated using oxygen isotopic fractionation between quartz and cassiterite, the OH-F exchange between muscovite and topaz and fluid inclusion homogenization temperatures. Based on the oxygen isotopic compositions of cassiterite and quartz separates in a vein (Chapter 2), the temperature is estimated to have been 473±15°C ($\Delta^{18}O_{quartz-cassiterite} = 7.4\pm.0.2‰$) using the experimental thermometer developed by Zhang et al. (1994). This temperature is 100°C higher than that predicted by the theoretical thermometers of Borshchevskii et al. (1983) and Zheng (1991) or the empirical thermometer of Alderton (1989) (Fig. 17). In order to obtain an independent estimate of the temperature, we calibrated the F-OH exchange between topaz and muscovite as a function of temperature and pressure (Chapter 4) using thermodynamic data for F and OH end-members of muscovite and topaz (Barton 1982; Barton et al. 1982; Zhu and Sverjensky, 1991). As a means of ensuring the best possible result, we restricted our analyses to those samples from drill hole 90-1 in which the muscovite does not have a significant phengitic component. The F-OH thermometer yielded temperatures between 470 and 490°C at pressures from 500 to 4000 bars (shown by the heavy lines in Figure 17). These temperatures are in very good agreement with those estimated using the experimental oxygen isotope thermometer of Zhang et al., (1994). As discussed earlier, most fluid inclusions homogenize in a very narrow temperature range between 220 and 280°C in the vein and various greisen samples, supporting our view that there was only one important episode of greisenization and that the temperature was essentially the same in all the alteration zones.

Figure 17 shows the vapour saturation curve for the above system at an average salinity of 30wt-%NaCl equivalent as measured in the quartz-topaz greisen, the isochores for the same salinity at the average $Th_{(L-V)}$ of 250°C and the bracketing isochores for fluid inclusions representing one standard deviation above (280°C) and below (220°C) the average $Th_{(L-V)}$ at the maximum and minimum salinities (38 and 25 wt-% eq.), respectively. The pressure obtained by projecting these isochores to the estimated

Figure 17: Pressure-temperature diagram showing P-T conditions during greisenization. The thin lines represent temperatures based on the $\delta^{18}O$ fractionation between cassiterite and quartz obtained using several different calibrations. The bold lines correspond to conditions calculated using the topaz-muscovite geothermometer. This geothermometer is based on the OH-F exchange between the two minerals. The shaded area represents the range in isochores from fluid inclusions. Also shown is the isochore for 30wt % NaCl eq. and an average homogenization temperature of 250°C, used to estimate the condition of greisen formation at 480°C and 4100 ±1000bars. The high temperature of formation of the deposit is confirmed by the dissolution of an Fe-chloride above 400°C in some fluid incluions

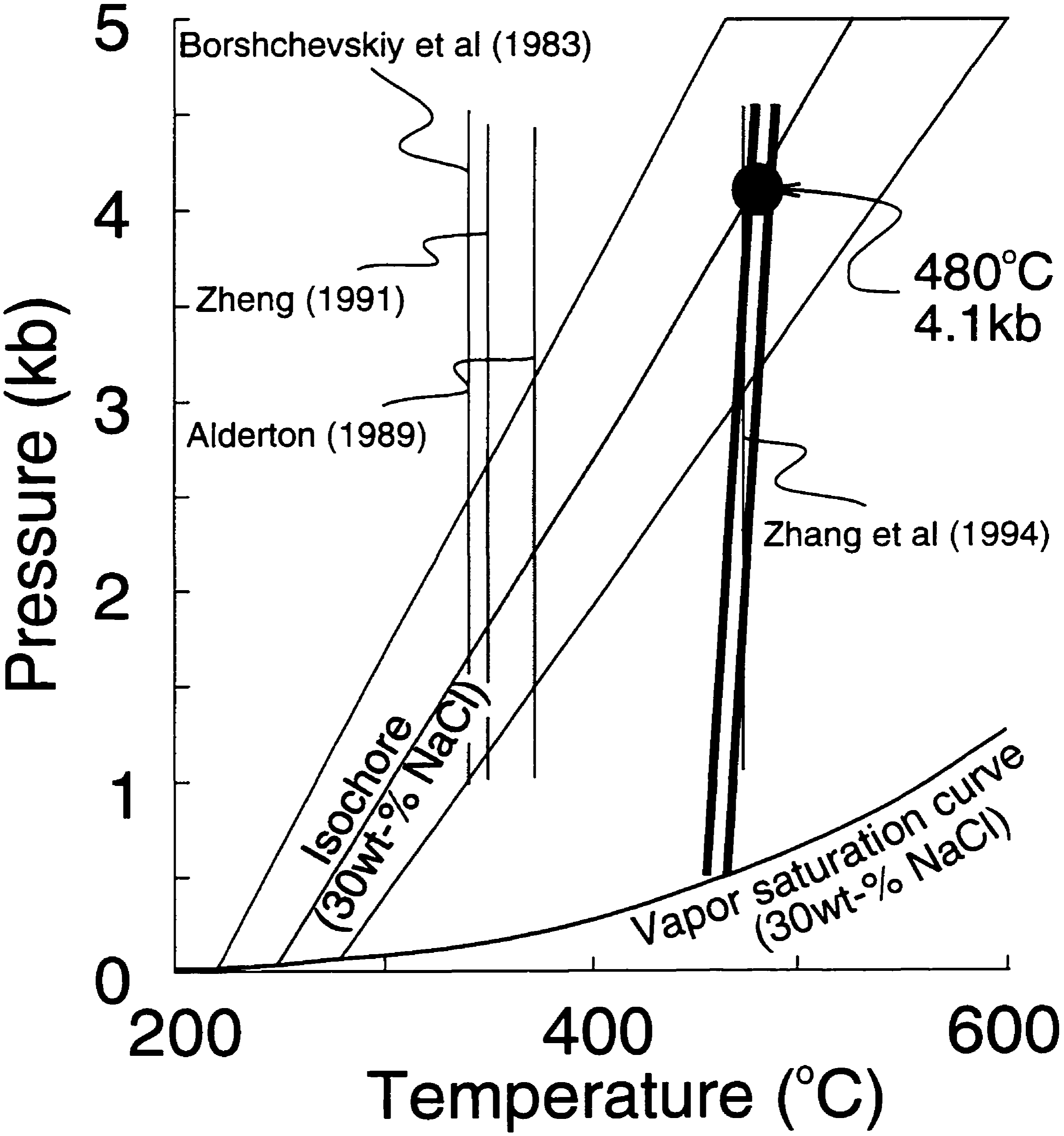

Pressure (kb)
5
4
3
2
1
0
200
400
600
Temperature (°C)
Borshchevskiy et al (1983)
Zheng (1991)
Alderton (1989)
480°C
4.1kb
Zhang et al (1994)
Isochore (30wt-% NaCl)
Vapor saturation curve (30wt-% NaCl)

temperature of greisen formation (~480°C) is 4100±1000 bars. This pressure is slightly above that estimated from metamorphic mineral assemblages (2.5 to 4.0Kbars) for the emplacement of the South Mountain Batholith at its northeastern end (Raeside et al., 1994).

CHEMICAL CHANGES IN THE FLUID DURING ALTERATION

We established earlier that all L-V±H±S inclusions were formed during a single event, i.e., greisenization, and that changes in fluid chemistry resulted from interaction of this fluid with the wall rock with which it equilibrated. The mineralizing fluid in the fracture (vein) was dominated by $NaCl^0$ and contained significant concentrations of Fe, Mn and Br. The concentrations of K and Ca were, however, relatively low, with K only becoming significant in the quartz-sericite greisen. The starting log fO_2 of the fluid was -24.7, i.e., between the Ni-NiO and the fayalite-magnetite-quartz buffers.

With increasing distance from the vein, eutectic temperatures and those of final ice melting decrease in the quartz greisen, due to an increase in the Fe content of the fluid. This is not apparent from the leachate data due possibly to the restricted number of samples that could be analyzed using this technique. However, the increase in the Fe concentration of the fluid predicted from eutectic temperatures is matched by a corresponding increase in the Fe content of the rock (Fig. 10). This behaviour of Fe was probably the result of the dissolution of pyrrhotite in quartz greisen (Fig. 8). At greater distance from the vein, the content of Fe in the rock decreases and T_e and Tm_{ice} increase, reflecting a decrease in the activity of Fe as a result of the precipitation of pyrrhotite. A similar process might have controlled the distribution of cassiterite, which is also less abundant in the quartz greisen than in the quartz-topaz greisen; an increase in the Sn content of the fluid between samples 10 and 100 is apparent from leachate analyses and correlates with a decrease in the Sn content of the rock towards the vein (Fig. 10).

Dissolution of pyrrhotite could also have been responsible for an increase in the Fe^{2+}/Fe^{3+} ratio in the fluid as iron in pyrrhotite is dominantly Fe^{2+}. This could explain the dip in fO_2 estimated from CO_2/CH_4 ratios in fluid inclusions (Fig 16): at a Log fO_2 of -24.7, the Fe^{2+}/Fe^{3+} is approximately 10^{-14}. Using the total Fe content obtained from leachate analyses (3.7wt-% or 25g/l), an increase in the concentration of Fe^{2+} from 25 to 39 grams per liter, at constant $a_{Fe^{3+}}$ in the fluid, could account for the estimated range of fO_2 values.

In addition to Fe and Sn, Zn and Mn also increased their concentration in the fluid, i.e., their concentration in the rock decreases towards the vein (Fig. 10), possibly as a result of the dissolution of sphalerite and cassiterite in quartz greisen (cassiterite in these samples contain up to 200 ppm MnO). Similarly, Nb and Br are only present in significant concentrations in the fluid next to the vein. Niobium was likely incorporated as a trace element in cassiterite in which can contain up to 5800 ppm Nb_2O_5 in these samples, and Br might have substituted for F^- in topaz. The high concentration of these components in fluid inclusions from the most altered rocks, indicates that they were introduced by the mineralizing fluid.

Sodium behaved differently to the above elements in that it increased continuously towards less altered rocks. This increase cannot reflect the dissolution of a mineral, as was proposed for Fe (Po), since no Na-bearing phase is present close to the vein, i.e., the Na content of the rock is low (Fig. 10). It is therefore likely due to a supply of Na to the fluid as a result of albite replacement further out in the alteration halo. The concentration of Rb also increased in the fluid with distance from the vein, due to the dissolution of K-bearing phases. This is reflected in a decrease in the Rb content of the rock towards the vein (Fig. 10). Thorium and Neodymium remained essentially unchanged in the fluid, suggesting that these elements were immobile during alteration. The same conclusion was drawn above from the whole rock geochemistry. This possibly applies also to: P and Y, although these elements appear to decrease slightly away from the vein; to Ce, U, Zr, Yb and Hf (not shown in Figure 15); and possibly to Ca, which would have been buffered to low concentrations by fluorite (Richardson and Holland 1979). Chlorine also remained constant in the fluid, due to the fact that none of the minerals incorporated significant amounts of this element.

ORIGIN OF THE METALS

In order to determine the source of the metals precipitated during greisenization we examined closely the chemistry of the least altered granites in both the Baby and Main Zones of the deposit. As discussed earlier, the leucogranite of the Baby Zone (DDH 90-1) is homogenous. The same is also true for the leucogranite in the Main Zone (Kontak, 1990). Moreover, the major element compositions of the two leucogranites are very similar. However, the trace element compositions differ significantly. In particular, the Th and La contents of the Baby Zone are appreciably higher than those of the Main Zone (Fig. 4). The same is true to a lesser extend for Ti, Li, Sc, Y, U and Zr. This suggests that the leucogranite in the Baby Zone was different prior to greisenization (more differentiated) to that in the Main Zone, and may even represent a separate intrusion. Mineralogically, this difference is apparent from the presence of magmatic topaz in the Main Zone, and its absence in the Baby Zone.

In Table 8 we report the concentrations, in the least altered leucogranites of the Main and Baby Zones, of elements enriched during greisenization. From this table it is evident that the concentration of these elements is systematically lower in the leucogranite of the Baby Zone. By contrast, alteration was more intense and these elements were more strongly enriched in greisens of the Baby Zone. This could indicate that elements precipitated in the greisen (Fe, Zn, Mo, Sn, F, S, P) were released from the leucogranite to the mineralizing fluid, and that this was more efficient in the Baby Zone. Release of these elements could then have occurred either by leaching of earlier crystallized phases (e.g. biotite was dissolved during early sericitization, see below) or by fractionation between a residual melt and the fluid.

This issue can be addressed in detail for Sn: Tin dissolves as Sn^{2+} in reduced melts (Johnston, 1965) or as Sn^{4+} in oxidized melts. In its higher oxidation state, tin behaves as a compatible element (crystal/melt distribution coefficient >1) and substitutes for Ti^{4+} or Fe^{3+} in mafic minerals like biotite (Lehmann, 1990). Consequently, oxidized magmas are depleted in Sn at an early stage of crystallization. By contrast, tin is present as Sn^{2+} in reduced melts and behaves as an incompatible element during fractional crystallization

Table 8: Selected average analyses of mobile elements from leucogranite in the Main and the Baby Zone

	Main Zone	Baby Zone
P_2O_5	0.49	0.10
F	0.79	0.50
S	535	0
Zn	468	104
Ga	35	26
Mo	4	0
Nb	31	20
Sn	102	23

P_2O_5 and F are in wt-% percents, others are in ppm.

(crystal/melt distribution coefficient <1). At East Kemptville, the freshest leucogranite contains approximately 100 ppm Sn (Kontak 1990) but no Sn could be detected (<0.01wt-%) in biotite inclusions in quartz, which suggests that the crystal/melt distribution coefficient was less than 1 and that tin was therefore present as Sn^{2-} in the melt and did not enter the crystal structure of biotite. This is consistent with the presence of a small amount of ilmenite at East Kemptville and with an fO_2 below the Ni-NiO buffer, i.e., below the ilmenite-magnetite boundary (Wones 1989). Consequently tin was able to concentrate in the residual magma by fractional crystallization and subsequently partition into a fluid phase, probably as a chloride complex (Jackson and Helgeson 1985).

ORIGIN OF THE FLUID

The above distribution of ore metals, and particularly tin, suggests that the mineralizing fluid was orthomagmatic, confirming earlier interpretations of oxygen isotopic data (Chapter 2 and Kontak, 1993). However, although some pegmatites are present in the northeastern part of the deposit, other signs that the magma achieved fluid saturation, e.g., miarolitic cavities, are missing, suggesting that the fluid separated from the magma at a very late stage. We propose that this separation resulted from a drop in pressure associated with tectonic fracturing that occurred prior to complete crystallization of the leucogranites (Fig. 1). The pervasive sericitization that affected all the leucogranite in the deposit might have been caused by this magmatic fluid phase. Such a fluid would have been initially in equilibrium with albite, muscovite and K-feldspar at high temperature (star in Figure 18) and, as a result of preferential partitioning of H_2S, HCl and HF into this phase, would have evolved to higher a_{H^-}, thereby causing sericitization. Simultaneously, some ore metals, e.g., Sn, would have been partitioned into this fluid and others enriched through the dissolution of magmatic phases, e.g., Fe which was enriched during the dissolution of biotite.

Separation of the fluid would have caused almost instantaneous quenching of the residual magma and prevented further fluid segregation, consistent with evidence of a

Figure 18: Activity-activity diagram showing the stability fields of albite, K-feldspar, paragonite, muscovite and pyrophyllite. The fluid phase that separated from the crystallizing magma was in equilibrium with albite, muscovite and K-feldspar (star). Partitioning of HCl, H_2S and HF into this fluid likely increased its acidity and caused the pervasive sericitization that affected the leucogranite at the scale of the deposit.

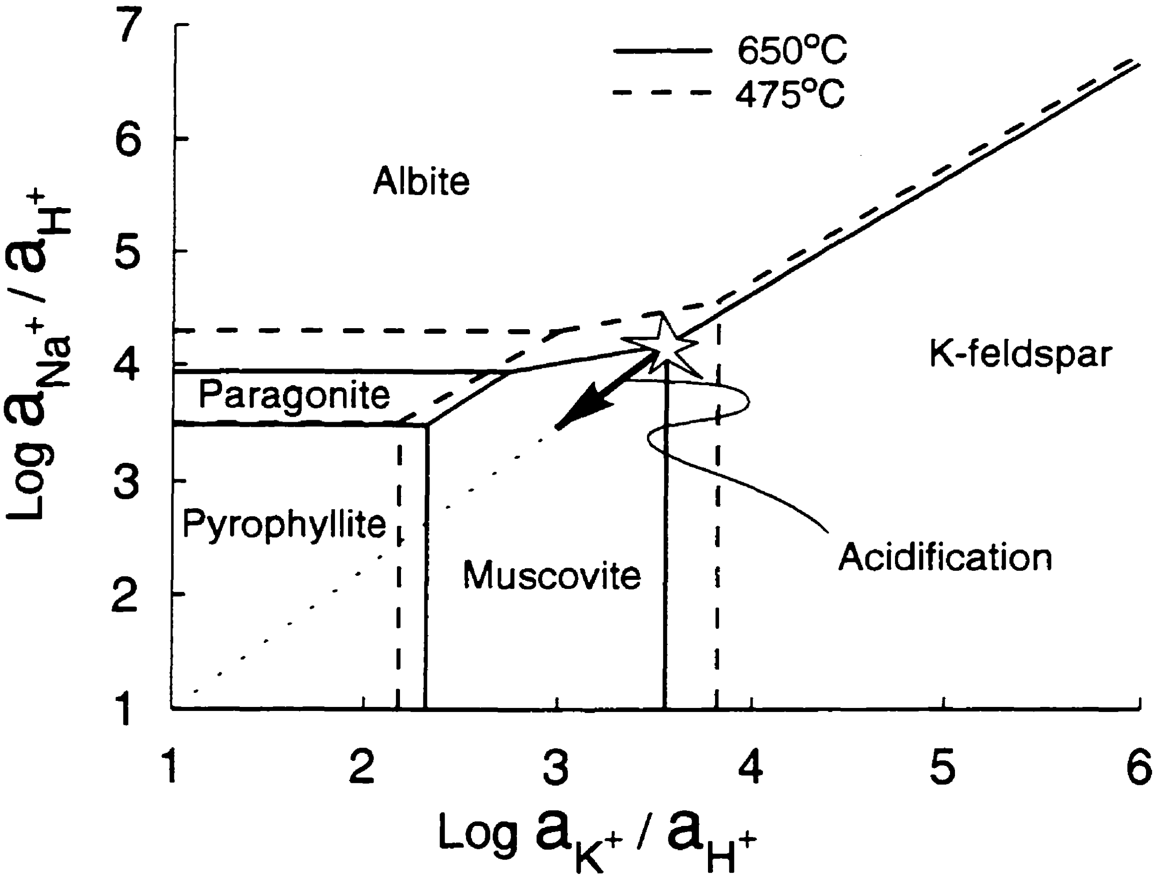
650°C
475°C
Albite
K-feldspar
Paragonite
Pyrophyllite
Muscovite
Acidification
Log a_{Na^+}/a_{H^+}
Log a_{K^+}/a_{H^+}
1
2
3
4
5
6
7

Figure 19: Model for the evolution of the hydrothermal system at East Kemptville. Prior to complete crystallization of the magma, fracturing caused a drop in pressure and allowed a fluid phase to separate (1). This fluid caused pervasive sericitization, transported the metals and was focused along fracture planes (2) where topaz, cassiterite and sulfides were deposited and the host rocks were altered to greisen (3). Additional cassiterite and sulphides were precipitated in the greisen

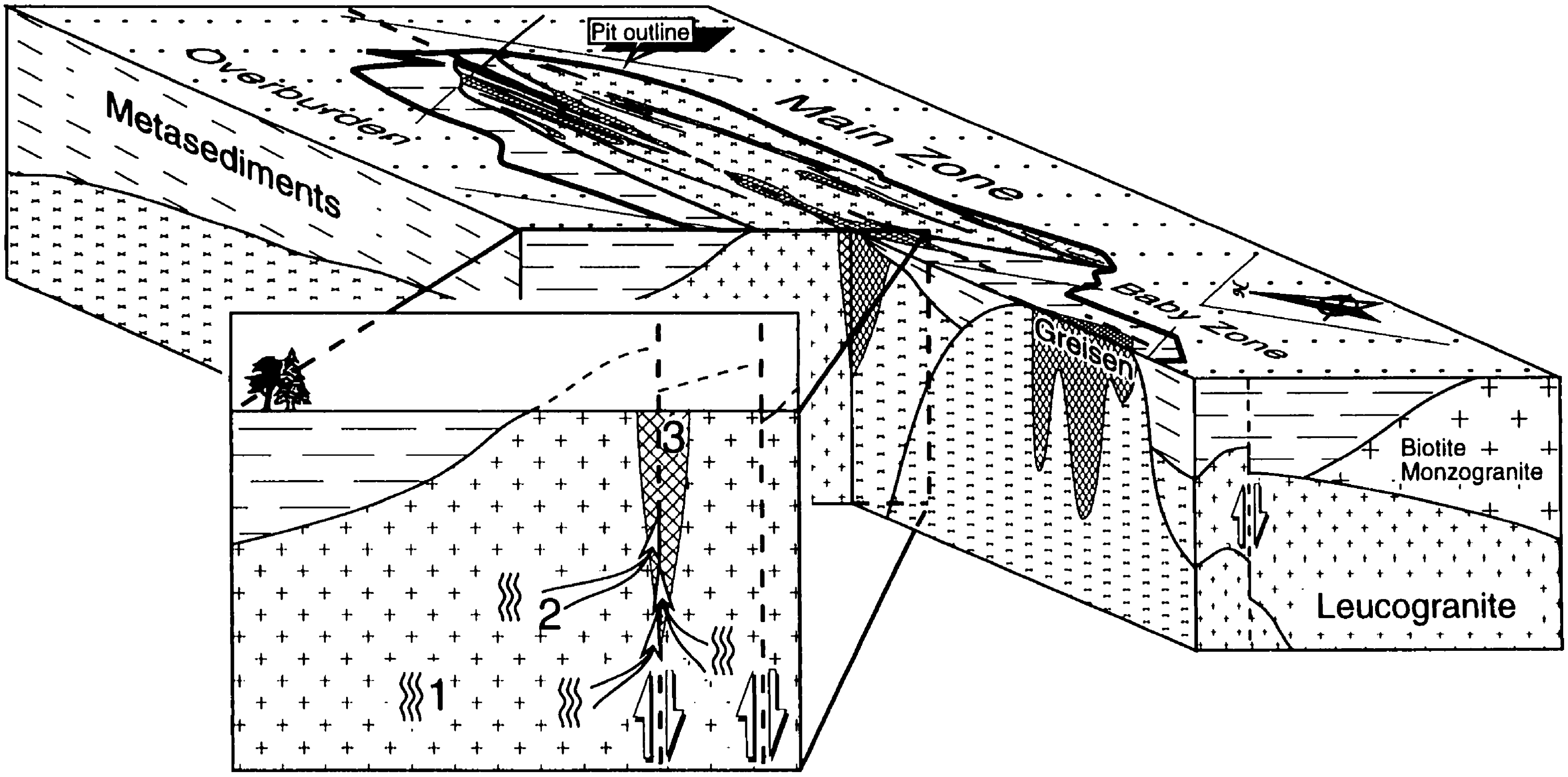
Pit outline
Overburden
Metasediments
Main Zone
Baby Zone
Greisen
Biotite Monzogranite
Leucogranite
1
2
3

single greisenizing event. After separation of the fluid phase, fault planes produced by concurrent tectonic fracturing are interpreted to have focused the fluid (Fig. 19), allowing it to escape (Halter et al., 1994) and interact with the leucogranite along these paths, causing greisenization. The higher ore grades in the greisen of the Baby Zone and the correspondingly lower abundance of Fe, Zn, Mo, Sn, F, S and P in the leucogranite of this zone might reflect a more efficient removal of ore metals by the fluid than in the Main Zone.

This model is similar to one proposed by Pollard and Taylor (1986) based on textural evidence, except that these authors suggest that the exsolved fluid remained trapped until later fracturing allowed it to escape. In both cases, only one fluid is invoked to explain pervasive alteration and the various greisen assemblages.

PHYSICOCHEMICAL CONTROLS ON CASSITERITE PRECIPITATION

At the conditions of greisen formation at East Kemptville, i.e., 480°C and 4.1kbars, the most important tin species in solution is $SnCl^-$ (Wilson and Eugster, 1990) and the reaction controlling cassiterite precipitation is therefore:

$$SnCl^- + H_2O + {}^1/_2O_2 + Cl^- \rightleftharpoons SnO_2 + 2HCl^0 \qquad (1)$$

Consequently, cassiterite could have precipitated due to an increase in fO_2, in a_{Cl^-}, or a decrease in $a_{HCl}0$, i.e. an increase in pH. A decrease in temperature would also have favored cassiterite precipitation, but we established earlier that temperature remained essentially constant during alteration and this parameter cannot therefore have been responsible for tin mineralization.

The change in oxygen fugacity of the fluid during greisenization was evaluated earlier from the CO_2/CH_4 ratio and shown to drop from -24.7 in the vein to a low of -25.2 in the most intensely mineralized quartz-topaz greisen (Fig. 16). As is evident from

Reaction (1), the change in fO_2 is opposite to that required to cause cassiterite precipitation. Based on mass balance calculations in a single zoned greisen, we reached the same conclusion in Chapter 2, namely that fO_2 decreased during early greisenization and could not have been responsible for cassiterite deposition.

Changes in a_{Cl^-} are difficult to quantify as the concentration of Cl^- in the fluid cannot easily be estimated separately from that bound to species such as $NaCl^0$, KCl^0, and HCl^0. However, since Fe and Zn sulphides were dissolved where cassiterite was precipitated, and Fe and Zn form strong Cl-complexes, a_{Cl^-} is likely to have decreased, which would have favoured cassiterite dissolution, not precipitation.

It therefore follows from the above discussion that the only factor which can account for cassiterite precipitation was the change in pH associated with alteration. We established that in the zoned greisen (Chapter 2) the replacement of muscovite by topaz and quartz was accompanied by a pH increase through the reaction:

$$4.50Ms + 5.99Al(OH)_3^0 + 1.92FeCl^- + 1.07ZnCl_2^0 + 17.07HF^0 + 3.30HCl^0 + 10.78H_2S^0 + 3.59O_2 + 1.92Cl^- \rightleftharpoons$$
$$16.09Qtz + 14.59Toz + 4.86Py + 1.07Sp + 9.12\,KCl^0 + 0.14NaCl^0 + 33.10H_2O$$

Since the same alteration sequence is observed in the samples from drill hole 90-1, we propose that a similar reaction occurred in the Baby Zone, and that pH also increased during the replacement of muscovite by topaz and quartz in these rocks, causing concurrent precipitation of cassiterite. We therefore conclude, that the observations made on the scale of the zoned greisen apply equally on the scale of the deposit.

FLUID-ROCK INTERACTION PROCESS

The changes in fluid composition discussed earlier provide important clues about the process which controlled formation of the alteration halos. For example, since pyrrhotite is absent in the unaltered leucogranite, its dissolution in quartz greisen suggests that it was precipitated close to the vein during an early stage of the alteration as a result of rapid equilibration of the fluid with the leucogranite (Fig. 20). At a later stage of the alteration, changes in fluid composition occurred more gradually and pyrrhotite was re-dissolved in the quartz greisen by the pyrrhotite-undersaturated fracture (vein) fluid. This process implies that with time, the alteration zones moved away from the vein and widened. The significance of this behaviour of pyrrhotite is that it would have affected the concentration of Fe in the fluid and since Fe has more than one valence, this can, in turn, lead to the formation of alteration zones more reducing or oxidizing than the fracture fluid or unaltered rock. At East Kemptville, this is apparent from the minimum in fO_2 in the quartz-topaz greisen.

The behaviour of Na, specifically its continuous increase in the fluid away from the vein, is particularly important in understanding the alteration process. The only reasonable explanation for this behaviour is that Na was transported from the albite-bearing zone towards the vein. This might be evidence that the distribution of Na and other components in the alteration halo was controlled by diffusion, since infiltration of fluid into the rock only transports components away from the vein. However, diffusion is a slow process (Chapter 2) and implies a static fluid. Yardley and Lloyd (1995) have shown that the fluid is not static during metasomatism and that the bulk of the flow is parallel to the metasomatic front. This is readily explained by the fact that the amount of fluid that can move into the rock from a fracture (vein) is very limited. On the other hand, if infiltration from the fracture is compensated by the release of fluid back to the fracture, the flow between the rock and the fracture might be appreciable. We therefore suggest that, although the overall fluid flow occurred parallel to the fracture, individual aliquots of fluid followed a more complex path, i.e., they moved from the fracture into the rock and back to the fracture, as illustrated by the flowlines in Figure 20. Since the introduction of fluid into the rock needs to be compensated, we refer to this process as "compensated infiltration", as opposed to simple infiltration. We propose that this compensated flow provided a transport mechanism which enabled components to move in directions of decreasing chemical potential gradients, irrespective of whether these were directed away from the fracture or towards the fracture. This created a distribution of the components similar to that produced by diffusion yet orders of magnitudes more rapidly.

Figure 20: Schematic representation of the formation of an alteration halo around a central fracture. With time the alteration halo widens and alteration zones move outwards. Phases precipitated close to the vein during an early stage of the alteration can therefore be redissolved during a later stage and so significantly change the chemistry of the fluid. The overall fluid flow is parallel to the vein but individual aliquots of fluid can move into the rock and return (dashed lines) to the vein through a compensated infiltration process (see text). This permits transport of components from the vein into the rock or vice versa depending on the chemical potential gradient.

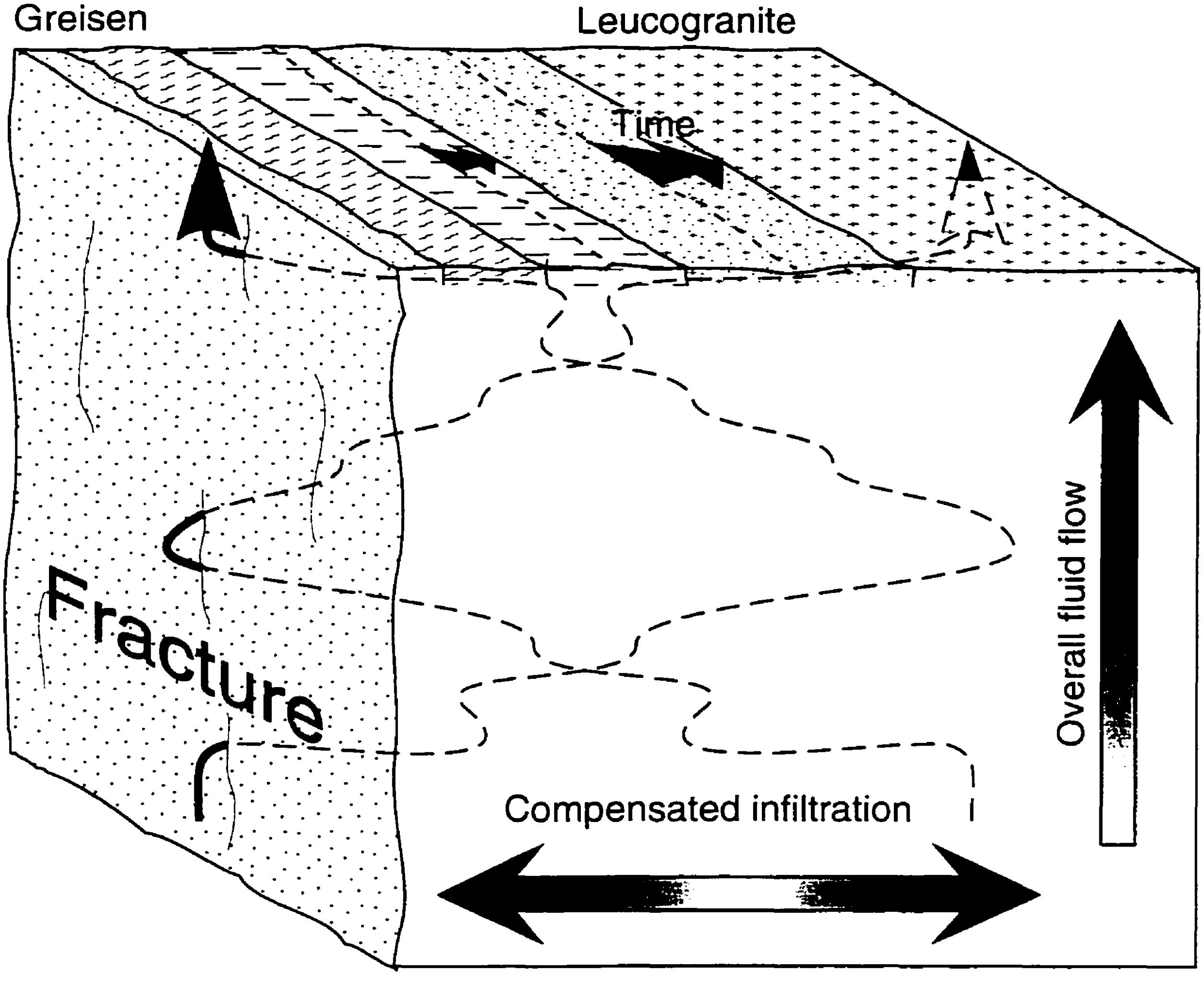
Greisen
Leucogranite
Time
Fracture
Compensated infiltration
Overall fluid flow

SUMMARY AND CONCLUSIONS

The East Kemptville tin deposit formed in a highly differentiated leucogranite of the Davis Lake Pluton. Prior to complete crystallization of the leucogranite, a pressure drop induced by tectonic fracturing caused separation of a magmatic aqueous fluid. This fluid caused pervasive sericitization of the feldspars and mobilized metals later precipitated in the greisen by dissolving magmatic phases (e.g., Fe) or by fractionation between the melt and the fluid (e.g., Sn). As a result of phase separation, the residual magma was quenched, preventing release of further generations of fluid. The exsolved fluid was focused along fracture planes and after a drop in P and T, interacted with the wall rock to produce greisens. This interaction first converted the leucogranite into a quartz-muscovite-albite assemblage by replacement of the K-feldspar with albite and quartz. Further alteration replaced albite with muscovite and quartz, converting the rock into a quartz-sericite greisen. Muscovite was, in turn, replaced by topaz and quartz in quartz-topaz greisen. Cassiterite and sulphides precipitated during this latter stage of alteration. Next to veins, quartz-topaz greisen was replaced by quartz-greisen, characterized by low cassiterite and sulphide concentrations.

Greisenization occurred at a temperature of approximately 480°C and a pressure 4.1±1.0kb and was caused by an NaCl-brine, with variable but lesser proportions of Fe, Mn and K. The concentration of Fe in the fluid increased in quartz greisen, i.e., as the Fe content of the rock decreased towards the vein. This suggest that minerals like pyrrhotite precipitated close to the vein at the onset of alteration and were dissolved and re-precipitated further away from the vein during later stages of the alteration process. Dissolution of pyrrhotite was responsible for a decrease in the fugacity of O_2 in quartz greisen by preferential release of Fe^{2-} to the fluid. Similarly to pyrrhotite, cassiterite was dissolved close to the vein and re-precipitated in quartz-topaz greisen in response to a pH increase of the fluid produced by its interaction with the wall rock. Changes in other parameters potentially important in controlling cassiterite solubility, remained constant (temperature) or acted against it's precipitation (fO_2 and a_{Cl^-}) in the most intensely mineralized greisen.

In contrast to pyrrhotite and cassiterite, the Na content of the fluid continuously increases in the greisen. This requires that Na and possibly other components were transported towards the vein during alteration, which cannot be caused by simple infiltration. We propose that this occurred through a compensated infiltration process in which small aliquots of fluid moved back and forth between the rock and the fracture, while the bulk of the flow was parallel to the fracture. As a result, the distribution of components in the greisen was controlled by chemical potential gradients, as is the case with diffusion, but rates of mass transfer by compensated infiltration were presumably orders of magnitude faster.

REFERENCES

Aja, S.U., Wood, S.A., and Williams-Jones, A.E., 1996, The aqueous geochemistry of Zr and the solubility of some Zr-bearing minerals: Applied Geochemistry, v. 10, p. 603-620.

Alderton, D.H.M., 1989, Oxygen isotope fractionation between cassiterite and water: Mineralogical Magazine, v. 52, p. 373-376.

Barton, M.D., 1982, The thermodynamic properties of topaz solid solutions and some petrologic applications: American Mineralogist, v. 67, p. 956-974.

Barton, M.D., Haselton, H.T. JR., Hemingway, B.S., Kleppa, O.J., and Robie, R.A., 1982, Thermodynamic properties of fluor-topaz: American Mineralogist, v. 67, p. 350-355.

Borshchevskii, Y.A., Borisova, S.L., Zakharova, O.Y., Lugov, S.F., Makeyev, A.M., Podolskii, A.M., and Politov, V.K., 1983, Oxygen-isotope systematic of tin deposits of the Northeast USSR: International Geological Review, v. 25, p. 107-116.

Bottrell, S.H., Yardley, B. and Buckley, F., 1988: A modified crush-leach method for the analysis of fluid inclusion electrolytes: Bulletin de Minéralogie, v. 111, p. 279-290.

Bray, C.J., and Spooner, E.T.C., 1992, Fluid inclusion volatile analysis by gas chromatography with photoionization/micro-thermal conductivity detectors: Applications to magmatic MoS_2 and other H_2O-CO_2 and H_2O-CH_4 fluids: Geochimica et Cosmochimica Acta, v. 56, p. 261-272.

Burt, D.M., 1981, Acidity-salinity diagrams - Application to greisen and porphyry deposits: Economic Geology, v. 76, p. 832-843.

Chatterjee, A.K., Strong, D.F., and Clarke, D.B., 1985, Petrology of the polymetallic quartz-topaz greisen at East Kemptville: Nova Scotia Department of Natural Resources, Open File Report 650, p. 151-196.

Dubessy, J., 1984, Simulation des équilibres chimiques dans le système C-O-H. Conséquences méthodoligiques pour les inclusions fluides: Bulletin de Minéralogie, v. 107, p. 155-168.

Durišová . J., Charoy, B., and Weisbrod, A., 1979, Fluid inclusion studies in minerals from the tin and tungsten deposits in the Krusné Hory Mountains (Czechoslovakia): Bulletin de Minéralogie, v. 102, p. 665-675.

Eadington, P. J., 1983, A fluid inclusion investigation of ore formation in a tin-mineralized granite, New England, New South Wales: Economic Geology, v. 78, p. 1204-1221.

Finlow-Bates, T., and Stumpfl, E.F., 1981, The behavior of so-called immobile elements in hydrothermally altered rocks associated with volcanogenic submarine-exhalative deposits: Mineralium Deposita, v. 16, p. 319-328.

Grant, J.A., 1986, The isocon Diagram - A simple solution to Gresens equation for metasomatic alteration: Economic Geology, v. 81, p. 1976-1982.

Haapala, I., and Kinnunen, K., 1982, Fluid inclusion evidence on the genesis of tin deposits, *in* Metallizations associated with acid magmatism: New York, Wiley-Interscience, p. 101-110.

Halter, W.E., Williams-Jones, A.E., and Kontak, D.J., 1994, Greisen zonation and mineralization process at the East Kemptville tin deposit, Yarmouth Country, Nova Scotia, *in* Mines and Minerals branch report of activities 1993: Nova Scotia Department of Natural Resources, Mines and Energy Branches, Report 94-1, p. 161-173.

Halter, W.E., Williams-Jones, A.E., and Kontak, D.J., 1995, REE mobility during albitite formation at the East Kemptville tin deposit, Yarmouth County, Nova Scotia: Nova Scotia Department of Natural Resources, Report 95-1, p. 91-97.

Ham, L.J., and MacDonald, M.A., 1994, Geological map of Wentworth Lake: Nova Scotia Department of natural Resources, Mines and Energy Branches, map 94-03.

Heinrich, C.A., 1990, The chemistry of Hydrothermal tin (- tungsten) ore deposits: Economic Geology, v. 85, p. 457-481.

Heinrich, C.A., Ryan, C.G., Mernagh, T.P., and Eadington, P.J., 1992: Segregation of ore metals between magmatic and brine vapor: A fluid inclusion study using PIXE microanalysis: Economic Geology, v. 87, p. 1566-1583.

Jackson, K.J., and Helgeson, H.C., 1985, Chemical and thermodynamic constrains on the hydrothermal transport of tin: I. Calculation of the solubility of cassiterite at high pressures and temperatures: Geochimica et Cosmochimica Acta, v. 49, p. 1-22.

Johnson, J.W., Oelkers, E.H., and Helgeson H.C., 1991, SUPCRT92, a software package for calculating the standard molal thermodynamic properties of minerals, gases, aqueous species, and reactions from 1 to 5000 bars and 0 to 1000°C: Computers and Geosciences, v. 18, p. 899-947.

Johnston, W.D., 1965, Oxydation-Reduction equilibria in molten Na_2O-$2SiO_2$ glass: Journal of the American Ceramic Society, v. 48, p. 184-190.

Keppie, J.D., 1979, Geological map of Nova Scotia: Nova Scotia Department of Mines and Energy.

Kontak, D.J., 1990, The East Kemptville topaz-muscovite leucogranite, Nova Scotia. I. Geological setting and whole-rock geochemistry: Canadian Mineralogist, v. 28, p. 787-825.

Kontak, D.J., 1991, The East Kemptville topaz-muscovite leucogranite, Nova Scotia. II. Mineral chemistry: Canadian Mineralogist, v. 29, p. 37-60.

Kontak, D.J., 1993, Geological, geochemical and isotopic studies of the East Kemptville Sn-(Zn-Cu-Ag) deposit, Yarmouth County, Nova Scotia, Canada: Quadrennial IAGOD Symposium, Eighth, Stuttgart, Germany, E. Schweizerbart'sche Verlagsbuchhandlung, 1993, Proceedings, p. 383-409.

Kontak, D.J., and Chatterjee A.K., 1992, The East Kemptville tin deposit, Yarmouth County, Nova Scotia: a Pb-isotope study of the leucogranite and the mineralized greisens-evidence for a 366 Ma metallogenic event: Canadian Journal of Earth Sciences, v. 29, p. 1180-1196.

Kontak, D.J., and Dorsal, J., 1992, The East Kemptville tin deposit, Yarmouth County, southwestern Nova Scotia: a lithogeochemical study of the wall rock metasedimentary rocks: Atlantic Geology, v. 28, p. 63-83.

Lehmann, B., 1990, Metallogeny of tin: Berlin, Germany, Springer-Verlag 211p.

MacDonald, M.A., 1994, Geological map of the South Mountain Batholith, western Nova Scotia: Nova Scotia Department of Natural Resources, Mines and Energy Branches, map 94-01.

MacLean, W.H., and Kranidiotis, P., 1986, Immobile elements as monitor of the mass transfers in hydrothermal alteration: Phelps Dodge massive sulfide deposit, Matagami, Québec: Economic Geology, v. 82, p. 951-962.

Moyle, J.E., 1985, East Kemptville tin project, *in* Guide to the granites and mineral deposits of southwestern Nova Scotia: Nova Scotia Department of Mines and Energy, Paper 85-3, p. 199-200.

Norman, D.I., and Trangcotchasan, Y., 1982, Mineralization and fluid inclusion study of the Yod Nam tin mine, southern Thailand, *in* Metallizations associated with acid magmatism: New-York, Wiley-Interscience, p. 261-272

O'Reilly, G.A. and Kontak, D.J., 1992: The East Kemptville tin deposit and the southwestern Nova Scotia Tin Domain: Nova Scotia Department of Natural Resources, Report 92-1, p. 65-74.

Pollard, P.J., and Taylor, R.G., 1986, Progressive evolution of alteration and tin mineralization: controls by the interstitial permeability and fluid fracture-related tapping of the magmatic fluid reservoirs in tin granites: Economic Geology, v. 81, p. 1795-1800.

Raeside, R.P., Mahoney, K.L., and Peskleway, C., 1994, The aureole of the South Mountain Batholith, Nova Scotia, *in* MacDonald D.R., ed., Program and summaries, eighteenth annual review of activities: Nova Scotia Department of Natural Resources, Mines and Energy Branches, Report 94-2.

Rankin, A.H., and Alderton, D.H.M., 1985, Fluids in granites from southwest England, *in* High heat production granites, hydrothermal circulation and ore genesis: London, England, Institution of Mining and Metallurgy, p. 287-299.

Richardson, C.K., and Holland, H.D., 1979, The solubility of fluorite in hydrothermal solutions, and experimental study: Geochimica et Cosmochimica Acta, v. 43, p. 1313-1325.

Richardson, J.M., 1988, Field and textural relationships of alteration and greisen-hosted mineralization at the East Kemptville tin deposit, Davis Lake Complex, southwest Nova Scotia, *in* Recent advances in the geology of granite-related mineral deposits: Canadian Institute of Mining and Metallurgy Special Volume 39, p. 265-279.

Richardson, J. M., Bell, K., Watkinson, D. H., and Blenkinsop, J., 1990, Genesis and fluid evolution of the East Kemptville greisen-hosted tin mine, southwest Nova Scotia, Canada, *in* Ore-bearing granite systems; petrogenesis and mineralizing processes: Geological Society of America Special Paper 246, p. 181-203.

Richardson, J.M., Spooner, E.T.C., and McAuslan, D.A., 1982, The East Kemptville tin deposit, Nova Scotia: An example of a large tonnage, low grade, greisen-hosted deposit in the endocontact zone of a granite batholith: Geological Survey of Canada Current Research, part B, paper 82-1B, p. 27-32.

Roedder, E., 1958, Technique for the extraction and partial chemical analysis of fluid-filled inclusions from minerals: Economic Geology, v. 53, p. 235-269.

Salvi, S. and Williams-Jones, A.E., 1996, Fluid-inclusions volatile analyses by gas chromatography: application of a wide-bore porous-polymer cappilary colomn to the separation of organic and inorganic compounds: Geochimica et Cosmochimica Acta, in press.

Schwartz, M.O., and Surjono, A., 1990, Greisenization and albitization at the Tikus tin-tungsten deposit, Belitung, Indonesia: Economic Geology, v. 85, p. 691-713.

Schwartz, M.O., and Askury, A.K., 1989, Geologic, geochemical and fluid inclusion studies of the Tin Granites from the Bujang Melaka Pluton, Kinta Valley, Malaysia: Economic Geology, v. 84, p. 751-779.

Seward, T.M., 1974, Determination of the first ionization constant of silicic acid from quartz solubility in borate buffer solutions to 350°C: Geochimica et Cosmochimica Acta, v. 38, p. 1657-1664.

Shepherd, T.J., Rankin, A.H., and Alderton, D.H.M., 1985a, A practical guide to fluid inclusion studies: Glasgow and London, England, Blackie.

Shepherd, T.J., Miller, M. F., Scrivener, R. C., and Darbyshire, D. P. F., 1985b, Hydrothermal fluid evolution in the relation to mineralization in southwest England with special reference to the Dartmoor-Bodmin area, *in* High heat production granites, hydrothermal circulation and ore genesis: London, England, Institution of Mining and Metallurgy, p. 345-364.

Spear, F.S., Rumble D. III, and Ferry, J.M., 1982, Linear algebraic manipulation of n-dimensional composition space, *in* Characterization of metamorphism through mineral equilibria: Mineralogical Society of America, Reviews in Mineralogy, v. 10, p. 105-152.

Štemprok, M., 1987, Greisenization (a review): Geologische Rundschau, v. 76, p. 169-175.

Sterner, M.S., Hall, D.L., and Bodnar, R.J., 1988, Synthetic fluid inclusions. V. Solubility relations in the system NaCl-KCl-H_2O under vapor saturated conditions: Geochimica et Cosmochimica Acta, v. 52, p. 989-1005.

Taylor, R.G., and Pollard, P.J., 1988, Pervasive hydrothermal alteration in tin-bearing granite and implications for the evolution of ore-bearing magmatic fluids, *in* Recent advances in the geology of granite-related mineral deposits: Canadian Institute of Mining and Metallurgy Special Volume 39, p. 86-95.

Tischendorf, G., 1977, Geochemical and petrographic characteristics of silicic magmatic rocks associated with rare-element mineralization, *in* M. Štemprok, L Burnol, and G. Tischendorf, eds., Metallization associated with acid magmatism: Geological Survey of Czechoslovakia, v. 2, p. 41-98.

Wilson, G.A., and Eugster, H.P., 1990, Cassiterite solubility and tin speciation in supercritical chloride solutions, *in* Fluid-mineral interactions: A tribute to H.P. Eugster: The Geochemical Scociety, Special Publication No 2., p. 179-195.

Wones, D.R., 1989, Significance of the assemblage titanite + magnetite + quartz in granitic rocks: American Mineralogist, v. 74, p. 744-749.

Wood, S.A., 1990, The aqueous geochemistry of the rare-earth elements and yttrium, 2. Theoretical predictions of speciation in hydrothermal solutions to 350°C at saturated water pressure: Chemical Geology, v. 88, p. 99-125.

Yardley, B.W.D., and Lloyd, G.E., 1995, Why metasomatic fronts are really metasomatic slides: Geology, v. 23, p. 53-56.

Zhang, L.G., Liu, J.X., Chen, Z.S., and Zhou, H.B., 1994, Experimental investigation of oxygen isotopic fractionation in cassiterite and wolframite, Economic Geology, v. 89, p. 150-157.

Zhang, Y.G., and Frantz, J.D., 1987, Determination of the homogenization temperatures and densities of supercritical fluids in the system $NaCl-KCl-CaCl_2-H_2O$ using synthetic fluid inclusions: Chemical Geology, v. 64, p. 335-350.

Zheng, Y.F., 1991, Calculation of oxygen isotope fractionation in metal oxides: Geochimica et Cosmochimica Acta, v. 55, p. 2299-2307.

Zhu, C., and Sverjensky, D.A., 1991, Partitionning of F-Cl-OH between minerals and hydrothermal fluids: Geochimica et Cosmochimica Acta, v. 55, p. 1837-1858.

INTRODUCTION TO CHAPTER IV

In the previous chapters, we established the origin of the mineralizing fluid and the metals, the effect of alteration on the chemistry of the fluid and the rock, and suggested controls on cassiterite precipitation. In particular, we suggested that the temperature at which greisenization took place was approximately constant across the alteration halo and that this temperature had to be above 250°C; the temperature at which fluid inclusions homogenize. However the exact temperature, as well as the pressure of the alteration are still unknown, yet these parameters are essential for later modeling of fluid-rock interaction.

In Chapter 4, we calibrate a geothermometer based on the F-OH exchange between muscovite and topaz to determine the temperature of greisenization. The pressure is also estimated using isobaric extrapolation of fluid inclusion data. In addition to East Kemptville, this geothermometer is tested in two other localities.

CHAPTER IV

CALIBRATION OF A MUSCOVITE-TOPAZ F-OH EXCHANGE GEOTHERMOMETER

WERNER E. HALTER

AND

ANTHONY E. WILLIAMS-JONES

DEPARTMENT OF EARTH AND PLANETARY SCIENCES, MCGILL UNIVERSITY
3450 UNIVERSITY STR. MONTREAL, QUEBEC, H3A 2A7

ABSTRACT

Recently reported thermodynamic data for the F^- endmembers of muscovite permitted calibration of a geothermometer based on the F-OH exchange between muscovite and topaz. The geothermometer provides reliable estimates for the temperature of greisen forming systems that are essentially independent of pressure. At an average pressure for hydrothermal systems of 2000 bars, the temperature can be calculated using the equation

$$T(^{\circ}C) = -1805.8x - 296.24$$

where x is equal to

$$1/\{2 \log (X_{OH}^{toz}/X_{F}^{toz}) + 2 \log (X_{F}^{ms}/X_{OH}^{ms})\}.$$

This geothermometer was tested with samples from three different localities where there had been previous estimates of the temperature. Calculated temperatures compared well with the previous estimates provided that the total content of doubly charges cations (Fe^{2+}, Mg^{2+} and Mn^{2+}) in the muscovite was less than 0.4 cations per formula unit (based on 22 oxygens).

INTRODUCTION

Temperatures at which greisens form have been poorly documented because of a lack of reliable geothermometers. The most widely used geothermometer is based on oxygen isotopic fractionation between cassiterite and quartz. However, this geothermometer cannot be confidently applied because of a large discrepancy between empirical (Borshchevskii et al., 1983; Alderton, 1989), theoretical (Zheng, 1991) and experimental calibrations (Zhang et al., 1994). Fluid inclusions could also provide information on the temperature of greisen formation, but this requires that the composition of the fluid and the pressure of entrapment be known.

The purpose of this paper is to calibrate a new geothermometer in order to obtain better estimates of temperature fro greisen systems. In similar rocks, the F-OH exchange between biotite and apatite has been successfully used as a geothermometer because of the small volume change associated with this substitution. We therefore use the same substitution, but in this case between topaz and muscovite, in order to estimate the temperature of formation of greisen assemblages. This geothermometer is calibrated using thermodynamic data on muscovite and topaz from Barton (1982), Barton et al (1982) and Zhu and Sverjensky (1991), and tested on samples from the East Kemptville tin deposit, Nova Scotia and two other localities.

METHODOLOGY

The exchange reactions between an (OH, F)-bearing phase Φ and a hydrothermal fluid can be written as:

$$\Phi(OH)_2 + 2\ HF^0 = \Phi(F)_2 + 2\ H_2O \qquad (1)$$

where $\Phi(OH)_2$ and $\Phi(F)_2$ are the pure hydroxyl- and fluoride-endmembers of the phase Φ. Hence, the F-OH exchange reactions between a fluid and topaz or muscovite are, respectively:

$$\underset{\text{fluor-topaz}}{Al_2SiO_4(F)_2} + 2\ H_2O = \underset{\text{hydroxy-topaz}}{Al_2SiO_4(OH)_2} + 2\ HF^0 \qquad (2)$$

$$\underset{\text{fluor-muscovite}}{KAl_3Si_3O_{10}(F)_2} + 2\ H_2O = \underset{\text{hydroxy-muscovite}}{KAl_3Si_3O_{10}(OH)_2} + 2\ HF^0 \qquad (3)$$

By subtracting reaction (3) from (2), the F-OH exchange reaction between muscovite and topaz is:

$$Al_2SiO_4(F)_2 + KAl_3Si_3O_{10}(OH)_2 = Al_2SiO_4(OH)_2 + KAl_3Si_3O_{10}(F)_2 \qquad (4)$$

fluor-topaz + hydroxy-muscovite = hydroxy-topaz + fluor-muscovite

and for this reaction

$$\log K_{(4)T,P} = -(G^{T,P}{}_{Al_2SiO_4(OH)_2} + G^{T,P}{}_{KAl_3Si_3O_{10}(F)_2} - G^{T,P}{}_{Al_2SiO_4(F)_2} - G^{T,P}{}_{KAl_3Si_3O_{10}(OH)_2}) / RT \qquad (5)$$

The thermodynamic data for these phases are listed in Table 1. Data for fluor-topaz and hydroxy-topaz are from Barton (1982) and Barton et al. (1982). The ΔH of hydroxy-topaz was obtained by adding the enthalpies of formation of the elements (Robie and Waldbaum, 1968 and Pankratz, 1982). Data for fluor-muscovite are from Zhu and Sverjensky (1991) and those for hydroxy-muscovite are from Johnson et al. (1991). Maier-Kelly heat capacity coefficients for the above phases were obtained by fitting the appropriate curve through heat capacity values calculated between 0 and 500°C (see Table 1 for sources of these data). The values for $\log K_{(4)T,P}$ at various temperatures and pressures were calculated from equation (5) using these thermodynamic data and the program SUPCRT92 (Johnson at al., 1991).

Table 1: Thermodynamic constants for F and OH endmembers of muscovite and topaz.

		F-muscovite	OH-muscovite	F-topaz	OH-topaz
ΔG^0 (J/mol)		-5768818 [1]	-5585738 [3]	-2907876 [4]	-2690674 [6]
ΔH^0 (J/mol)		-6107093 [1]	-5966565[3]	-3081500[4]	-2896080[7]
S^0 (J/mol*K)		297 [1]	284 [3]	105 [4]	100 [6]
V (cm^3/mol)		140.87 [1]	140.71 [3]	51.53 [6]	53.92 [6]
Heat capacity coefficients (c_p)	a	78.926 [2]	97.56 [3]	42.741 [5]	45.817 [8]
	b	0.040 [2]	0.026 [3]	0.013 [5]	0.014 [8]
	c	-1482661 [2]	-2544000 [3]	-1061331 [5]	-1134009 [8]

[1] Zhu and Sverjensky (1991)

[2] Calculated using data from Zhu and Sverjensky (1991)

[3] Helgeson et al. (1978)

[4] Barton et al. (1982)

[5] Calculated using data from Barton at al. (1982)

[6] Barton (1982)

[7] Calculated from the H of fromation of the elements (Robie and Waldbaum, 1968 and Pankratz, 1982)

[8] Calculated using data from Barton (1982)

The equilibrium constant $K_{(4)T,P}$ of the exchange reaction (4) at a given temperature and pressure can also be written as

$$K_{(4)T,P} = (a^{2}{}_{Al_2SiO_4(OH)_2}{}^{toz} * a^{2}{}_{KAl_3Si_3O_{10}(F)_2}{}^{ms}) / (a^{2}{}_{Al_2SiO_4(F)_2}{}^{toz} * a^{2}{}_{KAl_3Si_3O_{10}(OH)_2}{}^{ms}) \quad (6)$$

Since the electronegativity and the effective ionic radius for F^- and OH^- are quite similar, we can consider that OH^- and F^- mix ideally in most OH-F bearing phases $\Phi(OH, F)$, including topaz and muscovite (Zhu and Sverjensky, 1991). The activities of the fluoride and the hydroxyl component of a non-endmember phase $\Phi(OH, F)_2$ can therefore be estimated accurately by the mole fractions of OH^- and F^- in this phase. Accordingly,

$$\log K_{(4)T,P} = 2 \log (X_{OH}{}^{toz} / X_F{}^{toz}) + 2 \log (X_F{}^{ms} / X_{OH}{}^{ms}) \quad (7)$$

where X_F and X_{OH} are the mole fractions of the fluoride and the hydroxyl components of the phase. The mole fractions of fluor-muscovite and fluor-topaz in the two phases can be estimated easily from microprobe analyses of F. Assuming that the F-OH site is completely filled, the mole fraction of the OH-component is calculated by

$$X_{OH}{}^{ms,\,toz} = 4 - X_F{}^{ms,\,toz} - X_{Cl}{}^{ms,toz} \quad (8)$$

with formula units based on 22 and 10 oxygens for muscovite and topaz, respectively ($X_{Cl}{}^{ms,toz}$ is the mole fraction of chlorine).

If the values for $K_{(4)T,P}$ are calibrated at various temperatures and pressures using the thermodynamic data of Table 1 and equation (5), the conditions at which a muscovite-topaz pair formed can be estimated by comparing the value of $K_{(4)T,P}$ obtained from equation (7) with that calculated by equation (5).

We also tested the possibility of applying the F-OH exchange to topaz-apatite and muscovite-apatite pairs to provide an additional geothermometer for greisen systems. Unfortunately, the composition of apatite in fluorine-rich environments is very close to that of the pure fluor-apatite endmember, i.e., 96-98% of the hydroxyl site is filled with F.

Consequently, small errors in analyses for F in apatite will induce very large relative errors in estimates of OH^- contents based on site occupancy, and F-OH exchange involving apatite can therefore not be used to obtain reliable geothermometers for greisens unless the OH^- content can be estimated independently.

PRESSURE DEPENDENCE

Values of $\log K_{(4)T,P}$ were calculated at temperatures between 200 and 600°C and pressures between 500 and 4000 bars using the thermodynamic data in Table 1 and the program SUPCRT92 (Johnson et al., 1991). These values are presented in Table 2 and shown graphically as a function of pressure and temperature in Figure 1. For a given value of $\log K_{(4)T,P}$, the temperature can be estimated at various pressures using the equation

$$T(^{\circ}C) = ax + b \qquad (9)$$

in which x is equal to $1/(\log K_{(4)T,P})$ obtained from equation (7) and a and b are constants given in Table 3 for various pressures. The dependence of temperature on pressure is approximately 5°C/kbar (Fig. 1).

APPLICATION OF THE F-OH GEOTHERMOMETER

East Kemptville

The East Kemptville deposit, Nova Scotia is a classical greisen-hosed tin deposit formed through the alteration of leucogranite at the southwestern end of the 370 Ma South Mountain Batholith of the Meguma Terrane (Chapters 2 and 3). Alteration began with the replacement of K-feldspar and albite by muscovite to form a quartz-sericite greisen. With further alteration muscovite was replaced by topaz and formed quartz-topaz greisen next to veins. Muscovite and topaz are present in both the quartz-muscovite and the quartz-

Table 2 : values for log K at temperatures between 200 and 600°C and pressures between 500 and 4000 bars.

T(degC)	P(bars)	Log K	T(degC)	P(bars)	Log K	T(degC)	P(bars)	Log K
200	500	-3.645	340	500	-2.792	480	500	-2.293
200	1000	-3.659	340	1000	-2.803	480	1000	-2.302
200	1500	-3.673	340	1500	-2.814	480	1500	-2.311
200	2000	-3.687	340	2000	-2.825	480	2000	-2.32
200	2500	-3.701	340	2500	-2.836	480	2500	-2.328
200	3000	-3.715	340	3000	-2.846	480	3000	-2.337
200	3500	-3.729	340	3500	-2.857	480	3500	-2.346
200	4000	-3.743	340	4000	-2.868	480	4000	-2.355
220	500	-3.489	360	500	-2.705	500	500	-2.239
220	1000	-3.503	360	1000	-2.716	500	1000	-2.247
220	1500	-3.516	360	1500	-2.726	500	1500	-2.256
220	2000	-3.53	360	2000	-2.737	500	2000	-2.264
220	2500	-3.543	360	2500	-2.747	500	2500	-2.273
220	3000	-3.557	360	3000	-2.758	500	3000	-2.282
220	3500	-3.57	360	3500	-2.768	500	3500	-2.29
220	4000	-3.584	360	4000	-2.779	500	4000	-2.299
240	500	-3.347	380	500	-2.624	520	500	-2.187
240	1000	-3.36	380	1000	-2.634	520	1000	-2.196
240	1500	-3.373	380	1500	-2.645	520	1500	-2.204
240	2000	-3.386	380	2000	-2.655	520	2000	-2.212
240	2500	-3.399	380	2500	-2.665	520	2500	-2.221
240	3000	-3.412	380	3000	-2.675	520	3000	-2.229
240	3500	-3.425	380	3500	-2.685	520	3500	-2.238
240	4000	-3.438	380	4000	-2.696	520	4000	-2.246
260	500	-3.217	400	500	-2.549	540	500	-2.139
260	1000	-3.229	400	1000	-2.559	540	1000	-2.147
260	1500	-3.242	400	1500	-2.569	540	1500	-2.155
260	2000	-3.254	400	2000	-2.579	540	2000	-2.163
260	2500	-3.267	400	2500	-2.588	540	2500	-2.171
260	3000	-3.279	400	3000	-2.598	540	3000	-2.18
260	3500	-3.292	400	3500	-2.608	540	3500	-2.188
260	4000	-3.304	400	4000	-2.618	540	4000	-2.196
280	500	-3.097	420	500	-2.479	560	500	-2.093
280	1000	-3.109	420	1000	-2.488	560	1000	-2.101
280	1500	-3.121	420	1500	-2.498	560	1500	-2.109
280	2000	-3.133	420	2000	-2.507	560	2000	-2.117
280	2500	-3.146	420	2500	-2.517	560	2500	-2.125
280	3000	-3.158	420	3000	-2.527	560	3000	-2.133
280	3500	-3.17	420	3500	-2.536	560	3500	-2.141
280	4000	-3.182	420	4000	-2.546	560	4000	-2.149
300	500	-2.987	440	500	-2.413	580	500	-2.049
300	1000	-2.999	440	1000	-2.422	580	1000	-2.057
300	1500	-3.011	440	1500	-2.431	580	1500	-2.065
300	2000	-3.022	440	2000	-2.441	580	2000	-2.073
300	2500	-3.034	440	2500	-2.45	580	2500	-2.08
300	3000	-3.046	440	3000	-2.459	580	3000	-2.088
300	3500	-3.057	440	3500	-2.469	580	3500	-2.096
300	4000	-3.069	440	4000	-2.478	580	4000	-2.104
320	500	-2.886	460	500	-2.351	600	500	-2.008
320	1000	-2.897	460	1000	-2.36	600	1000	-2.016
320	1500	-2.908	460	1500	-2.369	600	1500	-2.023
320	2000	-2.92	460	2000	-2.378	600	2000	-2.031
320	2500	-2.931	460	2500	-2.387	600	2500	-2.038
320	3000	-2.942	460	3000	-2.396	600	3000	-2.046
320	3500	-2.953	460	3500	-2.406	600	3500	-2.054
320	4000	-2.965	460	4000	-2.415	600	4000	-2.061

Table 3: Coefficients for equation (9) at various pressures

Pressure	a	b
500	-1786.0	-296.57
1000	-1792.8	-296.53
1500	-1799.1	-296.33
2000	-1805.8	-296.24
2500	-1811.7	-295.90
3000	-1818.9	-296.00
3500	-1826.1	-296.10
4000	-1832.3	-295.83

Figure 1: Pressure-temperature diagram showing thermodynamically calculated values of log K for reaction (4). The slope of the lines is approximately 5°C per kbar.

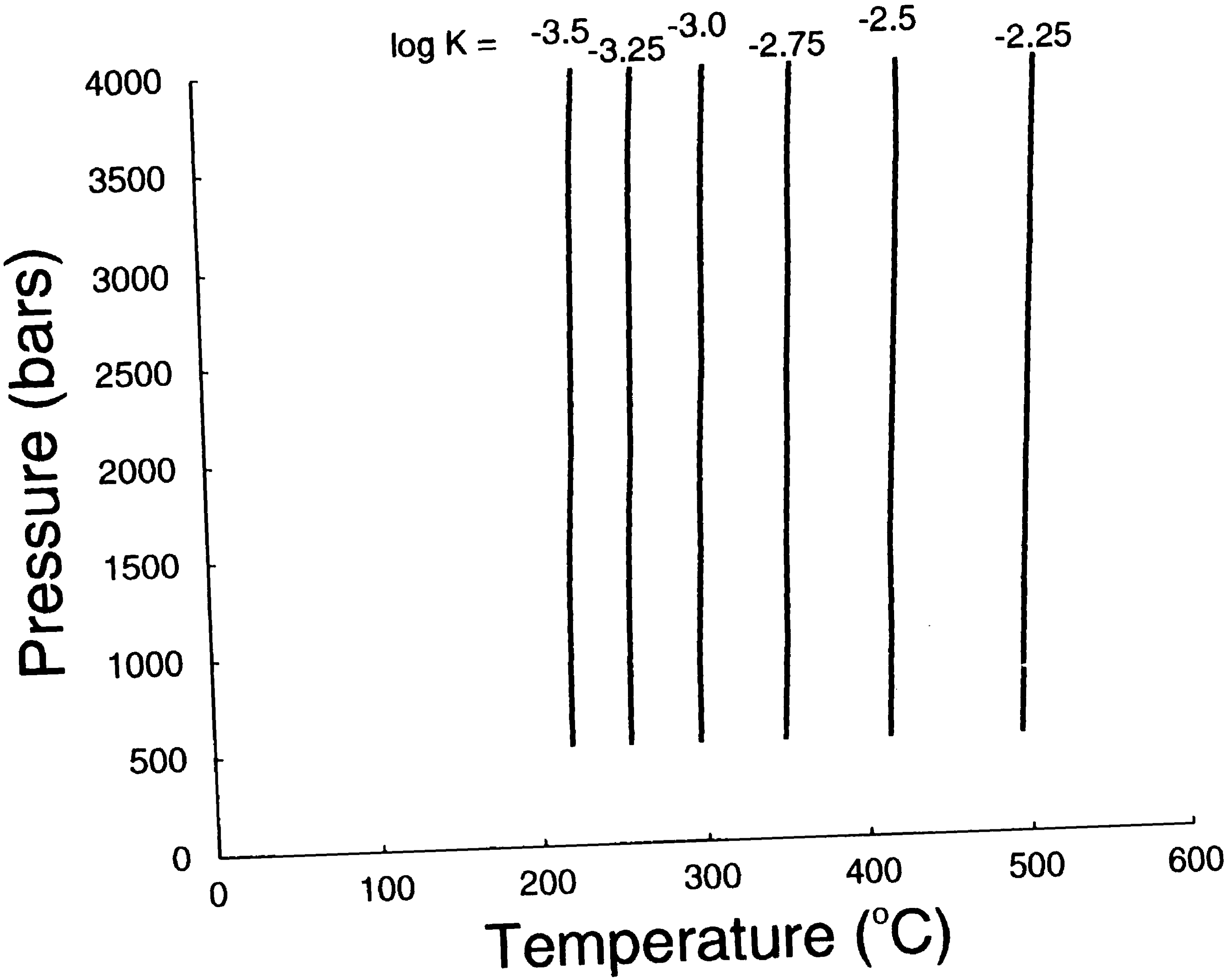
log K =
-3.5
-3.25
-3.0
-2.75
-2.5
-2.25
Pressure (bars)
4000
3500
3000
2500
2000
1500
1000
500
0
Temperature (°C)
0
100
200
300
400
500
600

topaz greisen and these rock types are therefore ideal candidates for testing the muscovite-topaz geothermometer developed above.

In order to be able to apply the muscovite-topaz geothermometer, the F content of the muscovite has to be a function only of the a_{HF^0} in the fluid. However, the proportion of F that can be accommodated by the muscovite structure is highly dependent on the concentration of doubly charged cations (M^{2+}), among which Fe^{2+} is the most important (Munoz, 1984). Muscovite with a high Fe content should therefore be avoided as it will only provide a maximum temperatures for the formation of the mineral assemblage.

At East Kemptville, the sample containing muscovite least enriched in Fe (sample 38.6) is from a vein. The F content of muscovite in this sample does not correlate with M^{2+} (Fig. 2), i.e., the presence of M^{2+} ions did not influence the incorporation of F^-. Unfortunately, in this sample, muscovite is typically "anhydrous" and dehydration changes the thermodynamic properties of these micas, making them unsuitable for geothermometry (Chapter 6); only one muscovite analysis yielded a stoichiometric composition, i.e., it was not dehydrated, and could therefore be used to reliably estimate the temperature of formation of the topaz-muscovite assemblage with the geothermometer. The composition of the latter muscovite is shown in Table 4, together with the average topaz composition in the same sample.

Stoichiometric muscovite is present in quartz-sericite greisen, but in these rocks the M^{2+} content of the muscovite is significant and correlates well with the F^- content (Figure 3). However, the dependence of the F^- content on that of M^{2+} decreases with decreasing M^{2+} concentration, and a third order regression through the data suggests that below a concentration of M^{2+} of approximately 0.4 cations per formula unit (based on 22 oxygens), the F^- content does not vary, i.e., it is independent of the M^{2+} concentration. This is the same conclusion as that drawn above for muscovite from the vein sample 38.6 (Figure 2). We therefore suggest that the F content (0.62) of the single muscovite which contains <0.4 M^{2+} per formula unit (Fig. 3) is the most appropriate to use in calculating the temperature of formation of the quartz-sericite greisen. The composition of the latter muscovite and the average composition of the co-existing topaz are given in Table 4. In

Table 4: Composition of Fe-poor muscovite and average composition of co-existing topaz

Sample	Vein		Quartz-ser. greisen		Triberg Granite		Seagull batholith	
	Musc.	Topaz	Musc.	Topaz	Musc.	Topaz	Musc.	Topaz
SiO_2	48.42	32.33	47.25	32.68	48.88	32.68	47.63	32.09
TiO_2	0.03		0.02		0.10		0.11	
Al_2O_3	34.35	55.30	33.66	55.25	30.91	55.37	28.42	55.38
FeO	0.72	0.01	2.43		2.82	0.07	3.93	0.02
MnO	0.05		0.27		0.30		0.06	
MgO	1.10	0.00	0.04	0.00	0.53		1.68	0.00
CaO	0.00	0.02	0.01	0.00	0.07	0.01	0.02	0.03
Na_2O	0.38		0.25		0.06		0.12	
K_2O	10.47		11.32		10.09		11.50	
F	1.53	15.14	1.47	15.24	0.98	16.20	2.21	15.88
Total	96.44	96.42	96.09	96.82	95.28	97.18	94.75	96.61
atoms per formula unit (calculated on 22 oxygens for muscovite and 10 oxygens for topaz								
Si	6.38	1.99	6.35	2.00	6.62	2.00	6.59	1.99
Ti	0.00		0.00		0.01		0.01	
Al	5.33	4.01	5.33	3.99	4.92	3.99	4.64	4.01
Fe	0.08	0.00	0.27	0.00	0.32		0.46	0.00
Mn	0.01		0.03		0.03		0.01	
Mg	0.22	0.00	0.01	0.00	0.10		0.35	0.00
Ca	0.00	0.00	0.00	0.00	0.01	0.00	0.00	0.00
Na	0.10		0.06		0.03		0.03	
K	1.76		1.94		1.74		2.03	
F	0.64	2.95	0.62	2.95±0.12	0.44	3.08	0.97	3.14±0.05
Total	14.53	8.95	14.68	8.95	13.80	8.08	15.08	9.15
OH (calculated)	3.36	1.05	3.38	1.05±0.12	3.56	0.92	3.03	0.86±0.05
F/OH	0.19		0.18		0.12		0.32	
OH/F		0.36		0.36		0.30		0.27
Log K		-2.33		-2.37		-2.85		-2.12

Cl is below detection limit in all the samples.

Figure 2: A plot of the concentration of F^- per formula unit (based on 22 oxygens) as a function of the proportion of M^{2+} cations in muscovite from a vein sample (38.6). At these low M^{2+} concentrations, the F content of the muscovite is independent of the M^{2+} concentration. The dashed line is a linear regression through the data.

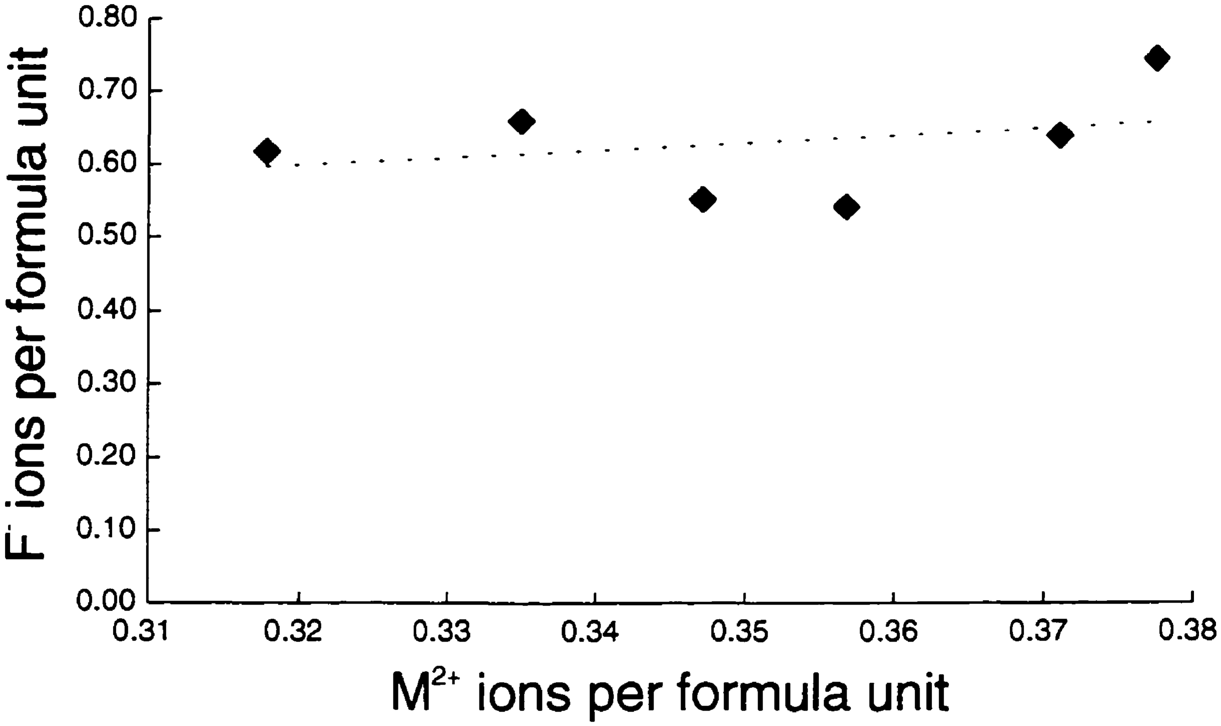

0.80
0.70
0.60
0.50
0.40
0.30
0.20
0.10
0.00
F⁻ ions per formula unit
0.31
0.32
0.33
0.34
0.35
0.36
0.37
0.38
M²⁺ ions per formula unit

Figure 3: The concentration of F^- anions versus the concentration of M^{2+} (cations per formula unit, based on 22 oxygens) in muscovite from samples in the quartz-sericite greisen. A third order polynomial fitted to the data (solid line) predicts that below 0.4 M^{2+} cations per formula unit, the F content does not change, i.e., it is independent of the M^{2+} concentration. The cross represents a stoichiometric mica from sample 38.6 (see text).

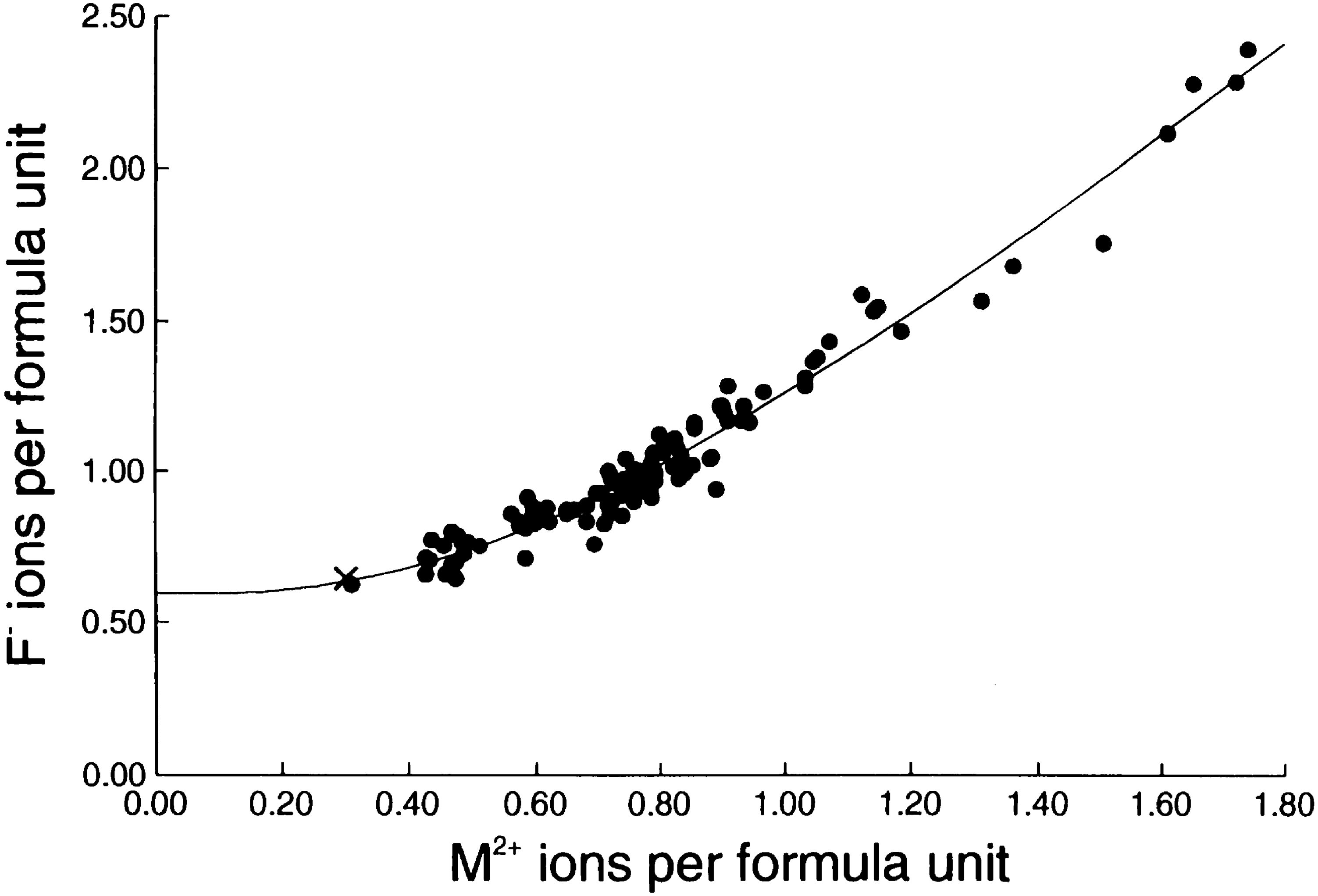
2.50
2.00
1.50
1.00
0.50
0.00
F^- ions per formula unit
0.00
0.20
0.40
0.60
0.80
1.00
1.20
1.40
1.60
1.80
M^{2+} ions per formula unit

this Table, the number of OH^- groups was calculated using equation (8) and $\log K_{T,P}$ using equation (7).

The $\log K_{T,P}$ values determined for the samples discussed above were used in equation (9) to calculate the temperatures of greisen formation. These temperatures vary between 454 and 476°C for the quartz-sericite greisen and between 468 and 490°C for the vein sample at pressures between 500 and 4000 bars. The heavy line in Figure 4 represents these conditions in P-T space. In the same samples, fluid inclusions in quartz contain liquid + vapour ± halite, have a salinity of 30 ± 5wt-% NaCleq. and are consistent with a single mineralizing event (Chapter 3). Inclusions that homogenize to the liquid phase do so at temperatures of 246 ± 32°C. The corresponding isochore intersects the muscovite-topaz geothermometer applied to the quartz-sericite greisen and the vein samples at temperatures of 476°C and 490°C, respectively and at a pressure of approximately 4.1 kbars (Fig. 4).

An independent estimate of the formation temperature of the East Kemptville greisens was made using the oxygen isotopic fractionation between cassiterite and quartz. A sample of vein material in quartz topaz greisen yielded $\delta^{18}O$ values for cassiterite and quartz of 3.0‰ and 10.4‰ respectively, corresponding to a $\Delta^{18}O$ of 7.4‰. The corresponding temperatures using the empirical geothermometer of Borshchevskii et al. (1983) and Alderton (1989) are 340°C and 372°C, respectively, and using the theoretical geothermometer of Zheng (1991) is 348°C. By contrast, the experimentally calibrated geothermometer of Zhang et al. (1994) yields a temperature of 473°C, which is in very good agreement with the temperatures calculated from the topaz-muscovite exchange reaction. We therefore conclude that greisenization at East Kemptville occurred at a temperature of 480 ± 15°C and a pressure of 4.1 ± 1.0 kbars.

Triberg Granite

Only one published study, namely that of Markl and Schumacher (1996) on the 325 ± 2 Ma Triberg Granite Complex in the Black Forest, Germany, reports analyses of topaz and

Figure 4: Pressure-temperature diagram showing conditions estimated for greisen formation at East Kemptville. The heavy lines represent the muscovite-topaz geothermometer and the thin lines various calibrations of the cassiterite-quartz oxygen isotopic geothermometer. The isochores are from fluid inclusion data in these rocks (Chapter 3), calculated using experimental data from Zhang and Frantz (1987). Greisenization at East Kemptville is estimated to have occurred at a temperature of approximately 480°C and a pressure of 4.1 kb.

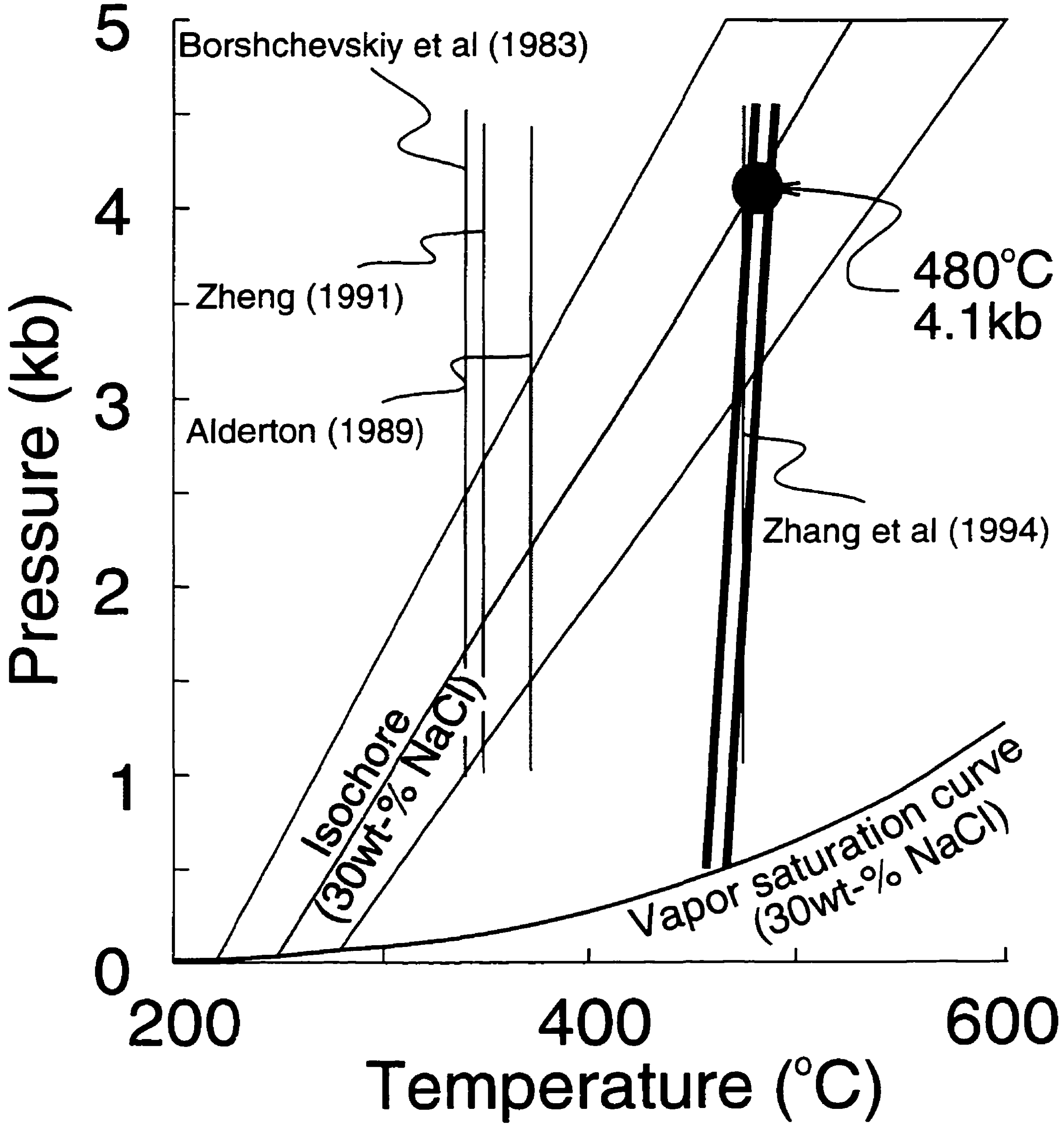

Pressure (kb)
5
4
3
2
1
0
Temperature (°C)
200
400
600
Borshchevskiy et al (1983)
Zheng (1991)
Alderton (1989)
Zhang et al (1994)
480°C
4.1kb
Isochore
(30wt-% NaCl)
Vapor saturation curve
(30wt-% NaCl)

muscovite from the same rocks. The complex comprises an assemblage of monzogranite, granodiorite and a two-feldspar, two-mica leucogranite which contains beryl-bearing pegmatites (Markl and Schumacher, 1996). Alteration by a late magmatic fluid, circulating in veins, affected the leucogranite and associated pegmatites and converted the intrusive rock into a topaz-, fluorite- and cassiterite-bearing quartz-muscovite greisen. In less altered rocks, beryl in the pegmatites was replaced by phenakite, muscovite and quartz at temperatures below 250°C (based on mineral stability relationships). Primary fluid inclusions in cassiterite homogenize to liquid at temperatures between 333 and 357°C and secondary inclusions in beryl from samples close to the most intensively greisenized part of the leucogranite homogenize at temperatures between 341 and 374°C. Unfortunately, the pressure was not estimated and the homogenization temperatures are therefore minimum temperatures of greisen formation. However, earlier studies of Black Forest granites suggest a shallow level of emplacement based on petrographic considerations (Emmermann, 1977), and Simon (1990) concluded from fluid inclusion microthermometry, feldspar geothermometry and cation thermometry that hydrothermal alteration in two mica granites of the Black Forest occurred at temperatures between 300 and 400°C at a depth of 4 to 7 km. If the same depth is assumed for the Triberg granite, pressure correction of the homogenization temperatures would yield trapping temperatures between 380 and 430°C (hydrostatic pressure) and 510 and 630°C (lithostatic pressure).

Average muscovite and topaz analyses from the same greisen are presented in Table 4. In these samples, muscovite contains very little Fe (<0.48 M^{2+} ions, calculated on 22 oxygens). The average F concentration of muscovite is 0.44 ± 0.02 F anions per formula unit and that of topaz is 2.94 ± 0.20 F anions (for 10 oxygens). The log K calculated using these data and equation (7) is -2.85 which corresponds to temperatures between 327 and 343°C at pressures between 500 and 4000 bars (equation 8). These temperatures are close to homogenization temperatures of fluid inclusions in the same samples and of hydrothermal alteration in other Black Forest granites.

Seagull Batholith

Samples from quartz-cassiterite-bearing greisens in the Seagull Batholith, Yukon Territory, supplied by Dr. I. Samson, provided an additional opportunity to test the topaz-muscovite geothermometer. The batholith is composed of a meta- to peraluminous, medium- to coarse-grained leucocratic granite of mid-Cretaceous age with a composition typical of highly differentiated granites (Sinclair and Richardson, 1992). The roof zone of the batholith is characterized by tin-rich tourmaline orbicules interpreted to have formed at the transition between the magmatic and the hydrothermal stage (Samson and Sinclair, 1992). Greisen occurs locally in this zone, around discrete cassiterite-sulphide-bearing veins (Mato et al., 1983). Based on fluid inclusion microthermometric data and a pressure of 1 kbar, (estimated from stratigraphic reconstruction; Layne and Spooner, 1991), the orbicules are interpreted to have formed at temperatures between 500 and 600°C (Samson and Sinclair, 1992). Similar or slightly lower temperatures are inferred for the formation of cassiterite-bearing veins and associated greisens, on the assumption that they formed from the same orthomagmatic fluids that produced the orbicules.

Muscovite is a minor phase in the topaz-bearing samples and unfortunately contains appreciable Fe (0.82 M^{2-} ions based on 10 oxygens). Table 4 reports average analyses for this muscovite (20 analyses) and of co-existing topaz (16 analyses). The log K calculated with equation (7) corresponds to a temperature of formation of approximately 560°C. Although this temperature is within the range given by Samson and Sinclair (1992) for the associated orbicules, it is a maximum temperature due to the high M^{2-} content of the muscovite, and likely overestimates the true temperature of greisen formation in this batholith.

SOURCES OF ERROR

The above examples suggest that the muscovite-topaz geothermometer developed in this paper yields reliable estimates of the temperature at which topaz and muscovite form during greisenization, provided that the concentration of Fe, Mn and Mg in muscovite is low, i.e., below 0.4 M^{2-} ions per formula unit (based on 22 oxygens).

A major source of error affecting the accuracy of the muscovite-topaz geothermometer is uncertainty in the fluorine analyses. We evaluated these uncertainties for topaz by repeated analyses (>18) of several homogenous crystals from the East Kemptville quartz-sericite greisen and obtained a standard deviation of 0.12 ions per formula unit (Table 4), which corresponds to an error of ± 4.0%. Owing to the variation in the Fe content of muscovite, it is not meaningful to calculate a standard deviation for the analyses of F in this phase, but if the same error of ± 4.0% is applied, the F content in muscovite varies by ± 0.025 anions per formula unit. Taking into account the standard errors for both topaz and muscovite, the range in temperature is 420 to 540°C at a pressure of 4 kbars, i.e., corresponding to an error of approximately ± 60°C or ±12.5%. This error is significant, but can be reduced if a larger number of analyses are made, and if analyses are restricted to Fe-poor muscovite.

An additional source of error is the thermodynamic data, but evaluation of this error is a complicated task which is well beyond the scope of the present paper (Anderson 1978; Chatterjee, 1991).

CONCLUSIONS

Using thermodynamic data on F^- and OH^- endmembers of muscovite and topaz we have been able to calibrate the F-OH exchange between these phases as a function of temperature and pressure. The effect of pressure on this exchange is approximately 5°C/kbar making it a potentially excellent geothermometer for application to greisens.

The F^- content of both phases can be determined from microprobe analyses and the OH^- content estimated from the occupancy of the hydroxyl site. The temperature of formation is calculated by comparing thermodynamically calculated values of log K for the exchange reaction

$$Al_2SiO_4(F)_2 + KAl_3Si_3O_{10}(OH)_2 = Al_2SiO_4(OH)_2 + KAl_3Si_3O_{10}(F)_2$$

fluor-topaz + hydroxy-muscovite = hydroxy-topaz + fluor-muscovite

with those obtained from the equation

$$\mathrm{LogK} = 2\log(X_{OH}^{toz}/X_F^{toz}) + 2\log(X_F^{ms}/X_{OH}^{ms})$$

assuming ideal mixing on the hydroxyl site. Errors associated with this thermometer due to uncertainties in the microprobe analyses are approximately 12.5%,.

We used this thermometer to establish the temperature and the pressure of greisenization at the East Kemptville tin deposit as 480°C ± 15°C. This is in very good agreement with temperatures obtained using the quartz-cassiterite oxygen isotope geothermometer of Zhang et al. (1994). The muscovite-topaz geothermometer was also tested on greisens from the Triberg granite (Germany) and the Seagull Batholith (Yukon) for which it yield temperatures of approximately 335 and 560°C, respectively. These temperatures are close to published fluid inclusion homogenization temperatures for Triberg samples and within the range of temperatures estimated for the formation of associated orbicules in the Seagull Batholith. The Seagull temperature is nevertheless a maximum value and may overestimate the temperature of greisen formation in the batholith.

We conclude that the muscovite-topaz geothermometer provides reliable temperature estimates for greisen formation, provided that the M^{2-} content of the muscovite is below 0.4 cations per formula unit (based on 22 oxygens), as is the case at East Kemptville and in the Triberg granite, but not for the Seagull batholith where the temperature may be overestimated.

REFERENCES

Alderton, D.H.M., 1989, Oxygen isotope fractionation between cassiterite and water: Mineralogical Magazine, v. 52, p. 373-376.

Anderson, G.M., 1978, Uncertainties in calculations involving thermodynamic data, *in* H.J. Greenwood, ed., Mineralogical Association of Canada Short Course, v.2, p. 199-215.

Barton, M.D., 1982, The thermodynamic properties of topaz solid solutions and some petrologic applications: American Mineralogist, v. 67, p. 956-974.

Barton, M.D., Haselton, H.T. Jr., Hemingway, B.S., Kleppa, O.J., and Robie, R.A., 1982, Thermodynamic properties of fluor-topaz: American Mineralogist, v. 67, p. 350-355.

Borshchevskii, Y.A., Borisova, S.L., Zakharova, O.Y., Lugov, S.F., Makeyev, A.M., Podolskii, A.M., and Politov, V.K., 1983, Oxygen-isotope systematic of tin deposits of the Northeast USSR: International Geological Review, v. 25, p. 107-116.

Chatterjee, N.D., 1991, Applied mineralogical thermodynamics, Berlin, Heidelberg, Germany, Springer-Verlag.

Emmermann, R., 1977, A petrogenitic model for the origin and the evolution of the Hercynian granite series of the Schwartzwald, Neues Jahrbuch für Mineralogie, Abhandlungen, v. 128, p. 219-253.

Helgeson, H.C., Delany, J.M., Nesbitt, H.W., and Bird, D.K., 1978, Summary and critique of the thermodynamic properties of rock-forming minerals: American Journal of Science, v. 278A, 229 p.

Johnson, J.W., Oelkers, E.H., and Helgeson H.C., 1991, SUPCRT92, a software package for calculating the standard molal thermodynamic properties of minerals, gases, aqueous species, and reactions from 1 to 5000 bars and 0 to 1000°C: Computers and Geosciences, v. 18, p. 899-947.

Layne, G.D., and Spooner, E.T.C., 1991, The JC tin skarn deposit, southern Yukon Territory. I. Geology, paragenesis and fluid inclusion microthermometry: Economic Geology, v. 86, p. 29-47.

Markl, G., and Schumacher, J.C., 1996, Spatial variation in temperature and composition of greisen-forming fluids: An example from the Variscan Triberg granite complex, Germany: Economic Geology, v. 91, p. 576-589.

Mato, G., Ditson, G., and Godwin, C.I., 1983, Geology and geochronology of tin mineralization associated with the Seagull Batholith, south-central Yukon Territory: Canadian Institute of Mining and Metallurgy Bulletin, v., 76, p. 43-49.

Munoz, J.L., 1984, F-OH and Cl-OH exchange in micas with applications to the hydrothermal ore deposits, *in* S.W. Bailey, ed., Micas: Reviews in Mineralogy, Mineralogical Society of America, v. 13, p. 469-494.

Pankratz, L.B., 1982, Thermodynamic properties of elements and oxides: U.S. Dept. of Interior, Bureau of Mines, Bulletin 672, 509p.

Robie, R.A., and Waldbaum, D.R., 1968, Thermodynamic properties of minerals and related substances at 298.15°K (25.0°C) and one atmosphere (1.013 bars) pressure and at higher temperatures: Bull. U.S. Geological Survey 1259.

Samson, I.M., and Sinclair, W.D., 1992, Magmatic hydrothermal fluids and the origin of quartz-tourmaline orbicules in the Seagull Batholith, Yukon Territory: Canadian Mineralogist, v. 30, p. 937-954.

Simon, K., 1990, Hydrothermal alteration of Variscan granites, southern Schwartzwald, Federal Republic of Germany: Contribution to Mineralogy and Petrology, v.105, p. 177-196.

Sinclair, W.D., and Richardson, J.M., 1992, Quartz-tourmaline orbicules in the Seagull Batholith, Yukon Territory: Canadian Mineralogist, v. 30, p. 923-935.

Zhang, L.G., Liu, J.X., Chen, Z.S., and Zhou, H.B., 1994, Experimental investigation of oxygen isotopic fractionation in cassiterite and wolframite, Economic Geology, v. 89, p. 150-157.

Zhang, Y.G., and Frantz, J.D., 1987, Determination of the homogenization temperatures and densities of supercritical fluids in the system $NaCl-KCl-CaCl_2-H_2O$ using synthetic fluid inclusions: Chemical Geology, v. 64, p. 335-350.

Zheng, Y.F., 1991, Calculation of oxygen isotope fractionation in metal oxides: Geochimica et Cosmochimica Acta, v. 55, p. 2299-2307.

Zhu, C., and Sverjensky, D.A., 1991, Partitioning of F-Cl-OH between minerals and hydrothermal fluids: Geochimica et Cosmochimica Acta, v. 55, p. 1837-1858.

INTRODUCTION TO CHAPTER V

Some parameters essential for the understanding of the formation of greisen-hosted tin deposits, e.g., pH, a_{Cl^-}, could not be accurately quantified in the investigation of the natural samples presented in Chapters 2 and 3. However, the temperature and pressure conditions determined in the previous chapter (5) and the information on fluid and rock composition allows modeling of the alteration using a computer program. This modeling is presented in the following chapter and results of this study provide additional insights on the chemical processes involved in greisenization.

CHAPTER V

MODELING FLUID-ROCK INTERACTION DURING GREISENIZATION AT THE EAST KEMPTVILLE TIN DEPOSIT: IMPLICATIONS FOR MINERALIZATION

WERNER E. HALTER

AND

ANTHONY E. WILLIAMS-JONES

DEPARTMENT OF EARTH AND PLANETARY SCIENCES, MCGILL UNIVERSITY
3450 UNIVERSITY STR. MONTREAL, QUEBEC, H3A 2A7

ABSTRACT

Interaction between a tin-bearing greisenizing fluid and a leucogranitic rock was modeled in order to evaluate the possible role of alteration induced changes in fluid chemistry in cassiterite deposition. The interaction was modeled using simple titration and multiple pass fluid flow models with the program CHILLER, modified to permit calculations at 450°C and 4.0kb. The compositions of the mineralizing fluid and the unaltered leucogranite were based, respectively, on analyses of fluid inclusions and whole-rock chemistry, of samples from the East Kemptville greisen-hosted tin deposit, Nova Scotia. The starting fluid contained 4.85m Cl, 3.7m Na, 0.53m Fe, and minor K, Si, F and Sn, and was at a pH of 3.0, while the leucogranite contained 35wt-% quartz, 29wt-% albite, 19wt-% muscovite and 17wt-% K-feldspar.

In both models, the calculations show that with increasing alteration, K-feldspar was the first mineral consumed, and that this was followed by replacement of albite by muscovite. With further alteration, muscovite was replaced by topaz and pyrrhotite, and cassiterite precipitated in quartz-topaz rocks. In the most altered rocks, only topaz and quartz are present. These changes accurately reproduce those determined for natural samples at East Kemptville. Only the multiple pass fluid flow model, however predicts the changes in fluid inclusion composition.

The multiple pass fluid flow model quantified changes in fluid composition as a function of its interaction with the wall rock and thus enabled us to assess better the factors that controlled cassiterite precipitation. Important conclusions of the model are that the fluid and the rock equilibrated at each stage of the alteration and the water/rock ratio remained constant across the alteration halo. We further concluded that phases precipitated close to the vein in an earlier stage of the alteration were re-dissolved with evolution of the mineralizing system. In particular, re-dissolution of cassiterite caused an increase in the concentration of $SnCl^-$ in the fluid. As a result, cassiterite saturated at a lower pH, and the chemical potential of $SnCl^-$ increased away from the vein. This could, in turn, explain the low tin grades at East Kemptville.

INTRODUCTION

Although many authors have documented the nature of hydrothermal ore deposits and provided data on the composition of fluid inclusions, very few attempts have been made to quantitatively model the ore forming process. This is particularly true for greisen-hosted tin deposits, where changes in fluid composition in natural samples have been reported (Durišová et al, 1979; Burt, 1981; Eadington, 1983; Mangas and Arribas, 1987; Bottrell and Yardley, 1988; Schwartz and Surjono, 1990), but only one study (Heinrich, 1990) has used computer modeling to quantitatively evaluate the effects of changes in fluid composition on cassiterite deposition. This study examined cooling, fluid rock-interaction and fluid mixing, and concluded that acid neutralization through fluid mixing is the most effective way to precipitate cassiterite. However, the assumed fluid salinity and temperature were substantially lower than those generally reported in greisen-type tin deposits and topaz, which is an ubiquitous phases in greisens, was not considered in the model.

In this paper, we model greisen-style tin mineralization using detailed information on fluid, mineral and rock compositions, from the East Kemptville deposit in Nova Scotia (Chapters 3 and 4). The purpose of the study was to quantify the chemical changes in fluid composition during interaction of the latter with the leucogranite host, and to thereby determine the controls of cassiterite deposition. Results of this modeling are compared to previously reported estimates of fluid inclusion chemistry and greisen mineralogy (Chapters 2 and 3), and used to evaluate the process responsible for the formation of veins.

THE GREISENIZING SYSTEM AT EAST KEMPTVILLE

The East Kemptville tin deposit provided the data for the starting fluid and rock compositions used in our calculations, and served as a natural example against which to compare the results of the modeling presented below. The deposit is located 25 km northeast of Yarmouth, Nova Scotia and formed in highly differentiated leucogranite of the Davis Lake Pluton, at the

Figure 1: Location of the East Kemptville tin deposit on a simplified geological map of the Meguma Terrane, Nova Scotia (after Keppie, 1979, and Kontak, 1990). The enlarged area of the South Mountain Batholith shows the Davis Lake Pluton (after MacDonald, 1994, and Ham and MacDonald, 1994), which hosts the mineralization. The fault that runs through the leucogranite is part of the East Kemptville-East Dalhousie fault zone (EKEDFZ), and controlled the location and the geometry of the mineralization at East Kemptville. TFZ refers to the Tobiatic Fault Zone.

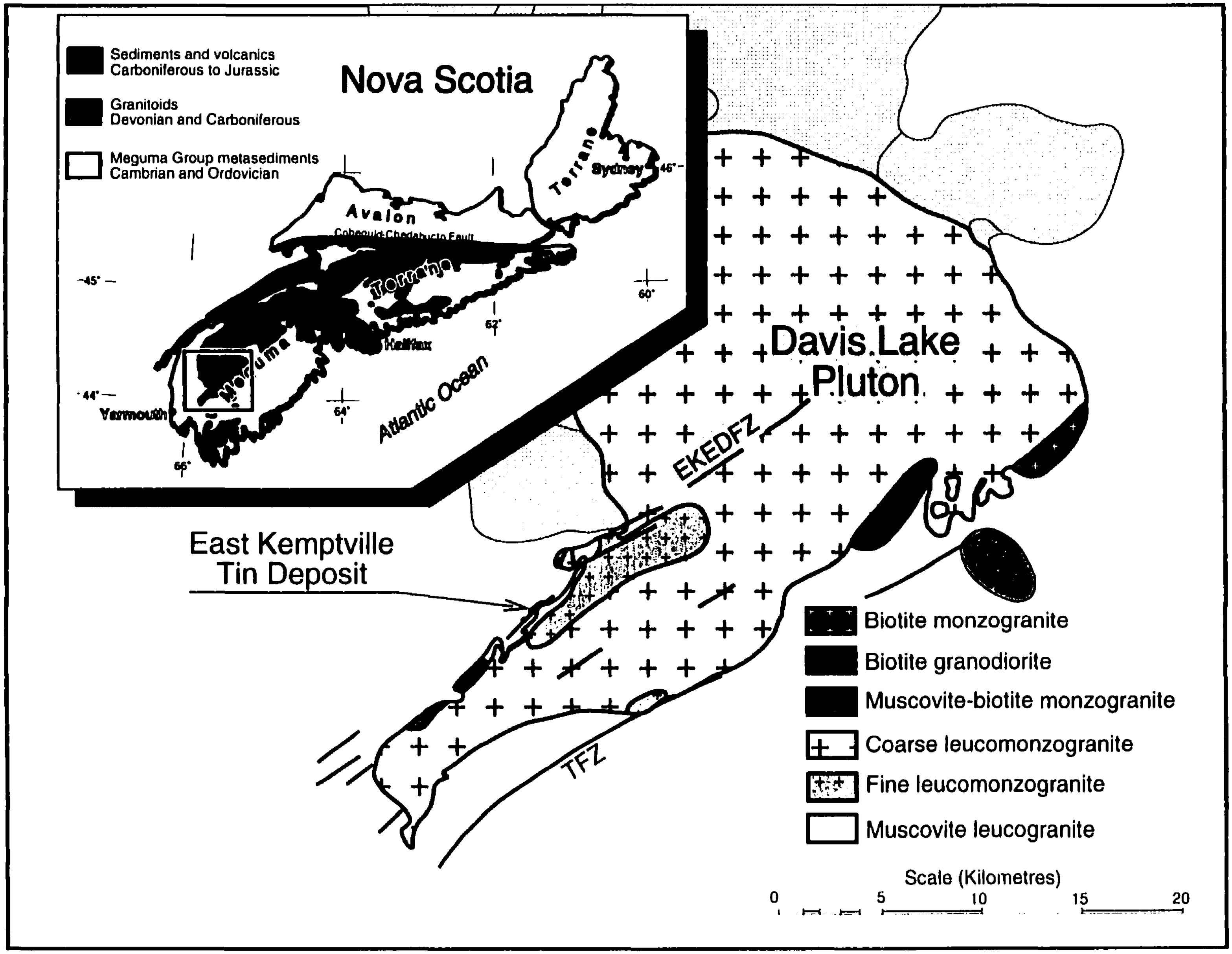
Sediments and volcanics Carboniferous to Jurassic
Granitoids Devonian and Carboniferous
Meguma Group metasediments Cambrian and Ordovician
Nova Scotia
Avalon
Cobequid-Chedabucto Fault
Terrane
Terrane
Meguma
Sydney
Halifax
Yarmouth
Atlantic Ocean
46°
45°
44°
60°
62°
64°
66°
Davis Lake Pluton
EKEDFZ
TFZ
East Kemptville Tin Deposit
Biotite monzogranite
Biotite granodiorite
Muscovite-biotite monzogranite
Coarse leucomonzogranite
Fine leucomonzogranite
Muscovite leucogranite
Scale (Kilometres)
0
5
10
15
20

southwestern end of the 370 Ma South Mountain Batholith of the Meguma Terrane in the Appalachian Orogen (Fig. 1). The leucogranite consists essentially of quartz, albitic plagioclase, K-feldspar, muscovite and locally topaz, with accessory biotite, apatite and zircon (Richardson et al., 1982; Richardson, 1988; and Kontak, 1990, 1991; Chapters 2 and 3). Cassiterite mineralization is hosted by zoned or massive topaz- and muscovite-bearing greisens; the latter massive greisens represent numerous superimposed zoned greisens. Greisenization is interpreted to have occurred as a result of the interaction of a late orthomagmatic fluid with the leucogranite at a temperature of 480°C and a confining pressure of 4.1 kb (estimated from oxygen isotopic fractionation between cassiterite and quartz, OH-F exchange between muscovite and topaz, and fluid inclusion isochores (Chapter 5)).

Figure 2 shows the variation in the abundance of major phases and cassiterite in an idealized alteration halo developed around a central vein in which mineralizing fluid was circulating. These changes in normative composition were deduced from the alteration sequences observed in a zoned greisen (Chapter 2) and variably greisenized samples from drill hole 90-1 (Chapter 3). The left margin of the diagram is the immediate wall to the vein. The abscissa records the degree of alteration. With increasing alteration (from right to left), K-feldspar is first replaced by albite and quartz. Complete replacement of K-feldspar coincides with the first appearance of small amounts of topaz as an alteration product. With further alteration albite is converted to muscovite and quartz in sericitized leucogranite, but the proportion of topaz remains essentially unchanged. Trace amounts of pyrrhotite can be present in this interval. Complete replacement of albite is followed by the replacement of muscovite by topaz and quartz in quartz-sericite greisen. In this zone, pyrrhotite becomes increasingly important and trace amounts of cassiterite can be present. Once topaz predominates over muscovite, the rock is termed a quartz-topaz greisen. In quartz-topaz greisen, the proportions of pyrrhotite and cassiterite increase to a maximum. Further alteration is characterized by decreases in the proportion of these phases in the most altered rocks, and by an increase in the proportion of quartz. This zone is referred to as the quartz-greisen and is evident in natural samples as a sulfide poor halo around veins.

Figure 2: An idealized section showing the normative mineralogy of altered rocks on one side of a vein at East Kemptville. The section is based on data for a zoned greisen (Chapter 2) and on data for samples from drill hole 90-1 (Chapter 3). The horizontal scale indicates decreasing alteration.

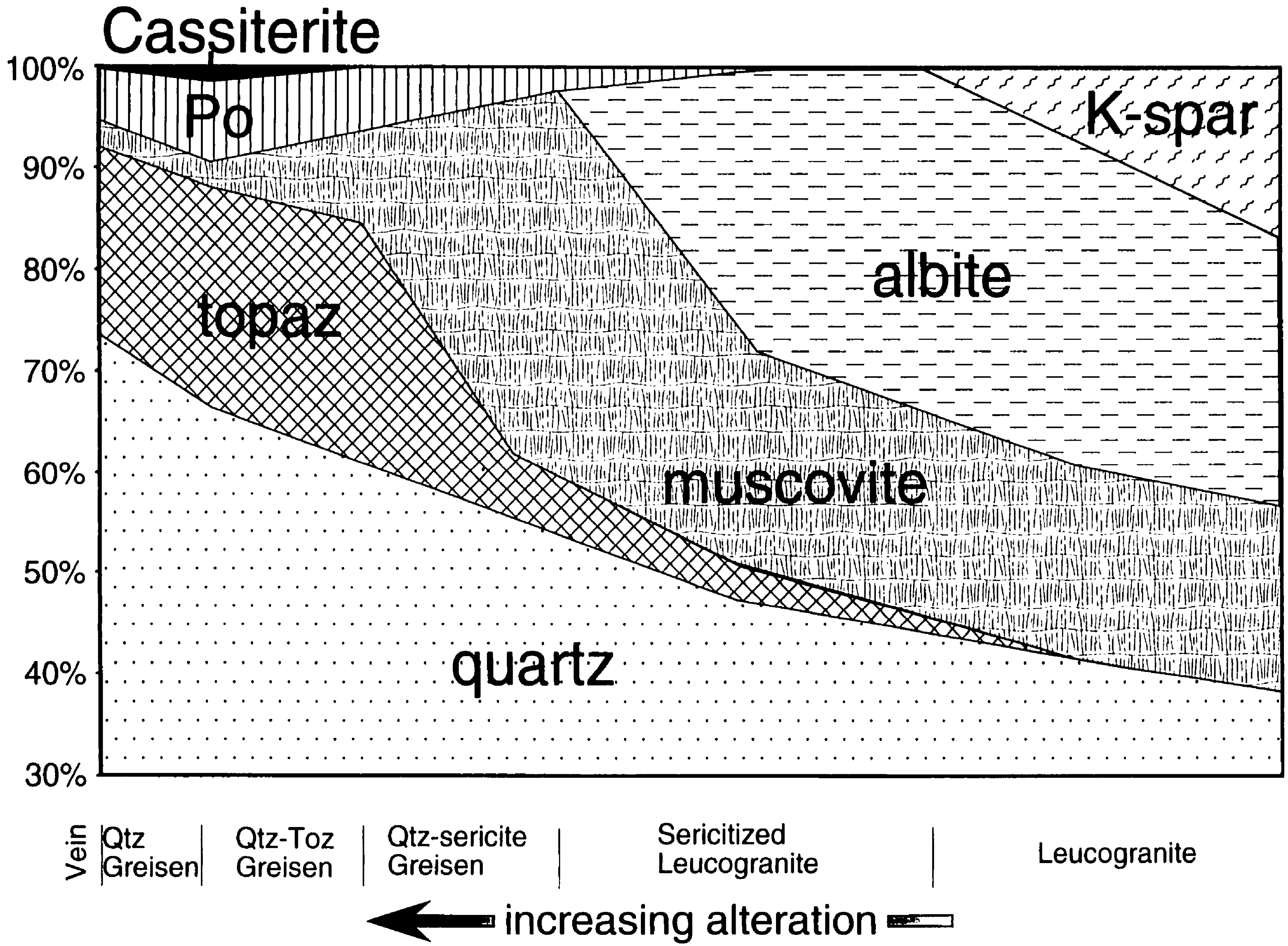
Cassiterite
Po
K-spar
albite
topaz
muscovite
quartz
100%
90%
80%
70%
60%
50%
40%
30%
Vein
Qtz Greisen
Qtz-Toz Greisen
Qtz-sericite Greisen
Sericitized Leucogranite
Leucogranite
increasing alteration

Changes in fluid inclusion compositions across this alteration halo were discussed in Chapter 3 and idealized changes are summarized in Figure 3. Eutectic temperatures, measured by microthermometry in greisen-related fluid inclusions, at first decrease in the quartz greisen with decreasing alteration (i.e., increasing distance from the vein) and then increase steadily toward less altered rocks. The oxygen fugacity (calculated using the CO_2/CH_4 ratio of fluid inclusions) behaves similarly. The NaCl content of the fluid, which was estimated from microthermometric and leachate analyses, increases continuously with decreasing alteration, and the a_{HF^0} in the fluid, calculated using the F content of topaz (see below), remains essentially constant in topaz-rich greisens, and then drops to a lower value in quartz-sericite greisen.

STARTING FLUID AND ROCK COMPOSITIONS

We used the fluid inclusion data presented in Chapter 3 and mineral equilibria to obtain our best estimate of the composition of the starting fluid (F_s), i.e., the fluid in the vein (Table 1). Based on the temperature of final ice melting, this fluid has a total salinity of 27 wt-% NaCl equivalent. Leachate analyses of fluid inclusions provided information on the relative abundance of cations and indicated that, besides Na, only Fe has a significant concentration. Based on the Na/Fe ratio and the total salinity, the concentration of Na is 3.7m and that of Fe is 0.53m. The pH of the solution was approximated using the topaz-muscovite equilibrium. However, this calculation requires that the concentration of K is known and, unfortunately, this was not possible from the leachate data due to contamination of the sample by muscovite. The K concentration was therefore calculated from the solubility of muscovite. Since the latter is dependent on pH, the K concentration and the pH of the fluid were obtained iteratively: The pH was assumed initially to be 3.5 and this value was used to calculate the K concentration. The latter value was employed to re-calculate the pH from the muscovite-topaz equilibrium, and the process was repeated until pH and the concentration of K were not changed significantly by additional iteration. Results of this iterative calculation yield an estimated starting pH of 3.0 and an initial K concentration of 0.08 moles per litre. Because muscovite is not saturated in the vein,

Figure 3: Variation in eutectic temperature T_e, fO_2 and molality of Na (fluid inclusion data; Chapter 3), and in a_{HF} (from topaz compositions), across the alteration halo. Eutectic temperatures and fO_2 show minima between the quartz greisen and the quartz-topaz greisen. The Fe content inferred from the eutectic temperatures is interpreted to have been at maximum between the two greisens. The molality of Na increased continuously before decreasing in the least altered sample, and a_{HF^0} remained essentially constant in topaz-rich rocks and dropped to a lower value as muscovite became more abundant.

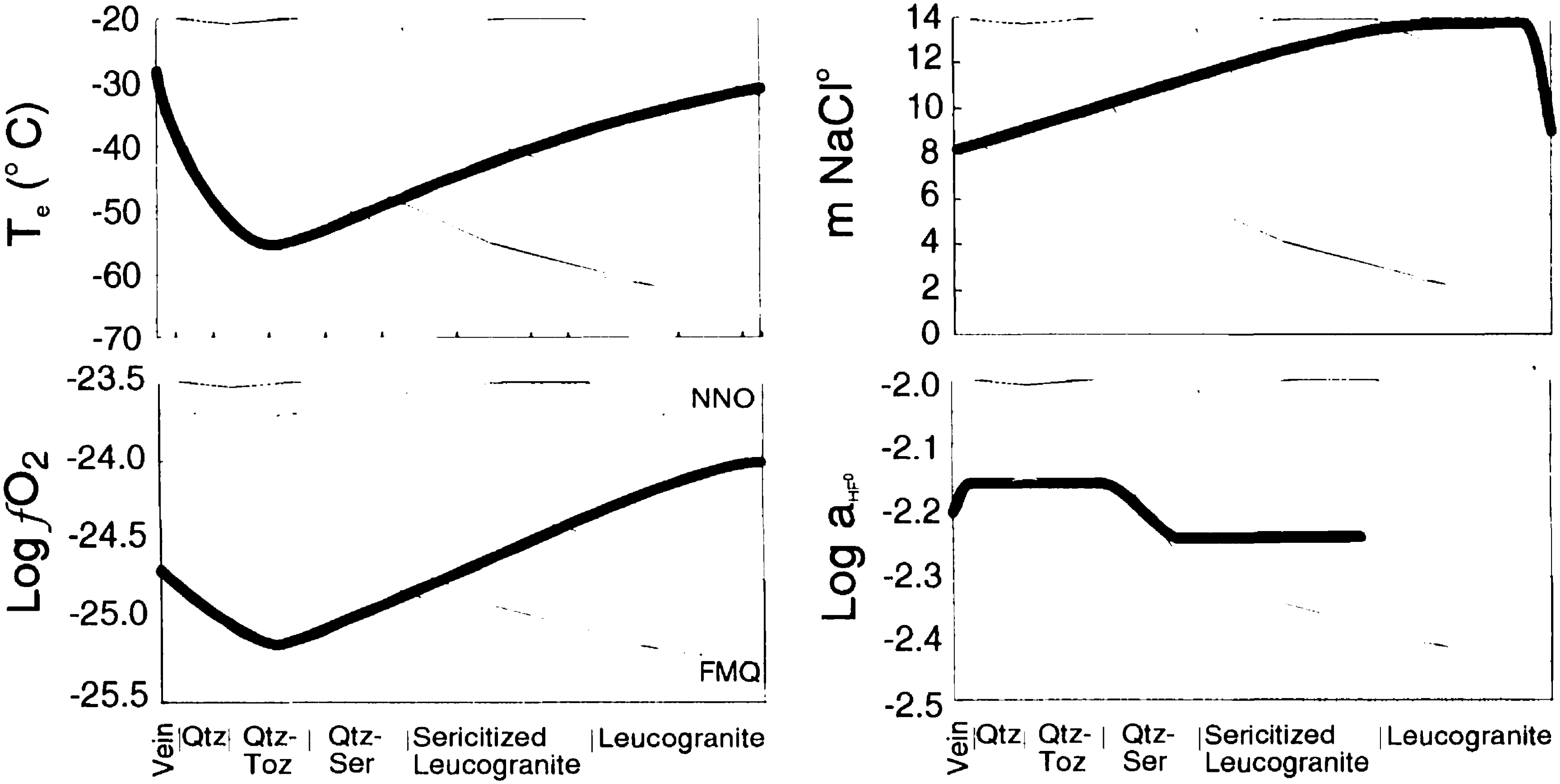

Te (° C)
-20
-30
-40
-50
-60
-70
m NaCl°
14
12
10
8
6
4
2
0
Log fO2
-23.5
-24.0
-24.5
-25.0
-25.5
NNO
FMQ
Log aHF°
-2.0
-2.1
-2.2
-2.3
-2.4
-2.5
Vein
Qtz
Qtz-Toz
Qtz-Ser
Sericitized Leucogranite
Leucogranite

Table 1: Concentration of components in the starting solution.

Component	Concentrations (m/l)	Determined by:
H^+	0.0010	muscovite-topaz equilibrium
Cl^-	4.8511	charge balance
fO_2	2.00E-25	gas chromatigraphic analyses of fluid inc.
SO_4^{2-}	-1.442E-08	equilib. with HS- at fO_2 cond. from GC
HS^-	0.0017	< pyrrhotite saturation
$SiO_2(aq)$	0.0851	Quartz saturation
Al	5.172E-05	topaz solubility
Fe	0.5300	leachate analyses
K	0.0809	muscovite solubility
Na	3.7000	microthermometry
F	0.0062	F content in Topaz
Sn	0.0014	< cassiterite saturation

these values represent minimum and maximum estimates, respectively. The Si and Al concentrations were estimated from the solubility of quartz and topaz, respectively, as both phases are present in the quartz greisen. The latter data were also used to estimate a_{HF^0}, from the equilibrium constant for the reaction:

$$Al_2SiO_4(F)_2 + 2H_2O = Al_2SiO_4(OH)_2 + 2HF^0$$

Hydroxy- and fluor-topaz were assumed to mix ideally as the electronegativity and the effective ionic radii of F^- and OH^- are quite similar (Zhu and Sverjensky, 1991), and a_{H_2O} was assumed to be unity. The value of a_{HF^0} calculated from this reaction was used to determine the a_{F^-} from the dissociation constant of HF^0 at the given pH. The total molality of F in the fluid was considered to be equal to the sum of the molality of HF^0 and F^-. Tin and sulphur concentrations were taken to be slightly lower than those required for cassiterite and pyrrhotite saturation, respectively, as both phases are not part of the mineral assemblage next to the vein, but saturate in quartz-topaz greisen. The value of fO_2 was estimated from gas chromatographic analyses of the ratio of CO_2 and CH_4 in the bulk inclusion fluid (Chapter 3). The concentration of Cl^- was assumed to be equal to the sum of cation charges.

The leucogranite used as the starting rock in our calculations contained 35wt-% quartz, 29wt-% albite, 19wt-% muscovite and 17wt-% K-feldspar, which is the normative composition of the least altered rock (Fig. 2). The compositions of these minerals and others formed during alteration are given in Table 2. They were assumed to be those of their end-members, except for muscovite and topaz, in which the F/OH ratios were taken to be 0.25 and 0.75, respectively, as suggested by microprobe analyses of these phases in samples from East Kemptville (Chapter 3). Thermodynamic data for these intermediate muscovite and topaz compositions were obtained assuming ideal mixing on the hydroxyl site (see above).

Table 2: Sources of thermodynamic data.

Phase	Data source
Muscovite $KAl_3Si_3O_{10}(OH_{1.5},F_{0.5})$	Zhu and Sverjensky 1991; Johnson et al., 1991
Topaz $Al_2SiO_4(F_{1.5},OH_{0.5})$	Barton, 1982; Barton et al., 1982
Albite $NaAlSi_2O_8$	Johnson et al., 1991
K-feldspar $KAlSi_3O_8$	Johnson et al., 1991
Quartz SiO_2	Johnson et al., 1991
Pyrrhotite FeS	Johnson et al., 1991
Cassiterite SnO_2	Johnson et al., 1991
HCl^0	Sverjensky et al., 1991
$Al(OH)_3{}^0$	Ragnarsdòttir and Walther, 1985
SnCi+	Wilson and Eugster, 1990
Other aqueous species	Johnson et al., 1991

MODELING

Method

The major components in the fluid and the phases described above are part of the system Na-Cl-K-Al-Fe-Si-Sn-S-H-O-F. The concentrations of the various aqueous species present in the starting solution for this system were calculated from the molalities of each element (Table 1) at 450°C and 4.0kb using a version of the program CHILLER (Reed, 1982, Spycher and Reed, 1989) and the accompanying database, modified to enable calculations at these high pressure and temperature conditions. The molalities, the activities and the activity coefficients of the most abundant aqueous species used in the calculations, are listed in Table 3. Equilibrium constants for the dissociation reactions of all species employed in CHILLER were obtained for the above conditions using SUPCRT92 (Johnson et al., 1991) and thermodynamic data from a variety of sources (Table 2). Only aqueous species present at the above conditions were included in the calculations; other aqueous species in the CHILLER database were suppressed. Activity coefficients of uncharged species were assumed to be unity and those of charged species were calculated using CHILLER and the extended Debye-Hückel equation from Helgeson (1981) at the model temperature. Solid phases included in the calculations are quartz, albite, K-feldspar, muscovite, topaz, pyrrhotite and cassiterite, and data for these phases were added (cassiterite) or modified in the database. Other solid phases were suppressed, i.e., not allowed to saturate.

Simple titration model

In our first set of calculations, we added successive aliquots of progressively larger masses of fresh leucogranite to one litre of starting solution, i.e., we followed the simple titration model developed by Helgeson (1970). This model is equivalent to a single pass of a fixed amount of fluid through the wall rock with a decreasing alteration capacity of the fluid

Table 3: Speciation of the starting solution.

Species	Molality	Log Molality	Activity	Log Activity	Gamma
H^+	0.001	-3.022	0.000	-3.629	0.247
H_2O			0.917	-0.038	0.917
Cl^-	2.147	0.332	1.077	0.032	0.502
SO_4^{2-}	0.000	-4.648	0.000	-6.764	0.008
HS^-	0.000	-6.068	0.000	-6.359	0.511
SiO_2(aq)	0.086	-1.068	0.086	-1.068	1.000
Al^{3+}	0.000	-8.938	0.000	-13.940	0.000
Fe^{2+}	0.216	-0.665	0.001	-3.107	0.004
K^+	0.040	-1.403	0.025	-1.605	0.628
Na^+	1.404	0.148	0.734	-0.134	0.523
F^-	0.000	-3.934	0.000	-4.402	0.341
Sn^{2+}	0.000	-9.056	0.000	-11.264	0.006
$Al(OH)_3^0$	0.000	-4.284	0.000	-4.284	1.000
HCl^0	0.007	-2.177	0.007	-2.177	1.000
HF^0	0.006	-2.211	0.006	-2.211	1.000
$FeCl^+$	0.269	-0.571	0.172	-0.765	0.639
$FeCl_2^0$	0.047	-1.325	0.047	-1.325	1.000
H_2 (aq)	0.000	-4.046	0.000	-4.046	1.000
KCl^0	0.042	-1.380	0.042	-1.380	1.000
$NaCl^0$	2.312	0.364	2.312	0.364	1.000
OH^-	0.000	-5.541	0.000	-5.978	0.365
H_2S^0	0.002	-2.774	0.002	-2.774	1.000
$SnCl^+$	0.001	-2.852	0.001	-3.046	0.639

away from the vein. Leucogranite was added in increments of first 0.1 gram, then of 1, 10, 100 and finally 1000g. At each step, minerals that became saturated were fractionated from the fluid. Changes in rock and fluid compositions resulting from this calculation are presented graphically in Figures 4 and 5. The alteration sequence obtained with this approach is remarkably similar to that observed in alteration halos at East Kemptville (Fig. 2): only topaz and quartz are stable next to the vein (equivalent to the quartz greisen in the alteration halo of Figure 2). After 0.5g of leucogranite were added to the fluid, cassiterite and pyrrhotite precipitated due to a pH increase; other factors that control the solubility of these phases, i.e., a_{Cl^-}, a_{SnCl^-}, fO_2 and a_{H_2S}, remained constant up to that point (quartz-topaz greisen). Subsequent addition of rock caused further increase in pH and a drop in a_{HF^0}, stabilizing muscovite over topaz (quartz-sericite greisen). This was accompanied by an increase in the concentration of aluminum in solution and by sharp decreases in fO_2 and a_{H_2S}. After further addition of leucogranite, albite saturated, producing a quartz-albite-muscovite assemblage (sericitized leucogranite). When 100g of leucogranite had been added, there were sharp increases in a_{KCl^0} and a_{Cl^-}, and a sharp decrease in a_{NaCl^0}, which caused the fluid to saturate with K-feldspar. Concurrently, a_{FeCl^-} dropped sharply due to the dissociation of this complex; $a_{Fe^{2-}}$ (not shown) increased. The activity of other components changed little during K-feldspar saturation. The a_{SnCl^-} decreased across the alteration halo as a result of cassiterite precipitation in two steps, namely as a_{HCl^0} decreased during muscovite and albite saturation, and subsequently during K-feldspar saturation. The fluid was close to equilibrium with the starting rock after addition of 600g of leucogranite, and subsequent additions produced no further changes in fluid composition.

Figure 4: Changes in the normative mineralogy of leucogranite produced by titrating increasing amounts of leucogranite in a starting fluid having the composition described in Table 1. The calculated changes resemble strongly those of the idealized alteration halo, i.e., with increasing water/rock ratio (to the left), K-feldspar first disappears, followed by albite and muscovite. At very high water/rock ratios close to the vein, only quartz and topaz are stable.

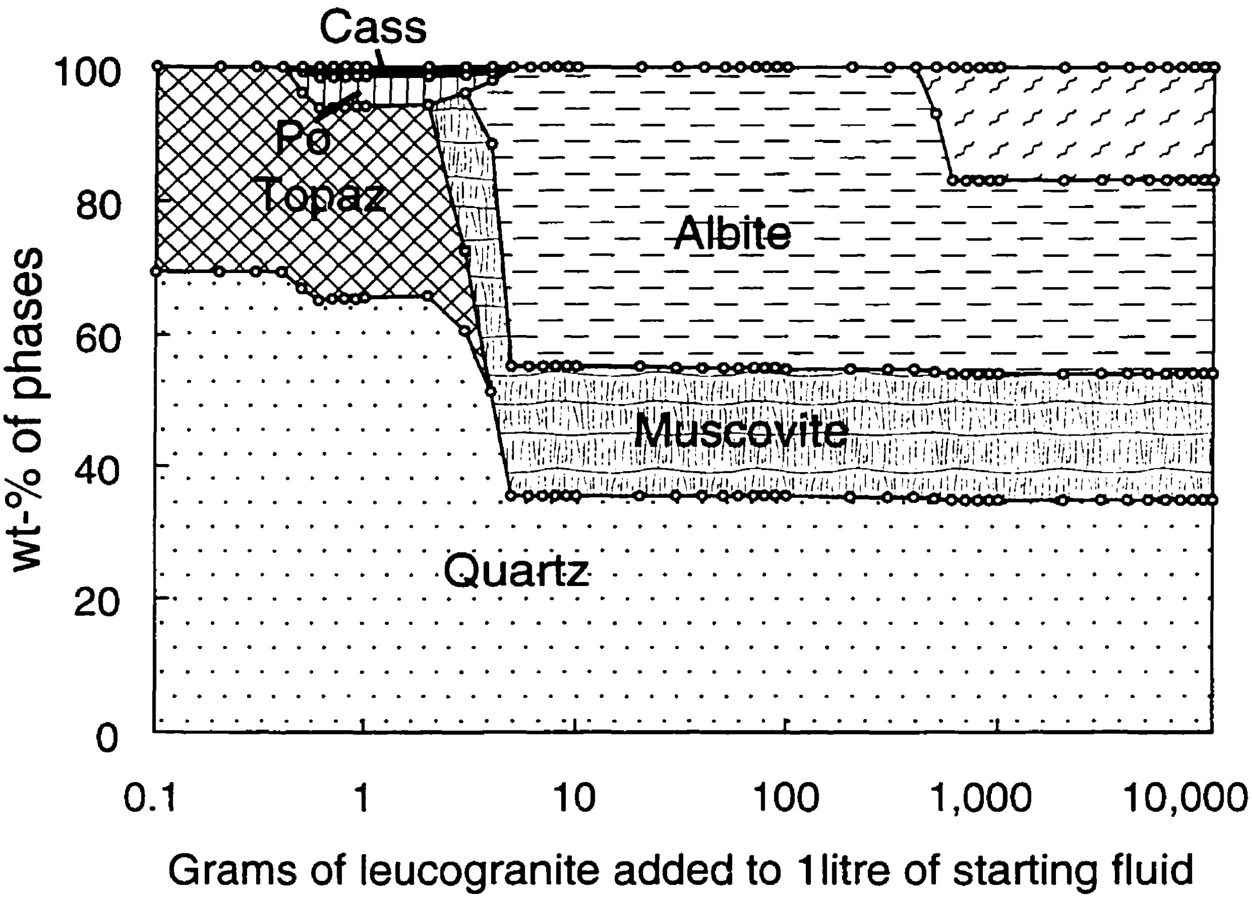
Cass
Po
Topaz
Albite
Muscovite
Quartz
wt-% of phases
0
20
40
60
80
100
0.1
1
10
100
1,000
10,000
Grams of leucogranite added to 1 litre of starting fluid

Figure 5: Profiles showing the concentration of major components in the fluid as a function of the amount of rock titrated into the starting fluid (Table 1). Apart from $Al(OH)_3^0$, the concentration of all components either increased or decreased monotonically. These changes only reflect some of those estimated from fluid inclusions in the East Kemptville greisen. See text for detailed discussion of the profiles.

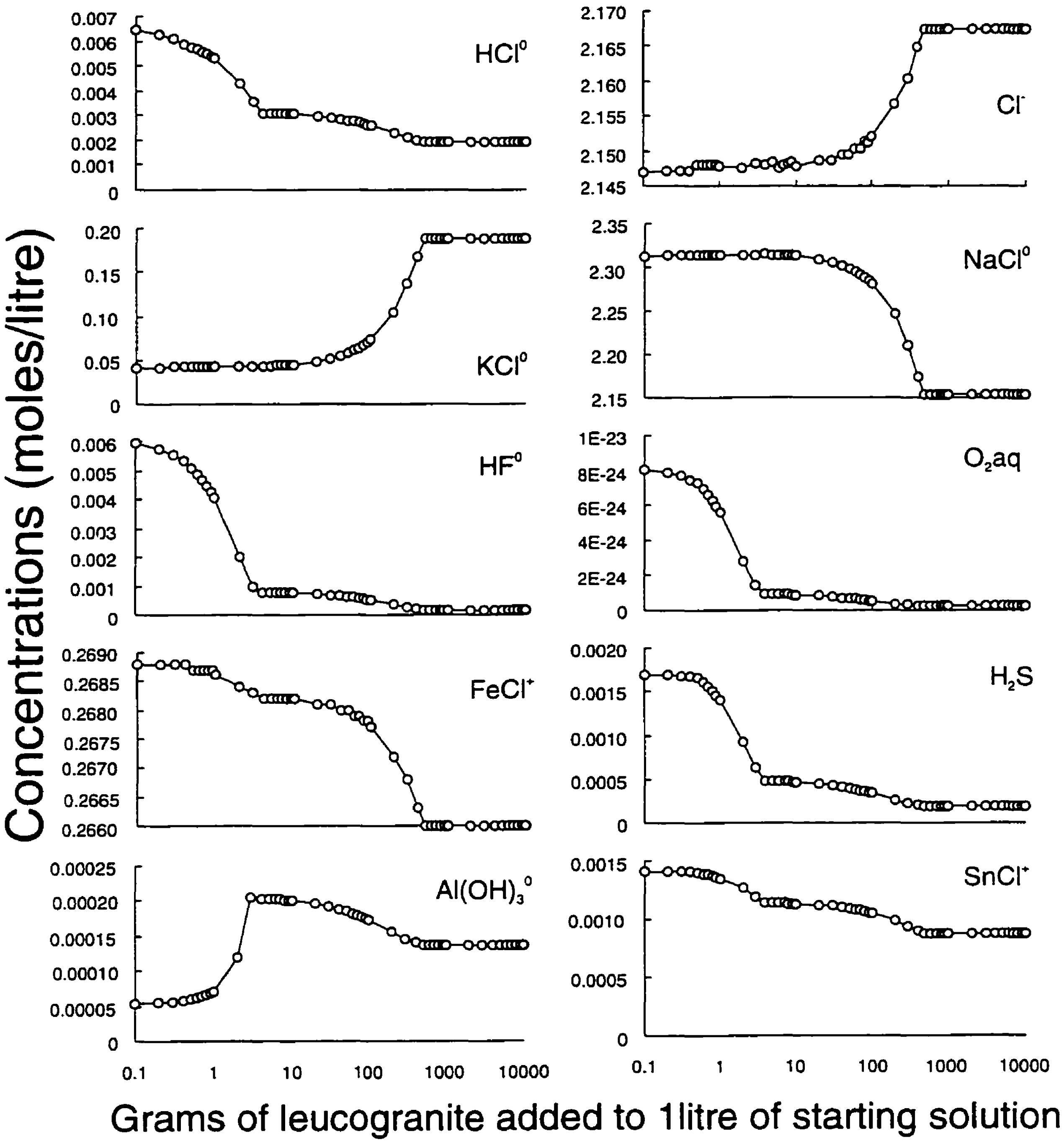

Concentrations (moles/litre)
HCl^0
0.007
0.006
0.005
0.004
0.003
0.002
0.001
0
Cl$^-$
2.170
2.165
2.160
2.155
2.150
2.145
KCl^0
0.20
0.15
0.10
0.05
0
NaCl^0
2.35
2.30
2.25
2.20
2.15
HF^0
0.006
0.005
0.004
0.003
0.002
0.001
0
O$_2$aq
1E-23
8E-24
6E-24
4E-24
2E-24
0
FeCl$^+$
0.2690
0.2685
0.2680
0.2675
0.2670
0.2665
0.2660
H$_2$S
0.0020
0.0015
0.0010
0.0005
0
Al(OH)$_3^0$
0.00025
0.00020
0.00015
0.00010
0.00005
0
SnCl$^+$
0.0015
0.0010
0.0005
0
0.1
1
10
100
1000
10000
Grams of leucogranite added to 1litre of starting solution

Multiple pass fluid flow model

The simple titration model provides an accurate prediction of the sequence of mineralogical changes during alteration, but we do not believe that this model correctly simulates the actual process of alteration, as it assumes that the fracture (vein) only remained open for a period of time sufficient for the infiltration of a single batch of fluid. Moreover, it requires the unreasonable conclusion that the fluid was able, from the onset of the alteration, to buffer the composition of a zone of rock having the width of the quartz-greisen. We propose rather that the influence of the fluid over the rock increased with time due to repeated overprinting of the rock by the fluid and that it only buffered the composition of the quartz greisen at a late stage of alteration. Hence, phases that precipitated at lower water/rock ratios in our model (cassiterite, pyrrhotite) must have formed close to the vein early in the alteration event and been re-dissolved in order to allow the quartz-greisen to form. We therefore discarded the simple titration model for a one-dimensional multiple pass fluid flow model similar to that described by Heinrich (1990). In this model, successive aliquots of fluid are passed through a segmented rock column, and attain local equilibrium with each rock segment before passing on to the next segment. Our model involved passing one litre aliquots of the starting fluid F_s through a column of leucogranite divided into 10 segments of 3g, one of 70g, one of 900g and one of 4000g, and allows each aliquot to equilibrate sequentially with the segments. With each new aliquot of fluid F_s the segments became progressively more altered.

Figure 6 shows the normative composition of the rock segments after one, four and seven aliquots of fluid were passed through the column, and illustrates the effect of successive fluid overprinting. The first aliquot of fluid that passed through the rock column produced the same alteration sequence as in the simple titration model. The most important changes in rock composition occurred close to the vein as the leucogranite there was most out of equilibrium with the altering fluid. After four aliquots of fluid had passed through the column, the closest segments were approaching equilibrium with the vein fluid and the quartz-topaz rich zone (i.e., the equivalent of the quartz-topaz greisen in the samples from East Kemptville) had widened significantly. Muscovite, albite and K-feldspar had stabilized further out in the alteration halo than after the previous pass. An important feature at this stage of the alteration was that in the first segment, the proportion of cassiterite and pyrrhotite had become smaller than in the second segment, suggesting that these minerals had started to dissolve close to the vein. After the 7th pass of fluid through the rock, the first segment was formed only of quartz and topaz, and therefore resembled quartz greisen; cassiterite and pyrrhotite had been completely dissolved from this segment. Concurrently with the formation of quartz greisen, all alteration zones continued to widen and move away from the vein.

Changes in the concentration of the most abundant aqueous species in the 1st, 4th and 7th aliquots of fluid after interaction with each wall rock segment are shown in Figure 7. As expected, the most significant changes during the first pass occurred close to the vein and progressively further out during subsequent passes of fluid, i.e., as the alteration front moves away from the vein. Hence, for example, changes in pH and therefore the concentration of HCl^0 between the 1st and the 10th segment of the rock column are abrupt and close to the vein in the first pass of fluid, but more gradual and further out in the 7th pass of fluid. Changes in the concentrations of KCl^0, Cl^- and $NaCl^0$ also occurred further out in the alteration halo as more fluid was passed through the rock column. The concentrations of $FeCl^-$, H_2S^0, O_2,aq. and $SnCl^-$, which decreased sharply between segment one and two in the first pass, increased in the first two segments in the 7th pass and only decreased further out in the alteration halo. The concentration of HF^0 decreased in the first segment after the first pass, and this was accompanied by an increase in $Al(OH)_3^0$. The locii of these changes (fronts) also moved away from the vein, i.e., to the 6th segment, in successive passes of fluid.

COMPARISON TO THE EAST KEMPTVILLE GREISENS

The mineralogical changes produced in both the single and multiple pass models are very similar to those observed in alteration halos around veins at East Kemptville (Fig. 2), i.e., they produce the same general sequence of alteration zones. However, the single pass or simple titration model does not satisfactorily predict the behaviour of several aqueous

Figure 6: A. Changes in the normative mineralogy of sequential segments in a rock column as a result of the passage of one litre of fluid through the rock. B. and C. show the same changes after 4 and 7, one litre aliquots were passed through the rock. Repeated overprinting of the rock column by the fluid progressively increased the widths of alteration zones. After the 7th aliquot of fluid passed through the rock column, all cassiterite and pyrrhotite initially precipitated in the 1st segment, had been re-dissolved and precipitated further out.

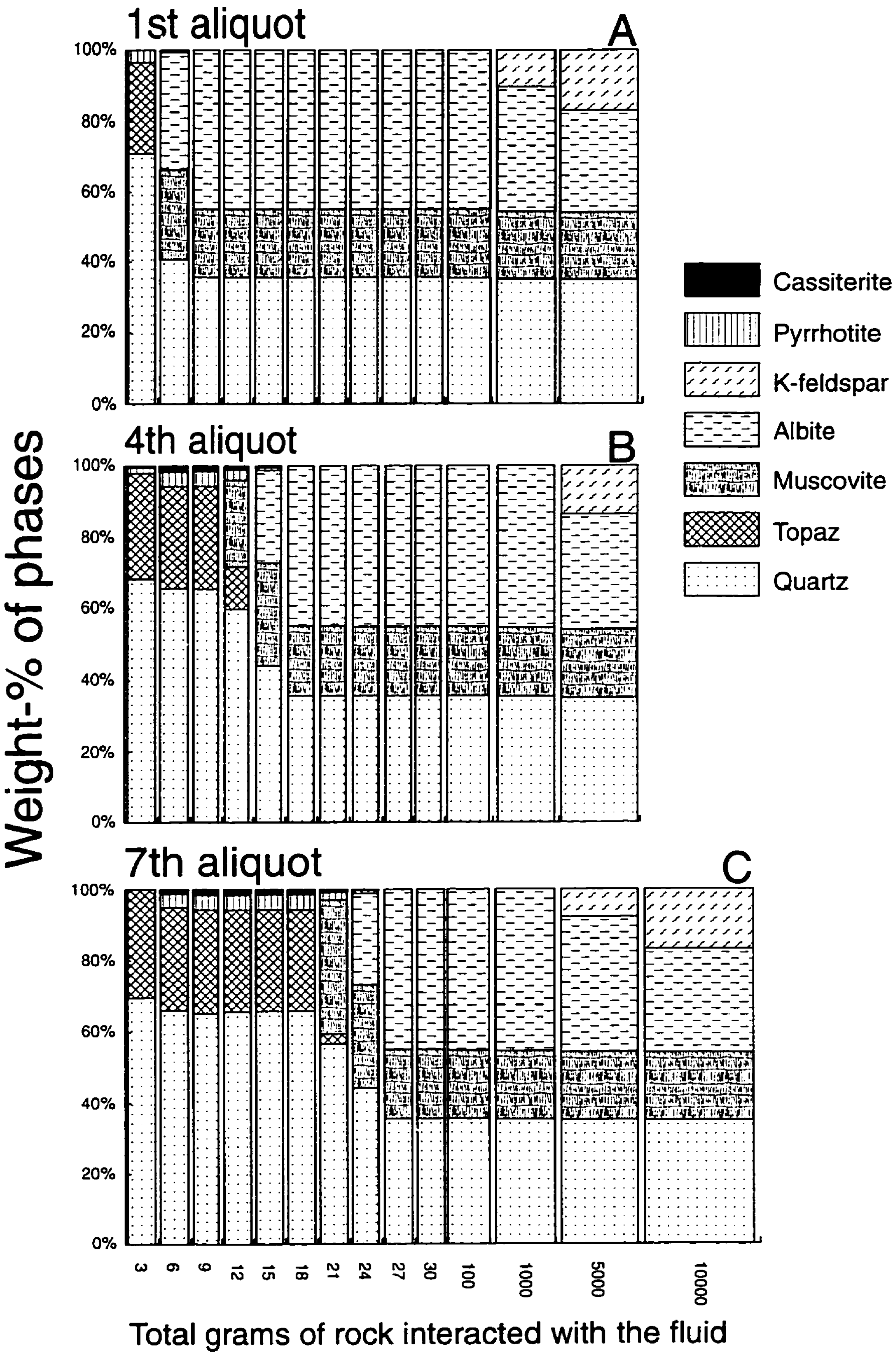

1st aliquot
A
4th aliquot
B
7th aliquot
C
100%
80%
60%
40%
20%
0%
Weight-% of phases
Cassiterite
Pyrrhotite
K-feldspar
Albite
Muscovite
Topaz
Quartz
3
6
9
12
15
18
21
24
27
30
100
1000
5000
10000
Total grams of rock interacted with the fluid

Figure 7: Profiles showing the concentration of major components in the 1st, 4th and 7th aliquots of fluid as a function of the mass of the rock column through which it was passed. As is apparent from the normative compositions, significant changes in fluid composition occurred progressively further into the column with each new aliquot of fluid. It is important to note that in the 4th and the 7th aliquots, the concentration of H_2S^0, $FeCl^-$ and $SnCl^-$ increase in the initial segments, before dropping to lower values. Similar changes were documented from fluid inclusion data for the East Kemptville greisens.

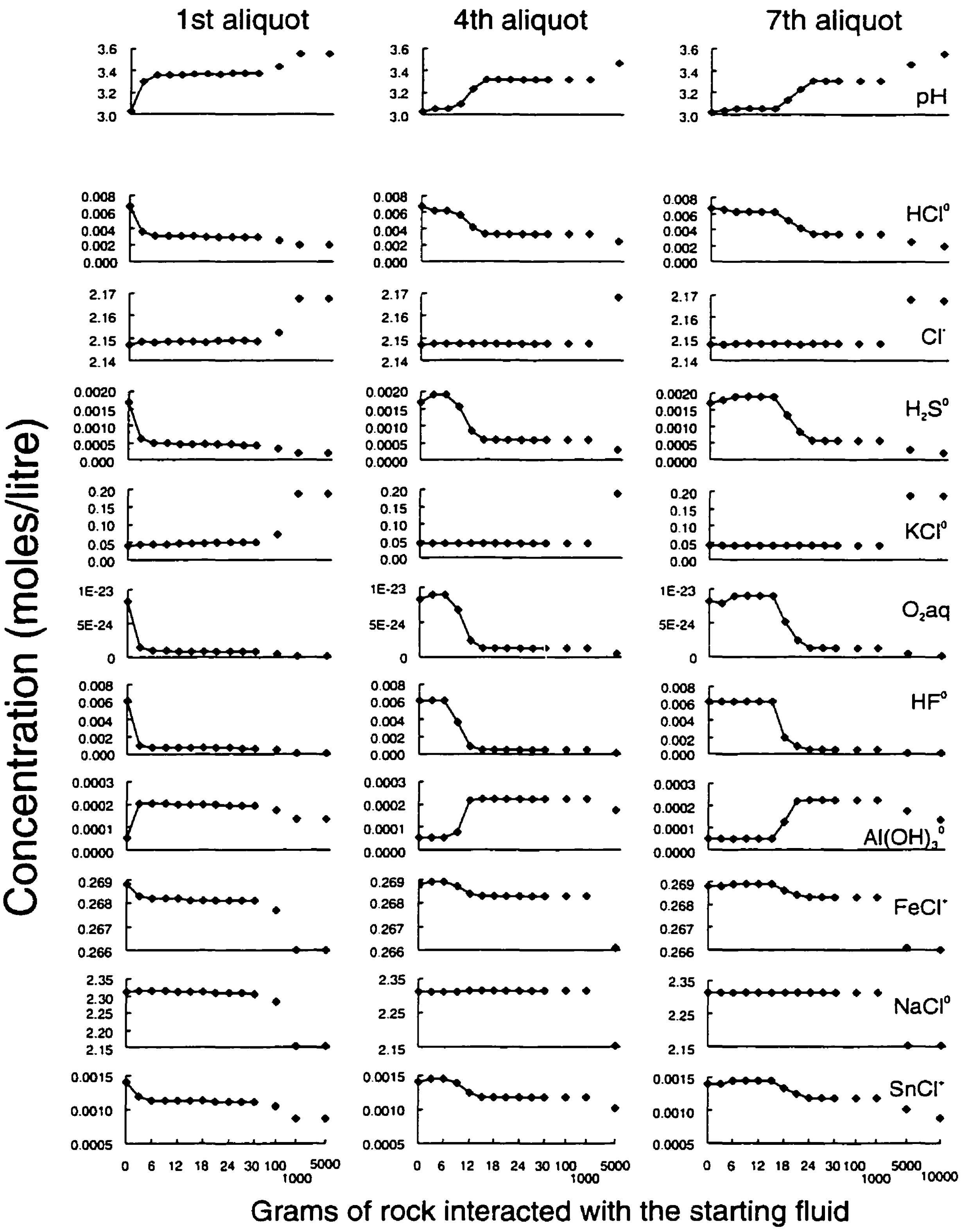
1st aliquot
4th aliquot
7th aliquot
pH
3.6
3.4
3.2
3.0
HCl°
0.008
0.006
0.004
0.002
0.000
Cl⁻
2.17
2.16
2.15
2.14
H₂S°
0.0020
0.0015
0.0010
0.0005
0.0000
KCl°
0.20
0.15
0.10
0.05
0.00
O₂aq
1E-23
5E-24
0
HF°
0.008
0.006
0.004
0.002
0.000
Al(OH)₃°
0.0003
0.0002
0.0001
0.0000
FeCl⁺
0.269
0.268
0.267
0.266
NaCl°
2.35
2.30
2.25
2.20
2.15
SnCl⁺
0.0015
0.0010
0.0005
0 6 12 18 24 30 100 1000 5000
0 6 12 18 24 30 100 1000 5000
0 6 12 18 24 30 100 1000 5000 10000
Concentration (moles/litre)
Grams of rock interacted with the starting fluid

species (Fig. 5). For example, in the simple titration model the concentrations of $FeCl^-$ and $SnCl^-$ decrease monotonically, whereas in the fluids that produced the East Kemptville greisens, the concentrations of Fe and Sn first decreased and then increased in the fluid with increasing distance from the vein. This is apparent from changes in eutectic temperatures of fluid inclusions (Fig. 2) and changes in the chemical composition of the rock (Chapter 3). Similarly, based on fluid inclusions data, the concentration of $NaCl^0$ increased with decreasing alteration before decreasing in the leucogranite in the presence of K-feldspar (Fig. 3), whereas in the single titration model it only decreased with decreasing alteration (distance from the vein; Fig. 5). Finally, a_{HF^0} is estimated to have increased with decreasing alteration to a maximum value before decreasing in less altered greisens (Fig. 3); the simple titration model only predicts decreasing a_{HF^0} with distance from the vein (Fig. 5). In contrast to the simple titration model, the multiple pass fluid flow model satisfactorily predicts all the changes in concentration of aqueous species discussed above, although in the case of $NaCl^0$ and HF^0 this is not evident on the scale of the diagram (Fig. 7). We therefore suggest that the multiple pass fluid flow model best reflects the alteration process that affected leucogranite at East Kemptville.

We further evaluated the appropriateness of the multiple pass fluid flow model by comparing calculated changes in fluid composition with those deduced from mass balance considerations on one side of a single zoned greisen (Chapter 2). The stage that represents best the zoned greisen is that obtained after four passes of fluid (Fig. 8). In Figure 9 we compare changes in fluid composition predicted by the model (first column) with those deduced from the zoned greisen, assuming the same starting fluid composition (second and third columns). In the second column, the changes take account of variations in the water/rock ratio, whereas in the third column a constant water/rock ratio is assumed. Profiles for most components calculated with the model compare very well with those deduced from compositional changes in the zoned greisen, regardless of whether the water/rock ratio correction was applied or not, thus further demonstrating the ability of the multiple pass fluid flow model to accurately characterize the greisenization process at East Kemptville. This, in turn, also confirms the validity of the starting assumption made

Figure 8: A comparison of the changes in normative mineralogy calculated using a multiple pass fluid flow model with those deduced from mass balance considerations for a zoned greisen (Chapter 2). The profiles compare very well, and differ only in that changes are gradual in the zoned greisen and abrupt in the calculated model.

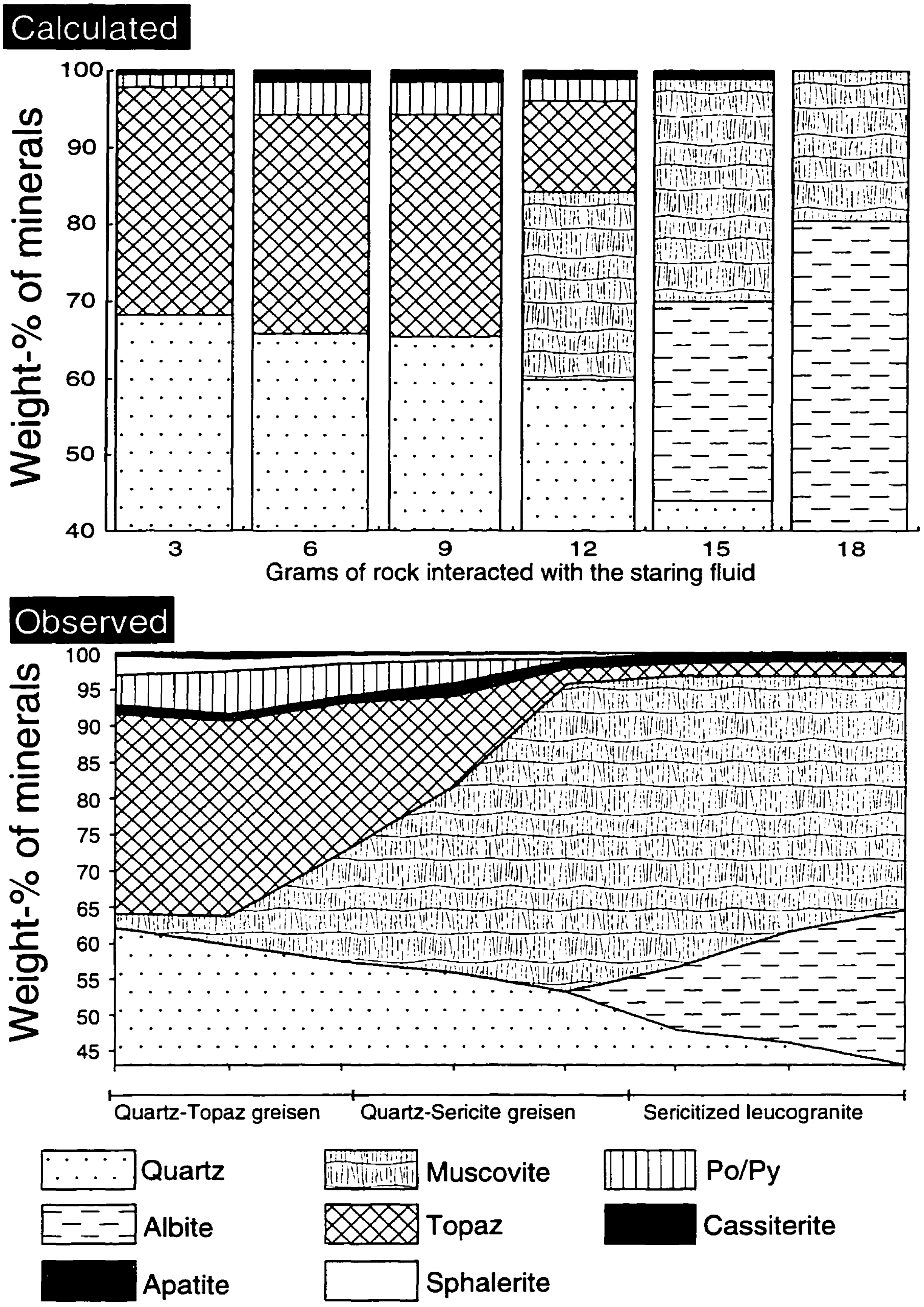
Calculated
Weight-% of minerals
100
90
80
70
60
50
40
3
6
9
12
15
18
Grams of rock interacted with the staring fluid
Observed
Weight-% of minerals
100
95
90
85
80
75
70
65
60
55
50
45
Quartz-Topaz greisen
Quartz-Sericite greisen
Sericitized leucogranite
Quartz
Muscovite
Po/Py
Albite
Topaz
Cassiterite
Apatite
Sphalerite

Figure 9: A comparison of the profiles in fluid composition calculated using the multiple pass fluid flow model with those estimated for a zoned greisen from mass balance considerations (Chapter 2), assuming the same starting composition. In the second column, changes determined for the zoned greisen were corrected for the water/rock ratio (estimated using oxygen isotope data). The third column shows the same profiles without this correction. Calculated profiles and those obtained from the zoned greisen are similar, but the changes are overestimated if the water/rock ratio correction is applied.

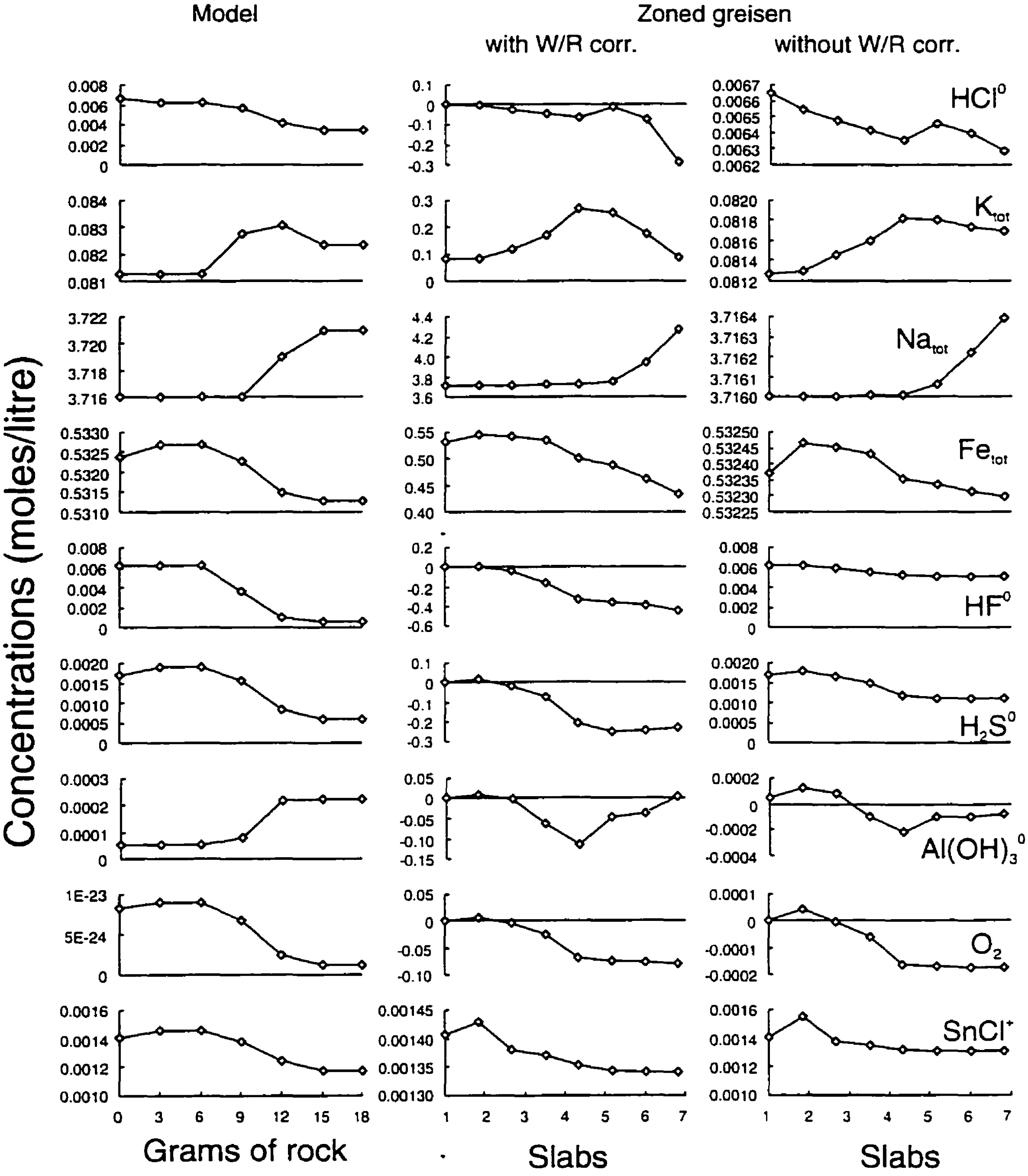
Model
Zoned greisen
with W/R corr.
without W/R corr.
Concentrations (moles/litre)
HCl^0
0.008
0.006
0.004
0.002
0
0.1
0
-0.1
-0.2
-0.3
0.0067
0.0066
0.0065
0.0064
0.0063
0.0062
K_{tot}
0.084
0.083
0.082
0.081
0.3
0.2
0.1
0
0.0820
0.0818
0.0816
0.0814
0.0812
Na_{tot}
3.722
3.720
3.718
3.716
4.4
4.2
4.0
3.8
3.6
3.7164
3.7163
3.7162
3.7161
3.7160
Fe_{tot}
0.5330
0.5325
0.5320
0.5315
0.5310
0.55
0.50
0.45
0.40
0.53250
0.53245
0.53240
0.53235
0.53230
0.53225
HF^0
0.008
0.006
0.004
0.002
0
0.2
0
-0.2
-0.4
-0.6
0.008
0.006
0.004
0.002
0
H_2S^0
0.0020
0.0015
0.0010
0.0005
0
0.1
0
-0.1
-0.2
-0.3
0.0020
0.0015
0.0010
0.0005
0
$Al(OH)_3^0$
0.0003
0.0002
0.0001
0
0.05
0
-0.05
-0.10
-0.15
0.0002
0
-0.0002
-0.0004
O_2
1E-23
5E-24
0
0.05
0
-0.05
-0.10
0.0001
0
-0.0001
-0.0002
SnCl$^+$
0.0016
0.0014
0.0012
0.0010
0.00145
0.00140
0.00135
0.00130
0.0016
0.0014
0.0012
0.0010
0
3
6
9
12
15
18
Grams of rock
1
2
3
4
5
6
7
Slabs
1
2
3
4
5
6
7
Slabs

in this model and in changes deduced from natural samples, that the fluid and the rock equilibrated locally. If, however, the water/rock ratio correction is applied to the chemical changes obtained from the zoned greisen (2nd column), these changes are largely overestimated; they compare much better to the modeled changes if a constant water/rock ratio is assumed.

In contrast to the components discussed above, significant differences are evident between calculated changes in the fO_2 of the fluid and those obtained from the CO_2/CH_4 ratio in fluid inclusions (Fig. 3). Owing to the high Fe content of this system, the fO_2 of the fluid was likely controlled by the Fe^{2+}/Fe^{3+} ratio in the fluid or in the rock. Unfortunately, at the low fO_2 conditions estimated from fluid inclusions (Table 1), this ratio is approximately to 10^{-14} and variations in Fe^{3+} could not be modeled accurately. Consequently, the modeled behaviour of fO_2 (Fig. 7) almost certainly does not represent the changes that occurred in the natural system.

An additional difference between the model and nature is that calculated changes in the concentration of components occur at relatively sharp alteration fronts, due to punctual dissolution or precipitation of a solid phase. By contrast, in the greisens, replacement of individual phases occurred progressively, suggesting that changes in fluid composition occurred the same way. This difference can be explained by the fact that in natural systems, the distribution of elements is controlled by chemical potential gradients through a compensated infiltration process (Chapter 3). As a result, changes in fluid and rock composition would have been progressive (Thompson 1959) as would have been changes in chemical potentials. Moreover, the multiple pass fluid flow model is uni-directional and only provides for transport of components away from the vein. Hence, the Na content, which appears to increase significantly in fluid inclusions across the alteration halo, increased only very little in the modeled fluid. However, since the chemical potential of most components in our system is higher in the vein than in the leucogranite (Fig. 7 and 9), uni-directional infiltration will transfer elements in the same direction as the compensated infiltration process in natural systems.

CHEMISTRY OF FLUID -ROCK INTERACTION

We showed above, that the multiple pass fluid flow model accurately predicts the changes in the concentration of components such as Fe, Sn and HF that were estimated from fluid inclusion and mineral analyses and satisfactorily explains the observed alteration. It is therefore reasonable to assume that the model predictions will also be valid for components such as a_{H^+} which could not be estimated directly for the greisens.

In Figure 7, the increase in pH of the fluid and the related decrease in the activity of HCl^0, occurred mainly as a result of feldspar dissolution. This took place close to the vein in the first pass of fluid as the rock column is composed of leucogranite. With progressive alteration of the column, first to a quartz-sericite greisen and then to a quartz-topaz greisen in subsequent passes, these changes occurred further out in the alteration halo. The concentration of Cl^-, which is important in the transport of almost all the components, depends on the activity of HCl^0 and thus on the pH. It remained essentially constant until segment 13 and only increased as the pH rose significantly due to the dissolution K-feldspar. Muscovite saturates at a KCl^0 concentration of approximately 0.05m and therefore buffered this component at very low values; the concentration of KCl^0 only increased significantly with the increase of pH in the least altered rocks. The profiles for H_2S^0 and O_2,aq. are similar and are marked by sharp decreases in the concentration of these components close to the vein in the first pass of fluid, in response to pyrrhotite and cassiterite precipitation, respectively. However, after several passes, pyrrhotite and cassiterite were dissolved in the 1st segment and re-precipitated further out (segment 6), causing the concentrations of H_2S^0, and O_2,aq. to increase between the 1st and the 2nd segment after the 7th pass. The concentration of HF^0 and $Al(OH)_3^0$ in the fluid were controlled by the solubility of topaz close to the vein and the solubility of muscovite in less altered rock, i.e., in the absence of topaz. This explains the steps in the profiles for these components at the muscovite-topaz equilibrium boundary and why this step moves outwards with each successive pass of fluid.

CASSITERITE PRECIPITATION

In Chapters 2 and 3 we showed that, at the conditions estimated for East Kemptville, the most important tin species in solution is $SnCl^-$ (Wilson and Eugster 1990). The H^+ and Cl^- ions are mainly associated in HCl^0 and the precipitation reaction of cassiterite is therefore:

$$SnCl^- + H_2O + {}^1/_2O_2 + Cl^- \rightleftharpoons SnO_2 + 2HCl^0; \quad K= 7.222 \cdot 10^{-11}$$

We concluded from changes in mineral and fluid compositions across the alteration halo that the main control on cassiterite precipitation was an increase in pH that accompanied the replacement of muscovite by topaz in quartz-topaz greisen (Chapter 2 and 3). We further concluded that changes in the two other parameters that could cause cassiterite to saturate (fO_2 and a_{Cl^-}) favoured its dissolution. As discussed earlier, however, our modeling only permits us to accurately quantity the changes in the pH or a_{Cl^-}; the calculated changes in fO_2 are considered unreliable because the very low concentration of Fe^{3+} could not be accurately approximated in the calculations.

The above calculations indicate that the activity of HCl^0 decreased in the first few segments, confirming conclusions drawn from the natural samples that this parameter favoured cassiterite precipitation. In contrast, a_{Cl^-}, which was thought previously to decrease in the fluid (Chapter 2), appears to increase and could equally explain tin mineralization. We therefore evaluated the relative importance of the changes in a_{HCl^0} and a_{Cl^-} on cassiterite precipitation by calculating the effect of their changes on the saturation index, SI. Cassiterite saturates if SI equals zero and an increasingly negative value indicates an increasing degree of undersaturation. In the vein, where no cassiterite is predicted to precipitate this index is -0.097 and only increases to -0.096 in response to the change in a_{Cl^-} after the seventh pass through the second segment, where cassiterite is predicted to precipitate. By contrast, the corresponding increase in SI as a result of the change in HCl^0 is to a value of -0.033. In other words, the change in a_{HCl^0} brings the fluid 63 times closer to saturation with cassiterite (SI = 0) than does the change in a_{Cl^-}. This confirms our earlier conclusions that cassiterite mineralization resulted mainly from a decrease in a_{HCl^0} during fluid-rock interaction, i.e., as a result of a pH increase during the formation of quartz-topaz greisen.

ALTERATION PROCESS

Hypotheses for the evolution of the alteration presented earlier (Chapters 2 and 3) were based on observations of the presently preserved nature of the alteration halo, i.e., its state after the termination of fluid-rock interaction. By modeling the process using multiple passes of fluid flow we had an opportunity to evaluate the changes in the fluid and the rock as a function of reaction progress: each successive pass of fluid simulates a more advanced stage of the reaction between rock and vein fluid. This model produced a series of alteration zones that were progressively more buffered by the fluid close to the vein, and alteration fronts, which migrated outwards with time. An important consequence of the model is that at a late stage of the alteration, the mineralizing fluid was able to re-dissolve earlier precipitated phases, potentially producing "geochemical cumulations", or locations in the alteration halo where the concentration of one or more components in the aqueous phase is higher than in surrounding rocks (Korzhinskii, 1970). These geochemical cumulations can significantly affect the conditions at which minerals saturate. For example, the concentration of $SnCl^-$ decreased sharply in the early stages of the first pass (open symbols) as a result of cassiterite precipitation in response to a pH increase (Fig. 10). In the same stages of the seventh pass (solid symbols) the concentration of $SnCl^-$ increased due to cassiterite dissolution. Consequently, the pH required for cassiterite precipitation in the first pass was 3.1, whereas after the seventh pass cassiterite saturated at a pH of 3.05. The implication is that cassiterite precipitated relatively close to the vein (in the second segment) as the a_{SnCl^-} was increased; if this did not occur, cassiterite would

Figure 10: Changes in pH and a_{Sn} in the fluid with increasing alteration (from left to right) calculated using the multiple pass fluid flow pass model. At the onset of alteration, changes in pH and a_{SnCl^+} occur rapidly and close to the vein (first pass; open symbols). With time, the halo wides and changes in pH and a_{SnCl^+} are more gradual (seventh pass, solid symbols). This results in the dissolution of some phases, e.g., cassiterite, and causes the formation of "geochemical cumulations", i.e., a zone in the alteration halo where the activity of a component in the fluid is higher than in the adjacent segments. This allows these particular components to be transported in two directions through compensated infiltration (Chapter 3), i.e., away from, and also towards the fracture (vein).

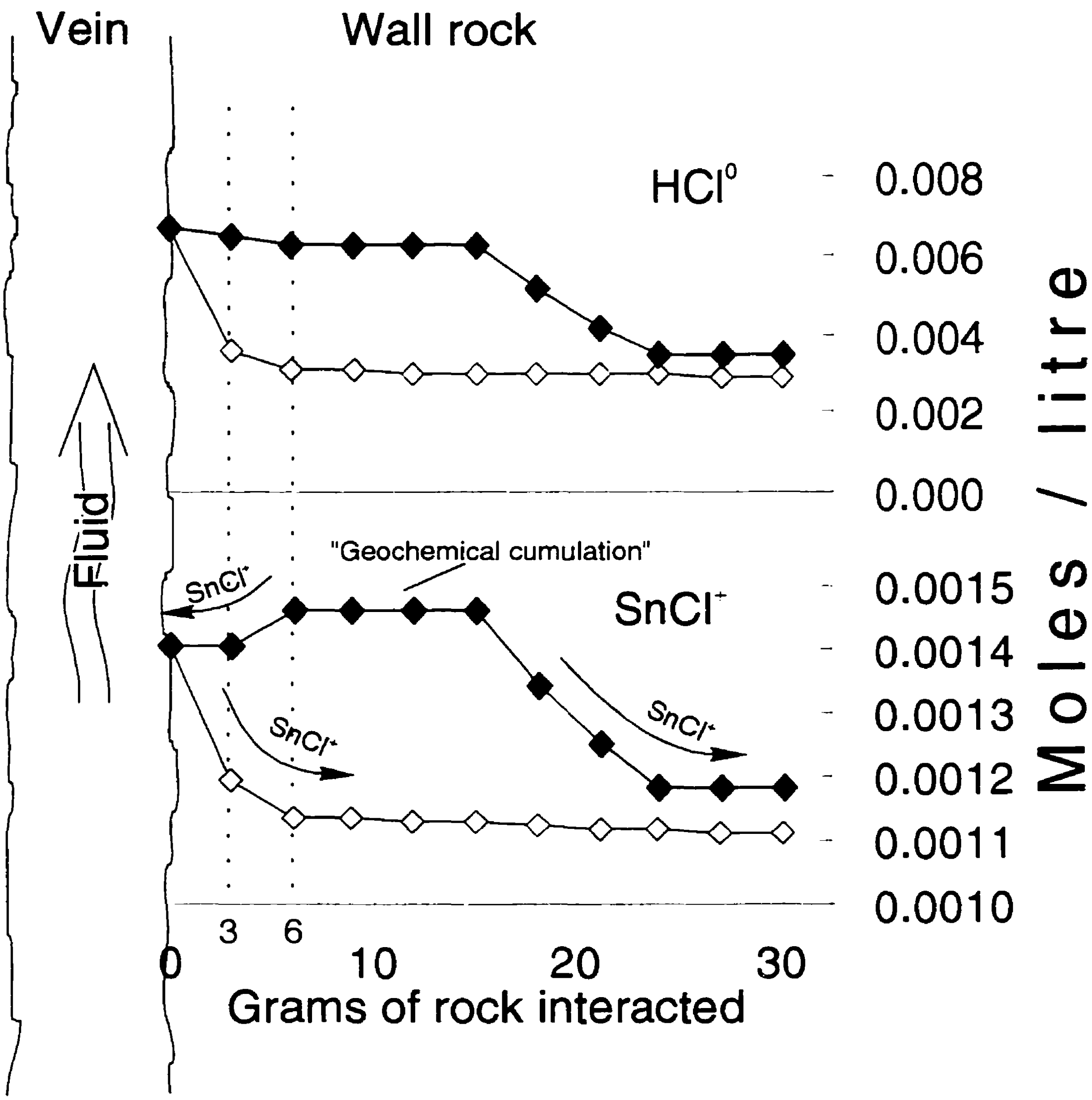
Vein
Wall rock
Fluid
HCl^0
0.008
0.006
0.004
0.002
0.000
"Geochemical cumulation"
SnCl$^+$
SnCl$^+$
SnCl$^+$
SnCl$^+$
0.0015
0.0014
0.0013
0.0012
0.0011
0.0010
Moles / litre
3
6
0
10
20
30
Grams of rock interacted

have precipitated only during dissolution of muscovite in the sixth segment (at a pH of 3.1).

Another important consequence of the creation of a geochemical cumulation in $SnCl^-$ is that a chemical potential gradient develops which promotes the transport of $SnCl^-$ back to the vein. This process can significantly affect the tin content of the wall rock during the formation of an alteration halo around a vein, as the geochemical cumulation can form an effective barrier across which Sn cannot be transported. This is not apparent from the above calculation because of the difficulty of modeling the transport of elements back to the vein, as discussed erlier.

Finally, if the model presented here satisfactorily simulates the alteration in natural systems, then if follows that the water/rock ratio remained constant across the alteration halo at any given time, i.e., each aliquot of fluid interacted with every rock segment even though its alteration capacity decreased away from the vein. This conclusion is contrary to the widely held view, based on $^{18}O/^{16}O$ ratios, that the water/rock ratio decreases continuously from the vein (Taylor, 1974). However, a constant water/rock ratio is supported by the fact that changes in fluid compositions deduced from natural samples (Chapter 2) compare much better to modeled changes if no correction for the water/rock ratio is applied (Fig. 9). It is also consistent with the compensated infiltration process proposed earlier (Chapter 3) in which the net addition of water to the rock is minimal. We suggest that the relative abundance of ^{18}O and ^{16}O is controlled by "isotopic" potential gradients in the alteration halo, analogous to chemical potential gradients.

SUMMARY AND CONCLUSIONS

Fluid-rock interaction and greisen formation around a central vein was simulated using simple titration and multiple pass fluid flow models. In the second model successive aliquots of fluid are passed through a segmented rock column, and equilibrated with each rock segment before passing on to the next segment. As a result, each segment of the column becomes progressively more altered as it equilibrates with each new aliquot of fluid. The multiple pass fluid flow model accurately predicts the changes in mineralogy and fluid chemistry estimated from samples of the East Kemptville tin deposit. The only obvious weakness of the model is that it assumes uni-directional infiltration and thus only provides for transport of components from the fracture (vein) to the rock. However, this was a relatively insignificant limitation in the case of East Kemptville as all important elements, except Na, were transported away from the vein.

The good agreement between the model and nature implies, that the assumption that the fluid and the rock equilibrated locally is valid. It also implies that the water/rock ratio remained constant across the alteration halo and that changes in isotopic composition of the wall rock during alteration do not reflect changes in water/rock ratios.

In contrast to conclusions drawn from fluid inclusion and whole rock analyses, modeled values of a_{Cl^-} increased during alteration and favoured cassiterite precipitation. However this increase in a_{Cl^-} did not significantly contribute to cassiterite saturation, which was caused mainly by a decrease in a_{HCl^0}. Re-dissolution of early precipitated cassiterite close to the vein affected the conditions at which this phase saturated during the later stages of the alteration, and caused a reversal in the chemical potential gradient for $SnCl^-$ in the most altered rocks which helped transport Sn back to the fracture (vein). This limited the amount of tin that could be introduced into the host rocks and may explain the comparatively low tin grades of the East Kemptville deposit and of other deposits which formed under similar conditions.

REFERENCES

Bottrell, S.H., and Yardley, B.W.D., 1988, The composition of a primary granite-derived ore fluid from S.W. England, determined by fluid inclusion analysis: Geochimica et Cosmochimica Acta, v. 52, p. 585-588.

Burt, D.M., 1981, Acidity-salinity diagrams - Application to greisen and porphyry deposits: Economic Geology, v. 76, p. 832-843.

Durišová , J., Charoy, B., and Weisbrod, A., 1979, Fluid inclusion studies in minerals from the tin and tungsten deposits in the Krusné Hory Mountains (Czechoslovakia): Bulletin de minéralogie, v. 102, p. 665-675.

Eadington, P.J., 1983, A fluid inclusion investigation of ore formation in a tin-mineralized granite, New England, New South Wales: Economic Geology, v. 78, p. 1204-1221.

Ham, L J., and MacDonald. M.A., 1994, Geological map of Wentworth Lake: Nova Scotia Department of natural Resources, Mines and Energy Branches, map 94-03.

Heinrich, C.A., 1990, The chemistry of Hydrothermal tin (- tungsten) ore deposits: Economic Geology, v. 85, p. 457-481.

Helgeson, H.C., 1970, A chemical and thermodynamic model of ore deposition in hydrothermal systems: Mineralogical Society of America, Spec. Pap. 3, 155-186.

Helgeson, H.C., Kirkham, D.H., and Flowers, G.C., 1981, Theoretical prediction of the thermodynamic behaviour of aqueous electrolytes at high pressures and temperatures. IV. Calculation of activity coefficients, osmotic coefficients, and apparent molal and standard and relative partial molal properties to 600°C and 5Kb.: American Journal of Science, v. 281, p. 1249-1516.

Johnson, J.W., Oelkers, E.H., and Helgeson H.C., 1991, SUPCRT92, a software package for calculating the standard molal thermodynamic properties of minerals, gases, aqueous species, and reactions from 1 to 5000 bars and 0 to 1000°C: Computers and Geosciences, v. 18, p. 899-947.

Keppie, J.D., 1979, Geological map of Nova Scotia: Nova Scotia Department of Mines and Energy.

Kontak, D.J., 1990, The East Kemptville topaz-muscovite leucogranite, Nova Scotia. I. Geological setting and whole-rock geochemistry: Canadian Mineralogist, v. 28, p. 787-825.

Kontak, D.J., 1991, The East Kemptville topaz-muscovite leucogranite, Nova Scotia. II. Mineral chemistry: Canadian Mineralogist, v. 29, p. 37-60.

Korzhinskii, D.S., 1970, The theory of metasomatic zoning: Oxford, England, Clarendon Press.

Mangas, J., and Arribas, A., 1987, Fluid inclusions study in different types of tin deposits associated with the hercynian granites of Western Spain: Chemical Geology, v. 61, p. 193-208.

MacDonald, M.A., 1994, Geological map of the South Mountain Batholith, western Nova Scotia: Nova Scotia Department of Natural Resources, Mines and Energy Branches, map 94-01.

Ragnarsdòttir, K.V., and Walther, J.V., 1985, Experimental determination of corundum solubilities in pure water between 400-700°C and 1-3kbars: Geochimica et Cosmochimica Acta, v. 49, p. 2109-2115.

Reed, H.M., 1982, Calculation of multicomponent chemical equilibria and reaction processes in systems involving minerals, gases and an aqueous phase: Geochimica et Cosmochimica Acta, v. 46, p. 513-528.

Richardson, J.M., 1988, Field and textural relationships of alteration and greisen-hosted mineralization at the East Kemptville tin deposit, Davis Lake Complex, southwest Nova Scotia, *in* Recent advances in the geology of granite-related mineral deposits: Canadian Institute of Mining and Metallurgy Special Volume 39, p. 265-279.

Richardson, J.M., Spooner, E.T.C., and McAuslan, D.A., 1982, The East Kemptville tin deposit, Nova Scotia: An example of a large tonnage, low grade, greisen-hosted deposit in the endocontact zone of a granite batholith: Geological Survey of Canada Current research, part B, paper 82-1B, p. 27-32.

Schwartz, M.O., and Surjono, A., 1990, Greisenization and albitization at the Tikus tin-tungsten deposit, Belitung, Indonesia: Economic Geology, v. 85, p. 691-713.

Spycher, N.F., and Reed, M.H., 1989, CHILLER : A program for computing water-rock reactions, boiling, mixing and other reaction processes in aqueous-mineral-gas systems: Unpublished report, Dept. of Geological Sciences, University of Oregon, Eugene, Oregon.

Sverjensky, D.A., Hemley, J.J., and D'Angelo, W.M., 1991, Thermodynamic assessment of hydrothermal alkali feldsar-mica-aluminosilicate equilibria: Geochimica et Cosmochimica Acta, v. 55, p. 989-1004.

Taylor, H. P., 1974, The application of oxygen and hydrogen isotope studies to problems of hydrothermal alteration and ore deposition: Economic Geology, v. 69, p. 843-883.

Thompson, J.B., Jr., 1959, Local equilibrium in metasomatic processes, *in* Abelson, P.H., ed., Researches in Geochemistry: New York, Wiley, p. 427-457.

Wilson, G.A., and Eugster, H.P., 1990, Cassiterite solubility and tin speciation in supercritical chloride solutions, *in* Fluid-mineral interactions: A tribute to H.P. Eugster: The Geochemical Scociety, Special Publication No 2., p. 179-195.

Zhu, C., and Sverjensky, D.A., 1991, Partitioning of F-Cl-OH between minerals and hydrothermal fluids: Geochimica et Cosmochimica Acta, v. 55, p. 1837-1858.

INTRODUCTION TO CHAPTER VI

Accurate determination of mineral compositions was required in the normative mineral calculation and in the modeling of the alteration. In Chapters 3 and 4, we mentioned that muscovite compositions used in these calculations are highly variable and that, in quartz-topaz greisen, muscovite generally yielded high totals during electron microprobe analyses, but did not discuss these data. In the following Chapter, we investigate the chemical variations and provide an explanation for these high totals of muscovite in quartz-topaz greisen.

CHAPTER VI

FORMATION AND COMPOSITION OF NATURALLY OCCURRING "ANHYDROUS" MUSCOVITE

WERNER E. HALTER

AND

ANTHONY E. WILLIAMS-JONES

DEPARTMENT OF EARTH AND PLANETARY SCIENCES, MCGILL UNIVERSITY
3450 UNIVERSITY STREET, MONTRÉAL QUÉBEC H3A 2A7

ABSTRACT

In highly altered rocks of the East Kemptville tin deposit, i.e., in quartz-topaz greisen, electron microprobe analyses of white micas consistently yield totals close to 100%. Comparison of these analyses with those of normal micas in slightly less altered rocks suggests that these high totals are due to dehydration. Sharp increases in the Si counts for these "anhydrous" muscovite crystals during the first 20-30 seconds of analysis, and the lack of similar increases in the Si counts for normal muscovite, suggest that the dehydration occurred during microprobe analyses. This, in turn, suggests that water was present as H_2O in the "anhydrous" mica, and not as structurally bound OH^- groups. Water molecules are interpreted to have formed from the conversion of two adjacent OH^- groups into an H_2O molecule which was trapped in the vacant site, and an O^{2-} ion bound to the structure. A possible reason for this conversion is the high F content of the mica, which would have caused a decrease in the thickness of the octahedral layer, and therefore the distance between OH^- groups. Formation of an O^{2-} ion was accompanied by the loss of an edge of the octahedral site which was therefore converted into a trigonal di-pyramid, and increased the stability of these micas.

Normal micas at East Kemptville have a composition between phengite and muscovite due mainly to a variation in the Fe^{2+} and Al^{3+} concentration, accompanied by a substitution of OH^- by F^-. In "anhydrous" micas, structural changes induced by the replacement of OH^- by O^{2-} allow a wider compositional variation than that reported for normal micas, and thus the substitution of Al^{3+} by Fe^{2+} produced compositions mid-way between di- and tri-octahedral structures.

INTRODUCTION

The water content of di-octahedral micas (estimated from the difference between the totals of electron microprobe analyses and 100%) is widely reported to vary between 3 and 5 wt%. However, in the East Kemptville tin deposit, Nova Scotia, di-octahedral micas in F-rich quartz-topaz greisen systematically yield totals of ~100%. Totals for di-octahedral micas in the other greisens and the sericitized leucogranite range from 95 to 97wt%, consistent with those expected for electron microprobe analyses of such micas. Reports of di-octahedral micas yielding high totals in electron microprobe analyses have been made for other F-rich rocks (Charoy et al., 1995). However, the reason of these high totals has not been explained.

In this study we present an explanation for the high totals of these micas involving the replacement of OH^- groups by O^{2-} and H_2O due to high F concentrations, and subsequent dehydration during electron microprobe analyses. We also examine the compositional changes that occurred in normal and "dehydrated" micas during progressive greisenization.

GEOLOGICAL SETTING

The East Kemptville tin deposit, Nova Scotia, developed in an evolved leucogranitic facies of the Davis Lake Pluton, at the southwestern end of the 370 Ma South Mountain Batholith in the Meguma Terrane of the Appalachian Orogen (Fig. 1). The least altered leucogranite of this intrusion has been described extensively by Richardson et al. (1982), Richardson (1988), Kontak (1990, 1991) and in Chapters 2 and 3. It consists of quartz, albitic plagioclase, K-feldspar, muscovite and topaz, with accessory biotite, apatite and zircon. The mineralogical changes that affected the leucogranite during greisen formation are presented in Figure 2, which represents one side of an idealized alteration halo formed around a central vein, and was constructed using samples from a drill core (90-1) described in Chapter 3. It is apparent from petrographic observations that, with increasing alteration in the leucogranite, albite

Figure 1: Location of the East Kemptville tin deposit on a simplified geological map of the Meguma Terrane, Nova Scotia (after Keppie, 1979, and Kontak, 1990). The enlarged area of the South Mountain Batholith shows the Davis Lake Pluton (after MacDonald, 1994, and Ham and MacDonald, 1994), which hosts the mineralization. The fault that runs through the leucogranite is part of the East Kemptville-East Dalhousie fault zone (EKEDFZ), and controlled the location and the geometry of the mineralization at East Kemptville. TFZ refers to the Tobiatic Fault Zone.

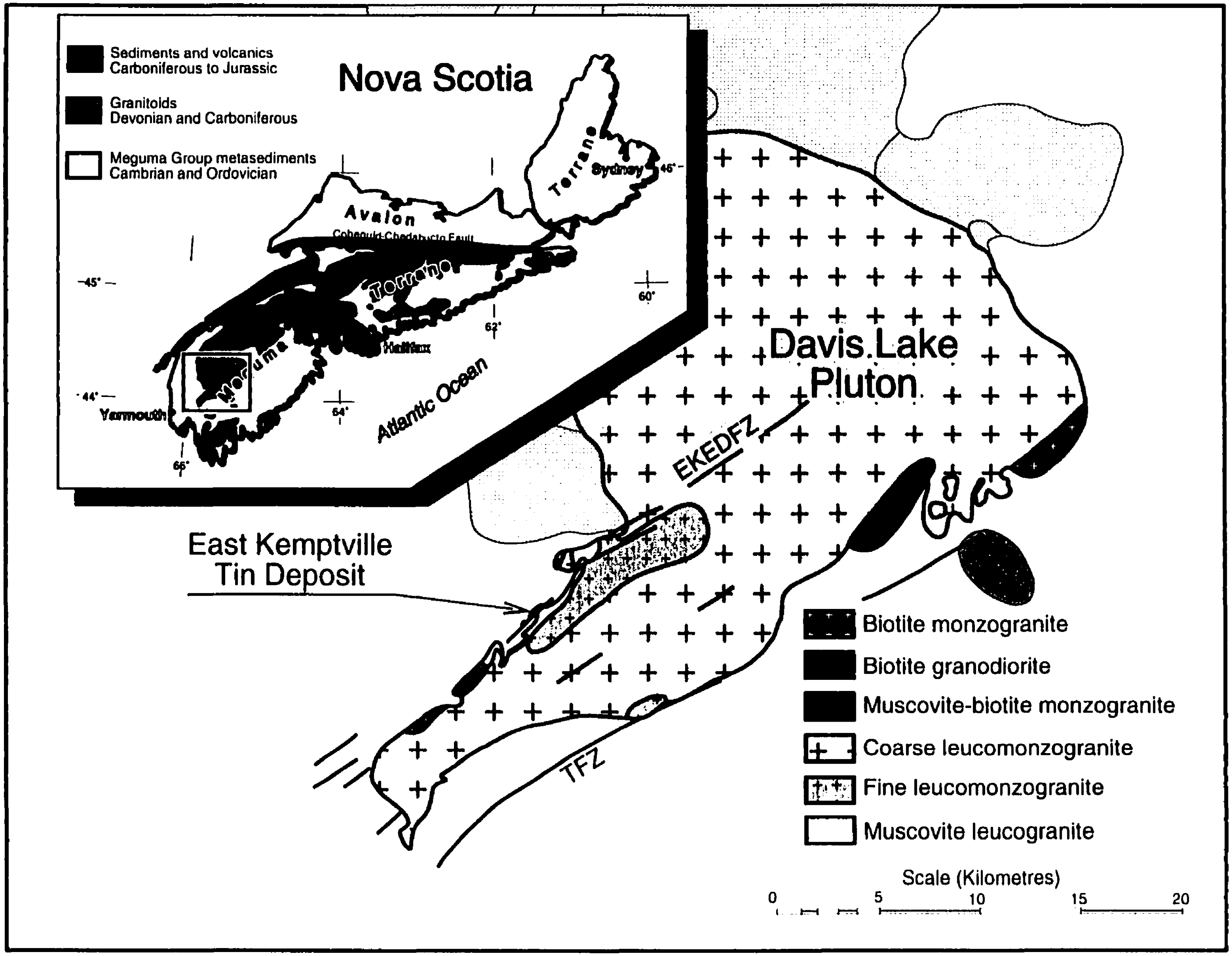
Sediments and volcanics
Carboniferous to Jurassic
Granitoids
Devonian and Carboniferous
Meguma Group metasediments
Cambrian and Ordovician
Nova Scotia
Avalon
Cobequid-Chedabucto Fault
Terrane
Sydney
Terrane
Meguma
Halifax
Yarmouth
Atlantic Ocean
46°
45°
44°
66°
64°
62°
60°
Davis Lake
Pluton
EKEDFZ
TFZ
East Kemptville
Tin Deposit
Biotite monzogranite
Biotite granodiorite
Muscovite-biotite monzogranite
Coarse leucomonzogranite
Fine leucomonzogranite
Muscovite leucogranite
Scale (Kilometres)
0
5
10
15
20

Figure 2: Calculated normative mineral compositions of all samples analyzed in drill hole 90-1. The horizontal scale was obtained by assuming a linear increase in muscovite between samples 188.5 and 222, followed by a linear increase in the proportion of albite up to sample 237, and eventually a linear increase in the proportion of K-feldspar. Spacing between samples was further adjusted in order to obtain an approximately linear decrease in the proportion of quartz (see Chapter 3 for more details). Samples used for muscovite analysis are framed.

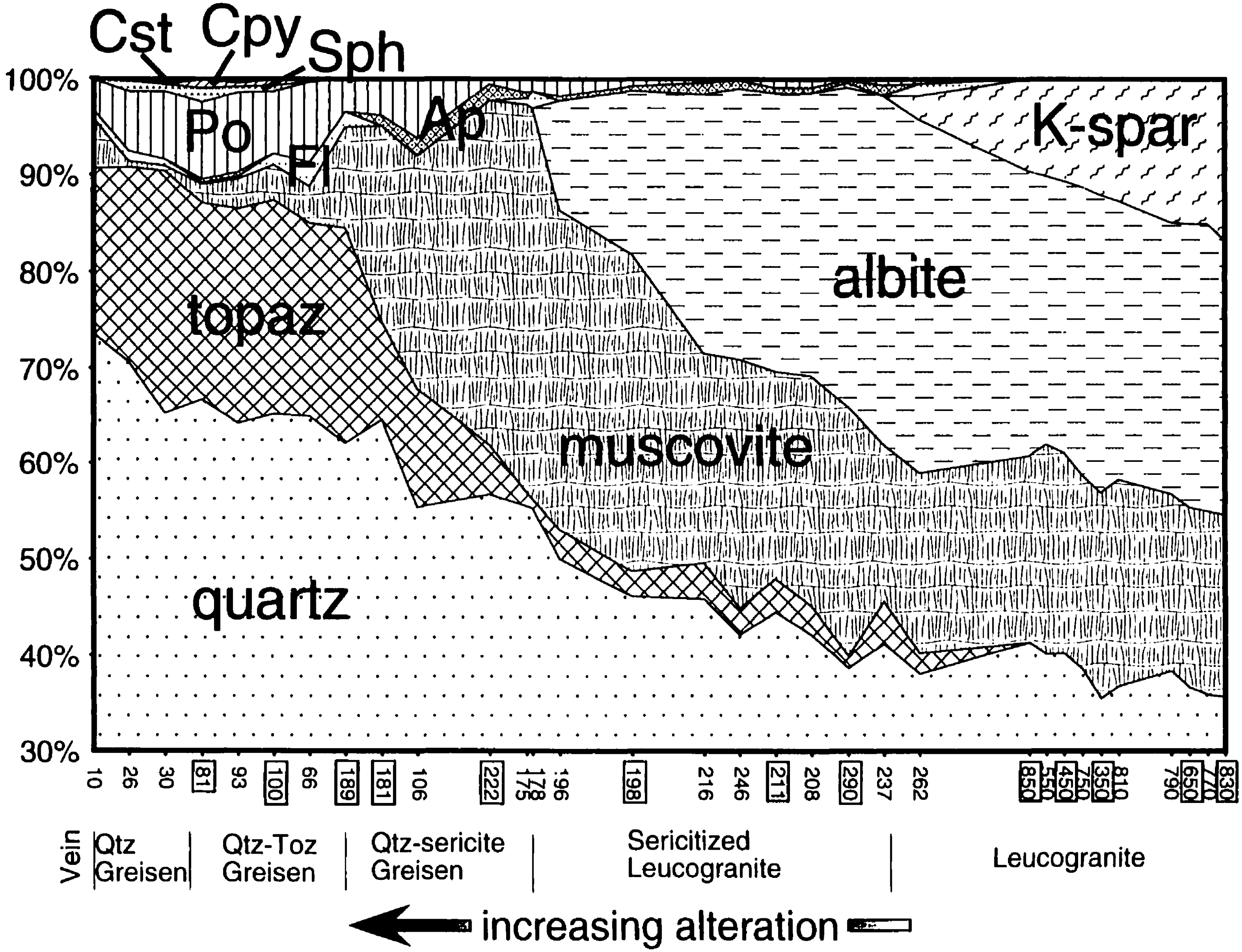
Cst
Cpy
Sph
Po
Fl
Ap
K-spar
albite
topaz
muscovite
quartz
100%
90%
80%
70%
60%
50%
40%
30%
10
26
30
81
93
100
66
189
181
106
222
178
175
196
198
216
246
211
208
290
237
262
850
550
450
750
350
810
790
650
770
830
Vein
Qtz Greisen
Qtz-Toz Greisen
Qtz-sericite Greisen
Sericitized Leucogranite
Leucogranite
increasing alteration

replaced K-feldspar forming "chess-board albite" and eventually homogenous albite when no further K-feldspar remained. With further alteration, albite was, in turn, replaced by sericite (muscovite), leading to the formation of quartz-sericite greisen which contains trace amounts of pyrrhotite and cassiterite. Close to veins and in highly altered zones, quartz-sericite greisen was replaced by quartz-topaz greisen, with topaz substituting for white mica. This greisen contains significant concentrations of pyrrhotite, sphalerite, chalcopyrite and cassiterite. The immediate wall to the vein is a quartz greisen characterized by lower topaz, sulphide and cassiterite contents than the quartz-topaz greisen.

ELECTRON MICROPROBE ANALYSES

White micas in selected samples of the different alteration zones described above (framed in Figure 2) were analyzed using an electron microprobe at standard operating conditions, i.e., with a beam current of 20 nanoamperes and an excitation voltage of 15 Kvolts. The electron beam diameter was 5µm and the counting times were 20 seconds for the major elements, 100 seconds for F and 10 seconds for the background. The average composition of these white micas in each sample are presented in Table 1. All analyses from samples between the least altered leucogranite and sample 181(except for sample 198) have totals between 95 and 97wt-%, i.e., similar to those of analyses reported in the literature. However, analyses of micas in more altered samples (189 to 38.6) consistently have totals close to 100%. Significantly, the composition of the mica in the least altered of these samples (189) is very similar to that of mica (with normal totals) in sample 181, if the analyses are normalized to the same total (Table 2). The same is true of micas in sample 38.6 from a vein which comprises both "normal" and "high" total populations. These observations suggest that micas yielding analyses with a high total represent "anhydrous" equivalents of the normal micas.

Possible explanations for the origin of the high totals are that they represent naturally occurring anhydrous micas or micas that underwent dehydration during analysis.

Table 1: Average muscovite analyses and normative compositions (based on 22 oxygens) in selected samples

Sample	38.6		71.8		81		100		189		181	
	wt-%	norm. 22O	wt-%	norm. 22O	wt-%	norm. 22O	wt-%	norm. 22O	wt-%	norm. 22O	wt-%	norm. 22O
SiO_2	50.02	6.35	45.20	6.36	46.46	6.50	49.26	6.55	49.03	6.46	46.66	6.42
TiO_2	0.06	0.00	0.16	0.00	0.22	0.02	0.11	0.01	0.02	0.00	0.03	0.00
Al_2O_3	35.82	5.36	24.70	4.09	25.71	4.23	29.22	4.58	31.72	4.92	30.43	4.94
FeO	1.14	0.12	14.91	1.77	11.20	1.33	8.00	0.89	6.06	0.67	5.52	0.64
MnO	0.05	0.01	0.74	0.09	0.48	0.06	0.27	0.03	0.28	0.03	0.34	0.04
MgO	1.15	0.22	1.40	0.30	1.14	0.24	0.70	0.14	0.28	0.06	0.17	0.03
Na_2O	0.33	0.08	0.14	0.04	0.17	0.05	0.13	0.03	0.17	0.04	0.27	0.07
K_2O	10.81	1.75	10.29	1.85	10.65	1.90	10.90	1.85	10.83	1.82	11.32	1.99
F	1.57	0.63	5.26	2.36	4.79	2.14	3.68	1.55	2.93	1.22	2.09	0.91
OH		3.37		1.64		1.86		2.45		2.78		3.09
Total	100.31		100.61		98.84		100.73		100.12		95.93	

Sample	222		198		211		273		290		850	
	wt-%	norm. 22O	wt-%	norm. 22O	wt-%	norm. 22O	wt-%	norm. 22O	wt-%	norm. 22O	wt-%	norm. 22O
SiO_2	47.28	6.44	49.75	6.57	46.59	6.49	45.33	6.49	47.50	6.90	46.75	6.53
TiO_2	0.09	0.01	0.15	0.01	0.13	0.01	0.28	0.00	0.10	0.01	0.41	0.04
Al_2O_3	30.85	4.95	30.11	4.73	28.71	4.71	26.02	4.76	22.76	3.87	27.53	4.53
FeO	5.00	0.57	6.69	0.73	6.88	0.81	10.47	0.75	9.35	1.18	7.72	0.90
MnO	0.22	0.03	0.46	0.05	0.48	0.06	0.31	0.04	0.90	0.12	0.38	0.05
MgO	0.41	0.08	0.24	0.05	0.20	0.04	0.83	0.04	0.17	0.04	0.45	0.09
Na_2O	0.15		0.12	0.03	0.14		0.14	0.04	0.12		0.14	
K_2O	11.31	1.97	10.56	1.78	11.29	2.01	11.19	1.99	11.02	2.04	11.32	2.02
F	2.05	0.88	3.56	1.46	2.74	1.22	3.39	0.89	5.89	2.78	2.18	0.97
OH		3.12		2.54		2.78		3.11		1.22		3.03
Total	96.51		100.18		96.03		96.61		95.34		96.01	

Sample	450		350		650		830	
	wt-%	norm. 22O	wt-%	norm. 22O	wt-%	norm. 22O	wt-%	norm. 22O
SiO_2	46.65	6.58	47.46	6.69	46.43	6.49	45.61	6.47
TiO_2	0.25	0.00	0.26	0.00	0.48	0.00	0.50	0.00
Al_2O_3	26.98	4.48	26.27	4.36	28.27	4.64	27.07	4.52
FeO	7.24	0.86	7.53	0.89	6.76	0.80	8.49	1.01
MnO	0.38	0.05	0.41	0.05	0.36	0.04	0.36	0.04
MgO	0.53	0.11	0.28	0.06	0.40	0.08	0.43	0.09
Na_2O	0.13	0.03	0.12	0.03	0.26	0.07	0.12	0.03
K_2O	11.41	2.05	11.26	2.02	11.33	2.02	11.29	2.04
F	3.27	1.46	3.64	1.62	2.66	1.19	2.10	0.95
OH		2.54		2.38		2.81		3.05
Total	95.49		95.71		95.83		95.11	

Table 2: Comparison between analyses of standard micas and micas with high totals

Sample	SiO_2	TiO_2	Al_2O_3	FeO	MgO	Na_2O	K_2O	F	Total
average low 38.6	48.42	0.03	34.35	0.72	1.1	0.38	10.47	1.53	96.44
average high 38.6	50.82	0.09	35.75	1.24	1.17	0.33	10.80	1.68	101.27
normalysed 38.6	50.85	0.03	36.07	0.76	1.16	0.40	10.99	1.61	101.27
sample 189	49.03	0.02	31.72	6.06	0.28	0.17	10.83	2.93	100.12
sample 181	46.66	0.03	30.43	5.52	0.17	0.27	11.32	2.09	95.93
normalysed 189	46.98	0.02	30.40	5.80	0.27	0.17	10.37	2.81	95.93

We investigated these possibilities by measuring the number of counts in consecutive 2 second intervals for the Si peak on crystals of "normal" and "anhydrous" mica using an electron beam with 5µm diameter and then expanding it to 15µm. It is apparent from Figure 3, that for a normal mica (sample 650), the number of counts per 2 seconds varies non-systematically in a narrow band for the first 125 seconds of the analysis and that there is no significant difference between the number of counts obtained with 5µm and 15µm diameter beams. Thereafter the number of counts with the 5µm beam increases gradually, while that with the 15µm beam remains the same. The number of counts per 2 seconds for the "anhydrous" mica, by contrast, increases rapidly in the first 20-30 seconds of analyses with a 5µm beam, whereas they vary within the same narrow range for the duration of the analyses (400 seconds) with a 15µm beam. The average difference in the number of counts with the two beam diameters is 3.3% and corresponds approximately to the proportion of H_2O present in micas. Three crystals in a sample of "anhydrous" mica (189) were re-analyzed with a 15µm beam and the compositions, presented in Table 3, have a total close to that expected for micas, i.e., no water was lost.

We conclude from the data presented above that the analyses in Table 1 with high totals (all analyses were conducted using 5µm beam diameter, which is standard for this type of analysis) represent early loss of H_2O during the analysis. This early water loss is confirmed by the fact that K, which is among the first elements to be considered during a microprobe analysis (i.e., before complete loss of H_2O), has approximately the same abundance in normal and "anhydrous" micas (Table 2), whereas Si and Al, which are analyzed some time later, i.e., after all the H_2O had been lost, are higher in the "anhydrous" mica.

Similar high totals in mica analyses have been reported in other high fluorine systems, e.g., by Charoy et al. (1995), and the normative K content calculated for these samples is low, as is the case in our samples. It is therefore possible that these high totals also reflect dehydration during analysis.

Figure 3: Variation in Si counts with time during electron microprobe analyses using beams with 5µm and 15µm diameters. Thin lines joint counts accumulated in 2 second intervals and heavy lines represent moving averages of the counts. A. Normal mica (sample 650). Si counts vary unsystematically in a narrow range for 125 seconds after which they gradually increase with the 5µm beam. B. "Anhydrous" mica (sample 189). Si counts increase by approximately 3.3% between 0 and 30 seconds of the analysis with the 5µm beam and then remain essentially constant. This suggests early dehydration during the analyses.

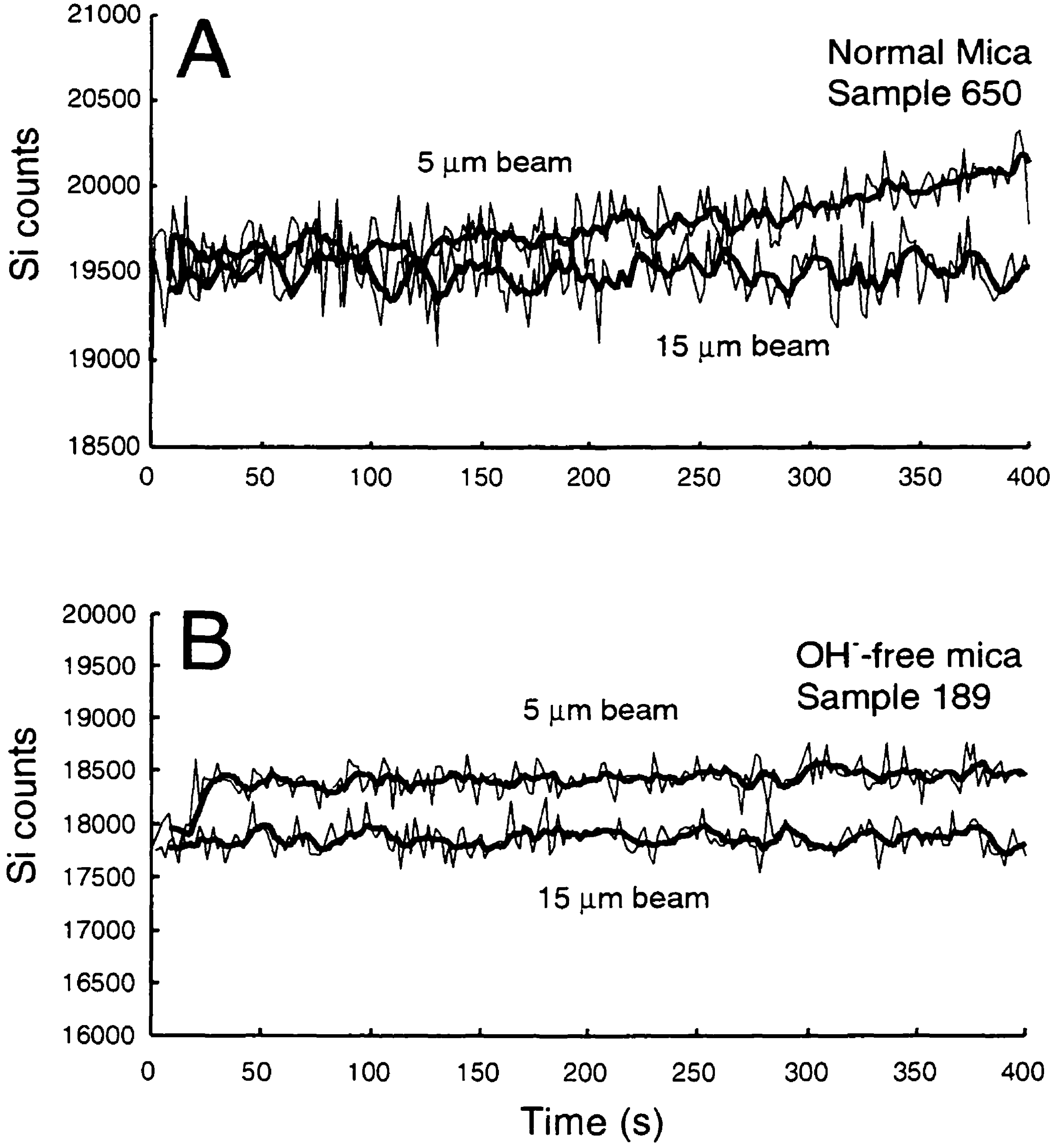
A
Normal Mica
Sample 650
5 µm beam
15 µm beam
Si counts
21000
20500
20000
19500
19000
18500
0
50
100
150
200
250
300
350
400
B
OH⁻-free mica
Sample 189
5 µm beam
15 µm beam
Si counts
20000
19500
19000
18500
18000
17500
17000
16500
16000
0
50
100
150
200
250
300
350
400
Time (s)

Table 3: Analyses of micas in sample 189 using a 15mm beam (colomn 1-4) and normalized average analyses using a 5mm beam

Samples	ms 189/1	ms 189/2	ms 189/3	Average	Avg.189normalized
SiO_2	45.10	45.27	45.55	45.31	46.31
TiO_2	0.17	0.02	0.01	0.07	0.02
Al_2O_3	30.21	29.75	30.00	29.98	29.96
FeO	5.85	6.09	5.28	5.74	5.72
MnO	0.23	0.24	0.21	0.23	0.26
CaO	0.00	0.03	0.01	0.01	
MgO	0.23	0.21	0.17	0.20	0.26
Na_2O	0.18	0.18	0.17	0.18	0.16
K_2O	11.55	11.62	11.69	11.62	10.22
F	2.24	2.05	2.00	2.10	2.77
Cl	0.01	0.02	0.02	0.01	
Total	94.82	94.60	94.26	94.56	94.56

MICA COMPOSITIONS

"Normal Micas"

Figure 4 is a graphical representation of the compositions of normal micas (open symbols) and "dehydrated micas" (solid symbols) on an Al-Si-M^{2+} triangular plot, where M^{2+} comprises Fe^{2+} and minor Mg^{2+} and Mn^{2+}. It is apparent from this figure, that the concentration of Al^{3+} and M^{2+} varied significantly, and from Figure 5 that these variations were accompanied by important changes in the F content.

In the least altered leucogranite (samples 833 to 292 in Figure 2), the composition of white mica is phengitic and is characterized by trends of increasing M^{2+} (Fe^{2+}) with Si^{4+} and F^- and trends of decreasing M^{2+} with Al^{3+} (Fig. 6). An additional feature of the distributions for M^{2+} vs Al^{3+} and Si^{4+} is that they have triangular forms on Figure 6 reflecting increasing divergence of Al^{3+} and Si^{4+} values with increasing M^{2+}. The trends can be explained by the substitution reactions:

$$1.5Si^{4+} + 1.7F^- \Rightarrow M^{2+} + 1.3Al^{3+} + 1.7OH^- \qquad (1)$$

and

$$2.33Al^{3+} + OH^- \Rightarrow M^{2+} + 1.25\ Si^{4+} + F^- \qquad (2)$$

as deduced from changes in the stoichiometric compositions, calculated for 22 oxygens (Table 1), in two samples, each containing mica affected by only one of the two substitution reactions. The triangular distribution is an effect of the combined substitution schemes 1 and 2. Thus, during early alteration the white mica tends to be enriched in M^{2+} at the expense of either Al^{3+} or Si^{4+}. The two reactions produce sympathetic changes in Si^{4+} and F^- and antipathetic changes in the concentration of Al^{3+} relative to these two elements.

With further alteration, albite was completely destroyed and white mica partially destroyed during the formation of quartz-sericite greisen (samples 292 to 181). In these

Figure 4: Compositions of white mica in the leucogranite and greisens from East Kemptville. The compositions are predominantly phengitic. Open symbols indicate normal micas and solid symbols refer to micas which yield high totals in electron microprobe analyses.

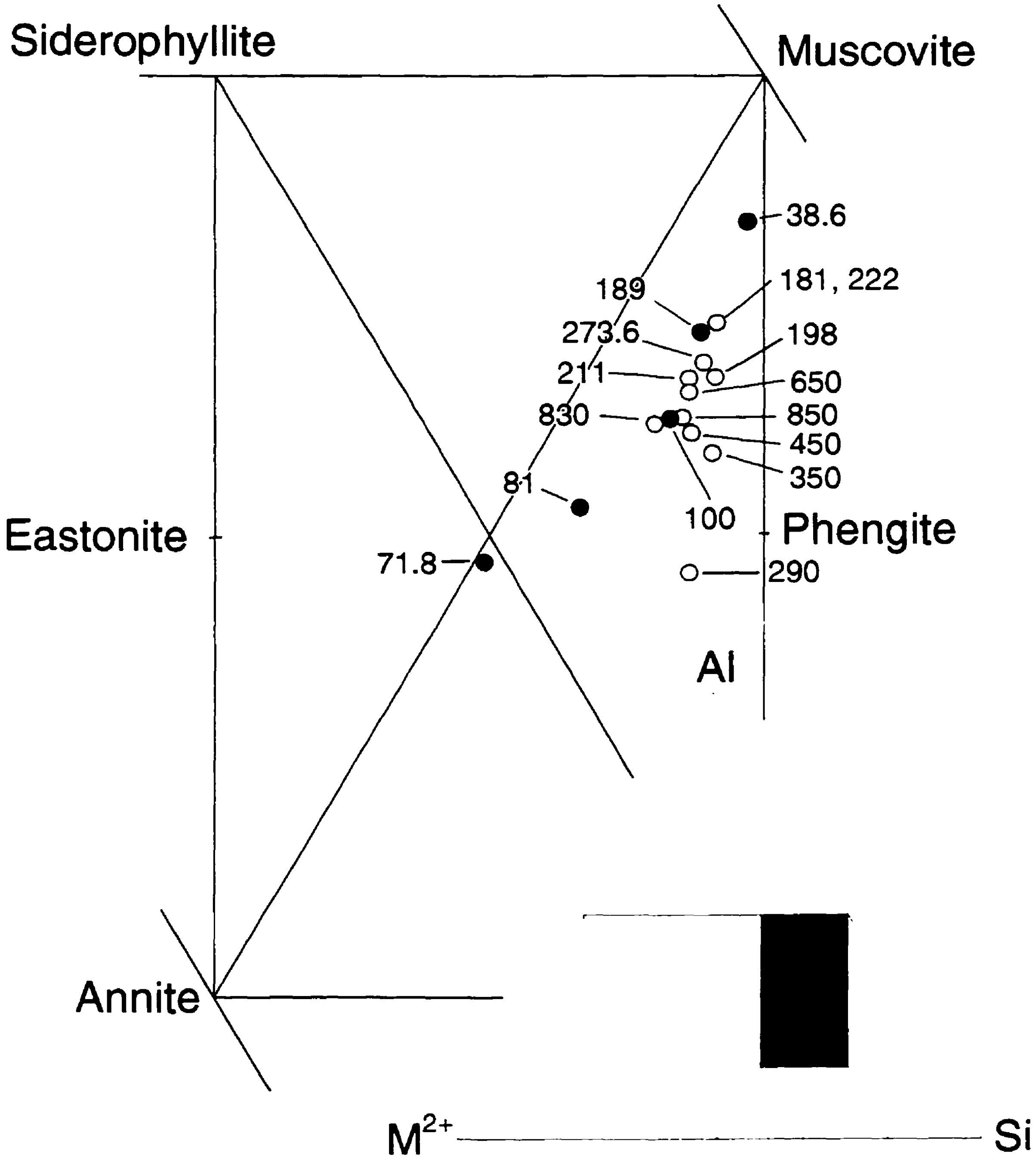
Siderophyllite
Muscovite
38.6
181, 222
189
273.6
198
211
650
830
850
450
350
81
100
Eastonite
Phengite
71.8
290
Al
Annite
M^{2+}
Si

Figure 5: Concentrations of Al_2O_3, FeO and F in micas as a function of alteration. In the leucogranite, increasing alteration is characterized by an increase in the Fe and F content of the micas. With further alteration the Al content then increases until sample 181 and the Fe and F concentrations decrease. Additional alteration is marked by an increase in the Fe and F contents to a maximum in sample 30. In the vein, micas have very low Fe and F contents and closely approximate a largely di-octahedral structure.

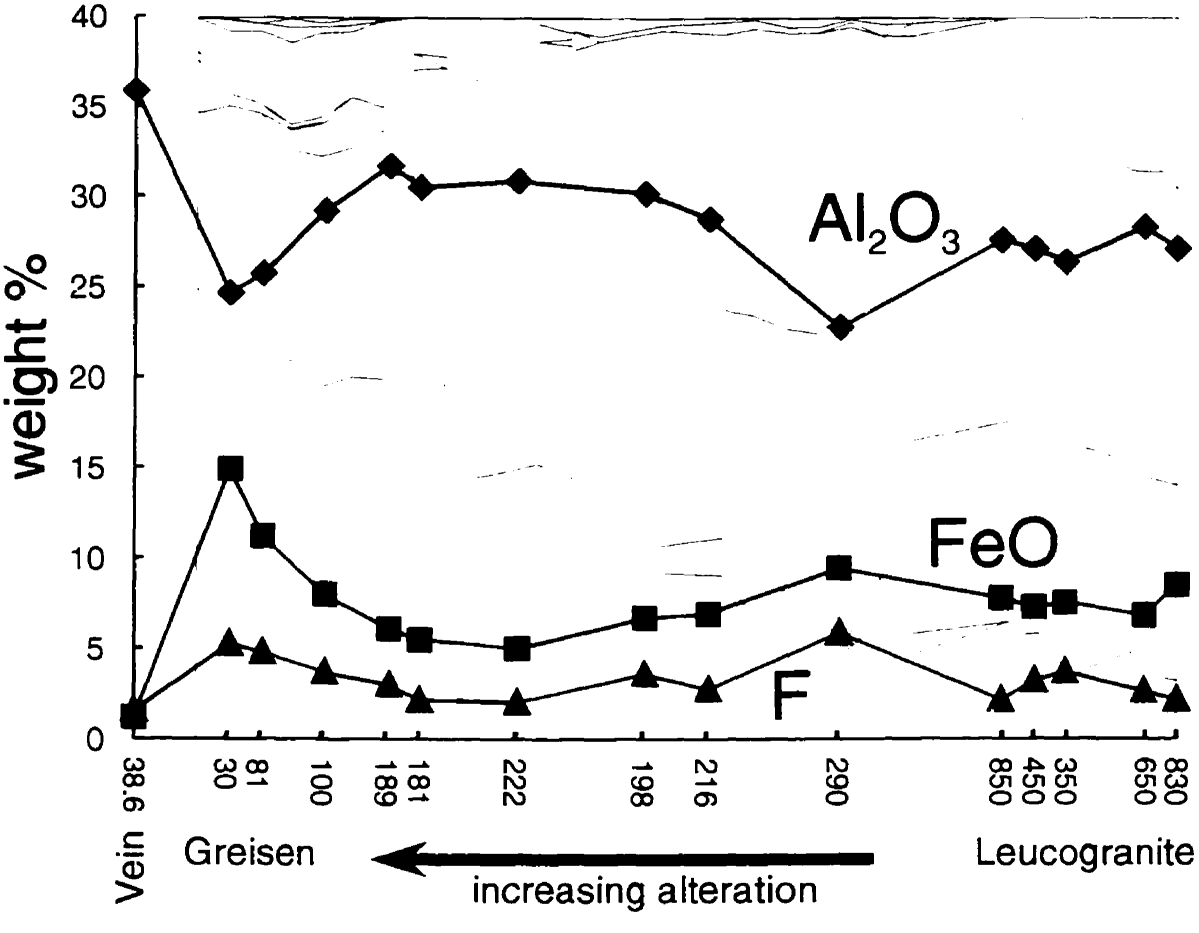

weight %
0
5
10
15
20
25
30
35
40
Al2O3
FeO
F
38.6
30
81
100
189
181
222
198
216
290
850
450
350
650
830
Vein
Greisen
increasing alteration
Leucogranite

Figure 6: Plots of M^{2+} vs Al^{3+}, M^{2+} vs F^- and M^{2+} vs Si^{4+} concentrations in micas from the leucogranite and the quartz-sericite greisen (in atoms per formula units). The lines are regressions through analyses of two samples in the leucogranite and all the normal samples between the leucogranite and sample 181. These lines were used to determine the coefficients of reactions (1) and (2) and (3).

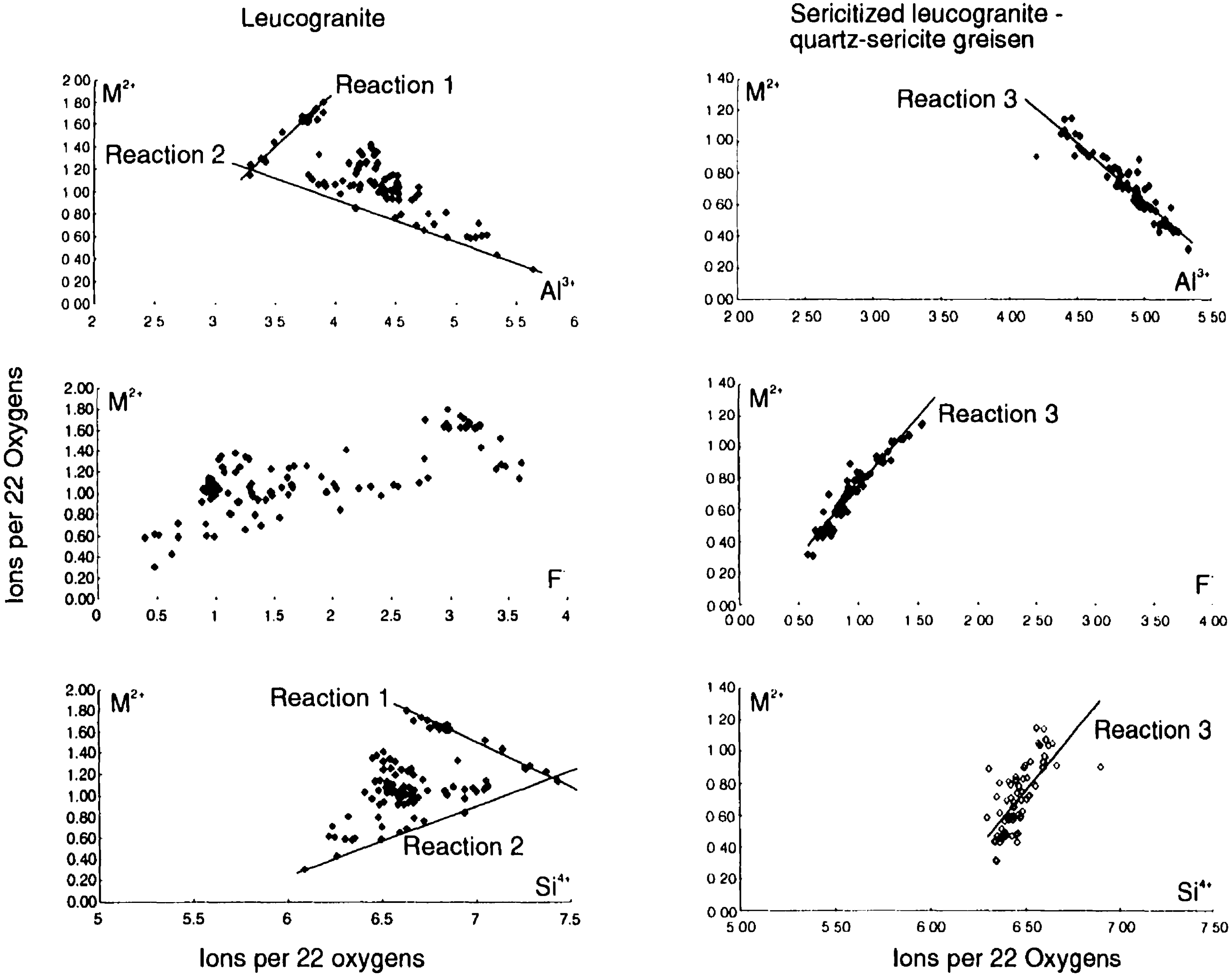
Leucogranite
Sericitized leucogranite - quartz-sericite greisen
Ions per 22 Oxygens
M^{2+}
Reaction 1
Reaction 2
Al^{3+}
2 00
1 80
1 60
1 40
1 20
1 00
0 80
0 60
0 40
0 20
0 00
2
2 5
3
3 5
4
4 5
5
5 5
6
Reaction 3
1 40
1 20
1 00
0 80
0 60
0 40
0 20
0 00
2 00
2 50
3 00
3 50
4 00
4 50
5 00
5 50
F^-
2.00
1.80
1.60
1.40
1.20
1.00
0.80
0.60
0.40
0.20
0.00
0
0.5
1
1.5
2
2.5
3
3.5
4
0 00
0 50
1 00
1 50
2 00
2 50
3 00
3 50
4 00
Si^{4+}
5
5.5
6
6.5
7
7.5
5 00
5 50
6 00
6 50
7 00
7 50
Ions per 22 oxygens
Ions per 22 Oxygens

greisens, the relationships among M^{2+}, Al^{3+}, Si^{4+} and F^- were controlled by the substitution reaction:

$$M^{2+} + 0.6Si^{4+} + 1.2F^- \Leftrightarrow 1.5Al^{3+} + 1.2OH^- \tag{3}$$

i.e., the proportions of M^{2+}, Si^{4+} and F^- decreased with increasing alteration at the expense of Al^{3+} and OH^- (Fig. 6).

"Dehydrated" Micas

The average compositions of "dehydrated" micas in quartz-topaz greisens are represented in Figure 4 by the solid circles and range from that of a nearly stoichiometric muscovite to a composition mid-way between muscovite and annite. In the latter case (sample 71.8), the dehydrated mica is therefore 50% di- and 50% tri-octahedral, a situation never encountered in normal micas. As is apparent from Table 1, the compositional variations are primarily in the proportion of Al, F and doubly charged M^{2+} cations (Fe^{2+}, Mg^{2+} and Mn^{2+}). Between sample 189 and the vein, the concentrations of Fe^{2+} and F^- increase sharply at the expense of Al^{3+} (Fig. 5). In sample 38.6, taken from a topaz-rich vein, Fe^{2+} and F^- drop to very low concentrations, and micas in this sample are highly enriched in Al^{3+}. Correlations among the concentrations of M^{2+}, Al^{3+} and F^- (Figure 7) all have very high regression coefficients (<0.94), which suggest that alteration was accompanied by the simple coupled substitution reaction:

$$2\ Al^{3+} + 3\ OH^- = 3\ M^{2+} + 3\ F^- \tag{4}$$

Vein sample 38.6 was not included to avoid erroneous correlations.

Figure 7: Plots of average M^{2+} vs Al^{3+}, F^- vs Al^{3+} and M^{2+} vs F^- concentrations (Table 1) in "dehydrated" micas from the quartz-topaz greisen (in atoms per two formula units). Correlations (dashed lines) suggest substitution of 2 Al^{3+} and 3 OH^- by 3 M^{2+} and 3 F^-.

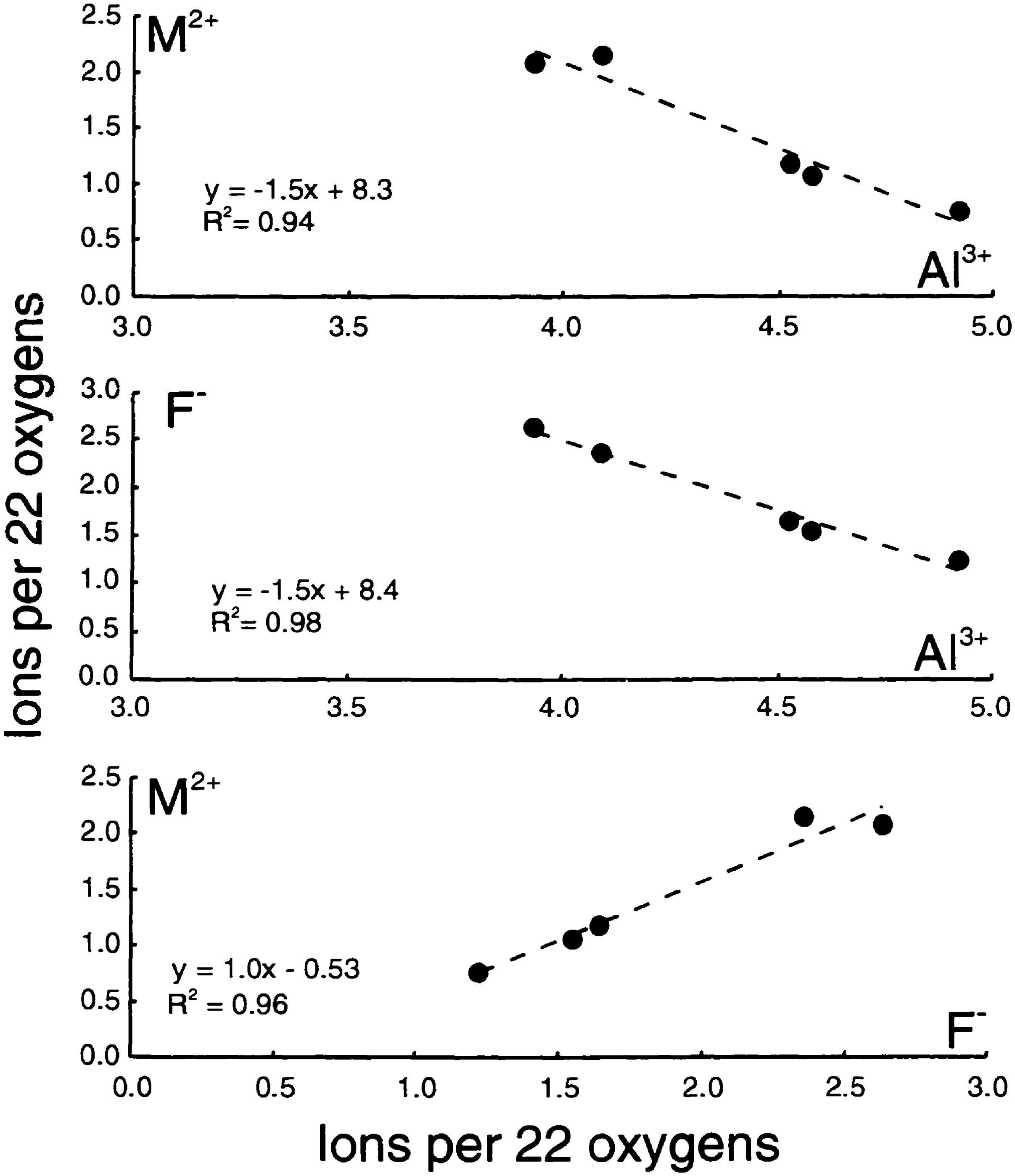
M^{2+}
y = -1.5x + 8.3
R^2= 0.94
Al^{3+}
2.5
2.0
1.5
1.0
0.5
0.0
3.0
3.5
4.0
4.5
5.0
F$^-$
y = -1.5x + 8.4
R^2= 0.98
Al^{3+}
3.0
2.5
2.0
1.5
1.0
0.5
0.0
3.0
3.5
4.0
4.5
5.0
M^{2+}
y = 1.0x - 0.53
R^2 = 0.96
F$^-$
2.5
2.0
1.5
1.0
0.5
0.0
0.0
0.5
1.0
1.5
2.0
2.5
3.0
Ions per 22 oxygens
Ions per 22 oxygens

CAUSES OF DEHYDRATION

The Role of Fluorine

The proportion of OH^- in micas that can be substituted by F^- is strongly dependent on the concentration of divalent cations, and in particular Fe^{2+} (Robert et al., 1993). In M^{2+}-rich (tri-octahedral) micas, the OH^- pair is oriented perpendicular to the sheet structure and complete substitution of OH^- by F^- is possible because this does not require any structural readjustment (Robert et al. 1993). By contrast, in di-octahedral micas, the H^- ion of the OH^- pair is oriented towards the vacant site in order to partially compensate for the deficiency of positive charges (Fig 8), and the H^- is attracted by the highly underbonded apical O^{2-} ion (Giese, 1984). This partial filling of the empty site cannot occur if F^- replaces OH^-, which greatly restricts the substitution of OH^- by F^- in di-octahedral micas. The maximum F/OH ratio is approximately 0.25 in these micas (Munoz 1984). An unusual feature of the micas in quartz-muscovite greisen at East Kemptville is that their F content remains very high due to the increase in the proportion of Al^{3+} at the expense of Fe^{2+} towards the vein (samples 290 to 181). In sample 181, this lead to the formation of purely di-octahedral mica, with a F content close to the highest predicted for these micas (F/OH is close to 0.25).

In addition to partially filling the empty octahedral site, the oxygen of the OH^- group and other apical oxygens are attracted along the edges of the octahedra diagonal to the octahedral layer, in order to partially shield the high repulsion between Al^{3+} cations in adjacent octahedral sites (Bailey 1984). In Figure 8, we schematically represent the repulsion of adjacent Al^{3+} cations by opposing arrows and the attraction of two O^{2-} or two OH^- groups on the edge of the octahedra by facing arrows. This attraction along edges diagonal to the octahedral layers leads to a shortening of these edges from a length of 2.7 to 2.9Å for unshared edges to a length of 2.3 to 2.5Å between Al^{3+} cations, and thus a decrease in the thickness of the octahedral layer (Bailey, 1984). Owing to the smaller size of F^- anions compared to the O^{2-} anion, the high F content mentioned above might decrease the c dimension of the unit cell as has been reported by Monier (1987) and further reduce the thickness of this layer.

Dehydration Mechanism

We showed above that water was initially present in the mica, but was released rapidly during electron microprobe analysis. In normal micas, OH^- groups are bound to the structure and therefore not easily released during analysis (sample 650 in Figure 3). However, the rapid dehydration of micas from the quartz-topaz greisen suggests that, in these micas, water was not bound to the structure as OH^- but was present as H_2O molecules. It is proposed that this H_2O formed in the structure as a result of the conversion of two OH^- groups into one O^{2-} ion and a H_2O molecule

$$2\ OH^- = H_2O + O^{2-} \qquad (5)$$

(Fig. 8) and that this reaction was promoted by the high F content which helped decrease the thickness of the octahedral layer. In the view of the fact that the distance between two OH^- groups (2.3 to 2.5Å) is approximately twice the radius of the OH^- anion in di-octahedral micas, it follows that thinning of the octahedral layer can only occur through the conversion of two OH^- groups into one O^{2-} and one H_2O molecule. As a result, one edge of the octahedral site was lost, and was replaced by a single oxygen anion, thereby converting octahedra into trigonal di-pyramids. The H_2O molecule produced by the fusion of the two OH^- groups remained trapped in the vacant site and the related O^{2-} anion acted as a very efficient shield between adjacent Al^{3+} cations.

The hypothesis of the conversion of two OH^- groups into one O^{2-} and an H_2O molecule has been suggested previously based on results of high temperature experiments (Eberhart, 1963; Zimmermann 1970) in which a weight loss, corresponding to the water content of mica, occurred during heating. Owing to the large size of the H_2O molecule, water can only escape the mica after its structure is damaged Nicol (1964). We suggest that H_2O formed in our "anhydrous" micas by the above reaction, and was trapped in the

Figure 8: Schematic representation of an octahedral layer of a di-octahedral mica. Diverging arrows represent repulsion between adjacent Al^{3+} ions, facing arrows the attraction between O^{2-} or OH^- groups which shield the Al-repulsion. Dashed lines represent additional bonding of H^+ with underbonded apical oxygens. Also portrayed is the conversion of two OH^- groups into one O^{2-} ion, bound to the structure and an H_2O, trapped in the vacant site.

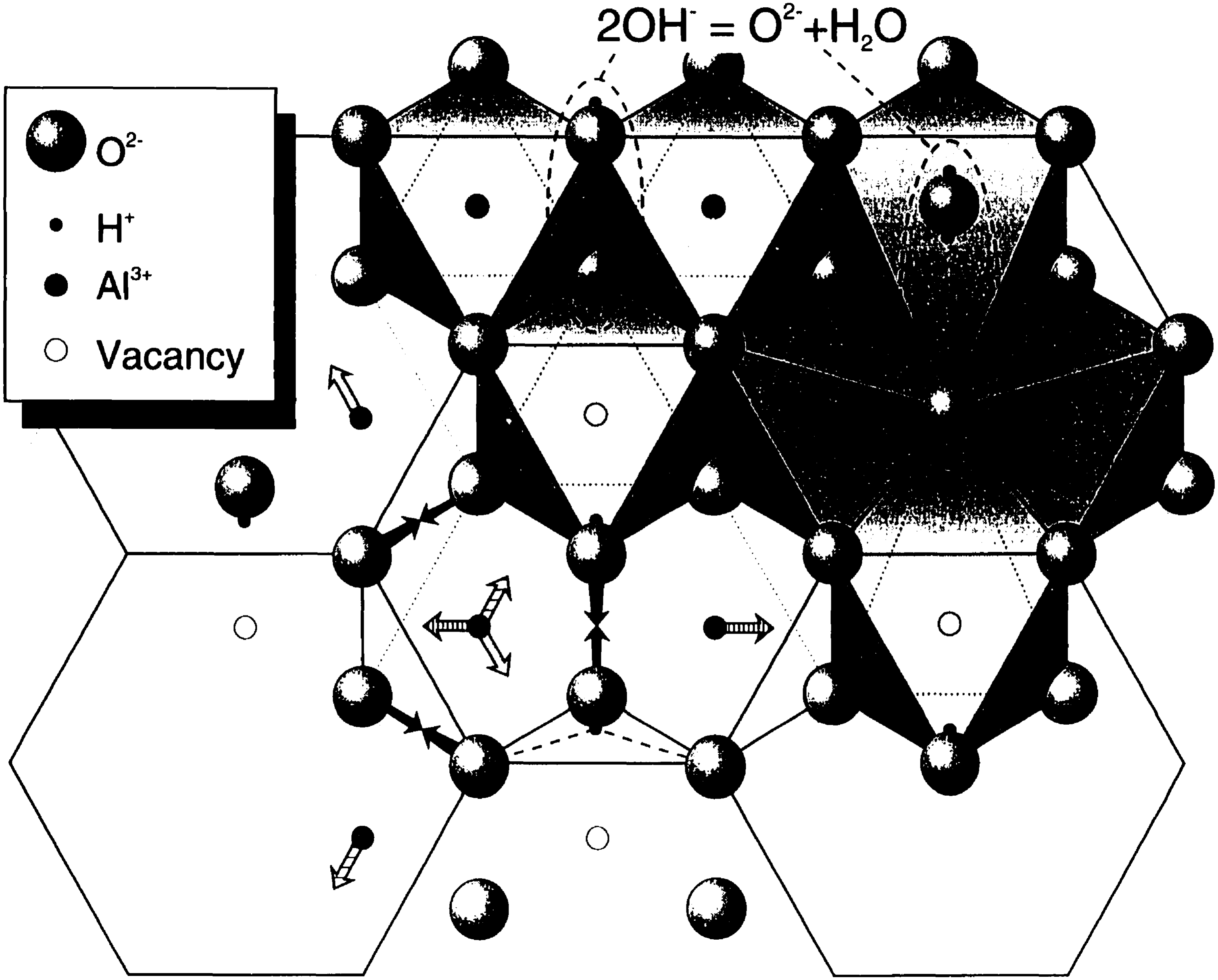
$2OH^- = O^{2-} + H_2O$
O^{2-}
H^+
Al^{3+}
Vacancy

vacant site until the damage to the structure by a focused (5μm) microprobe beam allowed the H_2O to escape; the larger beam (15μm) did not damage the structure of the muscovite sufficiently to permit the H_2O to escape. Dehydration does not occur in standard micas (sample 650 in Figure 3) because OH^- is bound to the structure of these micas and no H_2O is present.

CONSEQUENCES OF DEHYDRATION

Earlier, we discussed the compositional variations in dehydrated mica (Fig. 7) and suggested that substitutions in this mica were governed by the reaction:

$$2\ Al^{3+} + 3\ OH^- = 3\ M^{2+} + 3\ F^- \tag{4}$$

From the preceding section it is now apparent that these substitutions were more likely controlled by the reaction:

$$2\ Al^{3+} + 1.5\ O^{2-} = 3\ M^{2+} + 3\ F^- \tag{6}$$

where the proportion of oxygen involved in the reaction is determined by charge balance constraints. The substitution of a di-octahedral by a tri-octahedral arrangement (of 2 Al^{3+} by 3 M^{2+}) is thus accompanied by the replacement of 1.5 O^{2-} ions by 3 F^- ions. Compositions therefore lie between the two endmembers $KAl_{1.9}Si_{3.25}Al_{0.75}O_{10}(O)_1$ and $KFe_{2.9}Si_{3.25}Al_{0.75}O_{10}(F)_2$ and the solid solution between di- and tri-octahedral micas increases, allowing the formation of a phase with a composition exactly mid-way between the end-members.

In quartz-topaz greisen, increasing alteration was accompanied by an increase in the activity of fluorine and/or iron in the mineralizing fluid (Chapter 5) and therefore favour the right hand side of reaction (5). This substitution rebuilt octahedral sites since each O^{2-} ions was replaced by two F^- ions, thus converting trigonal di-pyramids back into octahedra. The substitution of one O^{2-} by two F^- ions was accompanied by the replacement of 2 Al by 3 Fe, presumably because O^{2-} was no longer available to shield the adjacent Al^{3+} cations. The formation of two OH^- groups from one O^{2-} ion and one H_2O molecule does not occur with high Fe concentration, possibly because of the stability of the H_2O molecule.

The substitution of two OH^- groups by O^{2-} and H_2O increases the possibility of compositional variations in these micas. As a result, the range in their stability is increased. This is apparent in the alteration halo described in Figure 2: the concentration of normal mica decreases regularly between samples 198 and 181 as it is replaced by topaz. It is likely that micas would disappear in rocks more altered than sample 181 if only normal micas were present. However, the increase in the stability of the mica due to the dehydration prevents further replacement by topaz and the proportion of anhydrous micas only decreases slightly with increasing alteration.

CONCLUSIONS

This study has documented the presence of di-octahedral micas at East Kemptville which yield totals in electron microprobe analyses equivalent to that of an anhydrous mica. This can probably be explained by the conversion in these micas of two OH^- groups into one O^{2-} ion and an H_2O molecule in the presence of a high concentration of fluorine. As a result, octahedral sites were turned into trigonal di-pyramids through the loss of an edge of the octahedra. The H_2O molecule created during this reaction remained trapped in the vacant octrahedral site until damage to the mica structure during microprobe analyses allowed it to escape, thereby resulting in high totals for the analyses. These OH^--free micas have a wider field of stability than normal micas and their compositions range from that of muscovite to a composition mid-way between muscovite and annite, i.e., a composition never encountered in normal muscovite.

REFERENCES

Bailey, S.W., 1984: Crystal chemistry of true micas, *in* S.W. Bailey, ed., Micas: Reviews in Mineralogy, Mineralogical Society of America, v. 13, p. 13-60.

Charoy, B., Chaussidon, M., and Noronha, F., 1995, Lithium zonation in white micas from the Argemela microgranite (central Portugal): an *in-situ* ion-electron-microprobe and spectroscopic investigation: European Journal of Mineralogy, v. 7, p. 335-352.

Eberhart, J.P., 1963, Etude des transformations du mica muscovite par chauffage entre 700 et 1200°C: Bulletin Société Française de Minéralogie et Cristallographie, v. 87, p. 213-251.

Giese, R.F. Jr., 1984, Electrostatic energy models for micas: *in* S.W. Bailey, ed., Micas: Reviews in Mineralogy, Mineralogical Society of America, v. 13, p. 105-144.

Kontak, D.J., 1990, The East Kemptville topaz-muscovite leucogranite, Nova Scotia. I. Geological setting and whole-rock geochemistry: Canadian Mineralogist, v. 28, p. 787-825.

Kontak, D.J., 1991, The East Kemptville topaz-muscovite leucogranite, Nova Scotia. II. Mineral chemistry: Canadian Mineralogist, v. 29, p. 37-60.

Monier, G. 1987, Cristallochimie des micas des leucogranites. Nouvelles données expérimentales et applications pétrologiques. Thèse d'Etat, Université d'Orléans. Géol. Géochim. Uranium, Mém. Nancy, 14, 347p.

Munoz, J.L., 1984, F-OH and Cl-OH exchange in micas with applications to the hydrothermal ore deposits, *in* S.W. Bailey, ed., Micas: Reviews in Mineralogy, Mineralogical Society of America, v. 13, p. 469-494.

Nicol, A.W., 1964, Topotactic transformation of muscovite under mild hydrothermal conditions: Clays and Clay Minerals, Proceedings of the 12th National Conference, Atlanta, Ga., p. 11-19.

Richardson, J.M., 1988, Field and textural relationships of alteration and greisen-hosted mineralization at the East Kemptville tin deposit, Davis Lake Complex, southwest

Nova Scotia, *in* Recent advances in the geology of granite-related mineral deposits: Canadian Institute of Mining and Metallurgy Special Volume 39, p. 265-279.

Richardson, J.M., Spooner, E.T.C., and McAuslan, D.A., 1982, The East Kemptville tin deposit, Nova Scotia: An example of a large tonnage, low grade, greisen-hosted deposit in the endocontact zone of a granite batholith: Geological Survey of Canada Current research, part B, paper 82-1B, p. 27-32.

Robert, J.-L., Beny, J.-M., Della Ventura, G., and Hardy, M., 1993, Fluorine in micas: crystal-chemical control of the OH-F distribution between trioctahedral and dioctahedral sites: European Journal of Mineralogy, v. 5, p. 7-18.

Zimmermann, J.-L., 1970, Contribution à l'étude de la déshydratation et de la libération de l'argon des micas: Geochimica et Cosmochimica Acta, v. 34, p. 1327-1350.

CHAPTER VII

CONCLUSIONS

CONCLUSIONS

The East Kemptville tin deposit formed in the apical part of the Davis Lake Pluton, at the Southwestern end of the 370 Ma peraluminous South Mountain Batholith. Two zones are distinguished in the deposit, the Main and the Baby Zone. During magmatic evolution, tin was present as Sn^{2+} in the melt and behaved as an incompatible element, i.e., it was enriched in the residual melt and did not enter the crystal structure of mafic phases. At a late stage of evolution of the magma, but before complete crystallization, large scale tectonic fracturing induced a drop in pressure and cause a fluid phase to separate (Fig. 1). This fluid was originally in equilibrium with the magmatic phases (quartz, albite, muscovite, K-feldspar), but preferential partitioning of HCl^0, HF^0 and H_2S^0 into this fluid decreased its pH and caused pervasive sericitization of the leucogranite.

Ore elements were enriched in the magmatic fluid by partitioning from the residual magma. Along with Sn, F, S and Fe, other elements partitioned into the fluid include Zn, P and Mo as indicated by the lower concentration of these elements in the leucogranite of the Baby Zone and their higher abundance in the greisen of that zone. The exsolved fluid was focused along the fault planes created during the tectonic event and caused greisenization in the apical part of the intrusion (Fig. 1).

The temperature of greisenization was estimated to be ~480°C as determined by a newly calibrated geothermometer based on the F-OH exchange reaction between muscovite and topaz, and a second geothermometer based on oxygen isotopic fractionation between cassiterite and quartz. The pressure was estimated to be 4.1 kbars using fluid inclusion homogenization temperatures and an isochoric extrapolation.

Two types of greisen are distinguished at East Kemptville, zoned and massive. Zoned greisens are characterized by symmetrical alteration halos around central veins. Massive greisens formed from the overlap of individual alteration halos in highly fractured zones. Analyses of mineralogical changes in a zoned greisen indicated that the leucogranite was first converted into a quartz-sericite greisen through the replacement of feldspars by muscovite. With further alteration, muscovite was, in turn, replaced by topaz in quartz-topaz greisen. Cassiterite and sulphide mineralization is associated with the latter alteration. In the better mineralized Baby Zone, quartz-topaz greisen is replaced by quartz greisen next to veins. These greisens are characterized by a high abundance of quartz and a lower abundance of topaz, sulphides and cassiterite.

In the zoned greisen, changes in normative composition with increasing alteration were used to determine alteration reactions that converted each alteration zone into one more altered. Relative changes in the concentration of aqueous species in the mineralizing fluid were calculated by balancing of these reactions for constant mass and charge. This indicated that cassiterite precipitation occurred in response to a pH increase which accompanied the replacement of muscovite by topaz. Other parameters potentially responsible for cassiterite precipitation, i.e. fO_2, and a_{Cl^-}, promoted its dissolution and could not account for the mineralization.

A study of samples from a 850m deep drill hole which cut through all the alteration zones present in the deposit indicated that the alteration sequence evident in greisens around individual veins also developed at the scale of the deposit. Analyses of fluid inclusions from all the alteration zones and variations in normative mineralogical compositions indicated that during interaction with the host rock, the fluid was first enriched in Fe and probably Sn due to the dissolution of pyrrhotite and cassiterite in quartz greisen. The concentration of these components subsequently decreased towards less altered rocks. The fO_2 of the fluid, estimated from the CO_2/CH_4 ratio in fluid inclusions, varied between the Ni-NiO and the FMQ buffer and dissolution of pyrrhotite was likely responsible for a decrease in fO_2 in quartz-topaz greisen. The NaCl content of the fluid was approximately 27wt-% in the vein and increases continuously to 40wt-% in less altered rocks. As this increase began in greisens devoid of Na-bearing phases, it follows that some Na had to be transported towards the vein from the zone where albite was dissolved. Based on these observations and the conclusions of others that infiltration of fluid from the fracture to the rock is limited (most flow is parallel to the vein), a model was formulated for the formation of alteration halos around veins in which individual aliquots of fluid could infiltrate the rock as they were compensated by the release of equivalent aliquots from the rock to back the fracture (Fig. 1). This created a distribution of elements similar to that of diffusion, i.e., controlled by chemical potential gradients, but presumably much more rapidly.

Computer modeling of the alteration accurately reproduced the zonal distribution of mineral assemblages and most changes in fluid chemistry observed in the samples from East Kemptville. Modeling further permitted quantification of the changes in compositional parameters that could not be measured directly, e.g., pH, and concentrations of K^+ and Cl^-, and confirmed that the pH change was the main control on cassiterite precipitation. It also simulated the dissolution of cassiterite and pyrrhotite, close to the vein, which was observed in natural samples. This simulation revealed that the conditions at which these phases precipitated were significantly modified by an increase in the Fe and Sn concentrations of the fluid. The increase in the Sn concentration raised its chemical potential away from the vein and this acted as barrier across which Sn could not be transported and could have been responsible for the low ore grades of the East Kemptville deposit (Fig. 1).

As the amount of fluid in the model remains unchanged across the alteration halo, it is suggested that the water/rock ratio was constant away from the vein in the natural samples, i.e., that changes in oxygen isotopic composition of the rock were not related to a change in the water/rock ratio. This information was not available at the time Chapter 2 was accepted for publication and the water/rock ratio in this chapter was therefore calculated to decrease with distance from the vein using oxygen isotopic data.

In quartz-topaz greisen of the deep drill hole, muscovite typically yields high totals during microprobe analyses. It is suggested that muscovite in this greisen was dehydrated during microprobe analyses because OH^- groups merged into a structurally bound O^{2-} and an H_2O molecule trapped in the vacant site, in the presence of high F concentrations.

Figure 1: Model for the evolution of the hydrothermal system at East Kemptville. Prior to complete crystallization of the magma, fracturing caused a drop in pressure and allowed a fluid phase to separate (1). This fluid caused pervasive sericitization, transported the metals and was focused along fracture planes (2) where topaz, cassiterite and sulphides were deposited and the host rocks were altered to greisen (3). Additional cassiterite and sulphides were precipitated in the greisen. The bloc diagram is a schematic representation of the formation of an alteration halo around a central fracture. With time the alteration halo widens and alteration zones move outwards. The overall fluid flow is parallel to the vein, but individual aliquots of fluid can move into the rock and return to the vein through a compensated infiltration process. This permits transport of components from the vein into the rock or vice versa depending on the chemical potential gradient. Also shown are the changes in pH and a_{Sn} in the fluid with increasing alteration. At the onset of alteration, changes in pH and a_{Sn} occur rapidly and close to the vein (open symbols). With time, the halo wides and changes in pH and a_{Sn} are more gradual (solid symbols). This results in the dissolution of some phases, e.g., cassiterite, and causes the formation of "geochemical cumulations", i.e., a zone in the alteration halo where the activity of a component in the fluid is higher than in the adjacent segments. This allows these particular components to be transported in two directions through compensated infiltration, i.e., away from, and also towards the fracture (vein).

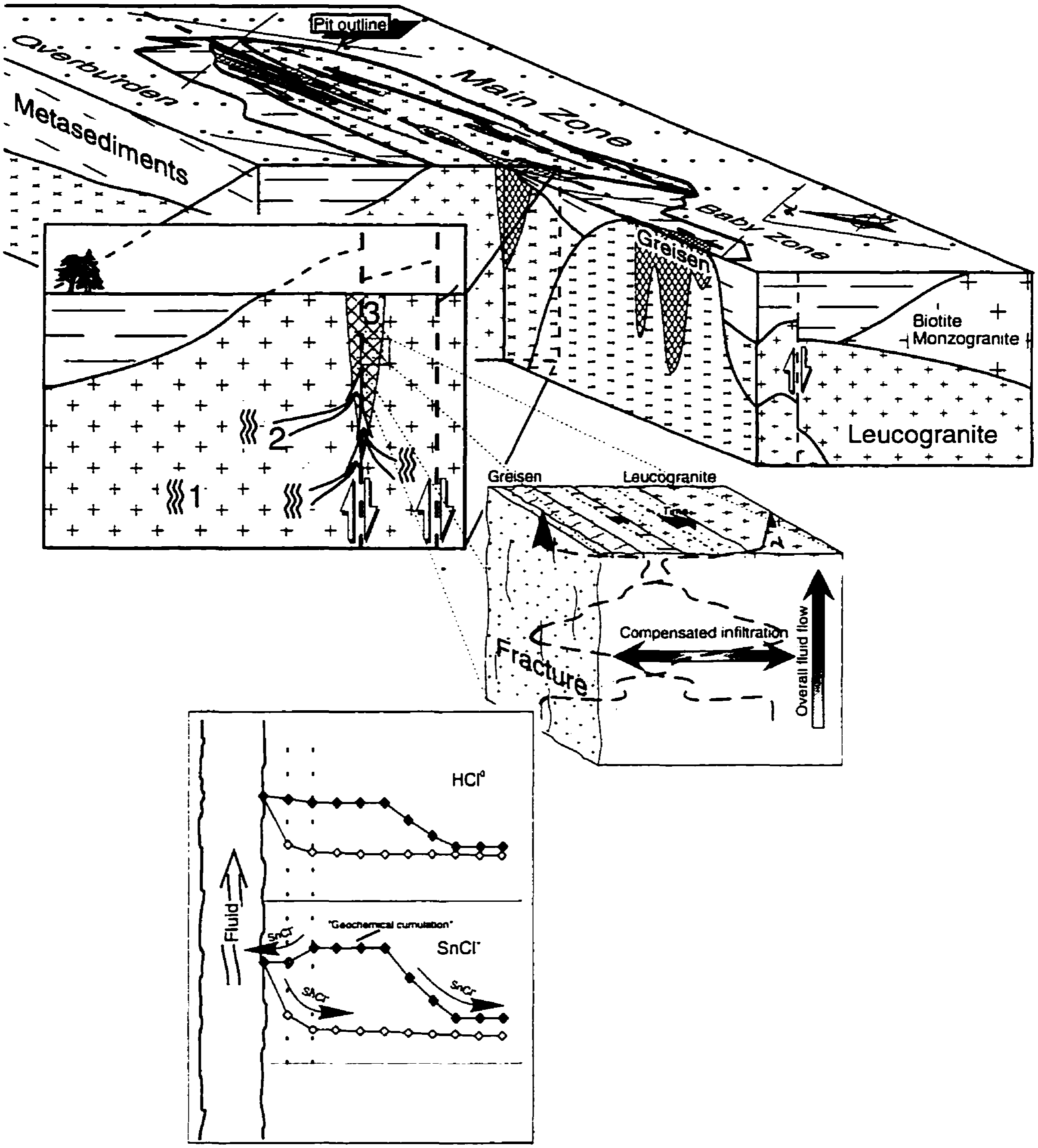
Pit outline
Overburden
Metasediments
Main Zone
Baby Zone
Greisen
Biotite Monzogranite
Leucogranite
1
2
3
Greisen
Leucogranite
Time
Compensated infiltration
Fracture
Overall fluid flow
HCl°
"Geochemical cumulation"
SnCl⁻
SnCl⁻
SnCl⁻
SnCl⁻
Fluid

CONTRIBUTIONS TO KNOWLEDGE

The following are the most significant contributions to knowledge from this thesis:

1. This study is one of the few in which the origin of the mineralizing fluid and the ore metals in greisenizing systems could be determined with any confidence.

2. The thesis is unique in its quantitative description of the systematic changes in fluid and rock composition during the formation of a greisen-hosted tin deposit.

3. A new hypothesis has been developed which satisfactorily explains the mechanism and the direction of mass transfer during the formation of alteration halos around veins. The hypothesis involves a compensated infiltration process in which small aliquots of fluid are transported back and forth between the fracture and the rock. This offers an attractive solution to the problem of explaining how components are transported towards the fracture and avoids having to invoke the unreasonably slow alternative mechanism of diffusion down a chemical potential gradient.

4. The computer based reaction path calculations presented in this thesis represent only the second attempt to model the formation of greisen-style tin mineralization, and the first to be based on an actual deposit. The model allowed accurate simulation of the alteration sequence in the samples and thus provided the first quantitative evaluation of the variation in physicochemical factors potentially responsible for cassiterite mineralization. The multiple pass fluid flow model, used in the calculations, also yielded a unique reconstruction of the evolution of an alteration halo through time. This, in turn, provided an explanation for why ore grades are low in some vein type deposits.

5. Systematic changes in the oxygen isotopic composition of altered rocks away from hydrothermal veins have long been interpreted to reflect corresponding decreases in

water/rock ratios. The data presented in this thesis invalidate this interpretation by showing that water/rock ratios are constant across alteration halos. Differences in oxygen isotopic composition between fresh and altered rocks are attributed, instead, to “isotopic” potential gradients produced by compensated infiltration.

6. A new geothermometer was calibrated using the F-OH exchange between muscovite and topaz. This geothermometer enables accurate estimation of the temperature at which greisens and other topaz-muscovite-bearing rocks form.

7. The thesis contains the first report of natural "anhydrous" muscovite. It also provides an explanation for the dehydration, based on the merging of two OH^- groups into one O^{2-} ion and an H_2O molecule, i.e., the conversion of some octahedral sites into trigonal di-pyramids, a process which had not yet been demonstrated to occur naturally.

RECOMMENDATIONS FOR FUTURE WORK

Newly available techniques for the analyses of individual fluid inclusions, e.g., laser ablation ICP-MS, synchrotron X-ray diffraction or PIXE (Proton Induced X-ray Emission) analyses, could provide further insights into changes in fluid compositions and thus help to better constrain the processes responsible for greisenization and the formation of other vein-type deposits. X-ray diffraction or High Resolution Transmission Electron Microscopy on "dehydrated" muscovite would place additional constraints on the structure of this muscovite as well as on the causes for its dehydration. The demonstration of the conversion of octahedral sites into trigonal di-pyramids would be a first report of such a phenomenon in natural samples. The newly calibrated geothermometer could be applied with more confidence if sample suites from other deposits were available to permit additional testing. A topic not addressed in this thesis is the formation of post-greisen veins, i.e., suphide and phosphate bearing veins, which are commonly associated with greisen style tin mineralization. Preliminary fluid inclusion work suggests that the fluid chemistry is similar to that of the greisenizing fluid. In phosphate-bearing veins, evidence of mixing between an NaCl-brine and a low salinity fluid suggests that these veins could form through the interaction of a meteoric fluid with the fluid responsible for greisenization, after the latter equilibrated with the host leucogranite.

APPENDIX 1

ELECTRON MICROPROBE ANALYSES OF MINERALS IN SAMPLE ZG106N FROM A ZONED GREISEN

(C.F. CHAPTER II)

Appendix 1: Electron microprobe analyses of minerals in the zoned greisen ZG106N (in wt-%).

Albite	SiO_2	TiO_2	Al_2O_3	FeO	MnO	MgO	CaO	Na_2O	K_2O	F	Total
slab 6	68.31	0.00	20.21	0.04	0.00	0.00	0.05	11.48	0.07	0.07	100.23
slab 6	68.58	0.00	20.38	0.00	0.00	0.00	0.01	11.58	0.06	0.00	100.60
slab 6	68.30	0.00	20.06	0.01	0.00	0.01	0.02	11.69	0.08	0.04	100.20
slab 6	68.64	0.00	19.74	0.00	0.01	0.00	0.02	11.71	0.08	0.00	100.20
slab 8	69.09	0.00	20.02	0.00	0.01	0.01	0.01	11.52	0.10	0.05	100.81
slab 8	69.14	0.01	20.12	0.00	0.00	0.01	0.02	11.65	0.05	0.03	101.01
slab 8	69.08	0.01	20.40	0.00	0.00	0.00	0.02	11.47	0.07	0.05	101.10
slab 8	68.66	0.00	19.76	0.04	0.01	0.00	0.01	11.61	0.07	0.00	100.15
slab 8	67.57	0.00	20.31	0.02	0.00	0.01	0.02	11.69	0.08	0.02	99.71
slab 8	68.52	0.00	20.44	0.02	0.00	0.00	0.03	11.48	0.08	0.00	100.58
slab 8	68.39	0.00	20.18	0.03	0.00	0.00	0.03	11.51	0.07	0.02	100.23
slab 8	68.14	0.00	20.16	0.01	0.02	0.00	0.06	11.42	0.08	0.00	99.90
slab 8	68.13	0.00	20.44	0.01	0.00	0.00	0.09	11.63	0.06	0.00	100.37
slab 8	67.87	0.00	20.13	0.01	0.01	0.00	0.02	11.63	0.07	0.06	99.80
slab 8	67.78	0.01	19.80	0.03	0.02	0.00	0.17	11.50	0.09	0.00	99.41
slab 8	68.29	0.02	19.76	0.01	0.02	0.00	0.00	11.62	0.08	0.00	99.80

Muscovite	SiO_2	TiO_2	Al_2O_3	FeO	MnO	MgO	CaO	Na_2O	K_2O	F	Total
slab 0	45.91	0.27	28.93	5.38	0.26	0.49	0.00	0.15	11.36	2.73	95.48
slab 0	46.43	0.32	29.02	5.13	0.22	0.52	0.00	0.17	11.35	2.57	95.73
slab 0	47.98	0.31	29.87	5.09	0.20	0.51	0.02	0.18	11.53	2.89	98.56
slab 0	47.85	0.27	29.59	5.47	0.23	0.54	0.02	0.15	11.46	2.91	98.48
slab 2	48.31	0.08	30.03	4.84	0.24	0.47	0.00	0.13	11.53	2.38	98.02
slab 3	46.90	0.08	30.39	5.00	0.14	0.43	0.00	0.11	11.38	2.69	97.11
slab 3	48.21	0.01	29.17	5.35	0.23	0.48	0.02	0.13	10.97	2.65	97.20
slab 3	47.46	0.26	30.38	5.05	0.20	0.38	0.00	0.16	11.51	2.65	98.05
slab 5	47.71	0.07	31.53	4.75	0.21	0.26	0.05	0.19	11.45	2.29	98.50
slab 5	46.75	0.17	29.76	6.84	0.25	0.11	0.00	0.17	11.57	3.14	98.75
slab 5	46.38	0.09	29.75	6.87	0.21	0.08	0.00	0.27	11.19	2.63	97.47
slab 5	45.68	0.02	31.02	6.34	0.17	0.09	0.00	0.16	11.36	2.49	97.34
slab 5	46.29	0.19	30.16	6.47	0.21	0.12	0.00	0.14	11.32	2.88	97.78
slab 6	46.70	0.08	30.26	6.00	0.28	0.23	0.00	0.13	11.58	2.69	97.94
slab 6	48.36	0.00	30.36	4.55	0.17	0.62	0.00	0.12	11.65	2.31	98.13
slab 6	46.64	0.08	29.66	6.66	0.26	0.10	0.00	0.14	11.57	2.57	97.68
slab 6	47.34	0.21	29.70	5.89	0.23	0.18	0.00	0.12	11.32	2.41	97.39
slab 8	48.39	0.03	30.40	4.86	0.21	0.58	0.00	0.17	11.56	2.70	98.88
slab 8	47.40	0.00	30.37	4.79	0.26	0.57	0.00	0.16	11.60	2.78	97.94
slab 8	47.34	0.00	30.95	4.66	0.22	0.47	0.00	0.16	11.64	2.71	98.15

Appendix I (cont.): Electron microprobe analyses of minerals in sample ZG106N (in wt-%)

Topaz	SiO_2	Al_2O_3	FeO	CaO	F	Total
slab 0	32.04	55.10	0.01	0.00	15.68	96.23
slab 0	32.24	54.84	0.00	0.00	16.64	96.72
slab 0	31.85	54.80	0.03	0.02	16.09	96.01
slab 0	32.12	54.86	0.00	0.00	16.38	96.47
slab 2	32.22	54.59	0.00	0.00	14.86	95.40
slab 2	32.13	54.50	0.02	0.00	14.76	95.19
slab 2	32.22	54.60	0.00	0.01	14.67	95.32
slab 2	32.31	54.23	0.01	0.01	15.03	95.26
slab 2	32.11	54.31	0.03	0.01	14.92	95.10
slab 2	32.21	53.99	0.02	0.00	14.98	94.90
slab 3	31.99	54.83	0.00	0.01	17.16	96.77
slab 3	32.01	54.47	0.01	0.01	17.47	96.61
slab 3	32.13	54.72	0.00	0.00	17.30	96.87
slab 3	31.59	54.60	0.03	0.00	17.32	96.25
slab 3	32.06	54.85	0.00	0.02	16.86	96.69
slab 3	32.01	55.16	0.00	0.00	16.99	97.01

Cassiterite	FeO	TiO_2	SnO_2	Total
slab 0	0.33	0.45	97.98	98.76
slab 0	0.04	0.05	99.26	99.35
slab 0	0.02	0.02	100.26	100.30
slab 0	0.20	0.38	98.93	99.51
slab 0	0.11	0.61	99.89	100.61
slab 0	0.14	0.48	99.29	99.92
slab 0	0.00	0.01	99.78	99.79
slab 0	0.05	0.15	100.45	100.65
slab 0	0.14	0.33	100.02	100.49
slab 0	0.01	0.05	99.52	99.58
slab 0	0.04	0.05	100.46	100.55
slab 0	0.18	0.30	97.89	98.36
slab 3	0.15	0.14	100.41	100.70

Sphalerite	Zn	Mn	S	Fe	Total
slab 0	55.06	0.08	33.9	10.66	99.69
slab 0	54.83	0.07	34.25	10.66	99.8
slab 0	55.12	0.06	34.17	10.59	99.94
slab 3	55.46	0	34.18	9.3	98.95
slab 3	54.92	0.08	33.9	10.27	99.17
slab 3	55.98	0.06	33.38	10.15	99.56

APPENDIX 2

ELECTRON MICROPROBE ANALYSES OF MINERALS FROM THE DRILL HOLE 90-1 (EXCEPT MUSCOVITE)

(C.F. CHAPTER III)

Appendix 2: Electron microprobe analyses of minerals in the drill hole 90-1 (in wt-%)

Topaz	SiO_2	Al_2O_3	FeO	MgO	CaO	F	Total
Sample							
38.6	32.54	55.21	0.00	0.00	0.00	15.31	96.62
38.6	32.54	55.33	0.00	0.00	0.00	15.55	96.88
38.6	30.80	55.60	0.05	0.01	0.10	15.50	95.52
38.6	32.60	54.86	0.01	0.00	0.03	14.53	95.91
38.6	32.73	55.36	0.00	0.00	0.01	14.61	96.56
38.6	32.64	54.71	0.01	0.00	0.02	14.65	95.86
38.6	32.32	55.25	0.00	0.00	0.00	15.01	96.27
38.6	32.33	55.72	0.00	0.00	0.00	15.66	97.11
38.6	32.47	55.67	0.01	0.00	0.01	15.46	97.11
71.8	32.96	55.87	0.00	0.00	0.01	16.13	98.18
71.8	32.79	55.57	0.00	0.00	0.00	16.11	97.69
181	32.01	54.82	0.02	0.00	0.00	15.48	95.81
181	32.14	54.58	0.03	0.00	0.01	15.23	95.57
181	32.30	54.64	0.06	0.00	0.02	15.51	95.99
181	32.68	54.98	14.00	-	-	0.05	95.82
181	32.61	54.99	14.28	-	0.00	-	95.87
181	32.63	55.01	13.94	-	0.01	0.03	95.74
181	32.68	54.95	14.33	0.00	0.00	0.03	95.96
181	32.57	55.14	14.20	-	0.01	-	95.95
181	32.95	55.12	14.16	-	0.00	0.00	96.27
181	32.70	54.68	16.50	0.01	0.00	-	96.94
181	32.61	55.41	16.47	-	0.00	0.00	97.57
181	32.93	55.42	15.99	-	0.00	0.02	97.62
181	33.04	55.44	16.36	-	0.00	0.07	98.02
181	32.78	55.35	16.16	-	-	0.02	97.52
181	32.88	55.64	15.39	-	-	0.00	97.44
181	32.89	55.56	15.46	0.00	0.02	-	97.42
181	33.04	55.51	15.40	0.01	0.00	0.01	97.48
181	33.04	55.67	15.87	0.00	-	0.05	97.95
181	32.6	55.53	15.34	0.01	0	0	97.02
181	32.63	55.49	14.92	0	0.01	0.03	96.81
181	32.87	55.33	15.38	0	0.01	0	97.12
181	32.76	55.66	14.46	0	0	0.04	96.83
181	32.49	55.46	14.59	0	0	0.04	96.44

Appendix 2 (cont.): Electron microprobe analyses of minerals in the drill hole 90-1 (in wt-%)

Biotite	SiO_2	TiO_2	Al_2O_3	FeO	MnO	MgO	Na_2O	K_2O	F	Total
Sample										
350	47.70	0.17	25.47	7.65	0.45	0.27	0.16	11.12	3.41	95.04
350	47.25	0.18	25.75	7.88	0.47	0.27	0.26	11.26	3.89	96.07
450	46.87	0.81	26.87	6.62	0.36	0.48	0.11	11.29	2.89	95.13
650	38.67	0.94	21.07	21.40	0.86	0.97	0.04	10.44	3.92	96.72
650	38.33	0.91	20.83	21.71	0.88	0.94	0.09	10.32	3.63	96.16
650	41.42	0.71	19.90	18.90	0.35	1.54	0.07	10.87	4.65	96.49
650	42.43	0.34	20.90	15.38	0.72	0.99	0.05	10.78	5.38	94.72
650	42.78	0.53	21.06	15.57	0.74	1.02	0.07	10.85	5.44	95.82
830	37.73	0.95	20.91	22.17	0.95	0.89	0.07	10.00	3.06	95.50
830	38.08	1.27	21.01	21.39	0.91	0.91	0.08	10.35	3.18	95.90
830	37.36	1.29	19.12	22.10	0.50	1.56	0.02	10.18	3.06	93.95
830	38.03	1.15	19.69	21.15	0.50	1.54	0.04	10.18	3.06	94.08
830	38.33	0.40	21.74	21.33	0.89	0.89	0.10	10.39	3.24	96.01
830	38.52	0.36	22.03	20.81	0.88	0.90	0.09	10.25	3.20	95.80
830	38.14	0.61	21.22	22.11	0.87	0.88	0.13	10.21	2.71	95.82
830	35.10	1.93	17.48	29.10	0.50	2.33	0.09	10.30	2.20	98.37
830	34.02	1.72	17.49	28.72	0.52	2.23	0.07	9.73	1.81	95.80
830	43.72	0.24	27.24	9.59	0.41	0.65	0.13	11.23	2.12	94.46
830	42.73	0.71	23.00	12.56	0.32	1.30	0.07	10.76	2.93	93.18
830	46.23	0.41	24.76	9.79	0.25	1.30	0.08	11.42	2.76	95.85
830	45.00	0.40	27.81	8.49	0.35	0.66	0.20	11.17	2.00	95.25
830	46.08	0.21	25.23	9.42	0.40	0.92	0.15	11.16	2.43	95.00
830	47.14	0.25	24.97	8.58	0.27	1.01	0.11	11.34	2.63	95.22
830	44.33	0.39	25.34	11.08	0.31	0.80	0.12	11.05	2.58	94.92

Annite	SiO_2	TiO_2	Al_2O_3	FeO	MnO	MgO	Na_2O	K_2O	F	Total
Sample										
71.8	44.07	0.24	23.35	15.32	0.72	1.47	0.12	10.37	5.35	99.01
71.8	43.83	0.08	23.37	15.81	0.76	1.52	0.11	10.28	5.49	99.05
71.8	42.64	0.16	22.78	17.15	0.8	1.38	0.17	10.18	5.81	98.67
71.8	46.67	0.1	23.06	13.86	0.65	1.6	0.14	10.3	6.1	99.94
71.8	43.34	0.11	24.04	16.9	0.82	1.51	0.13	10.5	5.32	100.45
71.8	44.3	0.19	23.07	15.36	0.76	1.58	0.09	10.51	6.03	99.36

Appendix 2 (cont.): Electron microprobe analyses of minerals in the drill hole 90-1 (in wt-%)

Sphalerite	Fe	Mn	Zn	Cu	Sn	S	Total
Sample							
38.6	9.41	0.09	56.74	0.13	0.00	33.00	99.37
38.6	9.00	0.07	56.65	0.18	0.00	33.03	98.94
38.6	9.03	0.08	56.68	0.14	0.00	33.01	98.94
66.2	9.04	0.07	58.07	0.01	0.00	33.23	100.41
66.2	9.39	0.09	57.29	0.02	0.00	33.10	99.88
66.2	9.44	0.09	57.73	0.04	0.06	33.06	100.41
66.2	9.56	0.09	57.74	0.01	0.00	33.13	100.54
66.2	8.44	0.05	58.99	0.04	0.00	33.28	100.80
181	9.63	0.15	56.98	0.06	0.00	32.57	99.39
181	9.68	0.14	56.50	0.07	0.00	32.67	99.06
181	9.68	0.14	56.78	0.02	0.00	32.83	99.46

Pyrrhotite	Fe	Mn	Zn	Cu	Sn	S	Total
Sample							
38.6	61.01	0.01	0.00	0.00	0.00	38.25	99.27
38.6	60.37	0.00	0.01	0.05	0.00	38.41	98.84
38.6	60.51	0.00	0.00	0.04	0.00	38.51	99.07
38.6	60.66	0.01	0.03	0.05	0.00	38.79	99.53
181	60.97	0.00	0.01	0.00	0.00	38.00	98.97
181	61.12	0.00	0.00	0.03	0.00	38.07	99.22
181	61.31	0.00	0.00	0.00	0.00	38.03	99.34

Cassiterite	FeO	MnO	SnO_2	WO_3	TiO_2	Ta_2O_5	Nb_2O_5	Total
Sample								
38.6	0.10	0.00	99.75	0.00	0.51	0.00	0.33	100.69
38.6	0.06	0.01	99.90	0.00	0.53	0.00	0.02	100.52
38.6	0.02	0.01	100.21	0.00	0.51	0.00	0.07	100.82
38.6	0.02	0.00	100.13	0.21	0.62	0.00	0.08	101.05
38.6	0.02	0.00	100.32	0.00	0.46	0.00	0.04	100.84
38.6	0.07	0.02	99.99	0.12	0.49	0.00	0.01	100.68
181	0.10	0.00	99.93	0.40	0.05	0.00	0.24	100.72
181	0.10	0.01	99.55	0.09	0.31	0.00	0.58	100.63
181	0.15	0.01	98.87	1.61	0.00	0.00	0.03	100.66

APPENDIX 3

ELECTRON MICROPROBE ANALYSES OF MUSCOVITE AND TOPAZ IN GREISENS FROM THE SEAGULL BATHOLITH, YUKON TERRITORY

(C.F. CHAPTER IV)

Appendix 3: Microprobe analyses of muscovite and topaz in greisens from the Seagull Batholith, Yukon Territory (in wt-%).

Muscovite	SiO_2	TiO_2	Al_2O_3	FeO	MnO	MgO	CaO	Na_2O	K_2O	F	Cl	Total
Sample												
STQ4	47.37	0.12	27.44	5.06	0.03	1.87	0.00	0.10	11.48	2.28	0.01	94.79
STQ4	49.02	0.08	26.44	4.85	0.06	2.40	0.00	0.05	11.31	2.32	0.00	95.55
STQ4	49.05	0.10	25.27	4.64	0.03	2.56	0.01	0.05	10.98	3.05	0.01	94.46
STQ4	47.91	0.13	27.37	5.15	0.06	1.96	0.00	0.08	11.25	2.66	0.00	95.45
STQ4	47.14	0.11	27.09	5.05	0.08	2.01	0.04	0.08	11.42	2.56	0.01	94.51
STQ4	47.63	0.11	28.42	3.93	0.06	1.68	0.02	0.12	11.50	2.21	0.00	94.75
STQ4	49.00	0.09	24.79	4.93	0.05	3.05	0.00	0.06	11.08	2.88	0.01	94.71
STQ4	48.38	0.12	25.92	4.22	0.06	3.37	0.02	0.07	11.31	2.97	0.01	95.19
STQ4	49.23	0.07	25.25	4.27	0.03	3.05	0.02	0.04	11.00	2.85	0.01	94.61
STQ4	47.89	0.10	25.51	4.57	0.07	3.68	0.01	0.11	11.34	3.06	0.01	95.06
STQ4	49.47	0.11	25.21	4.51	0.07	3.23	0.00	0.06	11.13	3.07	0.03	95.59
STQ3	48.48	0.20	24.27	6.56	0.13	3.05	0.02	0.04	10.02	2.97	0.04	94.52
STQ3	50.16	0.12	24.82	4.01	0.10	2.89	0.03	0.07	10.97	2.81	0.01	94.80
STQ3	49.13	0.09	25.16	4.11	0.09	2.97	0.01	0.08	11.16	3.11	0.01	94.59
STQ3	51.29	0.09	25.65	4.43	0.10	3.05	0.00	0.04	10.76	3.32	0.01	97.34
STQ3	51.19	0.06	25.96	4.06	0.05	2.95	0.02	0.06	10.87	2.83	0.01	96.87
STQ3	49.93	0.05	25.35	3.83	0.08	2.93	0.03	0.06	10.95	2.76	0.01	94.80
STQ3	49.07	0.18	24.41	5.80	0.09	2.99	0.02	0.05	10.78	2.92	0.03	95.09
STQ3	49.99	0.06	24.98	3.64	0.06	2.80	0.00	0.06	11.07	2.80	0.01	94.29
STQ3	51.91	0.05	26.31	3.81	0.07	3.00	0.02	0.04	8.88	3.55	0.01	96.14

Topaz	SiO_2	Al_2O_3	FeO	MgO	CaO	F	Cl	Total
Sample								
STQ4	31.85	55.23	0.00	0.00	0.00	15.72	0.00	96.19
STQ4	31.94	55.42	0.01	0.04	0.00	15.68	0.01	96.48
STQ4	32.19	55.21	0.01	0.01	0.00	16.31	0.01	96.86
STQ4	31.95	55.29	0.02	0.01	0.00	16.32	0.00	96.72
STQ4	32.36	55.09	0.08	0.00	0.00	16.07	0.00	96.83
STQ4	31.40	54.98	0.02	0.07	0.00	16.20	0.00	95.85
STQ4	32.12	54.98	0.01	0.01	0.00	15.78	0.00	96.24
STQ4	31.93	54.99	0.05	0.02	0.01	15.84	0.00	96.16
STQ4	31.86	55.28	0.00	0.06	0.00	15.89	0.00	96.41
STQ4	32.04	55.35	0.05	0.01	0.00	15.95	0.00	96.69
STQ4	32.08	55.23	0.04	0.00	0.01	15.79	0.01	96.52
STQ4	32.57	55.76	0.03	0.04	0.01	16.60	0.00	98.01
STQ3	32.61	55.38	0.01	0.00	0.03	16.20	0.00	97.40
STQ3	32.55	55.23	0.00	0.00	0.02	16.22	0.00	97.20
STQ3	32.21	55.40	0.03	0.08	0.02	16.15	0.00	97.08
STQ3	32.22	55.59	0.00	0.07	0.01	16.46	0.00	97.43

APPENDIX 4

MODIFICATIONS TO THE SOLTHERM DATABASE FROM CHILLER

(C.F. CHAPTER V)

Appendix 4: Modifications to the Solthem database from CHILLER

Activity and regression coefficients of CO_2 at the ionic strength of 0, 1, 2 and 3:

```
GN CO2 M#0 1.    1.    1.    1.    1.    1.    1.
LOG GN 0 0.    0.    0.    0.    0.
GN CO2 M#1 1.    1.    1.    1.    1.    1.    1.
LOG GN 1 0.    0.    0.    0.    0.
GN CO2 M#2 1.    1.    1.    1.    1.    1.    1.
LOG GN 2 0.    0.    0.    0.    0.
GN CO2 M#3 1.    1.    1.    1.    1.    1.    1.
LOG GN 3 0.    0.    0.    0.    0.
```

Debye-Hückle parameters and their regression coefficients:

```
ADH    .9495  .9495  .9495  .9495  .9495  .9495  0.9495
ADH     0.94951E+00-0.00000E-04 0.00000E-04-0.00000E-07 0.000000-09
BDH    .3840  .3840  .3840  .3840  .3840  .3840  .3840
BDH     0.38407E+00 0.00000E-04 0.00000E-05-0.00000E-08 0.00000E-11
```

BINACL and BIL parameters (Helgeson et al. 1981) and their regression coefficients:

```
BINACL  -1.577  -1.577  -1.577  -1.577  -1.577  -1.577  -1.577
BINACL  -.157760E+01-0.00000E-01 0.00000E-04 0.00000E-07-0.00000E-09
BIL     .22420  .22420  .2242   .2242   .2242   .2242   .2242
BIL     .224200E+00 0.00000E-02-0.00000E-04 0.00000E-07-0.00000E-10
```

Component species data:

```
H+            +1 308 1.00797                    1
H2O           00 1.  18.0153                    2
Cl-           -1 181 35.453                     3
SO4--         -2 315 96.0616                    4
HCO3-         -1 210 61.0172  1.0               5
HS-           -1 184 33.0720  1.0               6
SiO2(aq)      +0 4.0 60.0848                    7
Al+++         +3 333 26.9815                    8
Ca++          +2 287 40.08                      9
Mg++          +2 254 24.312                     10
Fe++          +2 262 55.847                     11
K+            +1 227 39.102                     12
Na+           +1 191 22.9898                    13
Mn++          +2 268 54.9380                    14
Zn++          +2 262 65.37                      15
Cu+           +1 190 63.54                      16
Pb++          +2 308 207.19                     17
Ag+           +1 220 107.87                     18
AuCl2-        -1 181 267.877                    19
HgCl4--       -2 300 342.402                    20
Sr++          +2 300  87.620                    21
Ba++          +2 322 137.340                    22
F-             -1 133  18.998                   23
Sb(OH)3       0 400 172.756                     24
```

```
H3AsO3       0 400 125.928                         25
Br-          -1 196 79.904                         26
HPO4--       -2 316 95.979                         27
Co++         +2 262 58.9332                        28
MoO4--       -2 315 159.938                        29
UO2++        2 500 270.03                          30
O2 aq.       0 004 32.000                          31
NH4+         +1 231 18.0386                        32
H3BO3        0 400 61.8331                         33
Ti(OH)4      0 400 115.909                         34
Ac-          -1 100 59.050                         35
Oxal=        -2 100 88.020                         36
C4H4O4=      -2 100 116.07                         37
Sn++         +2 300 118.70                         38
```

Derived species data:

```
Al(OH)3  0.2.00 4 3.   44-3.000 1 1.000 8 3.000 2
Al(OH)3    1.12   1.12   1.12   1.12   1.12   1.12   1.12             RS84
Al(OH)3  0.11200E+01-0.00000E+00 0.00000E-03-0.00000E-05 0.00000E-09
HCl     0.4.00 3-0.   -0 1.000 1 1.000 3
HCl      -1.42  -1.42  -1.42  -1.42  -1.42  -1.42  -4224               HH69
HCl     -0.142000+01-0.00000E-01-0.00000E-04 0.00000E-06-0.00000E-08
HF      0.4.00 3           1.000 1 1.00023
HF     -5.82  -5.82  -5.82  -5.82  -5.82  -5.82  -5.82                 WO82
HF     -5.82        -0.00000E-00-0.00000E-00 0.00000E-00-0.000000-00
FeCl+   1.2.31 3          1.   11  1.   3
FeCl+   -2.31    -2.31   -2.31   -2.31   -2.31   -2.31   -2.31         WO82
FeCl+  -2.31   E+00-0.00000E-02-0.00000E-04 0.00000E-06-0.00000E-09
H2 aq.  0.4.00 5        -0.25  1 -0.25 4 1.00  2 0.25  6
H2 aq.    5.017   5.017   5.017   5.017   5.017   5.017   5.017        AR82
H2 aq.  0.50170E+01-0.00000E-01 0.00000E-04-0.00000E-06 0.00000E-09
KCl    -0.4.00 3-0.   -0 1.00012 1.000 3
KCl      -0.193  -0.193  -0.193  -0.193  -0.193  -0.193  -0.193       HH69
KCl     -0.1930E+00-0.00000E-02-0.00000E-05-0.00000E-07
NaCl   -0.4.00 3-0.   -0 1.00013 1.000 3
NaCl    -0.466  -0.466  -0.466  -0.466 -0.466  -0.466  -0.466  -0.466  SC84
NaCl   -0.46600E+00 0.00000E-01-0.000000-03 0.00000E-06-0.00000E-09
O2 aq.  0.4.00 4         0.50  1 -0.5  6 0.50  4
O2 aq.    69.17   63.22   53.49   45.89   39.72   34.54   30.03        AR82
O2 aq.  0.75998E+02-0.29288E+00 0.82561E-03-0.16185E-05 0.13940E-08
OH-    -1.1.40 3 1.   44-1.000 1 1.000 2
OH-     9.57    9.57    9.57    9.57    9.57    9.57    9.57    9.57   SC84
OH-     9.57   E+00-0.00000E-01 0.00000E-03-0.00000E-06 0.00000E-09
H2S aq.  0.4.00 3-0.   -0 1.000 1 1.000 6
H2S aq.   -7.215  -7.215  -7.215  -7.215  -7.215  -7.215  -7.215      BA82
H2S aq. -0.72150E+01 0.00000E-01-0.00000E-04 0.00000E-06-0.00000E-09
SnCl+   1.2.31 3-0.   -0 1.00038 1.000 3
SnCl+    -8.186  -8.186  -8.186  -8.186  -8.186  -8.186  -8.186  -8.186  WE90
SnCl+   -0.81860E+01-0.00000E-01 0.00000E-05-0.00000E-07 0.00000E-10
H2O gas     18.01 1  1.000 2 1.000 6
H2O gas   -3.037  -3.037  -3.037  -3.037  -3.037  -3.037  -3.037  -3.037
H2O gas -0.30370E+01-0.00000E-01 0.00000E-03-0.00000E-06 0.00000E-09
H2O B.C -6191.41421  14.852822  -0.00914267 -66.3325857  0.182767    -.00013274
```

Mineral data:

```
albite    262.22 5  1.00013 1.000 8 3.000 7 2.000 2-4.000 1 0.0   0
albite    -1.91  -1.91  -1.91  -1.91  -1.91  -1.91  -1.91  -1.91
albite   -1.9100E+00-0.00000E-01 0.00000E-04 0.00000E-06-0.00000E-09 2.620
cassiter  150.70 5  1.00038 1.000 2 0.250 4 -.250 6 -1.75 1
cassiter -4.955  -4.955  -4.955  -4.955  -4.955  -4.955  -4.955  -4.955
cassiter -4.95500+00 0.00000E+00 0.00000E+00 0.00000E+00 0.00000E+00
feldsp-k  278.34 5  1.00012 1.000 8 3.000 7 2.000 2-4.000 1 0.0   0
feldsp-k  -2.698  -2.698  -2.698  -2.698  -2.698  -2.698  -2.698  -2.698
feldsp-k -2.698 E+00-0.00000E-01-0.00000E-04 0.00000E-06-0.00000E-09 2.557
muscovit  399.31 6  -9.50 1 1.00 12 3.000 7 5.500 2 3.000 8 0.5  23
muscovit -12.882 -12.882 -12.882 -12.882 -12.882 -12.882 -12.882 -12.882
muscovit-0.12882E+02-0.00000E+00 0.00000E-03-0.00000E-06-0.00000E-09 2.831
pyrrhoti   87.91 3  1.00011 1.000 6-1.000 1 0.0   0
pyrrhoti  -5.719  -5.719  -5.719  -5.719  -5.719  -5.719  -5.719  -5.719
pyrrhoti-0.57190E+01-0.00000E-02-0.00000E-04 0.00000E-06-0.00000E-09 4.830
quartz     60.08 1  1.000 7 0.0   0
quartz    -1.068  -1.068  -1.068  -1.068  -1.068  -1.068  -1.068  -1.068
quartz   -0.1068E+01 0.00000E-01-0.00000E-04 0.00000E-06-0.00000E-09 2.70
topaz      183.05 5 -4.500 1 2.000 8 1.000 7 2.500 2 1.5  23
topaz     -19.312 -19.312 -19.312 -19.312 -19.312 -19.312 -19.312 -19.312
topaz    -0.19312E+02 0.00000E-01-0.00000E-04 0.00000E-06-0.00000E-08 3.484
```

Reference:

Helgeson, H.C., Kirkham, D.H., and Flowers, G.C., 1981, The theoretical prediction of the thermodynamic behaviour of aqueous electrolytes at high pressures and temperatures. IV. Calculation of activity coefficients, osmotic coefficients, and apparent molal and standard and relative partial molal properties to 600°C and 5Kb.: American Journal of Science, v. 281, p. 1249-1516.

APPENDIX 5

ELECTRON MICROPROBE ANALYSES OF MUSCOVITE FROM THE DRILL HOLE 90-1

(C.F. CHAPTER VI)

Appendix 5: Electron microprobe analyses of muscovite in drill hole 90-1 (in wt-%)

Sample	SiO_2	TiO_2	Al_2O_3	FeO	MnO	MgO	Na_2O	K_2O	F	Cl	Total
38.6	49.22	0.04	36.62	1.33	0.04	1.12	0.32	10.92	1.35		100.42
38.6	50.04	0.03	36.20	1.11	0.05	1.13	0.28	10.83	1.65		100.63
38.6	49.99	0.05	36.30	1.12	0.05	1.19	0.35	11.03	1.39		100.89
38.6	50.61	0.09	36.12	0.88	0.03	1.18	0.30	10.89	1.56		101.02
38.6	50.44	0.09	35.68	1.36	0.08	1.17	0.40	10.73	1.60		100.90
38.6	51.42	0.10	35.44	1.47	0.06	1.17	0.30	10.78	1.88		101.89
38.6	48.42	0.03	34.35	0.72	0.05	1.10	0.38	10.47	1.53		96.44
71.8	44.90	0.20	23.71	15.82	0.77	1.55	0.09	10.13	5.62		100.45
71.8	44.16	0.18	23.41	16.19	0.77	1.50	0.12	10.52	5.66		100.15
71.8	47.92	0.11	24.86	12.61	0.55	1.64	0.16	10.54	5.76		101.77
71.8	43.95	0.15	23.98	16.51	0.81	1.51	0.15	10.36	5.70		100.74
71.8	44.43	0.15	24.60	16.54	0.79	1.51	0.12	10.20	5.32		101.44
71.8	44.15	0.22	24.09	16.63	0.79	1.48	0.18	10.00	5.85		100.95
71.8	44.03	0.17	24.05	16.22	0.75	1.52	0.09	10.42	5.48		100.46
71.8	43.93	0.15	23.26	17.26	0.87	1.49	0.13	10.17	5.61		100.53
71.8	44.95	0.18	23.84	15.53	0.73	1.53	0.09	10.46	5.39		100.45
71.8	44.13	0.17	23.94	16.25	0.75	1.52	0.08	10.44	5.28		100.37
71.8	44.23	0.26	23.10	15.84	0.76	1.54	0.14	10.02	5.70		99.23
81	46.93	0.37	28.71	8.11	0.50	1.04	0.32	10.80	3.61	0.02	98.89
81	46.27	0.42	28.82	8.37	0.51	1.08	0.29	10.87	3.62	0.04	98.76
81	46.39	0.39	28.20	8.56	0.54	1.06	0.25	10.87	3.50	0.05	98.34
81	46.14	0.09	27.53	9.49	0.47	1.02	0.18	11.07	3.76	0.02	98.18
81	49.61	0.17	28.85	6.77	0.38	1.33	0.13	11.33	3.57	0.02	100.65
81	47.53	0.09	28.77	9.02	0.31	1.01	0.15	10.82	3.73	0.02	99.89
81	49.16	0.07	28.81	7.32	0.21	1.08	0.20	10.96	4.14	0.02	100.23
81	48.84	0.06	28.45	8.11	0.34	1.10	0.25	10.84	3.79	0.02	100.21
81	50.38	0.07	29.43	6.80	0.25	1.04	0.19	10.66	4.13	0.03	101.23
81	49.85	0.06	28.37	7.68	0.21	0.97	0.13	10.89	3.82	0.01	100.38
81	49.74	0.03	27.88	7.61	0.29	1.31	0.11	10.73	4.25	0.01	100.19
81	49.49	0.10	29.22	7.23	0.22	0.91	0.13	10.93	3.76	0.01	100.40
81	47.41	0.10	27.69	8.61	0.25	0.93	0.14	10.71	3.89	0.03	98.13
81	48.95	0.07	27.69	8.52	0.27	1.10	0.09	10.73	3.82	0.01	99.65
81	48.71	0.11	28.63	8.29	0.23	0.92	0.24	10.81	3.70	0.05	100.16
81	50.18	0.09	29.30	6.79	0.26	1.14	0.18	10.67	3.89	0.01	100.86
81	47.21	0.28	27.34	9.67	0.41	1.18	0.21	10.68	4.42	0.02	99.55
81	47.37	0.41	28.59	9.11	0.41	1.16	0.22	10.67	4.00	0.01	100.30
81	42.84	0.41	23.27	15.48	0.74	1.13	0.13	10.55	5.22	0.04	97.58
81	43.43	0.32	22.70	14.78	0.73	1.15	0.20	10.73	5.40	0.07	97.22
81	42.24	0.42	22.81	15.51	0.84	1.06	0.14	10.56	5.31	0.05	96.69
81	42.31	0.40	22.13	15.33	0.78	1.11	0.19	10.40	5.12	0.07	95.66

Appendix 5 (cont.): Electron microprobe analyses of muscovite in drill hole 90-1 (in wt-%)

Sample	SiO_2	TiO_2	Al_2O_3	FeO	MnO	MgO	Na_2O	K_2O	F	Cl	Total
81	46.60	0.20	22.72	13.70	0.48	1.31	0.16	10.26	6.71	0.02	99.36
81	47.78	0.02	22.25	12.06	0.47	1.65	0.14	10.35	6.19	0.07	98.39
81	46.78	0.24	25.40	12.59	0.39	1.15	0.09	10.57	5.31	0.03	100.29
81	44.64	0.16	22.36	14.90	0.53	1.12	0.14	10.29	6.57	0.04	98.00
100	46.89	0.00	29.91	9.56	0.30	0.34	0.15	10.82	3.47	0.01	99.98
100	48.84	0.00	27.66	9.84	0.36	0.05	0.12	10.71	3.87	0.02	99.84
100	48.32	0.19	30.06	7.61	0.47	0.71	0.25	10.58	3.78	0.01	100.39
100	48.50	0.08	27.89	9.83	0.25	0.98	0.15	10.93	4.35	0.01	101.14
100	48.90	0.15	29.04	8.69	0.26	0.70	0.15	10.96	3.97	0.02	101.14
100	49.84	0.09	28.92	7.36	0.23	0.78	0.10	10.79	3.72	0.02	100.28
100	49.21	0.10	28.82	8.27	0.20	0.65	0.13	11.00	3.41	0.02	100.36
100	49.68	0.08	28.86	7.25	0.26	0.75	0.14	10.39	3.61	0.02	99.50
100	50.08	0.06	29.04	7.46	0.24	0.74	0.10	10.74	3.43	0.03	100.49
100	49.04	0.11	28.52	8.27	0.25	0.71	0.13	10.90	3.49	0.02	99.98
100	48.97	0.09	28.48	9.27	0.33	0.79	0.13	10.94	4.04	0.01	101.33
100	48.55	0.16	28.41	9.73	0.29	0.65	0.11	10.89	3.66	0.03	100.93
100	49.88	0.12	29.17	7.28	0.22	0.66	0.07	11.26	3.74	0.02	100.84
100	46.94	0.25	27.56	11.35	0.33	0.65	0.09	11.06	4.17	0.02	100.67
100	50.32	0.05	28.78	7.97	0.25	0.91	0.12	10.67	3.93	0.02	101.37
100	48.00	0.19	28.49	9.56	0.29	0.65	0.08	11.06	3.93	0.02	100.62
100	50.11	0.07	30.56	6.51	0.23	0.67	0.13	11.14	3.18	0.01	101.29
100	49.30	0.15	28.85	8.37	0.24	0.72	0.10	10.60	3.91	0.03	100.63
100	48.29	0.30	29.15	8.74	0.27	0.71	0.15	10.95	3.61	0.01	100.66
100	49.75	0.14	29.71	6.96	0.27	0.82	0.16	11.33	3.62	0.01	101.24
100	49.78	0.08	29.52	7.40	0.24	0.77	0.12	11.04	3.76	0.01	101.13
100	49.77	0.09	30.02	7.15	0.25	0.74	0.19	10.98	3.60	0.01	101.29
100	49.88	0.11	29.53	7.07	0.26	0.75	0.13	10.81	3.73	0.01	100.69
100	50.28	0.03	30.50	6.15	0.19	0.72	0.14	10.76	3.11	0.01	100.56
100	49.48	0.15	30.42	6.79	0.30	0.70	0.15	10.94	3.45	0.02	100.93
100	50.22	0.02	29.47	7.11	0.30	0.81	0.14	10.86	3.66	0.01	101.06
100	49.72	0.11	30.95	6.12	0.22	0.73	0.21	11.26	3.39	0.01	101.29
100	49.91	0.13	29.50	6.89	0.22	0.75	0.12	10.96	3.47	0.01	100.51
100	49.95	0.08	29.53	7.45	0.28	0.83	0.16	10.78	3.67	0.02	101.20
181	46.83	0.10	29.17	6.42	0.30	0.22	0.17	11.41	2.53		96.08
181	46.28	0.01	32.43	4.55	0.38	0.12	0.41	11.12	1.66		96.27
181	46.25	0.05	31.39	4.85	0.33	0.12	0.40	10.99	2.01		95.54
181	46.63	0.00	29.82	5.74	0.33	0.18	0.18	11.59	2.10		95.70
181	46.56	0.00	29.45	6.07	0.36	0.19	0.20	11.45	2.08		95.49
181	47.38	0.00	30.30	5.50	0.31	0.17	0.23	11.33	2.15		96.48
181	45.42	0.08	30.29	5.79	0.27	0.20	0.19	11.24	2.11	0.01	94.69

Appendix 5 (cont.): Electron microprobe analyses of muscovite in drill hole 90-1 (in wt-%)

Sample	SiO_2	TiO_2	Al_2O_3	FeO	MnO	MgO	Na_2O	K_2O	F	Cl	Total
181	45.10	0.04	30.55	5.52	0.27	0.19	0.25	11.55	2.00	0.05	94.67
181	44.42	0.07	28.77	8.05	0.44	0.20	0.17	11.45	2.86	0.02	95.24
181	46.57	0.06	29.08	6.08	0.35	0.25	0.14	11.42	2.54	0.01	95.43
181	45.29	0.04	29.77	6.42	0.33	0.20	0.15	11.67	2.38	0.01	95.25
181	46.15	0.07	29.60	5.82	0.30	0.22	0.14	11.65	2.29	0.00	95.28
181	46.08	0.04	29.66	5.60	0.28	0.28	0.22	11.55	2.14	0.01	94.96
181	45.96	0.08	29.42	5.72	0.30	0.23	0.13	11.49	2.18	0.01	94.60
181	46.28	0.04	29.22	5.49	0.36	0.27	0.22	11.16	2.19	0.00	94.33
181	45.91	0.10	28.69	6.60	0.33	0.32	0.16	11.40	2.35	0.01	94.90
181	46.03	0.09	29.35	6.00	0.30	0.24	0.18	11.68	2.16	0.00	95.14
181	44.91	0.18	30.55	5.49	0.27	0.21	0.16	11.39	1.94	0.01	94.30
181	44.98	0.10	30.93	5.14	0.22	0.26	0.21	11.48	1.87	0.00	94.42
181	45.13	0.07	30.18	5.29	0.32	0.32	0.34	11.20	2.16	0.01	94.11
181	44.44	0.19	29.87	6.18	0.36	0.27	0.34	11.21	2.17	0.01	94.12
181	46.12	0.03	30.20	5.95	0.27	0.19	0.20	11.31	2.05	0.04	95.48
181	46.56	0.02	28.97	6.06	0.33	0.20	0.18	11.52	2.32	0.00	95.19
181	46.19	0.03	29.44	5.93	0.32	0.19	0.15	11.71	2.12	0.00	95.19
181	45.86	0.12	30.94	5.16	0.22	0.19	0.18	11.44	1.99	-	95.26
181	45.54	0.18	30.00	5.89	0.37	0.17	0.28	11.19	2.27	0.01	94.96
181	45.90	0.16	30.74	5.26	0.24	0.22	0.19	11.48	2.02	0.01	95.36
181	45.57	0.08	30.51	5.60	0.33	0.16	0.31	11.19	2.03	-	94.92
181	45.37	0.16	30.29	5.86	0.28	0.21	0.20	11.43	2.23	0.01	95.08
181	45.30	0.15	30.00	5.95	0.33	0.26	0.35	11.12	2.39	0.01	94.84
181	45.44	0.14	30.17	6.53	0.36	0.25	0.29	11.14	2.32	0.00	95.67
181	45.60	0.36	30.49	5.73	0.25	0.26	0.22	11.28	2.20	0.01	95.47
181	45.93	0.06	30.47	5.94	0.30	0.15	0.23	11.27	2.24	0.00	95.64
181	45.18	0.46	29.55	6.74	0.29	0.29	0.25	11.30	2.36	0.02	95.43
181	46.41	0.29	29.17	6.42	0.27	0.23	0.18	11.27	2.45	0.01	95.67
181	45.99	0.26	29.63	6.03	0.31	0.26	0.20	11.27	2.19	0.00	95.22
181	45.91	0.30	30.05	5.80	0.24	0.18	0.19	11.47	1.94	0.01	95.27
181	46.07	0.29	30.64	5.57	0.30	0.17	0.18	11.60	1.89	0.01	95.92
181	47.15	0.01	29.04	6.69	0.36	0.20	0.18	11.28	2.66	0.01	96.47
181	46.86	0.02	28.63	6.64	0.34	0.21	0.18	11.38	2.59	0.00	95.77
189	50.28	0.00	33.54	4.59	0.22	0.15	0.22	10.58	2.32	0.01	100.93
189	49.99	0.03	34.52	3.47	0.14	0.11	0.25	10.80	2.07	0.01	100.51
189	48.01	0.07	31.28	6.16	0.35	0.26	0.18	10.70	2.95	0.02	98.79
189	49.03	0.01	32.80	5.10	0.26	0.25	0.19	10.95	2.66	0.01	100.15
189	50.63	0.00	32.38	5.01	0.30	0.26	0.16	11.05	2.59	0.01	101.29
189	48.47	0.01	33.30	5.19	0.25	0.24	0.20	11.01	2.65	0.01	100.20
189	49.03	0.02	33.58	5.40	0.24	0.19	0.17	10.53	2.65	0.01	100.75
189	47.44	0.12	29.55	8.11	0.33	0.35	0.19	10.71	3.14	0.02	98.64

Appendix 5 (cont.): Electron microprobe analyses of muscovite in drill hole 90-1 (in wt-%)

Sample	SiO_2	TiO_2	Al_2O_3	FeO	MnO	MgO	Na_2O	K_2O	F	Cl	Total
189	49.20	0.01	33.91	4.78	0.24	0.22	0.20	10.84	2.40	0.01	100.81
189	48.93	0.01	31.36	6.79	0.30	0.28	0.09	10.93	3.04	0.02	100.50
189	47.67	0.01	33.04	5.18	0.24	0.23	0.19	10.97	2.15	0.04	98.85
189	49.66	0.00	32.56	5.18	0.30	0.22	0.18	10.50	2.67	0.03	100.16
189	49.70	0.00	32.40	4.71	0.19	0.37	0.19	10.37	2.55	0.02	99.43
189	49.89	0.03	30.22	7.13	0.32	0.29	0.12	11.10	3.47	0.01	101.13
189	49.15	0.00	31.26	6.43	0.31	0.34	0.25	10.63	3.16	0.02	100.24
189	48.25	0.00	29.49	7.39	0.30	0.31	0.16	11.01	3.52	0.01	98.98
189	48.13	0.04	30.84	6.42	0.31	0.29	0.15	10.87	3.02	0.01	98.79
189	49.27	0.01	30.92	6.57	0.30	0.38	0.14	10.87	3.03	0.01	100.21
189	47.18	0.05	31.21	6.67	0.28	0.27	0.09	10.63	3.04	0.03	98.15
189	49.16	0.00	30.37	7.09	0.33	0.33	0.15	10.88	3.36	0.02	100.27
189	49.59	0.03	30.03	7.17	0.36	0.35	0.13	10.85	3.47	0.02	100.53
189	49.51	0.00	32.64	5.26	0.22	0.35	0.35	10.82	2.88	0.01	100.81
189	49.12	0.00	31.05	6.97	0.26	0.36	0.20	11.12	3.45	0.02	101.11
189	49.61	0.03	30.15	7.38	0.32	0.31	0.10	10.86	3.50	0.01	100.80
189	48.28	0.04	31.66	7.27	0.34	0.26	0.13	10.94	3.35	0.01	100.88
189	49.71	0.06	30.78	6.11	0.28	0.33	0.12	10.99	3.18	0.01	100.22
198	49.23	0.01	31.81	5.97	0.35	0.16	0.13	10.93	3.37	0.01	100.54
198	49.86	0.03	31.04	5.79	0.47	0.18	0.14	10.95	3.37	0.02	100.49
198	50.51	0.04	29.24	6.98	0.72	0.21	0.11	10.45	3.95	0.01	100.56
198	49.27	0.04	30.49	6.05	0.63	0.19	0.12	10.67	3.19	0.02	99.33
198	48.92	0.01	31.42	6.00	0.39	0.16	0.14	10.77	3.12	0.01	99.61
198	49.23	0.30	29.98	6.12	0.36	0.26	0.11	11.05	3.42	0.02	99.38
198	48.92	0.21	29.04	7.65	0.49	0.26	0.12	10.55	3.76	0.03	99.61
198	49.09	0.40	29.69	7.19	0.52	0.32	0.15	10.92	3.54	0.03	100.35
198	49.58	0.30	29.28	7.08	0.43	0.36	0.14	11.07	4.09	0.04	100.65
198	50.40	0.25	29.71	8.25	0.49	0.36	0.08	6.33	3.22	0.02	97.77
198	50.74	0.00	27.85	7.80	0.52	0.24	0.08	10.74	4.10	0.01	100.36
198	50.02	0.20	28.35	7.56	0.44	0.29	0.11	11.17	4.45	0.03	100.72
198	49.81	0.02	31.39	5.87	0.38	0.23	0.13	11.11	3.38	0.01	100.90
198	50.08	0.03	31.19	6.06	0.41	0.17	0.10	10.94	3.12	0.02	100.81
198	50.65	0.43	31.14	6.00	0.35	0.26	0.10	10.72	3.39	0.01	101.65
211	47.69	0.01	32.88	3.57	0.32	0.11	0.18	11.58	1.55	0.00	97.26
211	46.32	0.04	31.15	5.58	0.36	0.18	0.14	11.58	2.31	0.02	96.73
211	48.26	0.01	31.42	4.70	0.46	0.04	0.20	11.49	2.15	0.01	97.83
211	47.19	0.06	32.84	3.35	0.29	0.09	0.19	11.47	1.66	0.01	96.46
211	46.27	0.32	26.17	8.47	0.57	0.29	0.08	10.88	3.41	0.04	95.06
211	50.37	0.23	25.96	6.82	0.46	0.35	0.13	10.83	2.75	0.04	96.78
211	46.81	0.03	31.14	4.61	0.40	0.10	0.20	11.60	1.91	0.01	96.00

Appendix 5 (cont.): Electron microprobe analyses of muscovite in drill hole 90-1 (in wt-%)

Sample	SiO_2	TiO_2	Al_2O_3	FeO	MnO	MgO	Na_2O	K_2O	F	Cl	Total
211	47.25	0.02	33.66	2.43	0.27	0.04	0.25	11.32	1.47	0.01	96.09
211	47.17	0.07	29.46	5.52	0.38	0.19	0.11	11.57	2.26	0.01	95.78
211	47.53	0.00	33.88	2.52	0.24	0.07	0.22	11.42	1.37	0.01	96.70
211	43.88	0.30	24.00	12.12	0.80	0.25	0.18	10.75	4.87	0.03	95.12
211	43.55	0.36	23.39	12.62	0.91	0.26	0.12	10.67	5.08	0.02	94.83
211	43.16	0.28	23.47	12.38	0.88	0.27	0.17	10.62	4.81	0.02	94.01
211	46.37	0.18	29.16	5.69	0.37	0.18	0.16	11.32	2.36	0.01	94.80
211	47.04	0.08	30.78	5.05	0.30	0.20	0.15	11.54	1.99	0.01	96.29
211	46.46	0.31	26.88	7.73	0.54	0.33	0.10	11.07	3.05	0.03	95.21
211	47.30	0.11	27.66	7.13	0.38	0.28	0.09	11.46	2.65	0.01	95.97
211	46.28	0.00	29.82	6.36	0.37	0.06	0.15	11.48	2.26	0.01	95.84
211	46.16	0.02	29.83	6.22	0.44	0.18	0.11	11.52	2.47	0.01	95.92
211	47.51	0.28	26.90	7.93	0.48	0.26	0.12	11.45	2.92	0.02	96.63
211	47.27	0.28	26.42	8.02	0.43	0.28	0.11	11.44	3.10	0.01	96.08
211	44.63	0.18	27.58	9.01	0.57	0.19	0.09	11.00	3.24	0.02	95.13
211	44.65	0.22	27.18	9.98	0.69	0.18	0.10	10.81	3.47	0.03	95.82
211	46.07	0.05	30.37	6.18	0.42	0.22	0.14	11.48	2.42	0.03	96.38
211	47.33	0.03	31.57	4.44	0.49	0.08	0.20	11.55	1.91	0.01	96.80
211	47.32	0.02	29.21	6.46	0.40	0.21	0.11	11.64	2.34	0.01	96.73
211	47.66	0.06	27.17	6.83	0.39	0.32	0.12	11.34	2.90	0.02	95.56
211	44.87	0.24	26.02	10.25	0.65	0.23	0.09	10.84	3.69	0.03	95.38
211	43.86	0.22	26.30	11.30	0.77	0.22	0.11	11.02	3.84	0.03	96.04
211	46.82	0.11	28.68	7.08	0.46	0.18	0.13	11.40	2.67	0.02	96.44
211	47.14	0.36	26.63	7.91	0.52	0.40	0.10	11.31	3.23	0.05	96.29
211	47.25	0.24	27.37	7.18	0.44	0.38	0.09	11.35	2.85	0.02	95.96
211	43.57	0.33	25.15	11.99	0.79	0.21	0.14	10.94	4.57	0.03	95.79
211	46.64	0.31	25.65	8.21	0.53	0.37	0.12	11.17	3.52	0.07	95.11
211	47.37	0.20	25.92	7.87	0.52	0.24	0.10	11.21	3.98	0.02	95.75
211	46.36	0.03	28.57	6.89	0.43	0.19	0.12	11.21	2.75	0.02	95.43
211	47.06	0.01	32.10	3.76	0.30	0.06	0.21	11.55	1.50	0.00	95.93
211	45.22	0.03	30.16	6.85	0.45	0.19	0.13	11.49	2.12	0.02	95.76
211	47.77	0.02	28.19	6.98	0.38	0.26	0.11	11.52	2.78	0.01	96.84
211	47.77	0.03	27.77	7.20	0.44	0.28	0.09	11.41	2.65	0.01	96.53
211	47.82	0.01	31.88	3.50	0.68	0.03	0.18	11.49	1.84	0.01	96.67
211	48.08	0.00	31.98	3.85	0.35	0.06	0.15	11.38	1.79	0.01	96.88
211	48.25	0.00	32.40	3.35	0.35	0.06	0.17	11.34	1.56	0.01	96.84
222	47.61	0.05	30.66	4.61	0.23	0.36	0.13	11.43	1.94	0.01	96.20
222	47.50	0.03	30.98	4.45	0.18	0.37	0.13	11.55	1.93	0.01	96.31
222	48.08	0.00	31.72	4.42	0.20	0.40	0.15	11.60	1.95	0.01	97.73
222	47.92	0.01	31.11	4.43	0.15	0.39	0.14	11.52	2.01	0.01	96.84
222	45.55	0.01	29.68	8.08	0.24	0.37	0.14	10.49	1.75	0.02	95.58

Appendix 5 (cont.): Electron microprobe analyses of muscovite in drill hole 90-1 (in wt-%)

Sample	SiO_2	TiO_2	Al_2O_3	FeO	MnO	MgO	Na_2O	K_2O	F	Cl	Total
222	46.05	0.06	28.81	7.68	0.37	0.37	0.13	10.64	1.97	0.03	95.28
222	47.78	0.38	28.68	6.45	0.29	0.81	0.13	11.34	2.82	0.02	97.50
222	46.87	0.35	29.47	5.91	0.31	0.61	0.15	11.38	2.28	0.02	96.38
222	46.47	0.10	30.17	4.70	0.26	0.38	0.12	11.67	1.99	0.01	95.01
222	46.80	0.07	31.31	4.32	0.12	0.38	0.15	11.54	1.88	0.03	95.79
222	47.91	0.07	32.90	3.77	0.17	0.37	0.20	11.42	1.79	0.01	97.85
222	47.87	0.03	32.35	3.41	0.14	0.37	0.15	11.31	1.65	0.01	96.62
222	47.39	0.04	32.30	3.61	0.11	0.34	0.14	11.46	1.70	0.01	96.39
222	47.37	0.00	32.89	3.38	0.12	0.30	0.16	11.44	1.77	0.01	96.75
222	46.87	0.10	31.64	4.03	0.17	0.42	0.16	11.33	2.00	0.02	95.94
222	47.61	0.01	31.56	4.28	0.22	0.45	0.14	11.48	2.05	0.02	96.95
222	46.83	0.20	29.62	6.10	0.32	0.41	0.14	11.34	2.32	0.03	96.35
222	47.16	0.10	27.45	7.51	0.41	0.53	0.14	11.19	2.97	0.02	96.21
222	48.15	0.14	29.44	5.72	0.28	0.48	0.09	11.36	2.27	0.01	96.99
222	48.00	0.22	29.85	5.26	0.28	0.47	0.13	11.44	2.25	0.02	96.98
222	46.51	0.11	26.80	8.42	0.45	0.48	0.14	11.20	3.47	0.03	96.15
222	46.66	0.04	30.94	5.31	0.19	0.32	0.16	11.12	1.74	0.01	95.75
222	47.51	0.05	32.51	3.65	0.14	0.33	0.16	11.53	1.80	0.01	96.93
222	47.72	0.08	31.47	4.29	0.15	0.38	0.15	11.79	1.94	0.01	97.16
222	47.70	0.09	30.09	5.28	0.21	0.39	0.16	11.36	2.15	0.01	96.53
222	47.32	0.06	32.42	3.49	0.11	0.31	0.18	11.78	1.87	0.02	96.77
222	47.24	0.11	32.79	3.44	0.14	0.33	0.19	11.60	1.62	0.01	96.78
222	47.66	0.02	33.37	3.19	0.12	0.35	0.27	11.71	1.84	0.01	97.76
222	47.05	0.01	33.08	3.15	0.14	0.31	0.19	11.54	1.65	0.01	96.45
290	44.88	0.26	22.26	12.21	1.22	0.17	0.14	10.77	5.95	0.01	95.35
290	44.41	0.14	22.16	12.87	1.33	0.14	0.09	10.74	6.31	0.02	95.55
290	45.93	0.12	21.33	11.59	1.15	0.15	0.13	10.43	6.34	0.02	94.54
290	45.91	0.16	21.33	11.70	1.13	0.17	0.16	10.73	6.28	0.01	94.94
290	45.79	0.14	21.48	11.87	1.07	0.18	0.23	10.57	6.71	0.01	95.22
290	45.17	0.12	21.71	12.24	1.18	0.17	0.11	10.73	6.60	0.01	95.25
290	47.50	0.03	20.34	10.83	1.19	0.17	0.21	10.43	7.32	0.01	94.96
290	45.48	0.13	21.51	11.87	1.21	0.16	0.16	10.68	6.71	0.01	95.08
290	45.44	0.11	21.94	11.68	1.19	0.15	0.09	10.91	6.35	0.03	95.22
290	45.89	0.10	21.40	11.77	1.16	0.15	0.09	10.74	6.92	0.02	95.32
290	44.50	0.10	21.58	12.31	1.19	0.16	0.10	10.69	6.48	0.03	94.43
290	46.29	0.13	21.28	11.65	1.19	0.16	0.08	10.83	6.88	0.02	95.60
290	45.73	0.13	21.07	11.93	1.12	0.15	0.19	10.39	6.68	0.01	94.57
290	50.48	0.02	18.95	8.21	0.70	0.21	0.09	10.95	7.71	0.01	94.08
290	48.15	0.10	19.95	10.30	1.03	0.17	0.06	10.72	6.96	0.00	94.51
290	45.82	0.17	21.63	11.94	1.24	0.14	0.10	10.88	6.35	0.01	95.61
290	50.36	0.07	19.10	8.90	0.85	0.19	0.05	11.30	7.33	0.01	95.08

Appendix 5 (cont.): Electron microprobe analyses of muscovite in drill hole 90-1 (in wt-%)

Sample	SiO_2	TiO_2	Al_2O_3	FeO	MnO	MgO	Na_2O	K_2O	F	Cl	Total
290	46.08	0.16	21.44	11.89	1.17	0.16	0.27	10.44	6.95	0.02	95.64
290	46.22	0.12	21.60	11.64	1.12	0.17	0.14	10.66	6.87	0.01	95.65
290	45.85	0.12	21.15	11.60	1.15	0.14	0.15	10.95	6.63	0.02	94.96
290	45.64	0.16	21.45	11.59	1.18	0.16	0.13	10.95	6.55	0.04	95.07
290	47.85	0.05	28.58	5.27	0.46	0.15	0.11	11.46	3.17	0.02	95.76
290	48.54	0.14	24.01	7.25	0.66	0.17	0.10	11.26	5.35	0.01	95.26
290	48.68	0.11	27.63	5.81	0.52	0.18	0.10	11.39	3.54	0.00	96.47
290	49.19	0.07	22.52	8.12	0.70	0.21	0.06	11.28	6.05	0.01	95.66
290	49.14	0.08	22.85	7.77	0.76	0.19	0.10	11.35	5.64	0.00	95.50
290	48.72	0.06	23.12	7.82	0.61	0.19	0.10	11.23	4.89	0.01	94.74
290	47.78	0.03	30.73	4.60	0.42	0.12	0.23	11.43	2.30	0.05	96.71
290	48.35	0.09	22.95	7.91	0.71	0.18	0.20	11.38	5.53	0.04	95.02
290	48.09	0.15	29.30	5.04	0.52	0.11	0.15	11.43	2.88	0.04	96.48
290	49.38	0.00	25.22	6.36	0.60	0.16	0.09	11.21	4.67	0.01	95.74
290	48.68	0.11	22.10	8.45	0.75	0.17	0.09	11.30	6.14	0.01	95.20
290	48.37	0.09	27.98	5.97	0.59	0.20	0.12	11.37	3.06	0.01	96.47
290	49.33	0.06	19.68	9.17	0.87	0.19	0.11	11.23	7.39	0.04	94.96
290	49.45	0.08	19.75	9.16	0.76	0.18	0.09	11.20	7.48	0.01	95.02
290	49.35	0.00	19.44	9.26	0.87	0.19	0.05	11.19	7.74	0.01	94.85
290	48.78	0.16	23.86	7.90	0.75	0.18	0.08	11.20	5.17	0.01	95.91
350	47.62	0.21	26.82	7.11	0.43	0.28	0.13	11.47	3.23		95.94
350	47.41	0.13	27.07	7.21	0.43	0.22	0.08	11.47	3.07		95.83
350	47.81	0.58	25.32	8.01	0.44	0.29	0.09	11.28	3.51		95.86
350	47.88	0.28	24.49	7.93	0.37	0.29	0.08	11.37	4.52		95.33
350	45.99	0.20	28.41	7.50	0.39	0.27	0.12	11.55	3.35		96.36
350	45.66	0.58	30.13	6.30	0.37	0.22	0.24	11.36	2.55		96.34
350	48.14	0.14	24.83	7.81	0.44	0.36	0.12	11.11	3.70		95.11
350	48.34	0.14	25.16	7.63	0.40	0.30	0.15	10.35	4.34		95.03
350	48.29	0.06	24.18	8.24	0.42	0.30	0.11	11.41	4.48		95.63
450	46.41	0.11	28.95	5.85	0.32	0.42	0.14	11.46	2.57		95.24
450	45.95	0.05	31.21	4.49	0.24	0.28	0.17	11.57	2.11		95.19
450	47.54	0.17	26.66	6.92	0.39	0.56	0.14	11.59	2.97		95.70
450	46.99	0.38	25.95	7.68	0.40	0.61	0.14	11.40	3.70		95.77
450	47.17	0.51	24.86	8.12	0.44	0.64	0.10	11.29	4.22		95.59
450	47.26	0.30	26.31	7.16	0.34	0.62	0.10	11.46	3.32		95.50
450	44.78	0.34	25.05	10.04	0.54	0.60	0.12	11.12	4.60		95.27
450	45.37	0.47	26.55	8.23	0.42	0.55	0.11	11.34	3.56		95.16
450	47.58	0.08	26.78	7.26	0.38	0.55	0.12	11.37	2.96		95.85
450	47.40	0.07	27.50	6.69	0.32	0.51	0.12	11.46	2.72		95.65

Appendix 5 (cont.): Electron microprobe analyses of muscovite in drill hole 90-1 (in wt-%)

Sample	SiO_2	TiO_2	Al_2O_3	FeO	MnO	MgO	Na_2O	K_2O	F	Cl	Total
650	46.58	0.65	25.00	8.80	0.48	0.60	0.17	11.23	3.28		95.45
650	46.60	0.50	26.22	7.60	0.43	0.51	0.29	11.36	2.88		95.29
650	46.65	0.95	24.44	9.16	0.50	0.49	0.13	11.36	3.94		95.96
650	45.92	0.90	25.35	9.22	0.47	0.50	0.08	11.32	3.71		95.92
650	46.93	0.93	25.80	7.99	0.41	0.50	0.11	11.39	2.94		95.76
650	46.39	0.50	24.90	8.91	0.52	0.55	0.21	11.21	3.59		95.28
650	46.84	0.06	33.88	3.43	0.16	0.20	0.23	11.60	1.49		97.28
650	46.08	0.09	31.97	4.49	0.21	0.28	0.18	11.70	1.58		95.89
650	45.18	0.15	35.53	2.59	0.09	0.04	1.02	10.43	1.13		95.70
650	47.12	0.03	29.63	5.36	0.29	0.32	0.14	11.69	2.10		95.81
830	46.39	0.02	28.20	7.25	0.32	0.30	0.17	11.29	2.16		95.18
830	46.03	0.04	31.53	4.49	0.19	0.23	0.17	11.56	0.92		94.81
830	45.73	0.80	25.95	9.26	0.40	0.50	0.06	11.23	2.36		95.30
830	44.78	0.85	25.57	9.96	0.44	0.49	0.13	11.11	2.31		94.69
830	45.65	0.60	25.74	9.72	0.40	0.55	0.08	11.28	2.28		95.37
830	45.05	0.69	25.40	10.27	0.41	0.49	0.11	11.26	2.57		95.28
850	47.90	0.03	27.70	7.47	0.35	0.51	0.16	11.20	2.54	0.02	96.81
850	47.10	0.05	26.86	7.39	0.40	0.46	0.13	11.31	2.08	0.01	94.92
850	45.63	0.16	32.30	4.65	0.19	0.28	0.20	11.47	1.19	0.01	95.59
850	47.26	0.15	27.47	7.78	0.38	0.46	0.10	11.38	2.35	0.01	96.35
850	45.53	0.10	32.65	4.60	0.15	0.39	0.24	11.51	1.11	0.01	95.81
850	44.44	0.09	31.37	5.39	0.26	0.29	0.31	10.63	1.54	0.06	93.75
850	46.52	0.31	27.30	7.95	0.39	0.50	0.16	11.27	2.25	0.02	95.73
850	46.94	0.15	27.47	7.69	0.36	0.50	0.19	11.36	2.31	0.03	96.01
850	46.43	0.73	27.44	7.96	0.37	0.43	0.11	11.34	2.11	0.02	96.22
850	46.95	0.59	26.78	8.32	0.40	0.44	0.09	11.47	2.18	0.01	96.31
850	47.62	0.57	26.72	7.56	0.35	0.47	0.11	11.47	2.16	0.03	96.13
850	48.27	0.45	26.54	7.76	0.41	0.54	0.13	11.31	2.15	0.02	96.66
850	46.65	0.57	25.52	9.22	0.48	0.49	0.11	11.31	2.69	0.01	95.92
850	47.00	0.69	26.29	8.95	0.48	0.49	0.10	11.14	2.43	0.02	96.55
850	47.10	0.67	26.95	8.25	0.46	0.48	0.11	11.37	2.15	0.03	96.65
850	45.56	0.37	28.29	7.74	0.40	0.40	0.10	11.27	2.01	0.01	95.29
850	47.37	0.70	25.21	8.86	0.45	0.49	0.08	11.47	2.63	0.01	96.17
850	46.26	0.81	25.22	9.85	0.45	0.49	0.08	11.14	2.86	0.02	95.97
850	46.69	0.47	26.97	8.38	0.40	0.53	0.16	11.39	2.19	0.03	96.28
850	47.44	0.01	27.59	7.38	0.42	0.35	0.13	11.53	2.27	0.00	96.16
850	45.91	0.98	25.01	9.82	0.50	0.58	0.10	11.31	2.79	0.02	95.83
850	48.06	0.44	28.02	6.95	0.33	0.44	0.19	11.44	2.05	0.03	97.08

IMAGE EVALUATION
TEST TARGET (QA-3)

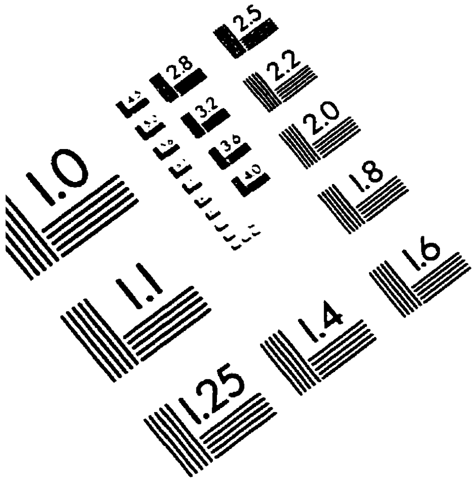

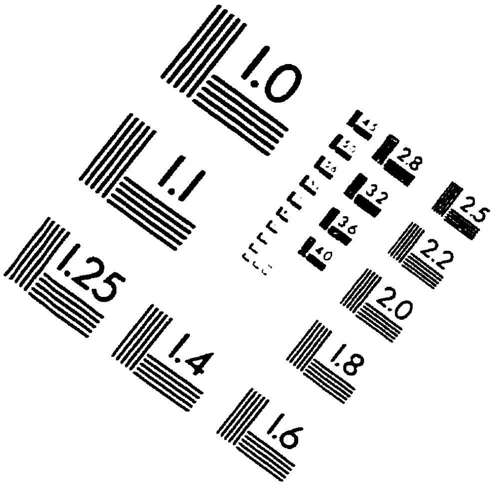

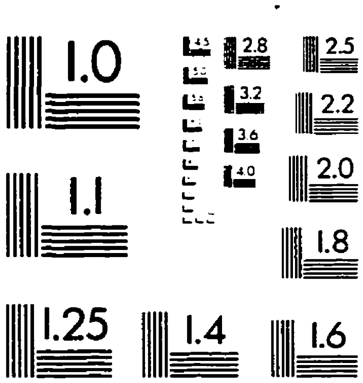

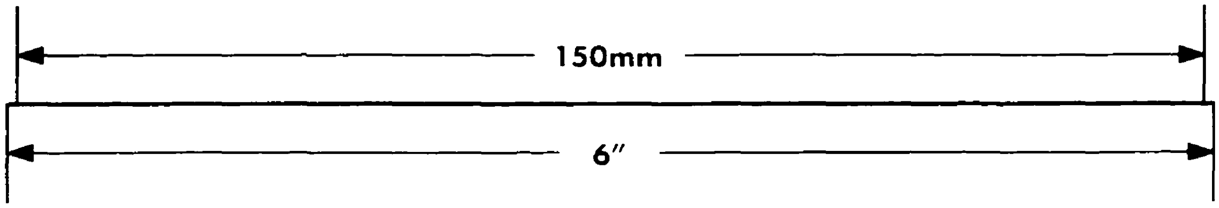

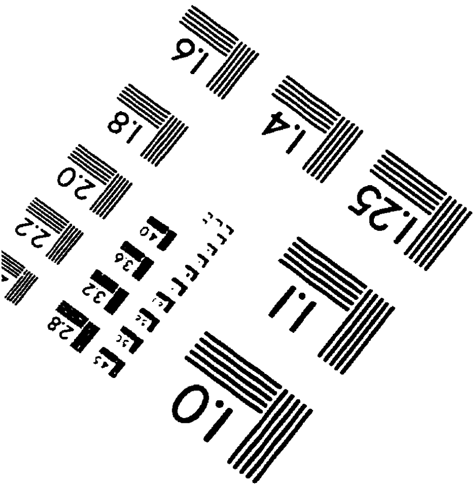

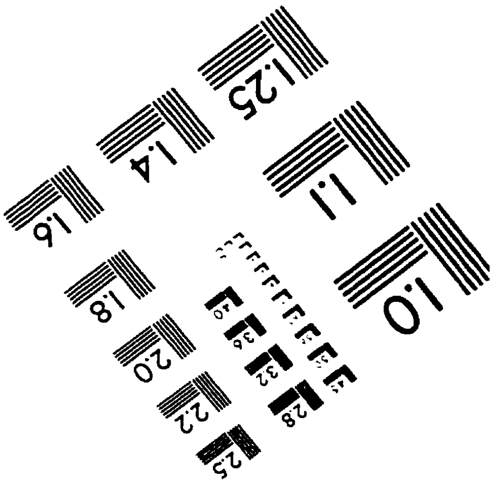

APPLIED IMAGE . Inc
1653 East Main Street
Rochester, NY 14609 USA
Phone: 716/482-0300
Fax: 716/288-5989